Investigating chromatin domain structures in living cells using histone pulse-labelling approaches

by

Filipe Alexandre Fernandes Duarte

Thesis submitted in partial fulfillment of the requirements for the degree of Doctor of Philosophy in Interdisciplinary Biomedical Research.

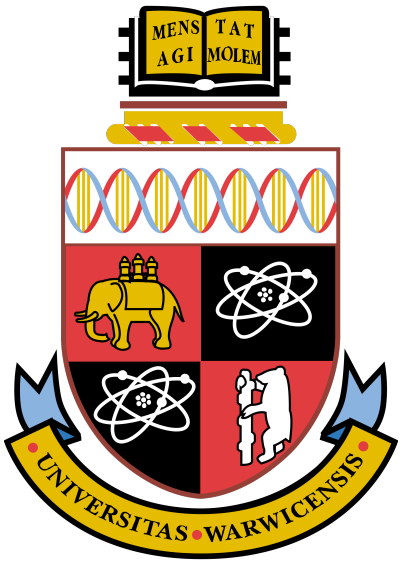

Warwick Medical School

The University of Warwick

July 2021

Contents

List of Figures

List of Tables

Acknowledgments

I would like to extend my deepest gratitude to my supervisors Dr Andrew Bowman and Prof Nigel Burroughs for their continuous support during my time at Warwick, their input was invaluable in carrying out the work presented in this thesis. I want to thank my advisory panel as well, Prof Steve Royle and Prof Mohan Balasubramanian, for their advice, which proved pivotal in this work. I would also like to thank the MRC DTP in IBR for the marvellous and supportive community they developed around the doctoral programme, which has not only given me the opportunity to fully capitalise on this degree, but has also created the conditions for me to expand my skills beyond it. I want to especially thank my IBR cohort for their companionship and support, which have made my PhD experience infinitely more enjoyable. I would also like to thank the whole of the Bowman lab, especially Dr Alonso Pardal who has been an invaluable soundboard and lab companion.

For their unconditional support and encouragement throughout all of my studies, being this degree no exception, I would like to thank my whole family, especially my mum, dad and sister. I would also like to thank my friends in Portugal, Britain, and all around the world, as well as my housemates throughout all these years for being my home away from home. This proved especially important during the last year, where Melissa and Jonny helped to cope with all the challenges of lockdown. I am very grateful for the time we all spent together over the years.

Declaration

This thesis is submitted to the University of Warwick in support of my application for the degree of Doctor of Philosophy. It has been composed by myself and has not been submitted in any previous application for any degree.

The work presented (including data generated and data analysis) was carried out by the author.

Abstract

3D genome organisation has been predominantly studied through next generation sequencing methodologies with conclusions often being made from population averages rather than single cells, or by fixed cell imagining techniques such as FISH. Studying its dynamics has been mostly limited to tracking one or two *foci*, integrated repetitive arrays, or has involved indiscriminate labelling of bulk chromatin.

As the domain structure of the genome is mirrored by its replication timing, I was able to use a recently developed technique (RAPID-release) where a short pulse of EGFP-tagged histones, during S-phase, is incorporated into distinct chromatin domains. As EGFP labeled H3.1 has a slow turnover in human chromatin, it was used as a location marker, allowing for the tracking of its position over time. I capitalised on this unique labelling ability to investigate the behaviour of chromatin domains in living cells, and across different time-scales using lattice light sheet microscopy.

I was able to characterise the dynamic characteristics of late-replicating domains, observing the presence of two populations with different dynamic features: high mobility domains and low mobility domains. I also investigated the effect of nuclear perturbation on the kinetics of the labelled chromatin by inducing DNA damage, where I observed a generalised increase in dynamic behaviour.

Finally, I adapted the RAPID-release technique to improve its kinetics and attempted to develop a parallel system that used orthologous components in order to expand on the capabilities of this system.

List of Abbreviations

3C – Chromosome conformation capture

3D – Three-dimensional

ABA – Abscisic acid

ABI1 – ABA Insensitive 1

AI – Auto inhibitory

AID1 – Auxin-inducible degron

AUX – Auxin

CID – Chemically induced dimerisation

CL – Chromatin loop

CP – Circularly permutated

CT – Chromosome territory

CTCF – CCCTC-binding factor

DSB – Double strand break

EGFP – Enhanced green fluorescent protein

FBS – Foetal bovine serum

FISH – Fluorescence *in situ* hybridisation

FKBP – FK-506 binding protein

FRB – FKBP12-rapamycin binding domain of mTOR

GFP – Green fluorescent protein

HCV – Hepatitis C virus

HDR – Homology-directed repair

HMD – High mobility domain

IRES – Internal ribosome entry site

IRR – IRES RAPID-release

L-15 – Leibovitz's L-15 Medium

LAD – Lamin associated domain

LLSM – Lattice light sheet microscopy

LMD – Low mobility domain

LOV2 – Light oxygen voltage

LSU – Large ribosomal subunit

MSD – Mean squared displacement

NAD – Nucleolus associated domain

NES – Nuclear export signal

NETs – Nuclear envelope transmembrane proteins

NHEJ – Non-homologous end joining

OMM – Outer mitochondrial membrane

OMP25 – Outer membrane protein 25-a

PBS – Phosphate buffer solution

PSF – Point spread function

Puro – Puromycin

PYL1 – Abscisic acid receptor PYL1

RAP – Rapamycin

RAPID-release – Rapamycin induced dimerisation release

RD – Replication domain

RFP – Red fluorescent protein

RPL5 – Ribosomal protein L5

RPL11 – Ribosomal protein L11

RTP – Replication timing programme

SD – Standard deviation

TAD – Topologically associated domain

TEV – Tobacco etch virus

TIR1 – Transport inhibitor response 1

TVMV – Tobacco vein mottling virus

Chapter 1

Introduction

1.1 Chromatin structure of higher Eukaryotes

The diploid human genome is comprised of 46 chromosomes, which together amount to approximately 6.5 billion base pairs. When stretched end-to-end this amount of DNA can exceed 2 meters in length, yet, it is packaged inside the approximately 10 μm in diameter nucleus of a single cell. With the sheer amount of information stored in a single genome, it is unrealistic to assume its dispersal within the nucleus is random, rather, for the prompt accessibility of this information, an intrinsic organisation must exist (Koonin and Wolf 2010).

Eukaryotic genomes are organised into chromatin, which is a structure comprised of proteins, RNAs and genomic DNA (Mondal et al. 2010; Ohta et al. 2010), and its integrity is crucial for genomic stability, gene regulation, replication, and repair (Bickmore 2013; Hübner, Eckersley-Maslin, and Spector 2013; Cardoso et al. 2012). Organisation is dependent on histones, the most abundant proteins in chromatin (Ohta et al. 2010). These form an octamer around which genomic DNA wraps. Two copies of histones H2A, H2B, H3 and H4 are encircled by a strand of DNA that wraps 1.65 times around the complex, corresponding to approximately 150 base pairs of DNA, with linkers between nucleosomes of

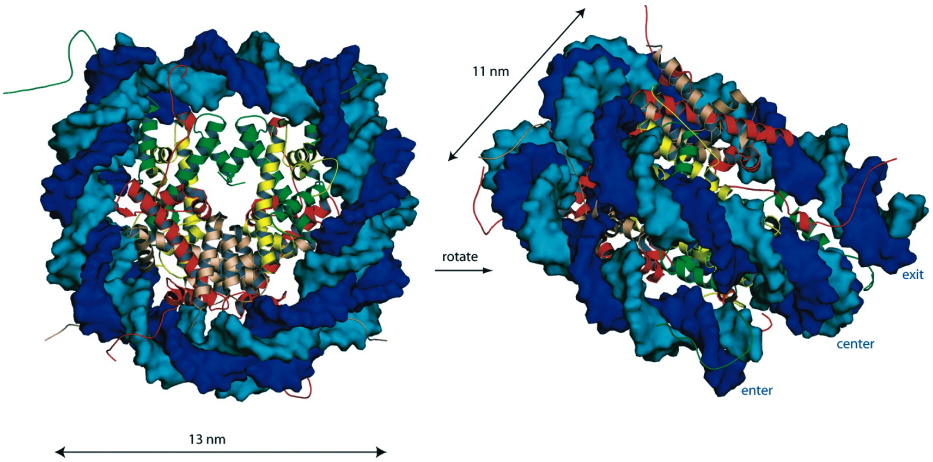

Figure 1.1: Diagram of the nucleosome, and the histones that compose it. Histone H3 in green, H4 in yellow, H2A in red, and H2B in pink. DNA strands in blue (Khorasanizadeh 2004).

around 20-60 base pairs. These form the basic repeating unit of chromatin – the nucleosome (Luger et al. 1997, figure 1.1).

From the nucleosome level and moving towards a macrometric scale, the genome is further organised into three dimensional (3D) structures in a hierarchical fashion, which not only contribute towards effective packaging, but also play an important role in regulation, genome stability and repair. This hierarchical 3D organisation is not static, its landscape changes as a result of stimuli in a way that impacts gene expression. The extent to which gene expression is impacted is widely debated, and many of the mechanisms that dictate specific spatial distribution are also not well known. What is certain is that much of what takes place in the nucleus requires physical interactions between different parts of the genome, making it clear that spatial distribution of genomic elements as well as how this changes through time play a key role in normal nuclear function (Fedorova and Zink 2008). This project focuses principally on genomic spatial organisation and dynamics, the aspects that may influence these features, and the methods used to study these phenomena.

1.1.1 Chromosome territories and compartments

Chromosomes are organised in hierarchical length scales within the nuclear space (Gibcus and Dekker 2013; figure 1.2). This organisation is a consequence of a variety of biological and biophysical phenomena that dictate structure at each of the hierarchical levels (N. Gilbert 2019; Zuin et al. 2014; Dixon, Jung, et al. 2015; Gibson et al. 2019). At the lowest level of resolution in this hierarchy we find the chromosome territory (CT). These are distinct nuclear regions to which a particular chromosome preferentially locates. It is within CTs that chromatin tends to interact with itself; interactions between different chromosomes are rarer than interactions between regions of the same chromosome (Szczepińska, Rusek, and Plewczynski 2019; Miguel R Branco and Pombo 2006).

Regarding their positioning within the nucleus, CTs' relative radial position seems to be dependent on the gene contents of each chromosome. Chromosomes that more are gene-rich tend to localise towards the centre of the nucleus whereas gene-poor chromosomes tend to localise towards the periphery (Boyle et al. 2001; Croft et al. 1999). Although this rule is generally applied, it is also true that CT positioning can be cell specific, suggesting a functional role to this characteristic (Hepperger et al. 2008). Furthermore, the distribution of chromatin within CTs tends to correlate with the gene contents as well, where gene-rich regions are located in the periphery of the CT, and gene-poor regions can be found in its centre (S. Shah et al. 2018). Interestingly, CTs of homologous chromosomes in diploid cells tend to locate away from each other (Heride et al. 2010; Selvaraj et al. 2013).

The formation of CTs has been postulated to influence the movement of the genetic material by preventing free diffusion of specific chromosomes from the periphery to the centre and *vice versa*. The formation of sub-chromosome scale domains in a preferential intra-chromosomal fashion resulted in the current idea of 'fractal globule' folding of chromosomes.

Chromosome territories are divided into different compartments that

differ in chromatin accessibility. These have been classified as A and B compartments. "A" compartments are characterised by their high CG content and their gene-rich nature. Histone modifications in the chromatin of these compartments are associated with higher levels of activity. Conversely, "B" compartments have a lower gene content and the histone modifications found there tend to be associated with gene silencing (Fortin and K. D. Hansen 2015). B compartments self-associate with greater affinity, and are located towards the periphery of the nucleus, corroborated by their high correlations with Lamin Associated Domains (LADs) and late-replicating chromatin (Ryba et al. 2010). The formation of these compartments is independent from the linear disposition of genes along the chromosome. Genes that are positioned at relatively long distances from each other from a linear standpoint can be associated with each other in a compartment of the same type, whereas genes that are linearly adjacent may be in different compartments (Lieberman-Aiden et al. 2009).

1.1.2 TADs, sub-TADs, and structures of the same order

At a higher resolution, compartments are sub-divided into Topologically Associated Domains (TADs). TADs are structures in the hundreds of kilobases scale that form through looping of linear chromatin, folding into roughly globular structures (figure 1.3 B). This assumption is derived from Hi-C and 5C data that shows a significantly higher level of interaction frequency within these regions than with neighbouring parts of the linear chromosome, suggesting a physical separation of the genome (figure 1.3 A). They are limited by boundary regions that insulate and separate neighbouring TADs into independent chromatin domains. These independent TADs can present vastly different gene expression patterns, even if they sit adjacent to each other in the linear chromosome (Dixon, Selvaraj, et al. 2012; Dixon, Jung, et al. 2015). Boundaries are often enriched with CCCTC-binding factor (CTCF) and cohesin – architectural

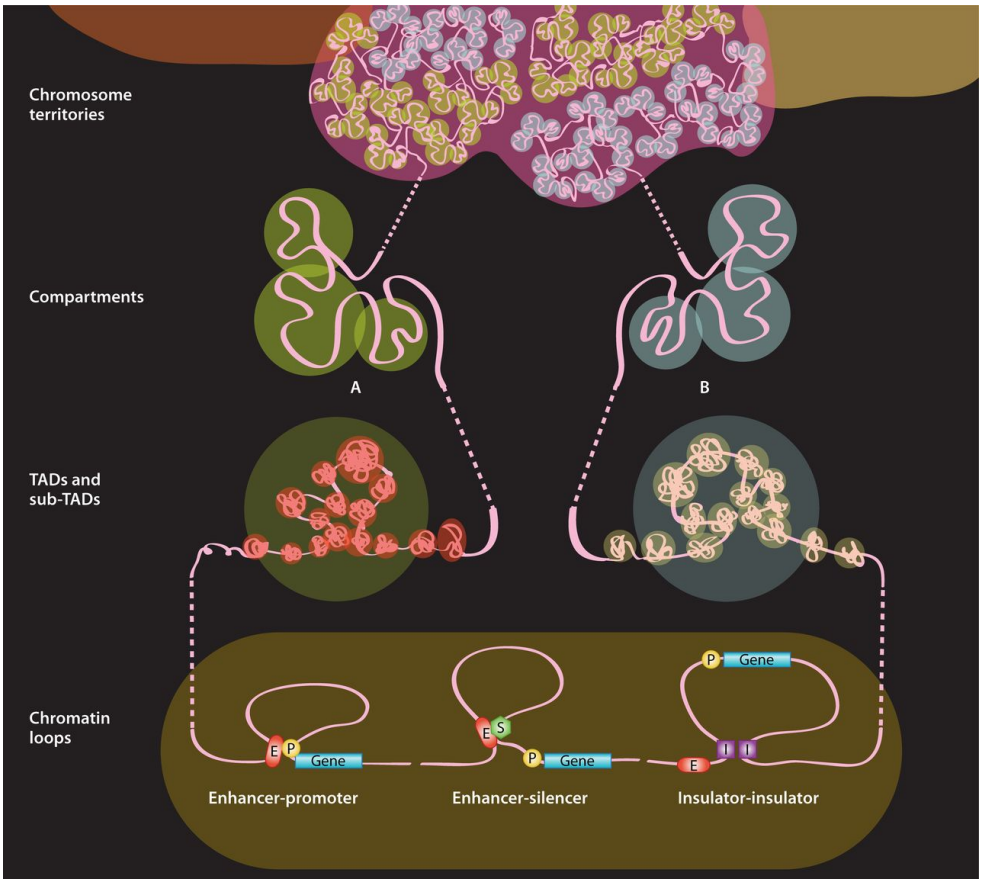

Figure 1.2: Illustration of the hierarchical organisation of the eukaryotic genome. Chromosome territories are the structures of lowest resolution, followed by compartments, TADs and sub-TADs, and chromatin loops (Fraser et al. 2015).

proteins that are thought to be responsible for the looping of the TAD itself (Zuin et al. 2014). The "loop extrusion" model describes TAD formation through the assembly of a cohesin ring around a DNA loop, which is extruded until a physical barrier (CTCF) stops the process (Nuebler et al. 2018; Sanborn et al. 2015; figure 1.3 C). It is also common to find histone modifications associated with active-gene regions, house-keeping genes, tRNA genes, and short interspersed nuclear elements (SINEs) in the regions that make up the boundaries between TADs (Dixon, Selvaraj, et al. 2012; Rao, Huntley, et al. 2014; Sexton et al. 2012).

The fact that genes within the same TAD are co-expressed during cell differentiation alludes to a functional and regulatory role of these structures (Nora et al. 2012). But perhaps more illustrative of their functional importance is the fact that most gene regulation events that require enhancer-promoter contacts happen within the same TAD. Indeed, if TADs are partially fused by deletion of boundary regions, gene expression profiles are affected (Bar Yaacov et al. 2019; Welch et al. 2020). TADs are widely conserved across organisms, cell types, and even developmental stages, however, it is within TADs that genome interactions change, to form structures termed sub-TADs which depend on cell type and stimuli (Shen et al. 2012; Bar Yaacov et al. 2019). Sub-TADs rely on different structural proteins than TADs for their formation and maintenance. Here, not only CTCF and cohesin, but also Mediator complex seem to be crucial, and at this level boundaries seem to be more dynamic and less strongly defined (Van De Werken et al. 2012). Sub-TAD topology appears to be much more intimately related to the levels of genomic activity than structures at lower resolutions (Phillips-Cremins et al. 2013). However, at this scale it is still unknown how sub-TADs interact with each other and how the boundaries between them represent and impose their functional role.

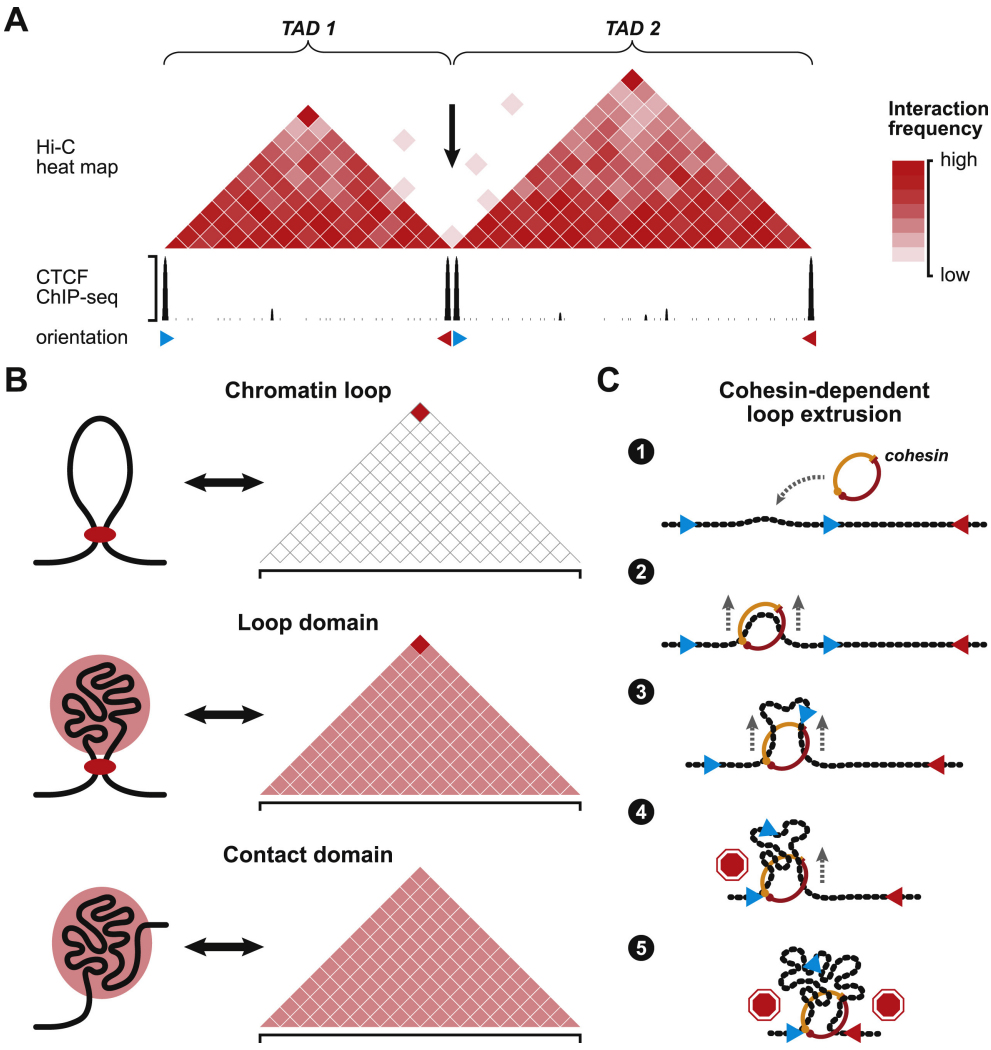

Figure 1.3: Topologically associated domain formation through loop extrusion. **A** Topologically associated domains are regions of the genome where greater frequency of contacts can be observed between genes in a Hi-C heat map. CTCF (red and blue triangles) marks the boundaries between TADs. **B** Chromatin structures with different architectures give rise to different Hi-C heat maps depending on how genes interact. **C** Illustration of the cohesin-dependent loop extrusion model for the formation of chromatin structures. Cohesin binds to the linear chromosome followed by extrusion of the DNA polymer through the cohesin ring until two correctly oriented CTCF sites converge and halt further extrusion (Chang, Ghosh, and Noordermeer 2020).

Structural proteins in more detail

Interplay between cohesin and CCTF is thought to play a central role in spatial organisation of chromatin structures. CTCF is a highly conserved protein that performs multiple functions (Ohlsson, Renkawitz, and Lobanenkov 2001; Phillips and Corces 2009). The variety of roles it performs is dependent on the DNA sequence to which it binds, allowing for different downstream effects by triggering different pathways (Filippova et al. 1996). However, CTCF's influence on genome architecture comes from its insulator features. Its presence at boundaries between hetero and euchromatin enforces their active/inactive contrast (Cuddapah et al. 2009; Narendra et al. 2015). CTCF depletion leads to an increase in interaction between elements in different TADs and reduces the ones within the same TAD, this illustrates that CTCF has an important role in physically segregating portions of the genome, preventing the access of enhancers foreign to a particular domain, and promoting the interactions of those within the same TAD (T. H. Kim et al. 2007; X. Xie et al. 2007).

Cohesin is a protein complex that was first identified as crucial in the segregation of chromosomes during both mitosis and meiosis (Michaelis, Ciosk, and Nasmyth 1997; Guacci, Koshland, and Strunnikov 1997). It is comprised, in somatic cells, of structural maintenance of chromosomes protein 3 (SMC3), structural maintenance of chromosomes protein 1 (SMC1), double-strand-break repair protein RAD21 homolog (RAD21) and cohesin subunit SA-1 (SA1) or cohesin subunit SA-2 (SA2) (Losada, M. Hirano, and T. Hirano 1998; Michaelis, Ciosk, and Nasmyth 1997; Guacci, Koshland, and Strunnikov 1997). The complex forms a ring composed of a SMC1 and SMC3 heterodimer, and RAD21, where SA1/2 bind, working as platforms for other factors to bind the complex (figure 1.4). DNA enters and leaves the ring through the opening of the interfaces between RAD21 and the SMC subunits on the side opposite to the hinge domains, where an ATP-binding cassette-like domain with ATPase activity can be found (Gruber, Haering, and Nasmyth 2003).

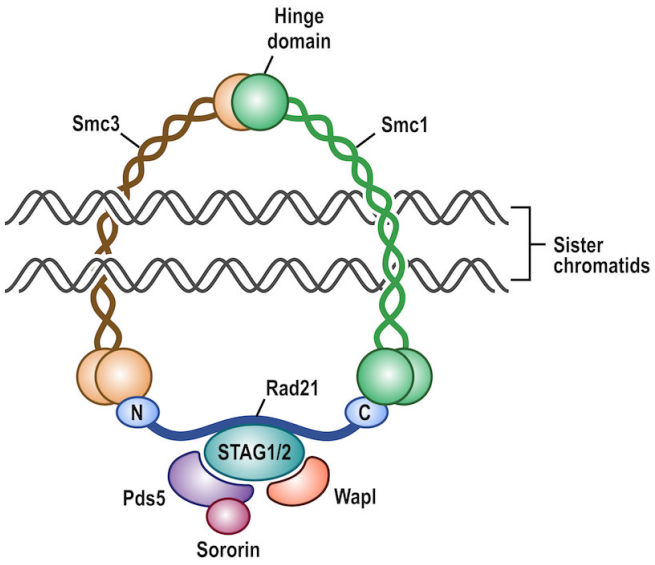

Figure 1.4: Diagram of the Cohesin complex (Solomon, J.-S. Kim, and Waldman 2014).

The cohesin complex's relationship with interphase genome architecture derives from its influence on promoter-enhancer looping in certain genes like Nanog and Ultrabithorax (Kagey et al. 2010). Unlike CTCF, whose binding site distribution across the genome is conserved, cohesin binding is carried out in a more tissue specific manner, therefore, both these structural proteins can be found independent of each other. Despite this, there is still extensive co-localisation of the two proteins, especially at TAD border sites (Schmidt et al. 2010). The most striking consequence of cohesin depletion is the reduction of intra-TAD associations and disruption of sub-TAD integrity, which takes place without disruptions to the overall TAD localisation and stability. This is linked to cohesin's role in enhancer-mediated activation of genes which takes place within TADs and is central in the generation of sub-TADs, highlighting its role in genome architecture at these length scales (Zuin et al. 2014; Sofueva et al. 2013).

Regardless of CTCF's and cohesin's central role in genome architecture, there are other proteins, complexes, and RNAs that also contribute towards it. The Mediator complex, for example, is known to be essential in bringing together promoters and enhancers to form chromatin loops

through interactions with cohesin (Kagey et al. 2010). Polycomb proteins have also been linked to the assembly of chromatin loops in highly repressed chromatin and can influence the way chromatin is compartmentalised (Boettiger et al. 2016). More recently evidence has shown that polycomb can also play a role in changing the conformation of chromatin to favour enhancer-promoter contacts in HoxA genes in a way crucial for their correct expression (Gentile et al. 2019; Schoenfelder et al. 2015).

LADs, NADs and the interaction of the genome with nuclear structures

Chromatin domains can interact with different structures present in the nucleus, for example, the nucleolus and the nuclear lamina. Interactions with these structures often have functional and structural consequences for gene expression and chromatin compartmentalisation (Zuleger et al. 2013). Lamin proteins are intermediate filaments adjacent to the inner nuclear envelope that interact with nuclear envelope transmembrane proteins (NETs); they are able to bind chromatin constituents like heterochromatin protein 1 and nucleosomes (Prokocimer et al. 2009). When this kind of interaction takes place, chromatin domains can be sequestered and anchored to the lamina, limiting their migration within the nucleus. Chromatin domains that undergo these interactions are called Lamin Associated Domains (LADs), these are heterochromatic and tend to present gene-poor features in the case of conserved LADs. However, LADs can also be comprised of gene-rich regions of the genome that have been silenced, which is the case of cell-specific LADs (Amendola and Van Steensel 2014). Also associated to the lamina with high affinity are telomeres, with disruptions to these interactions having significant consequences on the architecture of the genome (Gonzalez-Suarez et al. 2009; Shoeman and Traub 1990; Dechat et al. 2004). Interactions between the genome and the nuclear lamina are not solely structural, however. By binding NETs, LADs can be affected by forces and phenomena that take place in the cytoplasm through the transduction of

mechanical forces fostered by LInker of Nucleoskeleton and Cytoskeleton (LINC) complexes (Lombardi et al. 2011).

The nucleolus is a high-density region in the the nucleus where rRNA synthesis and pre-ribosome assembly take place. It forms from the coalescence of regions of different chromosomes that contain rRNA genes that are transcribed by RNA polymerase I. These structures too, interact with chromatin domains to form Nucleolus Associated Domains (NADs). NADs are gene-poor with high A/T content, and their identities overlap with LADs extensively, presenting identical characteristics (Kind et al. 2013). In fact, known LADs and NADs were found to co-localize often, suggesting that redistribution between the two structures takes place, possibly after a round of cell division. An example of this is the location of centromere clusters, these structures tend to localise towards the periphery of the cell together with heterochromatic DNA, however, when these are not found at these locations, they can be found in regions adjacent to the nucleolus (Weierich et al. 2003). Therefore, it is possible that similar factors target the inactive chromatin to either the lamina or nucleoli (Thomson et al. 2004). Both LADs and NADs reach dimensions of 0.1 to 10 Mbp, which is in the same order of magnitude to those of TADs, which reach sizes ranging between 0.1 to 1 Mbp (Pope et al. 2014; Dixon, Selvaraj, et al. 2012).

TADs and replication

Further evidence of the importance of TADs as functional structures of the 3D genome is the role they play in the regulation of DNA replication timing (Pope et al. 2014). Genome replication occurs in a particular order, termed the replication timing programme (RTP), where different regions are replicated at different points of S-phase (Rhind and D. M. Gilbert 2013). Initial studies of this phenomenon, using fluorescent nucleotide analogs, showed the formation of structures known as replication *foci*, which presented different spatial patterns that were dependent on S-phase timing. Replication *foci* that appeared at the beginning of S-

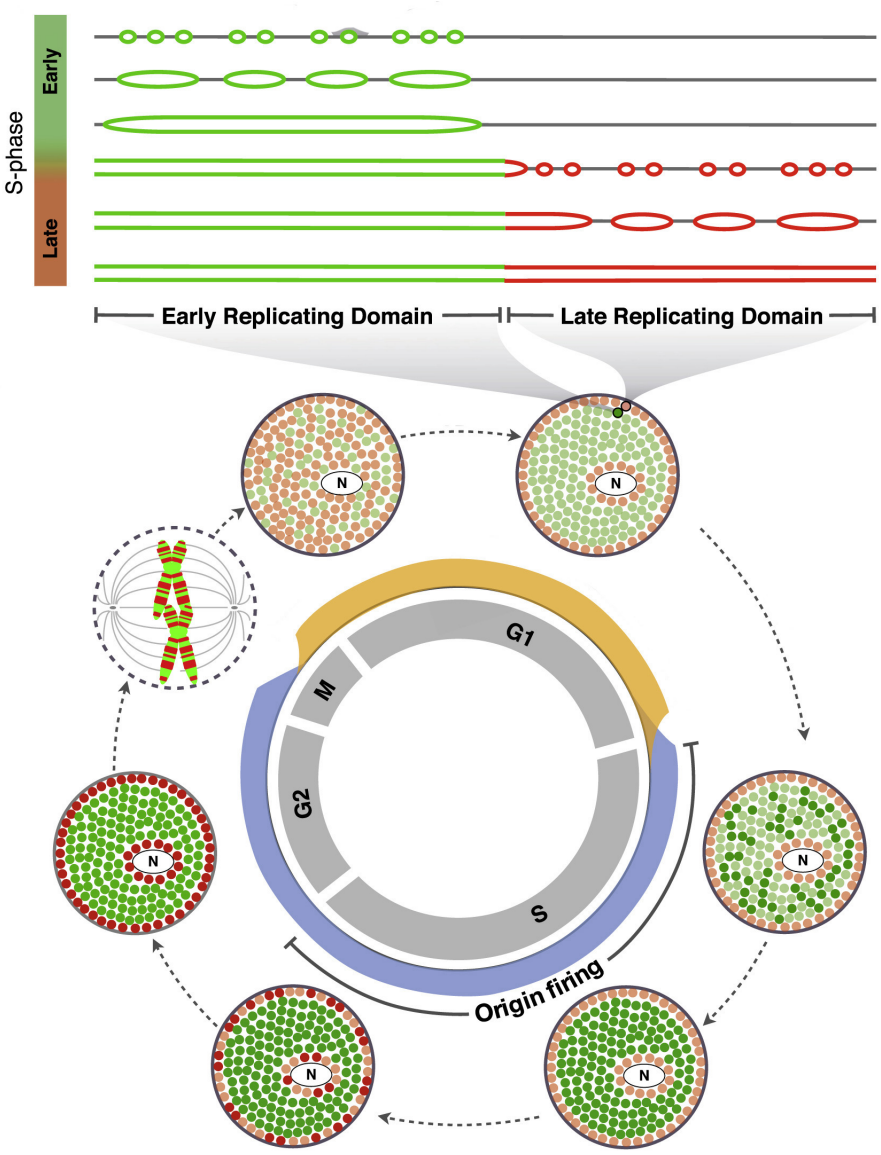

Figure 1.5: TADs as replication timing regulators. Different parts of the genome replicate at different stages of S-phase. Early replicating domains (green dots) are located towards the centre and late replicating domains towards the periphery of the nucleus (red dots). Replication of an individual TAD is contained and isolated to that particular domain, working as a regulator of replication (adapted from Rivera-Mulia and D. M. Gilbert 2016).

phase were dispersed throughout the nucleus and had small dimensions, whereas late S-phase *foci* were larger and located in the periphery of both nuclei and nucleoli (Nakamura, Morita, and Sato 1986; Nakayasu and Berezney 1989). With the employment of genome-wide methods, units of replication timing regulation were identified. These were comprised of clusters of replicons that fired simultaneously and in accordance with the RTP. Replication domains (RDs) were, therefore, perceived as structures that physically compartmentalised DNA and temporally segregated its replication, with RDs with the same RT programme being found undergoing replication simultaneously (Pope et al. 2014; Rhind and D. M. Gilbert 2013; figure 1.5). Parallels were made between the timing of replication and gene expression, becoming clear that early replicating domains were correlated with active euchromatin, which was located in A compartments (discussed above), whereas, late replicating domains were associated with heterochromatin in B compartments (Dixon, Selvaraj, et al. 2012; Moindrot et al. 2012; Yaffe et al. 2010).

Later studies revealed that the boundaries of RDs were coincident with those of TADs and that the physical compartmentalisation TADs conferred upon the genome was in fact responsible for upholding the different replication timings seen in the RTP (Pope et al. 2014). To further corroborate this close relationship between TADs and replication domains, it was later found that as replication timing changes during cellular differentiation, so do interactions between TADs, suggesting a migration of TADs between compartments, and a consequent change of their replication timing (Takebayashi et al. 2012). The same relationship was found between RDs and LADs/NADs. The boundaries of these chromatin domains also correlated with those of RDs, especially those with high A/T content that were known to be replicated at the end of S-phase and were located in the periphery of the nucleus (Pope et al. 2014; Peric-Hupkes et al. 2010).

1.1.3 Smaller scales of genome organisation

At the scale of sub-TADs and smaller, genome spatial organisation is intimately related to transcription regulation. Chromatin loops are the next observable structures and where the line is drawn between these and sub-TADs can be blurry. Chromatin loops form by two distal elements coming together. This happens within the same chromosome (*cis*) but an analogous process can also take place between chromatin belonging to two different chromosomes (*trans*) (Zhang et al. 2013; Monahan, Horta, and Lomvardas 2019). Unsurprisingly, it has been shown that chromatin loops that occur in *trans* are composed of elements that locate at the periphery of chromatin territories (Monahan, Horta, and Lomvardas 2019). Looping of chromatin is linked primarily to enhancer-promoter interactions. These cell specific events are important for cell identity maintenance and for regulating the levels of expression of particular proteins (Zhang et al. 2013). Just like the integrity of sub-TADs, chromatin loops are sensitive to cohesin depletion and are seen to dissociate under these conditions, affecting gene expression. However, chromatin loops are known to reappear once cohesin depletion is lifted (Rao, Huang, et al. 2017).

Looping of enhancers into promoter regions has also been shown to alter the physical properties of the environment of the locations in which it takes place through liquid-liquid phase separation (Hnisz et al. 2017). Together, looping and biophysical environmental changes generate what has been called "transcription hubs", where ideal conditions for effective transcription are found (Boija et al. 2018). It is thought that the biophysical changes in transcription hubs appear due to the specific electrostatic interactions generated by the presence of transcription factors and appropriate histone modifications at abundant concentrations (Sabari et al. 2018; Shrinivas et al. 2019).

At the supra-nucleosomal scale, the structure of chromatin and its behaviour in interphase are highly debated. Here, as a result of electron microscopy studies, the 30 nm fibre model gained traction. This model

describes a solenoid one-start helix where nucleosomes sit next to the adjacent nucleosome in the fibre to create a helical fibre 30 *nm* in diameter (Finch and Klug 1976). A second model was subsequently proposed, and later resolved through crystallography, where a 30 *nm* fibre was assembled in a zig-zag, two-start helix pattern. In this instance, nucleosomes adjacent along the strand are positioned opposite each other in the 30 nm fibre, the linker DNA crisscrossing in the centre (Bednar et al. 1998; Schalch et al. 2005).

Despite observations of this structure through electron microscopy, the 30 *nm* fibre only assembles in the presence of abundant linker histone (H1) and in a salt-dependent manner, leading to mounting challenges to this model's validity *in vivo* (Thoma, Koller, and A. Klug 1979). If H1 is depleted there is unravelling of the 30 *nm* solenoid to yield disordered chromatin that resembles a 10 *nm* fibre (Allan et al. 1981). Therefore, there has been a shift towards the 10 *nm* model as being the one that is more physiologically relevant to the majority of the genome of interphase cells. This corresponds to the classic "beads on a string" model that is widely accepted, and presents nucleosome density along the DNA strand as a regulatory feature of chromatin. In this instance, nucleosomes organise in "clutches" along the fibre, interspersed with regions of low nucleosome density. The former is associated with heterochromatin, whereas the latter with active euchromatin (Ricci et al. 2015).

It is possible however, that the two models could exist simultaneously and that chromatin fibres adopt different conformations that reflect its plasticity requirements. There have been studies suggesting this to be the case, where it was posited that the chromatin fibre is likely to resemble the 30 *nm* fibre model punctuated with regions that fit with the 10 *nm* description. These are also likely to be dependent on the transcriptional characteristics of each region of the genome, with heterochromatin being more regularly packaged than euchromatin (N. Gilbert 2019).

In conclusion, to achieve packaging of DNA into the cell nucleus in a way that allows for genome stability, maintenance, and the effective

retrieval of information crucial for cell homeostasis, a hierarchical organisation system has evolved. This system is highly complex, ranging from the μm scale of CTs to the 10 nm scale of nucleosomes, and relies on a myriad of proteins and RNAs to be achieved. Despite the advances made in the field of genome architecture, due to the complexity of eukaryotic genome organisation, many aspects remain elusive, especially at smaller scales.

1.2 Dynamics of the genome

1.2.1 Mitosis

The way the genome is organised and packaged is complex in its own right and the structures described above are far from being static. Indeed, the genome is highly dynamic in ways that depend on the stage of the cell cycle, transcription, and genome integrity.

During mitosis, the genome experiences a drastic change in structural arrangement, from dynamic events that tightly package chromatin into mitotic chromosomes, followed, after cytokinesis, by de-compaction of chromosomes into their interphase arrangement. These dynamic structural changes disrupt genomic structures, which, when the process is complete, reassemble and resume their roles.

TAD disassembly takes place through the removal of CTCF from TAD boundaries, followed by their reorganisation into tightly packed chromatin loops of much smaller dimensions. In turn, these associate to make up the mitotic chromosome prior to segregation (Eagen, Hartl, and Kornberg 2015; Naumova et al. 2013). These processes are dependent on condensins, protein complexes present in all eukaryotes that resemble cohesins (T. Hirano 2016). It has been suggested that the generation of these loops is achieved through loop extrusion (Goloborodko, Marko, and Mirny 2016), however, there are other theories that attempt to explain this phenomenon, such as chiral looping (T. Hirano 2012) and pairwise interactions (Cheng et al. 2015). Changes in structure are clearly visible

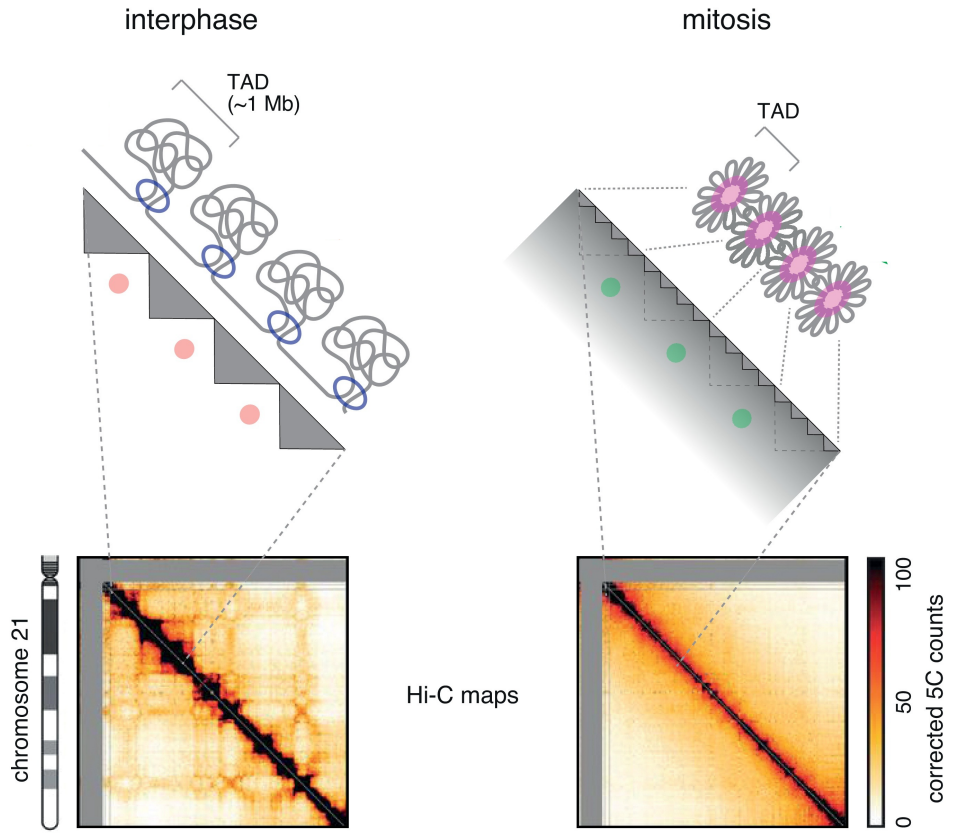

Figure 1.6: Changes in chromatin architecture during chromosome condensation. Interphase chromosomes must condense for segregation to take place during mitosis. This process perturbs the interphase chromatin architecture, altering structures and interactions within the genome. Condensins in pink and cohesins in blue (adapted from Kinoshita and T. Hirano 2017).

in Hi-C maps, where the long range interactions that characterise TADs disappear to give rise to interactions that take place almost exclusively between DNA that is contiguous along the linear chromosome (figure 1.6). Because of this, all inter-chromosomal interactions also cease to exist, as the chromatin at the edge of CTs is tightly packaged into the mitotic chromosome, leaving no room for interactions with DNA in *trans*. The reverse process takes place after cell division, where CTCF associates with their genomic *loci*, and the long range interactions that characterise TADs are restored, reinstating interphase architecture (Naumova et al. 2013).

1.2.2 Changes in transcription and gene expression

In an interphase context, different gene expression states give rise to different chromatin dynamics. Studies on the movement of individual genes have shown that at locations where transcription takes place, the movement of chromatin increases (Neely et al. 1999). This happens whether polymerases are catalytically capable of transcribing the DNA or not, suggesting that the chromatin environment assembled to promote transcription drives this increase in movement, and not the transcription of DNA itself (Neumann et al. 2012). Unsurprisingly, the *loci* of genes that require enhancer-promoter contacts also present increased dynamics when actively expressed, this is because different parts of the linear chromosome must be brought together for transcription to take place, which is very much a dynamic event in and of itself (Gu et al. 2018).

Some authors propose a "stirring model" to explain increased contact frequency between enhancers and promoters where contacts happen stochastically due to increased mobility of the chromatin, generated by the assembly of a transcription-prone environment. They posit that it is through this increase in random movement within the TAD, that enhancers and promoters interact, and not due to the formation of stable loops (Gu et al. 2018). This is in contrast with chromatin loop model that defends that sustained contact between the two elements is indeed necessary (Babokhov et al. 2020). It is likely that the truth lies somewhere in between the two models, since some studies have indicated that loops are dynamic structures themselves, breaking apart and reforming within timescales of tens of minutes (A. Hansen et al. 2018). Indeed, the same study suggested that larger Mb structures like TADs behave the same way.

Changes in dynamics associated with transcription/gene expression can also be observed at global nuclear scales. Interestingly, at these scales, transcription levels have the opposite effect of the one described above. Cells with decreased transcriptional activity show greater general chromatin movement, whereas, cells with higher levels of expres-

sion present a more constrained nuclear environment (Shaban and Seeber 2020). This suggests that when gene expression is active, local transcription-friendly environments are assembled, and chromatin is brought together under these environments and localised constrictions are created, which translate into a global reduction in correlated motion across the nucleus. When local constraints are lacking, chromatin is freer to diffuse. This is illustrated by the less sharp borders between neighbouring domains that can be seen when studying contact frequencies. This phenomenon further illustrates the correlation between genomic architecture and function (Nagashima et al. 2019; Babokhov et al. 2020).

During cell differentiation, when major changes in gene expression/ transcription take place, changes in dynamics are also observed. This is seen at the TAD level, where long-range TAD-TAD interactions as well as TAD location, can be affected (Paulsen et al. 2019). This is because, as seen before, the spatial organisation of TADs is intimately related to the expression profile of the genes included within them, therefore, new transcriptional needs lead to new spatial arrangements (Paulsen et al. 2019; Beagan et al. 2020; figure 1.7). As the activation of certain genes and deactivation of others take place, enhancer-promoter contacts change. "Rewiring" is crucial for lineage specific expression patterns as cells specialise in their function (Bonev, Mendelson Cohen, et al. 2017).

These changes also dictate that TADs containing genes that are inactivated become part of B compartments and locate accordingly within the nucleus (Paulsen et al. 2019; figure 1.7). Migration between compartments has been widely observed in neuron differentiation, and similar phenomena can also be observed in other lineages. For example, in adipose tissue differentiation, the existence of "TAD cliques" has been described, these are groups of TADs with similar repressed state chromatin that associate towards the periphery of the nucleus and interact with LADs (Paulsen et al. 2019). These cliques have their TAD composition change as adipose cells progress through differentiation. Here, an increased number of TADs join the "cliques", as cells further commit to

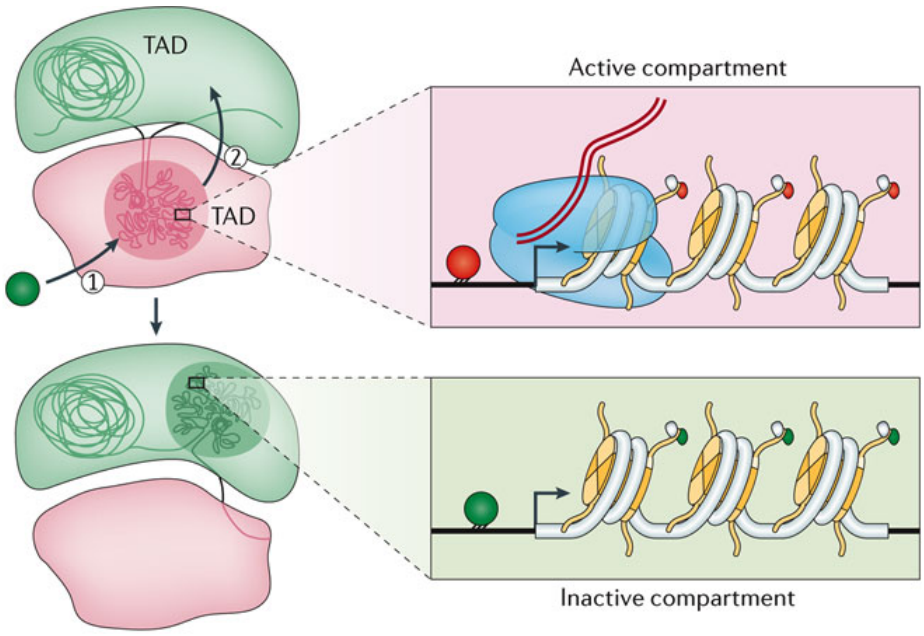

Figure 1.7: Dynamic events in the genome as a consequence of gene expression alteration. When particular genes are silenced they migrate from active into inactive compartments. Red circles represent gene activating factors, green circles represent gene repressive factors (adapted from Bonev and Cavalli 2016).

their fate. The reverse is also true, where the number of TADs in cliques and associated with LADs decreases when cells are reprogrammed into pluripotent states, as these require access to genes that would otherwise be silent (Stadhouders et al. 2018). This illustrates well the dynamics of genomes at a larger scale that is crucial for appropriate gene expression landscapes.

Despite the general rule of correlation between peripheral nuclear location and gene silencing, there are exceptions. This is the case with chromatin in close proximity to the nuclear pore complex. Here, despite the proximity to the nuclear lamina, heterochromatin exclusion zones can be found, these vary in size but have as a common feature their cone-like structure and the presence of euchromatin (Brown et al. 2008).

1.2.3 DNA damage and repair

The response to genotoxic stress is a process that elicits dynamic events in the nucleus. Dynamic changes in regions of damage can be attributed to the breaks in chromatin fibres and their impact in the physical properties of the polymer. Changes in dynamics can also be considered as the consequence of the response to said lesion by either the accumulation of repair proteins, which indirectly change the dynamics of chromatin, or even that the movement observed plays an active role in repair (Becker et al. 2014; Gandhi et al. 2012; Dion, Kalck, et al. 2012; Lottersberger et al. 2015; Zidovska, Weitz, and Mitchison 2013).

The two mechanisms used to repair double strand breaks (DSB) are non-homologous end joining (NHEJ) and homology-directed repair (HDR). The former relies on direct re-ligation of the two DNA ends, whereas the latter utilises the uncorrupted copy of the damaged DNA in its homologous chromosome to repair damage. HDR is a less error prone mechanism of repair than NHEJ, and is primarily prevalent in S-phase and G2, whereas NHEJ seems to be preferred in G1 (Lieber 2010). Whereas NHEJ can be performed in whatever location the break takes place, as long as the necessary machinery is present, HDR requires contact between the damaged DNA and its homologous counterpart. The necessity for two independent parts of the genome to co-localise means that one, or both of the copies must travel and scan, at least, a portion of the nuclear volume before finding the relevant partner (Dion and Gasser 2013). At this stage the chromatin structure and arrangement play important roles, as different levels of openness can hinder the progression of this scanning step (Agmon et al. 2013; Soutoglou et al. 2007).

DSB repair is regulated by the DNA damage checkpoint machinery, DNA repair factors, and some chromatin remodelers. Studies have shown that removal of these factors, be that through deletion or inhibition of some of their components, reduces the mobility and dynamics of chromatin. Conversely, their activation has the opposite effect (Seeber, Dion, and Gasser 2013; Miné-Hattab and Rothstein 2012; Dion, Kalck, et al.

2012; Burgess et al. 2014; Luijsterburg et al. 2012).

There have been studies that suggest that the relocation of DSB sites takes place not only due to the need to find the homologous pair to a damage site, but also to prevent aberrant recombination events (Tsouroula et al. 2016). Because heterochromatin is rich in repeating sequences, recombination between non-homologous chromosomes can take place, which has the potential to generate highly deleterious chromosomal aberrations. When DSBs are repaired through HDR, they are first excluded from the heterochromatic compartment, and repair only begins once DSB site sequestration has taken place (Tsouroula et al. 2016).

The involvement of actin and actin-associated proteins in DSB repair has long been described, with actin's failure to polymerise and crosslink, as well as inhibition of nuclear myosin I, leading to impaired HDR (Spichal et al. 2016; Evdokimova et al. 2018; Marnef et al. 2019). Indeed, recent evidence highlighted a direct role of nuclear F-actin in the transport of DSB sites, to which Arp2/3 is recruited to promote actin polymerisation and growth towards the nuclear periphery. Myosin is also recruited to the site to transport and anchor it to the nuclear pore or inner nuclear membrane proteins (Christopher P. Caridi et al. 2018). Despite its role in DNA repair, actin has also been associated with other nuclear functions such as *loci* translocation for regulatory purposes (Dundr et al. 2007; Chuang et al. 2006).

In yeast, there is a clear dynamic response of chromatin to genotoxic stress at the whole nucleus level, however, there is still debate whether the same takes place in mammalian cells (Miné-Hattab and Rothstein 2012). Some studies in mammalian cells suggest that there is no, or negligible changes in chromatin dynamics after DSB induction (Bonin et al. 2018; Whitefield et al. 2018), whereas others reported an increase in dynamics at the global level under these conditions (Lottersberger et al. 2015; Zidovska, Weitz, and Mitchison 2013). It is likely that changes are dependent on cell type and the nature of the DNA damage. Nevertheless, studies that set out to explore mechanisms through which dynamic

changes take place in the presence of DNA damage, have described the involvement of INO80 (inositol requiring 80) chromatin remodeling complex which promotes degradation of histones and consequent chromatin decompaction when DSBs are induced, which leads to changes in chromatin characteristics and, consequently, its dynamic behaviour (Hauer et al. 2017; Seeber, Dion, and Gasser 2013; Neumann et al. 2012). Besides INO80, other families of chromatin remodelers have also been shown to play a role in altering chromatin in the context of DNA damage repair, for example SWI/SNF (switching defective/sucrose nonfermenting), CHD (chromodomain, helicase, DNA binding) and ISWI (imitation switch). These remodelers are key in the removal of nucleosomes from the damage site, be that through nucleosome sliding or ejection, to allow the access of repair machinery, facilitating nucleotide excision repair (Chai et al. 2005; Aaron A Goodarzi, Kurka, and Jeggo 2011; Stanley, Moore, and Aaron A. Goodarzi 2013).

There are also studies that suggest that chromatin movement observed in the context of damage repair may have a component that derives from forces that are relayed from microtubules. Here, the treatment of cells with compounds that prevent polymerisation or favour catastrophe, like nocodazole, decrease chromatin mobility, even during interphase (Lottersberger et al. 2015). The same was true upon removal of dynein and the linker of nucleoskeleton and cytoskeleton (LINC) complex, suggesting that this effect takes place through forces applied onto the nucleus itself or relayed through the complexes that link the cytoskeleton and nucleoskeleton. These findings are not just relevant in the context of DNA damage repair but apply to general chromatin mobility as well (Bronshtein et al. 2015).

1.3 Methods of higher order chromatin analysis

1.3.1 Exploring chromatin architecture

The complexity of the genomic structures that allow for efficient packaging of DNA and regulation of all aspects of its function have been slowly but steadily discovered throughout the past few decades. The discovery of the ever-increasing complexity of nuclear architecture has been possible due to three different types of method that have been improving at a rapid pace, these are: imaging-based, ligation-based, and non-ligation based 3D genome mapping methods.

Imaging-based techniques

Even though this type of method employs techniques that span both light and electron microscopy, the most commonly applied technique is DNA-fluorescence *in situ* hybridisation (DNA-FISH). This technique relies on the hybridisation of fluorescently-tagged probes to their complementary target genes. DNA-FISH techniques are used to label and determine the position and distances between particular *loci* of interest (Maass et al. 2018; Finn et al. 2019). These techniques are limited by both the diffraction limit of light microscopy, and the limits in base pair resolution dictated by the size of the probes themselves (Miguel R Branco and Pombo 2006; Nora et al. 2012). The latter limitation is often a trade off between resolution and signal intensity, as probes that cover a longer genomic length allow for a stronger signal but with lower resolution.

Different modalities of FISH looked to tackle some of these problems, for instance, cryo-FISH, which relies on freezing and slicing of nuclei into 100-200 *nm*-thick sections prior to probe hybridisation allowing for greater hybridisation efficiency and higher resolution labelling of genomic *loci* (Miguel R Branco and Pombo 2006; Ferrai et al. 2010; Simonis et al. 2006; Barbieri et al. 2017). Furthermore, developments on probe technology itself has allowed to increase the resolution of standard FISH

from approximately 100 Kb to 15 Kb and smaller (Beliveau, Joyce, et al. 2012). These advances in probe technology have also led to the creation of multiplexed super-resolution fluorescence *in situ* hybridization, which has been instrumental in mapping chromatin domain structure and location. It relies on sequential hybridisation of 30 Kb stretches of DNA with probes that contain a 20 nucleotide readout sequence that is specific to each of them, and to which a dye-labelled complementary probe binds. After imaging the *loci* to which each specific probe binds, the signal is extinguished by removal of the dye or by photobleacing, and another round of hybridisation and labelling takes place. Once the process is complete for the thousands of *loci*, the images are used to generate a three dimensional map of the hybridised chromatin in 30 Kb segments which can be individually identified (Beliveau, Joyce, et al. 2012; Beliveau, Boettiger, et al. 2015; Bintu et al. 2018).

Despite their undeniable contribution in providing structural information, DNA-FISH-derived techniques rely on permeabilisation and fixation of cells so probes can enter nuclei, and for the target DNA to melt. Therefore, they do not allow for the observation and imaging of living cells.

Ligation-based techniques

Ligation-based methods (figure 1.8) derive from the chromosome conformation capture (3C) assay developed by Dekker *et al.* in 2002 (Job Dekker et al. 2002). These rely on chromosome crosslinking, genome shearing, and proximity ligation to generate a snapshot of the conformation of nuclei at a particular point in time. From here, a 3C library of the nucleus can be generated by purifying the ligation products. From this library it is possible to quantify, through PCR, the proximity of two *loci* of interest, averaged across the cell population.

Whereas 3C allows the establishment of a proximity relationship between two known *loci*, 4C and 5C (methods derived from 3C) allow for more complex relationships to be established. The former is capable of

establishing a relationship between a *locus* of interest and the rest of the genome, and the latter is used to explore the contacts between several *loci* against each other (Van De Werken et al. 2012; Nora et al. 2012; Kundu et al. 2017; Loviglio et al. 2017). But perhaps the most commonly used derivative of 3C is High throughput chromosome conformation capture (Hi-C), which allows for the exploration of genome-wide interactions (Lieberman-Aiden et al. 2009). This method relies on biotin-streptavidin interactions to purify the 3C library in order to reduce background before sequencing. Genome conformation capture, a parallel technique to Hi-C, avoids this step by sequencing the entire library, something that is becoming increasingly cheaper and easier, with the added benefit of controlling for biases that could otherwise be introduced by purification steps (Rodley et al. 2009). Even though these techniques are dependent on cell fixation and population averages, the development of single cell Hi-C techniques has taken place, albeit at lower resolutions. These rely on crosslinking and *in situ* proximity ligation followed by nuclear isolation, and the ultimate generation of libraries from individual nuclei (Nagano, Lubling, Yaffe, et al. 2015; Nagano, Lubling, Várnai, et al. 2017).

The methods described above provide useful information on DNA-DNA interactions, however, they do not discriminate how these interactions take place. By allying 3C methods with chromatin immunoprecipitation (ChIP) it is possible to assess the proteins that mediate the observed interactions. This takes place by either sonicating and immunoprecipitating crosslinked chromatin before ligation, as it is the the case with chromatin interaction analysis by paired-end tag sequencing (ChIA-PET; Fullwood et al. 2009), or by performing the pull-down step after proximity ligation and DNA shearing take place, for example Hi-ChIP and proximity ligation-assisted chromatin immunoprecipitation sequencing (PLAC-seq; Mumbach et al. 2016).

An advantage of sequencing based methods is that their resolution is not dependent on light diffraction or fluorescent signal intensity as is the

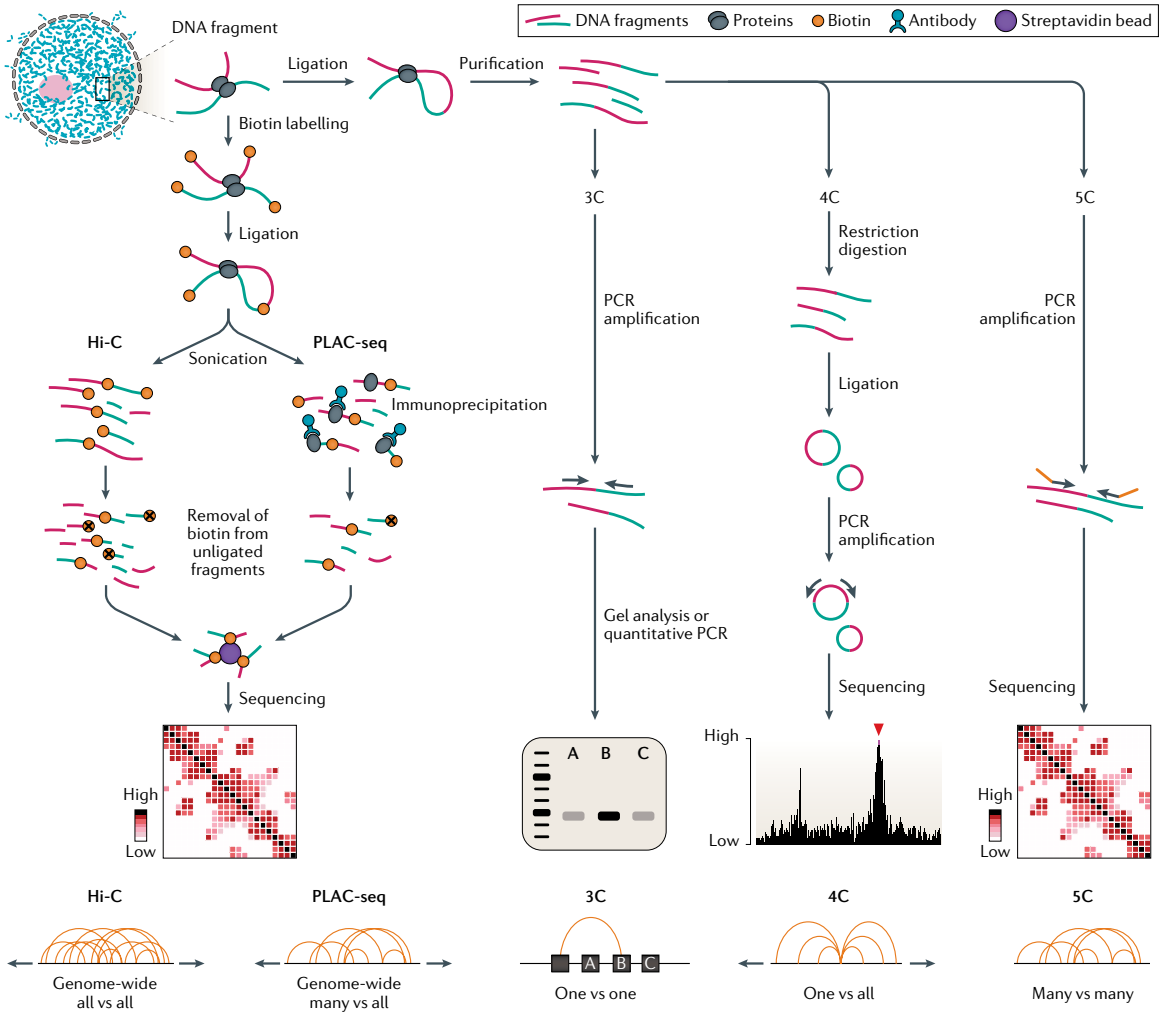

Figure 1.8: Ligation-based techniques for genome architecture investigation derived from the 3C method. Ligation based methods measure contact frequencies of *loci* pairs and rely on crosslinking, shearing and ligation of DNA. In 3C-derived methods, information can be extracted on the contact frequency between two *loci* (3C), one *locus* and the reminder of the genome (4C), or between many different parts of the genome (5C). In Hi-C and PLAC-seq ligation products are tagged with biotin for enrichment, and in PLAC-seq the DNA bound to the protein of interest is immunoprecipitated. These two methods allow the extraction of information about genome-wide interactions and protein-DNA interactions (Kempfer and Pombo 2020).

case with FISH and other microscopy-related methods. They are dependent however, on sequencing depth, which must be optimised for the type of interaction of interest, since the resolution necessary to study TADs and compartments is less than that needed to study smaller structures (Rao, Huntley, et al. 2014).

Ligation-free techniques

Methods that rely on ligation between DNA fragments to discern their interaction partners inevitably lead to the identification of fewer interactions than those that take place in reality. This is because these methods are intrinsically two dimensional; neighbouring fragments can only be ligated upstream or downstream of the original sequence, therefore if more than 2 or 3 DNA segments were in contact, only a proportion of those interactions would be identified. To attempt the elimination of this bias, ligation-free methods have been recently developed (figure 1.9).

The general approach to eliminating the ligation step in 3D mapping methods is to attribute the same "barcode" to the genomic fragments that interact together. Genome architecture mapping (GAM) is a method that relies on cryosectioning ultra-thin ($\sim 200\ nm$) slices of a frozen population of sucrose-embedded cells (figure 1.9). Following this, slices of individual nuclei are isolated, PCR amplified, and barcoded. The process is repeated for hundreds of nuclei slices, each slice with its own barcode, before DNA is pooled and sequenced. *Loci* that localise closer in space are more likely to have been extracted in the same slice, and therefore present the same barcode, whereas distant *loci* will seldom belong to the same slice and therefore will not display the same barcode. The process is repeated for hundreds of nuclear slices, and the data from the cell population is pooled. Through the application of statistical models it is possible to infer whether two or more *loci* co-localise within a specific radius, depending on the frequency with which they localise in the same slice. The resolution of this method is entirely dependent on the number of nuclear slices produced; 400 slices sequenced with a depth of 1 million

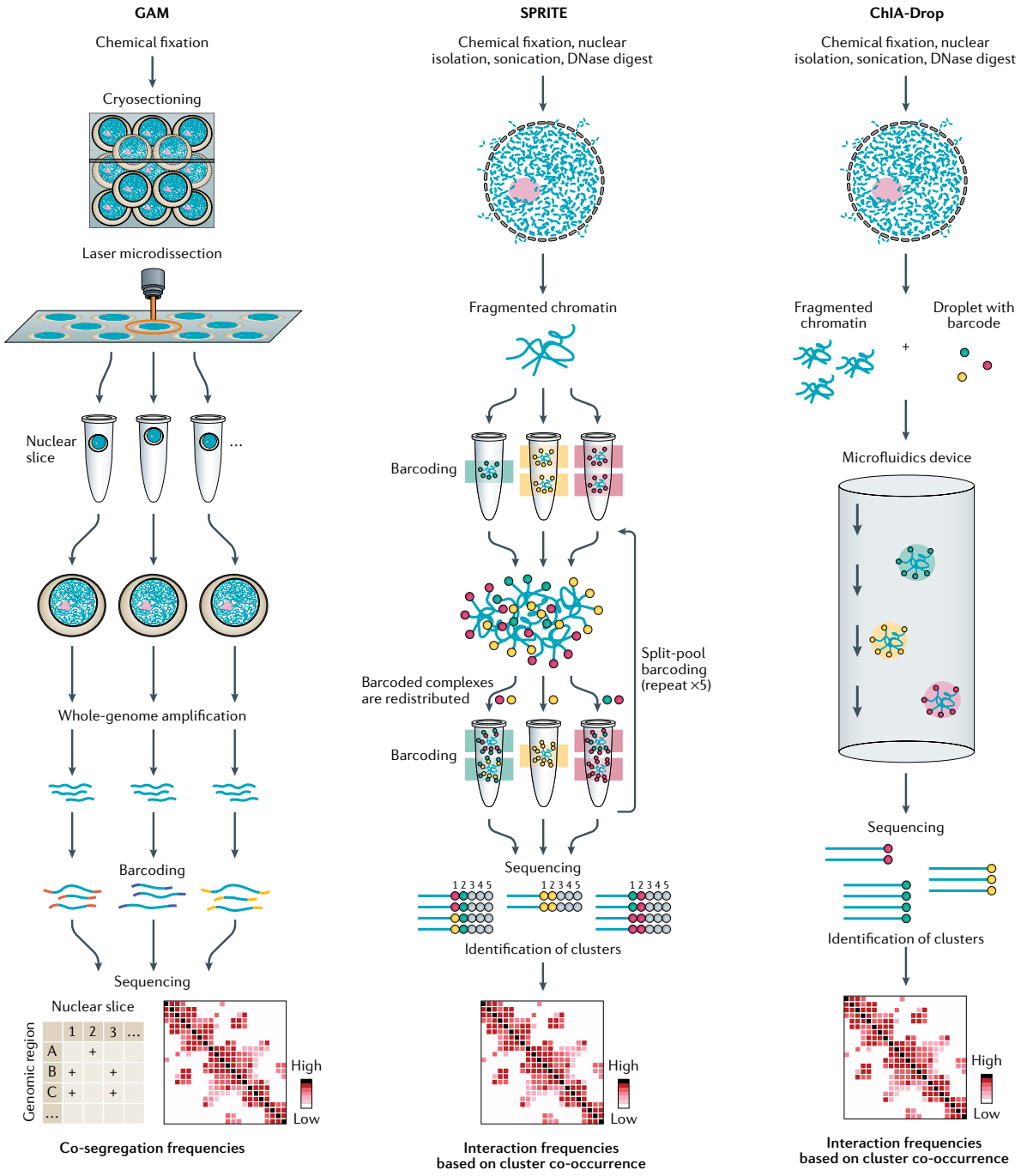

Figure 1.9: Ligation-free techniques for genome architecture investigation through crosslinking and barcoding of DNA fragments. Fragments in spatial proximity will display identical barcodes. In GAM, the nucleus is divided into slices, and fragments in the same slice will display an identical barcode. In SPRITE and ChIA-drop, DNA is sheared to separate DNA clusters. In the former, barcoding is done sequentially after several rounds of cluster separation, barcoding and pooling. In the latter, barcoding is done through microfluidic separation and barcoding of chromatin clusters (Kempfer and Pombo 2020).

reads yields a resolution equivalent to that of Hi-C (30 kB), however, a greater number of slices must be produced for greater resolution to be achieved (Beagrie et al. 2017).

Two other methods that rely on barcoding for interaction identification are SPRITE and ChIA-Drop (figure 1.9). Unlike GAM, both these methods apply a crosslinking step before chromatin shearing and barcoding. In the case of the former, the resulting sheared chromatin is separated across a 96-well plate and barcoded, these are then pooled and the process is repeated several times before sequencing takes place. Chromatin fragments belonging to the same complex will present the same barcode, as they were present in the same wells at each barcoding step (Quinodoz et al. 2018). The latter performs its barcoding step through the employment of microfluidics, where individual chromatin complexes are enclosed within droplets containing barcoding reagent before sequencing takes place. Sequences that present the same barcode are those that were cross linked together, and remained associated in the same droplet during the barcoding process (Zheng et al. 2019). Both these methods allow for all fragments within a complex to be identified, rather than only those that have been ligated together. These three methods have been employed to study super enhancer, TAD long-range interactions, and interactions involving more than three *loci* (Beagrie et al. 2017). Indeed, SPRITE has been able to detect interactions between *loci* belonging to different chromosomes that interact with other nuclear structures such as nucleoli and splicing speckles (Pombo and Miguel R. Branco 2007).

Furthermore, some ligation-free methods that are able to determine DNA-Protein interactions have been developed. These are DamID and TSA-seq. The former uses DNA adenine methyltransferase (Dam) fused to the DNA-binding domain of the protein of interest. When the DNA-binding domain interacts with its target sequence, Dam methylates the adenines included in a GATC sequence in its vicinity. The whole genome is then digested with a methylation-sensitive restriction enzyme and adapters are added to the methylated fragments so these can be se-

lected for sequencing. This method has been successful at mapping LADs through the identification of the interactions between DNA and Lamin B1, for example (Peric-Hupkes et al. 2010; Guelen et al. 2008). TSA-seq employs a slightly different approach in that an antibody against the protein of interest is fused to horseradish peroxidase. Horseradish peroxidase produces biotin-conjugated tyramide free radicals which bind to macromolecules in the vicinity. DNA that has been biotin-tagged can then be isolated and sequenced to reveal the *loci* that were located in close proximity to the protein of interest. This method has been especially useful in mapping the spatial relationship between genes and splicing machinery (Chen et al. 2018).

1.3.2 Exploring chromatin dynamics

Despite the advances made in the field of nuclear architecture, it remains challenging to infer how these structures change over time. In many cases, the methods that so expertly allow for detailed exploration of genome structure, are not ideal to explore their temporal dimension, in large due to the need for fixation. However, some methods have made it possible to explore the way in which chromatin landscapes change over time, which is crucial to determine its role.

Single *locus* to few *loci* imaging

Together with improving microscopy methods that present higher sensitivity and resolution, a number of methods have been developed that allow for labelling of single genomic *loci*. One of the first methods to be used was the fluorophore-tagged lac repressor/operator array system (figure 1.10 A). Here, fluorophore-tagged lac repressors bind to an array of lac operators that have been introduced to the target *locus*, which can be visualised and tracked (Robinett et al. 1996; Marshall et al. 1997). Through the introduction of an identical system that relies on the tet operator system, it was possible to label different *loci* in the same nucleus, increasing the complexity of possible studies in living cells (Michaelis,

Ciosk, and Nasmyth 1997). A downside of these techniques, beyond the limited number of *loci* that can be labelled, is that they rely on the introduction of an approximately 10Kb operator array into the target *locus*. This both limits the technique to cells whose genomic manipulation is easily achieved, and its resolution.

Fluorescently tagged zinc finger proteins (ZF) and transcription activator-like effectors (TALEs) have also been employed to label individual *loci* (figure 1.10 B). These have the added benefit of not being necessary to alter the target *locus*, as they can be engineered to bind to specific DNA sequences. On the other hand, the fact that they must be specifically designed for a particular sequence also means that they lack versatility. Furthermore, to maximise the signal, ZFs and TALEs are routinely used only in repetitive sequences, not unlike the systems described above (Seeber, Hauer, and Gasser 2018).

In an effort to reduce the limitation of only being able to label repetitive sequences, be those endogenous or inserted, the ANCHOR3/ParB DNA system was developed (figure 1.10 A). This relies on the introduction of an ANCH unit sequence into the *locus* of interest, where a dimer of fluorophore-labelled ParB protein binds. Following this, additional ParB proteins are recruited to the site and bind to the adjacent DNA along the strand, spanning approximately 1Kb, enough to enable visualisation of the *locus*. It is true that ANCHOR/ParB has the advantage of being employable in non-repetitive sequences of the genome, however, it still requires targeted insertion of DNA elements onto the target *locus*, albeit of much smaller Kb lengths than what was previously necessary (Saad et al. 2014; Germier et al. 2017).

More recently, with the discovery and development of CRISPR/Cas9 technologies (figure 1.10 C), some of these challenges were effectively tackled. Methods derived from this technology rely on editable sgRNAs that lead a catalytically inactive Cas9 protein towards the *locus* of interest (Jinek et al. 2012). This eliminated the need for the engineering of specific proteins, like ZFs and TALEs to target specific *loci*, as well as

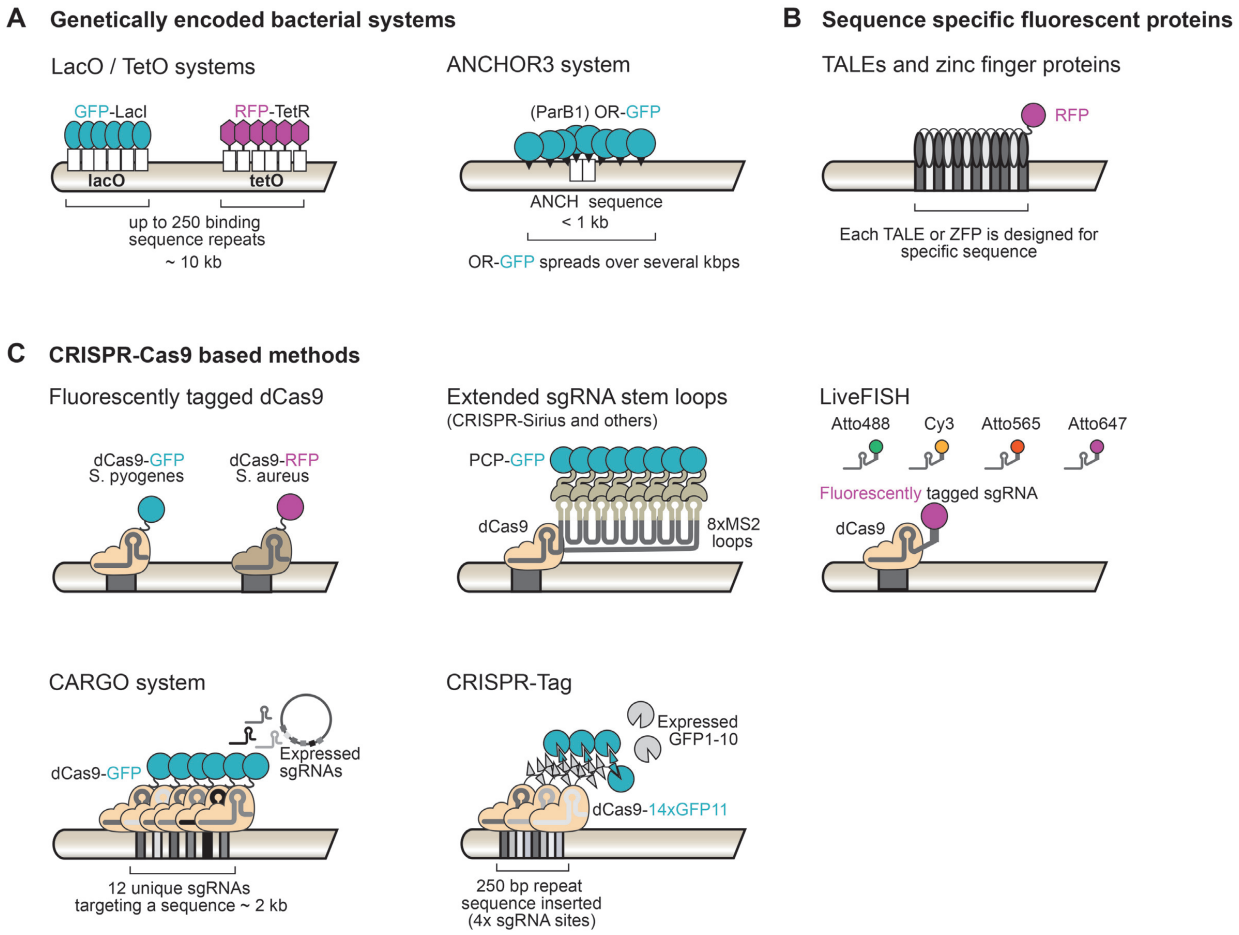

Figure 1.10: Methods for single *locus* dynamics investigation. **A** Genetically encoded bacterial systems make use of DNA sequences inserted into the *loci* of interest onto which fluorescent tags bind. **B** Sequence specific fluorescent proteins are DNA binding proteins designed to bind to a specific endogenous sequence. **C** CRISPR-Cas9 based methods make use of the sgRNA directed binding of a catalytically inactive Cas9 nuclease to report on *loci* location. Tagging can be achieved though the modification of Cas9 or the sgRNA (adapted from Shaban and Seeber 2020).

removing the need for inserting exogenous DNA sequences in regions of interest. CRISPR/Cas9 methods of *loci* labelling fall broadly into two categories: the ones where Cas9 is engineered to generate a signal, and those where engineering takes place on the sgRNA.

The simplest approach in the engineered Cas9 category is the fusion of a fluorescent tag to the Cas9 protein, however, one fluorescent molecule cannot produce a signal strong enough for visualisation. Therefore, it is necessary to recruit more fluorescent proteins to the *locus*. This can be achieved by expressing several different sgRNAs that target Cas9 proteins to the same *locus* in a non-competitive manner. An example of this approach is the Chimeric array of sgRNA oligonucleotides (CARGO) system (Gu et al. 2018). CRISPR-Tag operates slightly differently, where the signal is amplified through the tagging of Cas9 with a tail-like array of GFP11/GFP10 fluorescent proteins. This tagging system is composed of tethered GFP10, which is a fragment of GFP, where GFP11 (the remaining fragment) binds to yield a functional fluorescent protein. However, this method relies on the insertion of a 250bp sequence in the *locus* of interest where several tagged Cas9 bind (Chen et al. 2018; Kamiyama et al. 2016). Another method that relies on a principle similar to that of CRISPR-Tag is SunTag. SunTag is a scaffold that can be fused to a protein of interest that contains 10-24 copies of the GCNA epitope, which binds EGFP-scFV antibody fusion protein. By using SunTag fused to Cas9 (with the appropriate gRNAs) and expressing EGFP-scFV, it is possible to label specific *loci* across the genome (Tanenbaum et al. 2014).

Methods that explore the sgRNA for signal generation can operate quite differently, LiveFISH consists on the addition of a Cy3-labelled (fluorescent) sgRNA to cells expressing Cas9; because the signal of these molecules is stronger than that of EGFP, single molecule observations are possible (H. Wang et al. 2019). Operating in a very different manner is CRISPR-Sirius, here the sgRNA is engineered to display RNA stem-loop structures that recruit RNA-binding proteins even when bound to the Cas9 protein. These RNA-binding proteins are fluorescently labelled,

therefore, when the Cas9 protein binds to a *locus*, the amplified signal can be visualised (S. Wang et al. 2016; Ma, Tu, Naseri, Chung, et al. 2018; Fu et al. 2016; Ma, Tu, Naseri, Huisman, et al. 2016).

The methods used to track a single or a few *foci* outlined above have been crucial in the discovery of important biological processes, for example, through the application of LacO arrays, it was possible to observe the nuclear location and timing of gene expression *in vivo* (Tsukamoto et al. 2000) and the more modern CRISPR/Cas9 systems have been employed to study the dynamics of chromatin during DNA repair (H. Wang et al. 2019).

Whole chromatin dynamics

Beyond the methods that give insight into the movement of particular *loci*, there are those that allow for the exploration of the dynamics of chromatin as a whole. Singe particle tracking photoactivated localization microscopy (sptPALM) is one of these methods that uses photoactivatable fluorophores that can be fused to DNA-associated proteins *e.g.* histones (figure 1.11 A). Through several iterations of activation and tracking, followed by bleaching, this method can be used to infer the direction and speed in which a particular fluorophore is moving. By applying this to a high number of labelled DNA-associated proteins, is it possible to extract the dynamic characteristics of the global chromatin. This is a powerful method that allows for single nucleosome tracking, however, each particular fluorophore only remains active during timescales of seconds, therefore, dynamic events that occur in timescales of greater lengths cannot be observed (Manley et al. 2008; Shinkai et al. 2016; Holcman, Hoze, and Schuss 2015).

A different strategy used for bulk and global chromatin dynamics exploration relies on the labelling of bulk chromatin. In some of these techniques, this step can be achieved by using intercalating agents like Hoechst or even nucleotide analogs. After bulk labelling, cells are imaged through a time span of tens of seconds and maps of the global

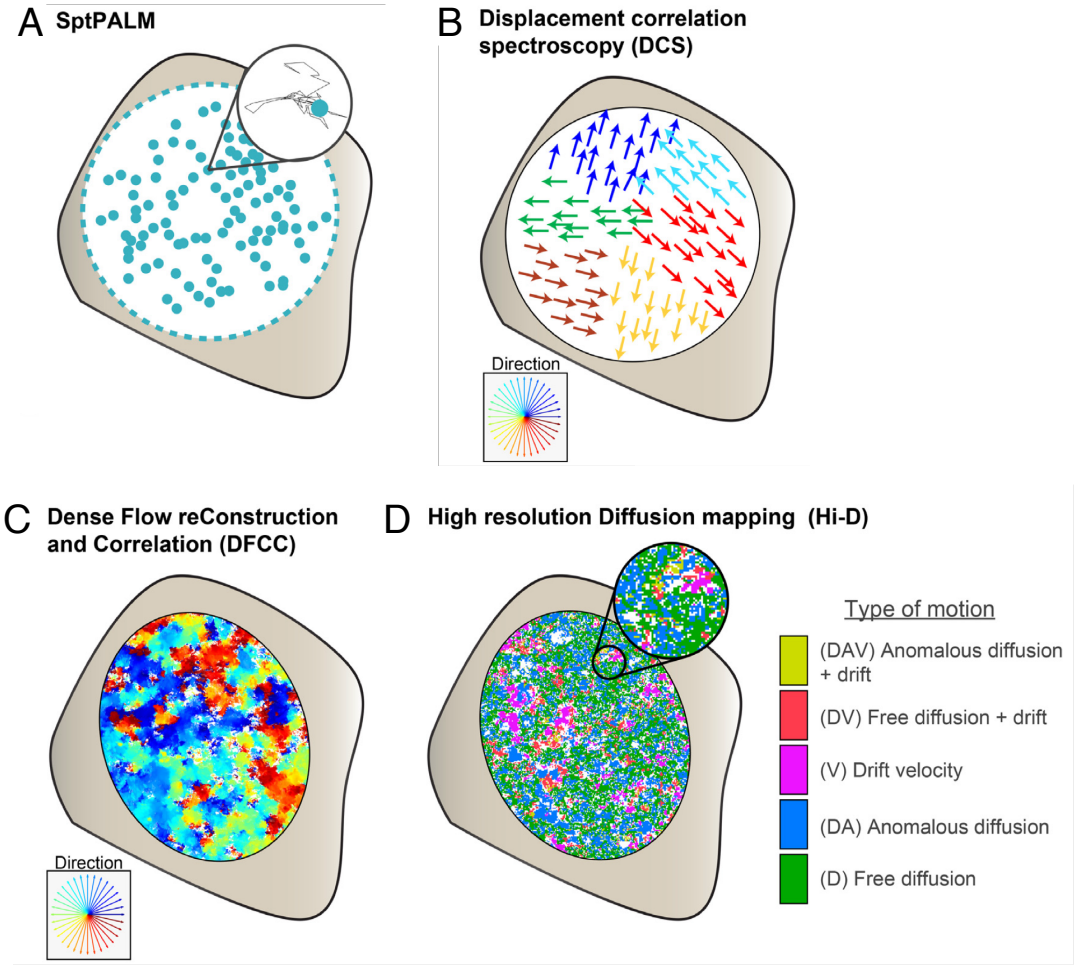

Figure 1.11: Methods for general chromatin dynamics analysis. **A** spt-PALM in association with single particle tracking for whole chromatin dynamics investigation. **B** Displacement correlation spectroscopy (DCS) for generation of global direction and magnitude of movement maps. **C** Dense Flow reconstruction and Correlation (DFCC) for generation of direction and magnitude maps with greater resolution than DCS. **D** High resolution diffusion mapping for determination of chromatin physical parameters in specific nuclear regions (adapted from Shaban and Seeber 2020).

direction and magnitude of chromatin movement are generated. In the case of displacement correlation spectroscopy (DCS), these are created through the employment of particle image velocimetry algorithms and auto-correlation functions over particular time-lags (Zidovska, Weitz, and Mitchison 2013; figure 1.11 B). With the objective of increasing the resolution of DCS dynamics maps, Dense Flow reconstruction and Correlation (DFCC) employs optical flow to capture the movement of chromatin and calculate the direction and magnitude of its movement (figure 1.11 C). By computing the correlation between flow fields DFCC is capable of yielding maps with *nm* resolution (Shaban, Barth, and Bystricky 2018).

In order to be able to not only analyse the global and bulk movements of chromatin but also calculate physical parameters like mean squared displacement (MSD), DFCC was further optimised into High resolution Diffusion mapping (Hi-D; figure 1.11 D). This technique estimates the trajectory of each pixel in the nucleus, allowing for the calculation of the MSD of chromatin in all regions of the nucleus simultaneously, and the generation of maps of the dynamic landscape (Shaban and Seeber 2020). As above, these techniques are employed over time-spans of tens of seconds which prevents the capture of dynamic events that span greater intervals. The computational power necessary to employ them is also highly intensive.

Because these methods allow for the analysis of chromatin movements as a whole, DCS, for example, has allowed for the discovery of coherent chromatin movement regions. These are parts of the nucleus, in the 4-5 μm scale, whose chromatin moves in the same direction in an ATP-dependent manner (Zidovska, Weitz, and Mitchison 2013).

1.4 Scope of the thesis

Much has been discovered regarding the structure and dynamics of chromatin. Advancements in techniques that allow further scrutiny of the nuclear environment push our knowledge in this field still further.

However, challenges remain, especially when studying the dynamics of chromatin structures, particularly at the Mb length scales (the scale of TADs). The work outlined in this thesis describes my contributions towards closing the gap on what is known about chromatin dynamics at these particular scales.

I hypothesised that late replicating TADs presented, in general, relatively low dynamism within the nuclear space, and that, for the most part, their position did not change significantly within time scales of tens of minutes. I further hypothesised that a small minority of TADs would not follow the same dynamic patterns of the majority of the population and present a more dynamic behaviour; and that through the introduction of perturbations to cell homeostasis (*e.g.* DNA damage), the number of these dynamic domains could be altered, linking highly dynamic behaviour of chromatin structures of this scale to important cellular events such as maintenance of genome integrity.

I explored these hypotheses through the employment of RAPID-release (a recently developed pulse-labelling technique), where I labelled TADs through their histone component. This allowed for the investigation of their behaviour in living cells, and in real time, across different timescales. Using state-of-the-art high resolution live-cell imaging approaches, the description of TADs position through time provided data for mathematical analysis of their dynamics. Parameters such as velocity, displacement, and spatial distribution were extracted. Additionally, due to the labelling stability granted by RAPID-release, it was possible to image cells for as long as 1-3h, and, because of the employment of lattice light sheet microscopy, it was also possible to image them as frequently as every second, albeit not in the same experiment. Here I also describe how the parameters extracted on the dynamics of TADs were altered in the presence of perturbations to cell homeostasis, in particular post-DNA damage induction. The evidence collected pointed towards the existence of a large population of chromatin domains that had relatively low mobility, along with a smaller population of chromatin domains that

displayed greater displacement and were, therefore, more dynamic, as hypothesised. Furthermore, I observed that the relative abundance of each of these types of chromatin domain was affected by the introduction of DNA damage, where its presence led to an increase in the number of more dynamic domains.

In this thesis I also describe how RAPID-release was altered and adapted in order to improve some of its features, such as consistency of kinetics between cells, and usability. This was done to facilitate its employment in other areas of research and to make it as versatile as possible. Ground work was also laid for the creation of an orthologous system to RAPID-release, relying on alternative components, to allow the generation of two different pulses within the same cell; a feature that could be advantageous in monitoring multiple structures or pulse-labelling at differing time points.

Ultimately, the work presented here has contributed towards understanding chromatin dynamics and stability, which are crucial aspects in cell function. Informing on how genetic material organises and moves within the nucleus can help understand disorders connected with aberrant gene expression, linked with inappropriate nuclear architecture and dynamics.

Chapter 2

Materials and Methods

2.1 Molecular biology

Nomenclature and ID references of plasmids and primers is written in accordance to that used in the Bowman laboratory database for molecular biology.

2.1.1 RAP-IRR

The first step in RAP-IRR assembly was the creation of the vector pmCherry-IRES-EGFP-Puro (Cl 1121) by digestion of pmCherry-C1 (Cl 0396) and IRES-EGFP-Puro (Cl 0970) with the enzymes XhoI and MfeI. This was a transfer of the IRES-EGFP-Puro cassette into the vector pmCherry-C1. pmCherry-IRES-EGFP-Puro was then subjected to an inverse PCR using the primers P1278 and P1279 to yield pmCherry-IRES-EGFP (Cl 1122). pmCherry-IRES-EGFP was digested using XhoI and SmaI and Gibson assembled with gBLOCK® (IDT) P1282 to form pmCherry-NES-FKBP-TVMV-AI-IRES-EGFP (Cl 1123). This vector was subsequently digested with Esp3I and HpaII and Gibson assembled with gBLOCK® P1283 to yield pmCherry-NES-FKBP-TVMV-AI-IRES-EGFP-TVMVx2-FRB-NES-OMP25 (Cl 1124, figure 2.1).

To generate vector pEGFP-TVMVx2-FRB-NES-OMP25-IRES-mCherry-NES-FKBP-TVMV-AI (Cl 1162, figure 2.2), Cl 1124 was digested with AgeI and SpeI to generate the cassette mCherry-NES-FKBP-TVMV-

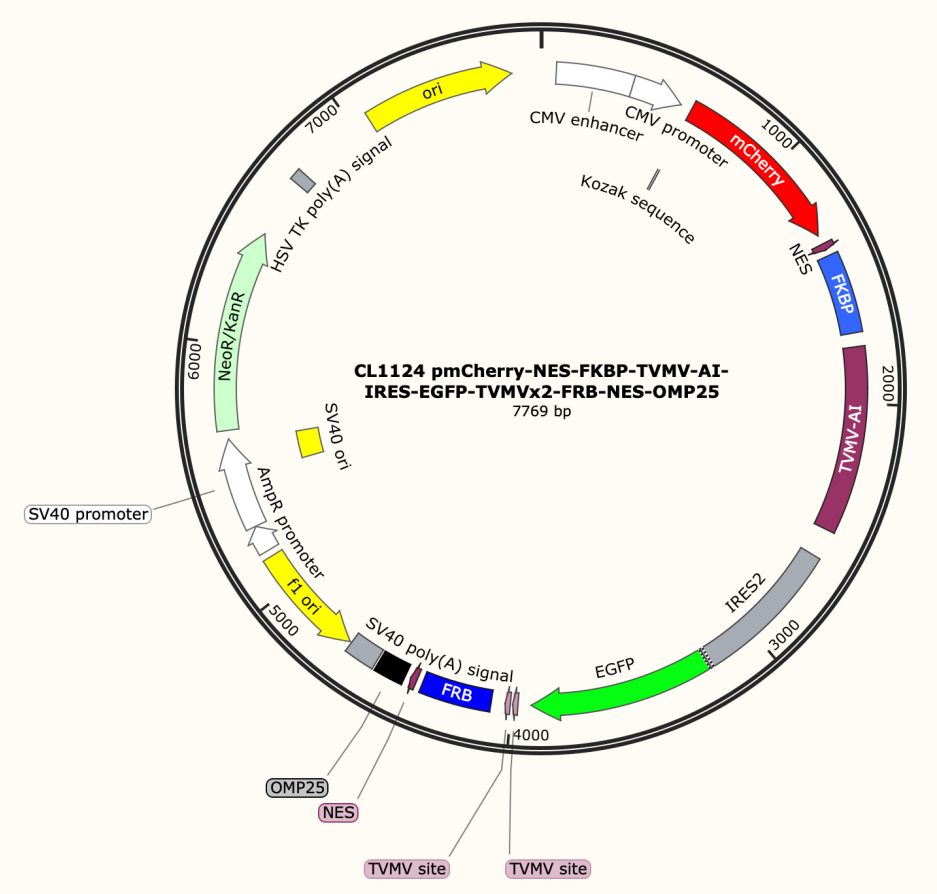

Figure 2.1: Map of plasmid CL1124, pmCherry-NES-FKBP-TVMV-AI-IRES-EGFP-TVMVx2-FRB-NES-OMP25.

AI. This cassette was subjected to PCR using the primers P1366 and P1367 to generate compatibility with the first portion of IRR. Cl 1124 was also digested with EcoRV and BstxI to generate the cassette EGFP-TVMVx2-FRB-NES-OMP25. This cassette was subjected to PCR using the primers P1368 and P1369 to generate compatibility with the second portion of IRR. Finally, Cl 1124 and the amplified mCherry-NES-FKBP-TVMV-AI cassette were digested with EcoRV and BstxI and ligated together. The resulting vector was digested with AgeI and SpeI, together with the amplified EGFP-TVMVx2-FRB-NES-OMP25 cassette and ligated.

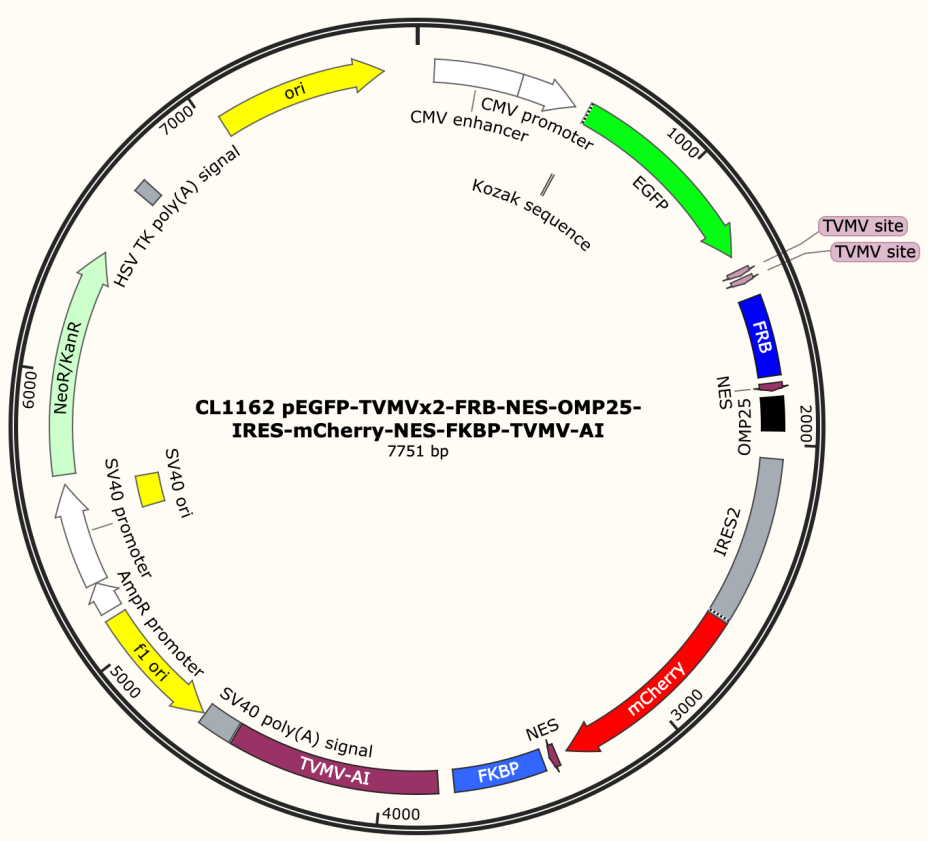

Figure 2.2: Map of plasmid CL1162, pEGFP-TVMVx2-FRB-NES-OMP25-IRES-mCherry-NES-FKBP-TVMV-AI.

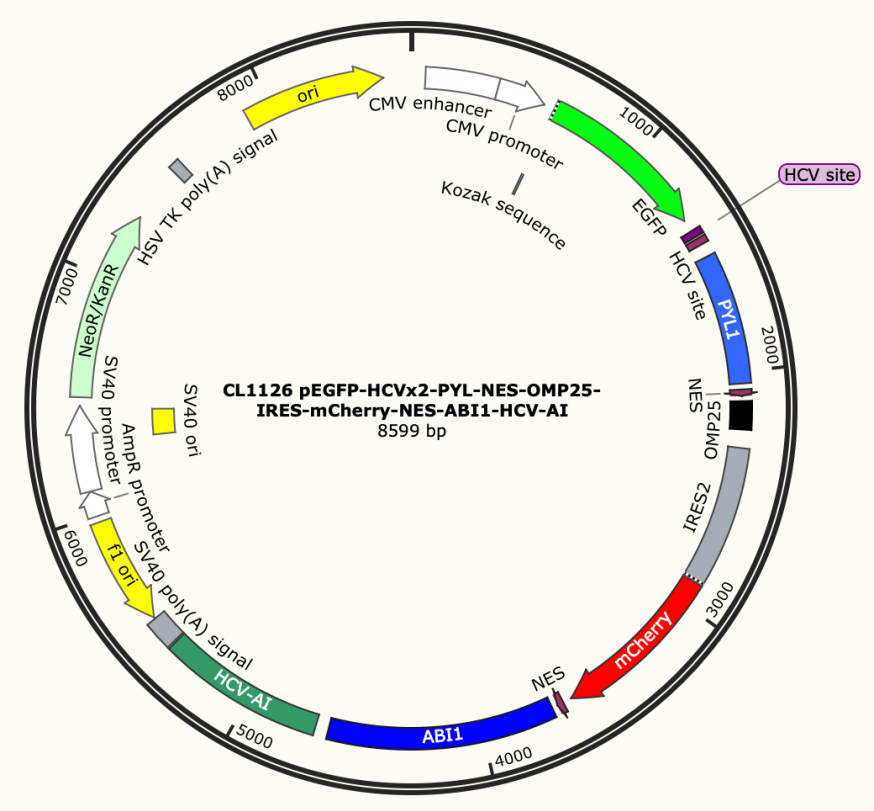

Figure 2.3: Map of plasmid CL1126, pEGFP-HCVx2-PYL1-NES-OMP25-IRES-mCherry-NES-ABI1-HCV-AI.

2.1.2 ABA-IRR

ABA-IRR was produced by the replacement of the TVMVx2-FRB-NES cassette by HCVx2-PYL1-NES through Gibson assembly of BglII and BamHI digested Cl 1162 and gBLOCK® P1285. Followed by the replacement of the FKBP-TVMV-AI cassette by ABI1-HCV-AI through ligation of EcoRI and EcoRV digested PCR products of gBLOCK® P1284 amplified with primers P1392 and P1393. This yielded plasmid pEGFP-HCVx2-PYL1-NES-OMP25-IRES-mCherry-NES-ABI1-HCV-AI (CL1126, figure 2.3).

2.1.3 AUX-IRR

AUX-IRR was produced by the replacement of the TVMVx2-NES-FRB cassette by TEVx2-NES-TIR1 through Gibson assembly of BglII and BamHI digested Cl 1162 and gBLOCK® P1287. Followed by the re-

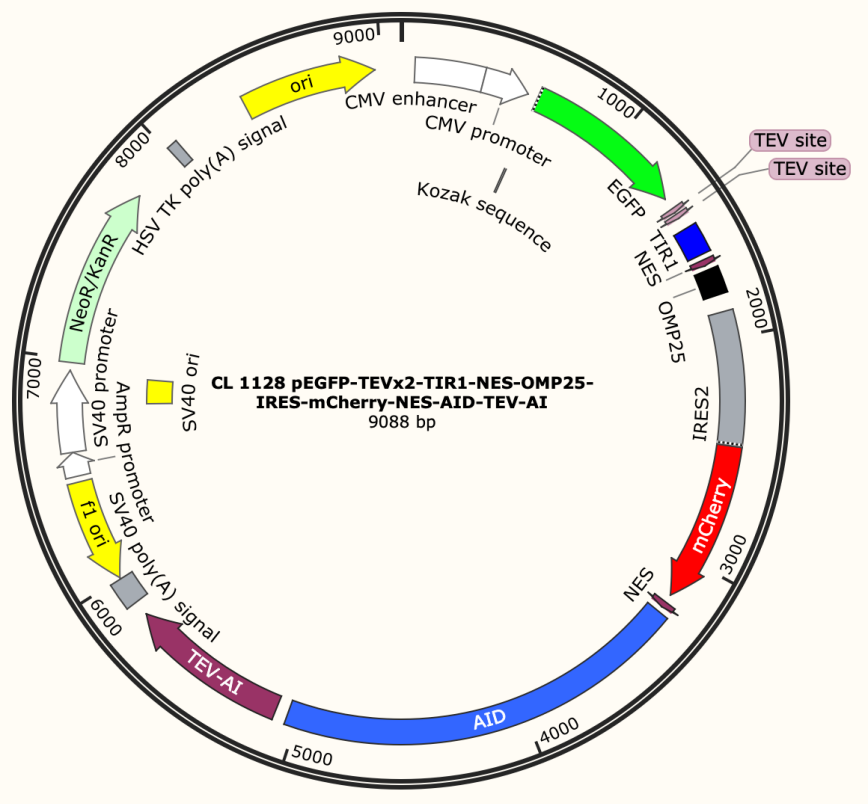

Figure 2.4: Map of plasmid CL1128, pEGFP-TEVx2-TIR1-NES-OMP25-IRES-mCherry-NES-AID-TEV-AI.

placement of the FKBP-TVMV-AI cassette by AID-TEV-AI through ligation of EcoRI and EcoRV digested PCR products of gBLOCK® P1286 amplified with primers P1392 and P1394. This yielded plasmid pEGFP-TEVx2-TIR1-NES-OMP25-IRES-mCherry-NES-AID-TEV-AI (CL1128, figure 2.4).

2.1.4 HALO-IRR

HALO-IRR (Cl 1246, figure 2.5) was assembled by digesting Cl 1162 with AgeI and BglI and subjecting the open vector to Gibson assembly with the PCR products of pHAT1-StrepII-HALO-HDR-donor (Cl1238) with the primers P1379 and P1380.

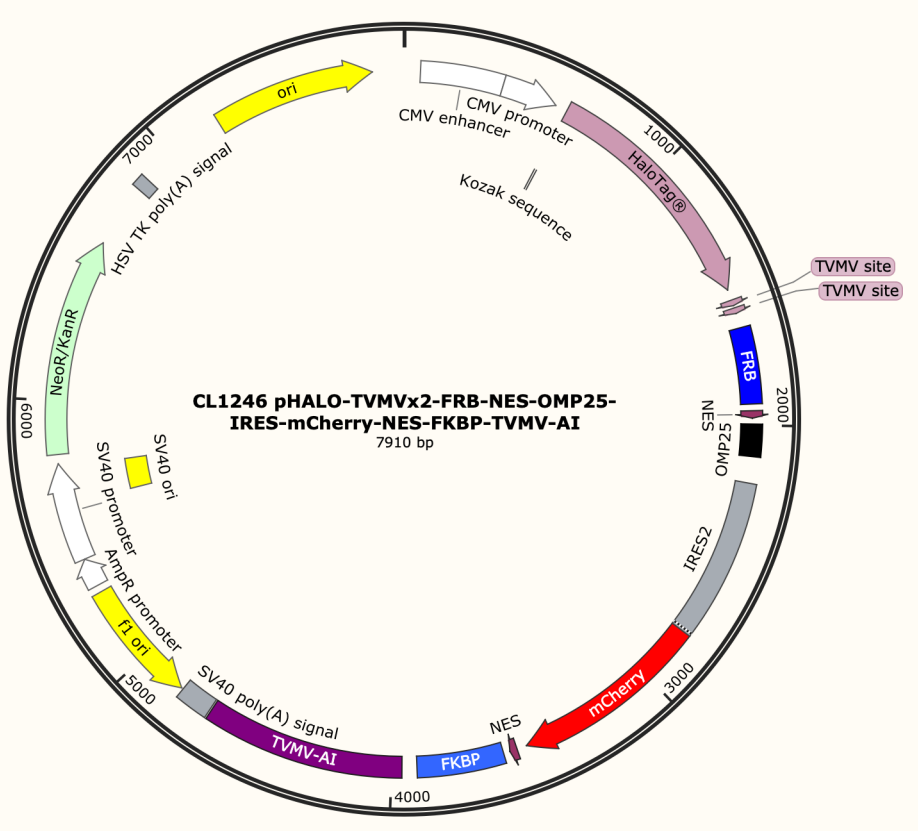

Figure 2.5: Map of plasmid CL1246, pHALO-TVMVx2-FRB-NES-OMP25-IRES-mCherry-NES-FKBP-TVMV-AI.

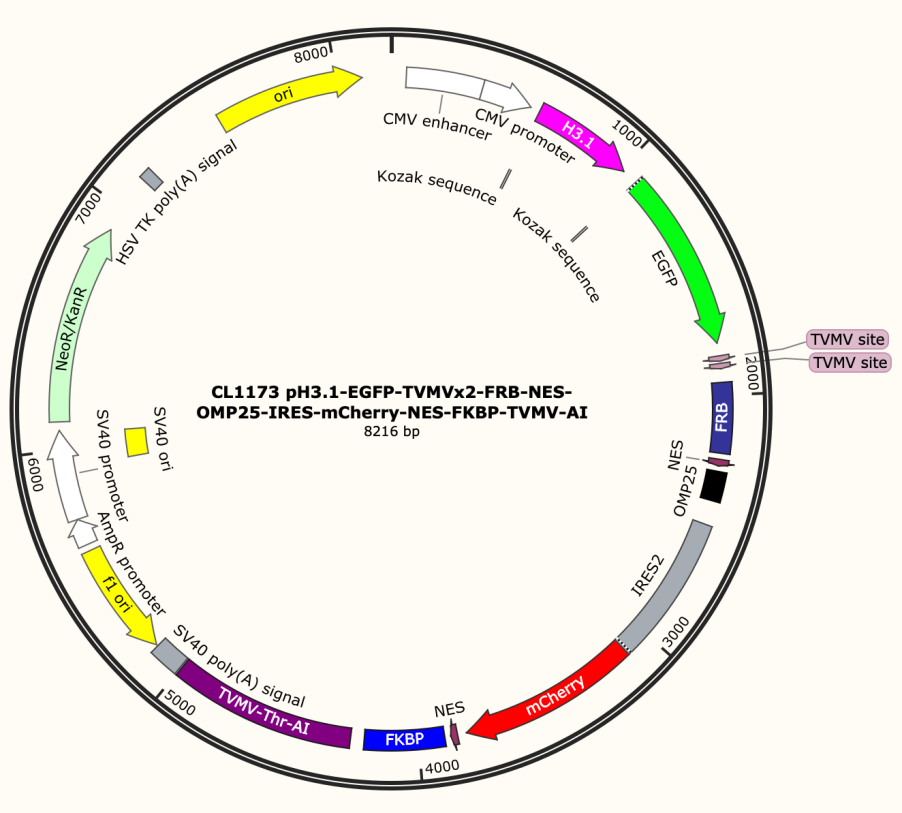

Figure 2.6: Map of plasmid CL1173, pH3.1-EGFP-TVMVx2-FRB-NES-OMP25-IRES-mCherry-NES-FKBP-TVMV-AI.

2.1.5 Cargo-IRR

H3.1-IRR (Cl 1173, figure 2.6) was generated by digesting Cl 1162 with AgeI and subjecting it to Gibson assembly with the PCR products of pH3.1-EGFP-HCVx2-FRB-OMP25 (Cl 1057) with the primers P1338 and P1341.

RPL11-IRR (Cl 1234, figure 2.7) was assembled by digesting Cl1162 with AgeI and subjecting it to Gibson assembly with the PCR products from HeLa cell cDNA amplified with primers P1427 and P1428.

2.1.6 Circular permutation of ABI1

The structure of the PYL1-ABI1 dimer in complex with abscisic acid was visualised using PyMol (Schrödinger) to identify a suitable location for the new N and C-termini (R137 – N-terminus, G126 – C-terminus). The circular permutation of ABI1 (CPABI1) was generated by PCR using

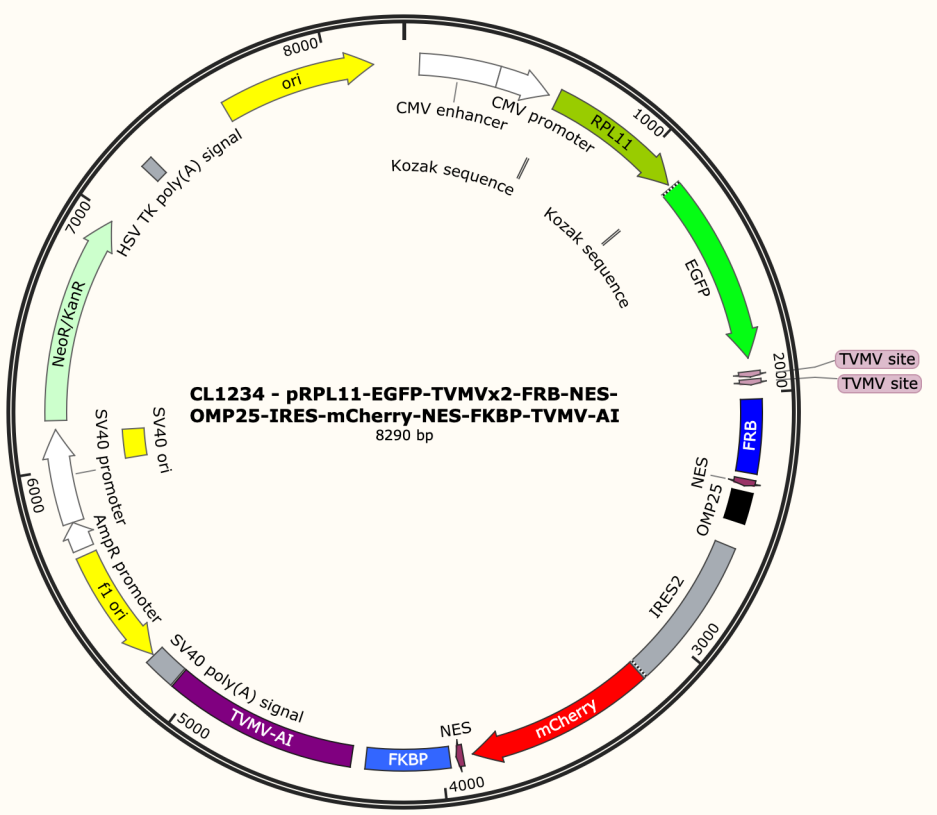

Figure 2.7: Map of plasmid CL1234, pRPL11-EGFP-TVMVx2-FRB-NES-OMP25-IRES-mCherry-NES-FKBP-TVMV-AI.

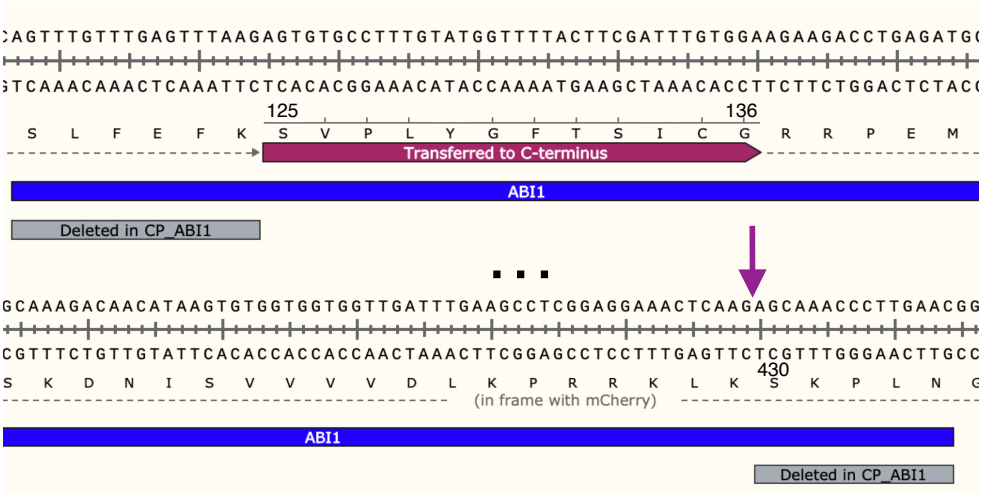

Figure 2.8: Circular permutation of ABI1, CL 1257, pEGFP-HCVx2-PYL-NES-OMP25-IRES-mCherry-NES-CPABI1-HCV-AI. Grey blocks show the deleted base pair sequences of the ABI1 gene in its circularly permutated version. The purple block shows the sequence transferred from the N to the C-terminus of the protein. Purple arrow indicates the transferred sequence's new position within the gene.

the primers P1439 and P1440, and as a template a gel purified segment of ABA-HCV containing solely the original ABI1 gene by digestion of Cl 1126 with the enzymes EcoRI and XhoI. The first six amino acids of the truncated ABI1 (S119-N434) were deleted and the following twelve amino acids (S125-G136) were transferred to the 3' end of the gene into position 430 (figure 2.8). Finally, the end five amino acids (S430-N434) were deleted to generate the final pEGFP-HCVx2-PYL-NES-OMP25-IRES-mCherry-NES-CPABI1-HCV-AI (Cl 1257).

2.1.7 IRR combinatorial assembly

pEGFP-HCVx2-FRB-NES-OMP25-IRES-mCherry-NES-FKBP-HCV-AI (Cl 1240, figure 2.9) was generated by sequentially swapping PYL1 and ABI1 in Cl 1126 by FKBP and FRB from Cl 1162 by using the enzymes AscI and BamHI, and EcoRI and XhoI, respectively.

pEGFP-TVMVx2-PYL1-NES-OMP25-IRES-mCherry-NES-ABI1-TVMV-AI (Cl 1241, figure 2.10) was generated by sequentially swapping FKBP

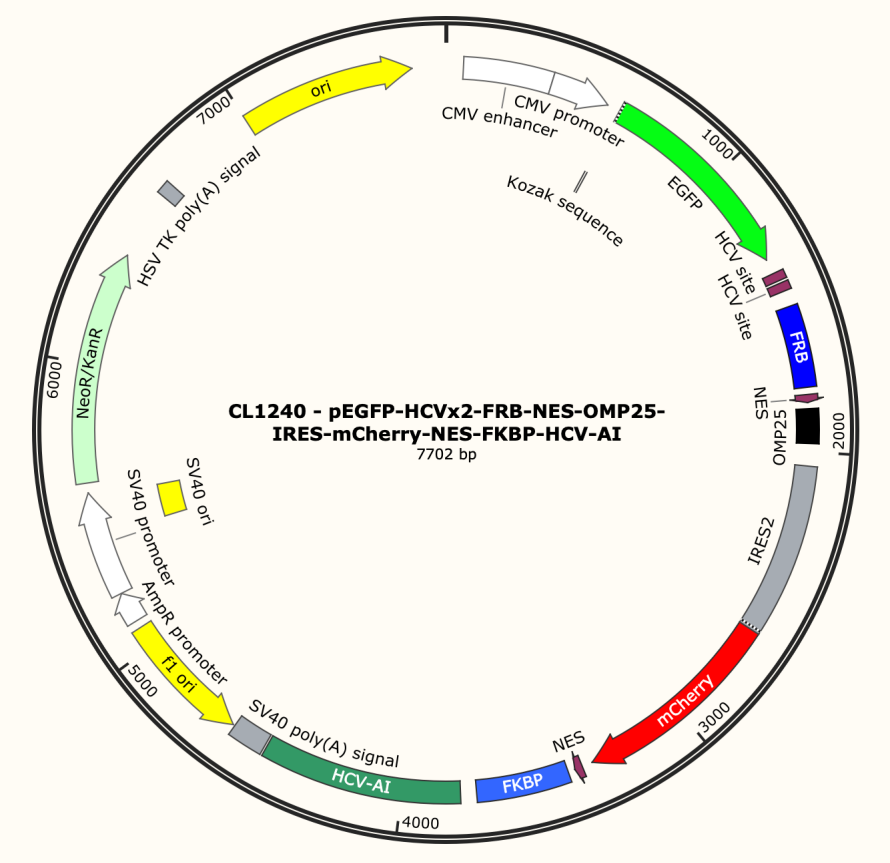

Figure 2.9: Map of plasmid CL1240, pEGFP-HCVx2-FRB-NES-OMP25-IRES-mCherry-NES-FKBP-HCV-AI.

and FRB in Cl 1162 by PYL1 and ABI1 from Cl1126 by using the enzymes AscI and BamHI, and EcoRI and XhoI, respectively.

pEGFP-HCVx2-ABI1-NES-OMP25-IRES-mCherry-NES-PYL1-HCV-AI (Cl 1258, figure 2.11) was generated by ligating the AscI and BamHI digested Cl 1126 and PCR products of Cl 1126 with the primers P1435 and P1436 also digested with AscI and BamHI. Followed by the ligation of the previously generated plasmid digested with EcoRI and XhoI and the PCR products of Cl 1126 with the primers P1437 and P1438 were also digested with EcoRI and XhoI.

All plasmids were sequenced to ensure there were no mutations.

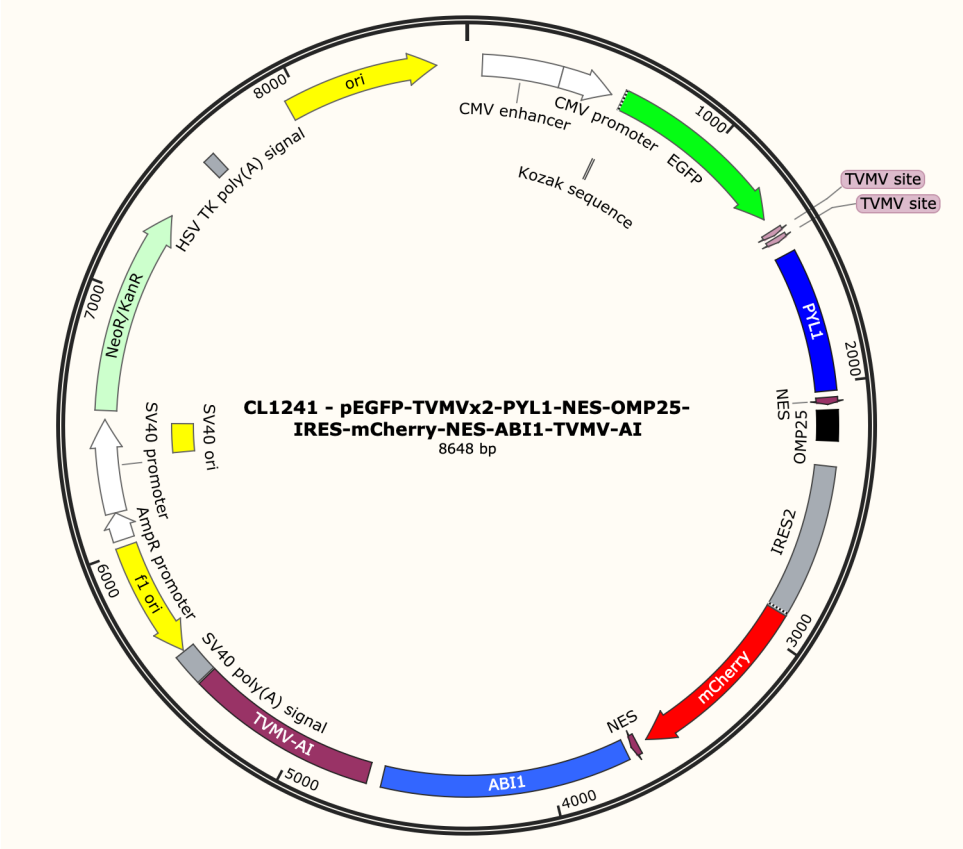

Figure 2.10: Map of plasmid CL1241, pEGFP-TVMVx2-PYL1-NES-OMP25-IRES-mCherry-NES-ABI1-TVMV-AI

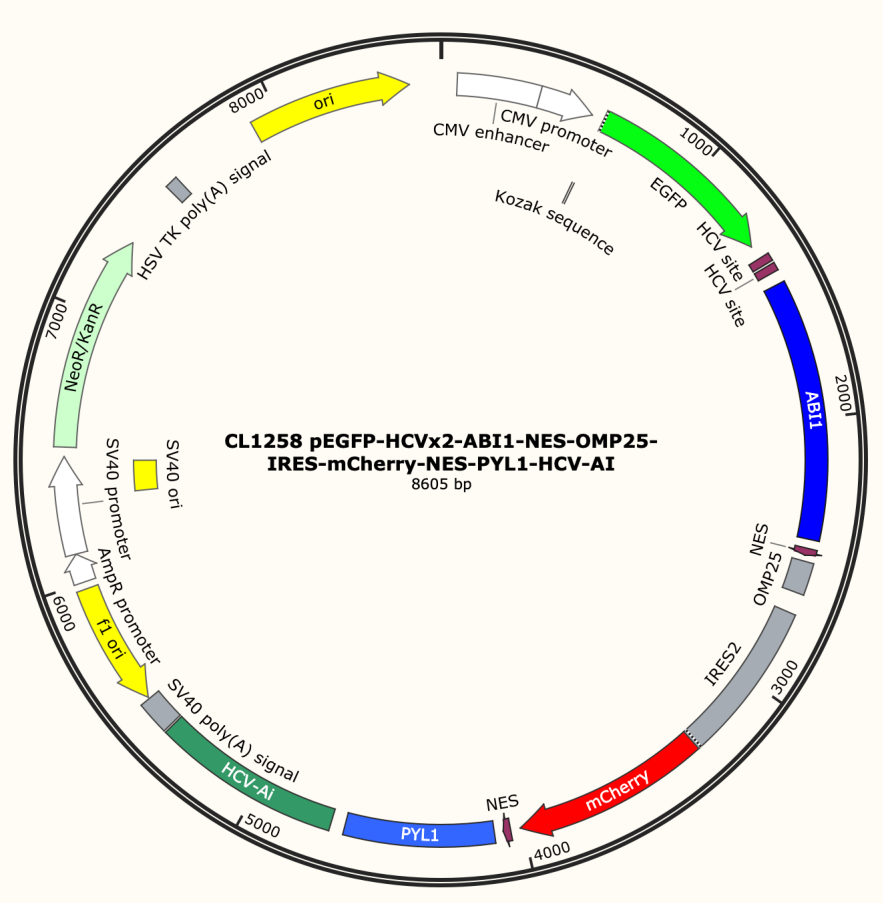

Figure 2.11: Map of plasmid CL1258, pEGFP-HCVx2-ABI1-NES-OMP25-IRES-mCherry-NES-PYL1-HCV-AI

2.2 Cell biology

2.2.1 Cell culture

All tissue culture steps were undertaken in a Labculture PLUS ESCO Class II Biosafety Cabinet Tissue culture hood and incubation of the cells took place at 37°C and 5% CO_2 with DMEM, high glucose, GlutaMAX medium with 10% fetal bovine serum (FBS) and 100U/ml penicillin/streptomycin. The cells used throughout all work were Hela Kyoto cells originally obtained from ATCC and maintained in the laboratory. RAPID-release stable cells line was created by subsequent transfection of each of the elements of RAPID-release into the cell line mentioned above and incubated in the presence of puromycin ($1\mu g/ml$) for selection and maintenance purposes.

2.2.2 Transfections

Transfections were carried out 48h prior to imaging using *FuGENE* from *PROMEGA* according to protocols published by the supplier, using a 3:1 ratio of μl of reagent to μg of plasmid DNA. Transfections were performed in 8-well μ-Slide chambers (ibidi) for direct use in imaging. For transfection purposes cells were kept in DMEM, high glucose, GlutaMAX medium with 10% fetal bovine serum (FBS) and 100U/ml penicillin/streptomycin.

2.2.3 Cell synchronisation

Cells were synchronised using a double thymidine block. HeLa cells were grown to approximately 25% confluency and treated with thymidine at 2 mM concentration for 14h. After this period the medium was removed and cells were washed with PBS. The medium was replaced with fresh DMEM containing 24 μM deoxycytidine, and incubated for 9h. The medium was again removed, cells were washed with PBS, and fresh DMEM medium was replaced. Thymidine was added to a final

concentration of 2 mM, and cells incubated for 14h. After this period, the medium was removed, cells were washed with PBS, and fresh DMEM supplemented with 24 μM deoxycytidine was added.

This is in accordance with the protocol in *Cell Cycle Synchronization, chapter 10, Synchronization from Early S: Double Thymidine Block.* (Futcher 1999).

2.2.4 Immunostaining of γH2AX

Cells were exposed to zeocin at the concentration of 1000 $\mu g/ml$ in L-15 imaging medium for 1h and 4h. After this period cells were washed with PBS and the medium was replaced with methanol at -20°C and cells were incubated at -20°C overnight for fixation. Cells were then washed with PBS and blocked with 5% BSA in TBST with 0.3% Triton X-100 for 40 minutes. After this cells were washed with PBS and were left incubating overnight with a 1:500 dilution of primary antibody (Cell Signalling Technology, Phospho-Histone H2A.X (Ser139) (20E3) Rabbit mAb #9718) with 1% BSA. The primary antibody solution was removed and cells were washed with PBS. The secondary antibody solution (dilution 1:2000) with 1% BSA was added and cells were incubated for 1h at room temperature. Cells were washed once more and mounted onto a microscope slide using mounting resin. Imaging was performed using a confocal spinning disc microscope as described in subsection 2.3.1.

2.2.5 Chromatin immunoprecipitation

DNA preparation

Approximately 3 million stably transfected HeLa cells expressing H3.1-RAPID-release were seeded into a 10 cm culture dish and subjected to synchronisation according to section 2.2.3 (except for asynchronous cell ChIP). After a period of 1, 3, 5, or 7h (three repeats per time point) from the last block lift, RAP was added to the cells for a final concentration of 0.1 μM and cells were incubated until 8h after block release, at which

point they were washed with PBS at 37°C and fixed with 1% formaldehyde for 10 minutes in an orbital shaker. After this period, samples were quenched with $2.5M$ glycine for 5 minutes and washed twice with PBS containing protease inhibitors. PBS with protease inhibitors was added to the fixed cells and these were scraped and transferred to a 15ml tube for centrifugation ($1000g$, for 5 minutes at 4°C) and the supernatant was removed. Cells were resuspended in lysis buffer from the ChromoTek GFP-Trap® Magnetic Agarose kit (gtma-20) and placed on ice for 30 minutes, being vigorously pipetted every 10 minutes and diluted with 0.3 ml of dilution buffer from the same kit with protease inhibitors. Lysates were transferred to microcentrifuge tubes and sheared through sonication using a Bioruptor® by Diagenode for 3 cycles of 10 minutes with on/off periods of 30 seconds. The resulting sheared samples were then centrifuged at 20 000 g for 15 minutes and 4°C, and supernatants were collected.

DNA immunoprecipitation

GFP-Trap® Magnetic Agarose beads were resuspended by inverting the tube, and 25 μl was transferred to microcentrifuge tubes and washed with ice-cold dilution buffer before being separated with a magnet and the supernatant discarded. The sheared DNA samples were added to the beads and incubated with rotation for 1h at 4°C. After this period, beads were separated, the supernatants were discarded, and resuspended in washing buffer. This process was repeated twice and the beads were transferred to clean microcentrifuge tubes during the last wash. After the supernatant was completely removed, acidic elution buffer was added to the beads and these were constantly pipetted for 1 minute at room temperature. Beads were then separated, supernatants were collected and neutralised with neutralisation buffer, and the process repeated once more. The collected supernatants were diluted with 50 μl of dilution solution and RNAse was added, followed by a 45 minute incubation at 45 °C. After this, samples were incubated overnight at 65°C. Proteinase

K was added, and the samples were incubated for 1h at 60°C. Finally, samples were purified using a Monarch® PCR & DNA Cleanup Kit.

Sequencing and alignment

Fragment library preparation was performed by Novogene (Cambridge) using an NEBNext® Ultra™ II DNA Library Prep Kit for Illumina® (E7645, E7103) and sequencing was carried out through Illumina® High Throughput Sequencing (PE150) with a depth of 30 Million paired reads per sample. Mapping of the reads was performed against the *//ftp.ensembl.org/pub/release-82/gtf/homo_sapiens/* reference Human genome using the Burrows-Wheeler Alignment (BWA) Tool software (H. Li and Durbin 2009).

Data was visualised and aligned with existing replication domain data (reference Int93773609 from Florida State University replication domain database) using Integrated Genomic Viewer (IGV, Broad Institute and the Regents of the University of California) software and compared with Hi-C data from the YEU lab (Northwestern University, reference GM12878; Y. Wang et al. 2018).

2.3 Imaging

All imaging was performed with cells in Gibco™ Leibovitz's L-15 Medium with 10% fetal bovine serum (FBS) and 100 U/ml penicillin/streptomycin.

2.3.1 Confocal microscopy

Confocal microscopy images presented in Chapter 3 were acquired using a spinning disc confocal microscope using and UltraVIEW VoX Live Cell Imaging System (Perkin Elmer) at 100X objective magnification in an environmental chamber at 35°C. The imaging volume of 10 μm and the Z-spacing between images was 1 μm. The 488 nm laser was used at 4% power with an exposure time of 180 ms.

Images presented in Chapter 4 were acquired in the same microscope

as above at 60X objective magnification. The imaging volume was 15 μm and the Z-spacing between images was 1 μm. The 488 nm laser was used at 17.5% power with an exposure time of 180 ms, and the 561 nm laser was used at 34% power with an exposure of 360 ms.

2.3.2 Lattice light sheet microscopy

Lattice light sheet microscopy was performed using the WarwickCAMDU-operated lattice light sheet microscope in dithered mode with 62.5x magnification. The set up operated an immersion lens into a L-15 media bath at 37°C where the sample sat on a 5mm glass cover-slip mounted onto a medical grade steel holder using vacuum grease.

For long-term imaging, images were acquired every 30 seconds with the 488 nm laser at minimum power. The imaging volume was 18 μm and the exposure time was 35 ms. For short-term fast imaging, images were acquired every second with the 488 nm at 3 % laser power. The imaging volume was 13 μm and the exposure time was 5 ms.

2.4 Tethered cargo release procedures

2.4.1 EGFP-histone pulse for chromatin labelling

For confocal microscopy, RAPID-release stable cells were seeded into an 8-well μ-Slide chamber (ibidi) for direct use in imaging and subjected to a double thymidine block according to subsection 2.2.3. Five hours post block removal, rapamycin was added to the well to a concentration of 0.1 μM. The media in the μ-Slide was changed to L-15 3h after the addition of rapamycin and cells were imaged with the parameters specified in subsection 2.3.1.

For LLSM, RAPID-release stable cells were seeded into a 6-well plate containing a 5mm glass cover-slip compatible with the LLSM sample holder. They were subjected to a double thymidine block according to subsection 2.2.3. Five hours post block removal, rapamycin was added

to the well to a concentration of 0.1 μM. Three hours after the addition of rapamycin the cover-slip was mounted onto the sample holder and transferred to the L-15 bath mounted onto the LLSM at 37°C for thermal equilibration, imaging commenced 1h after that with the parameters specified in subsection 2.3.2.

For DNA damage experiments in LLSM the protocol followed was the same as above, except the L-15 medium bath contained 500 $\mu g/ml$ or 1000 $\mu g/ml$ of Zeocin, according to the required concentration.

2.4.2 Real-time cargo release

In the case of real-time cargo release by RAPID-release or IRR, cells were transfected according to subsection 2.2.2 and imaged according to subsection 2.3.1. Here, T=0s time-points were recorded prior to the addition of rapamycin to the imaging medium. To commence the release, rapamycin was added to the cell media to a final concentration of 0.1 μM, and one minute later the image acquisition was initiated, images were captured every minute after this point for a duration of 20-30 minutes. For the abscisic acid-induced release, the same protocol was followed except the final concentration of abscisic acid was 10 μM. For the rapamycin-induced release events recorded in the presence of abscisic acid, the latter was added 5 minutes prior to the addition of rapamycin, the concentration of each of these was as previously described. For the auxin-induced release the same protocol was followed except the final concentration of auxin was 100 μM.

2.4.3 HALO-tagging

Ligand OregonGreen was added to imaging medium to a final concentration of 1 μM and incubated for 15 minutes. After this, cells were washed with PBS and fresh L-15 medium. The medium was finally replaced by fresh L-15 prior to imaging. Cells were imaged according to subsection 2.3.1.

For cells exposed to rapamycin prior to ligand addition, this took place 30 minutes before OregonGreen was introduced into the medium.

2.5 Data processing and analysis

Image processing was carried out using *ImageJ* (Schindelin et al. 2012). R was used for the statistical and graphical analysis of the extracted data.

2.5.1 RAPID-release and IRR kinetics analysis

Cell segmentation was performed manually with Z planes projected with maximal pixel intensity, partitioning the cell into three compartments: the nucleus, the cytoplasm, and the whole cell. Release from the outer mitochondrial membrane (OMM) was characterised by the variation in standard deviation of pixel intensity of the whole cell segment.

2.5.2 Deskew and deconvolution

Deskewing of the images was performed using the SlideBook 6 deskew tool with an angle of 57.2°.

Deconvolution of the images was achieved through the application of the Constraint Iterative (20 iterations) deconvolution tool also from SlideBook 6. This tool applied a calculated point spread function (PSF) without scaling to the original data pixel intensity range, in order to prevent fluctuations of the absolute intensity of the labelled structures between time-points.

2.5.3 Registration parameters

Registration was performed using the *ImageJ* plug-in *Descriptor-based series registration* (Schindelin et al. 2012) with the parameters detailed in table 2.1.

Brightness of detections	Interactive
Approximate size of detections	Interactive
Type of detections	Interactive
Subpixel localisation	3-dimensional quadratic fit
Transformation model	Rigid(3D)
Regularize model	Yes
Images are roughly aligned	Yes
Number of neighbours for the descriptors	3
Redundancy for descriptor matching	2
Significance required for descriptor match	3
Allowed error for RANSAC	3
Global optimization	All-to-all matching with range
Range for all-to-all matching	5
Image fusion	Fuse and display
Interpolation	Linear interpolation

Table 2.1: Parameters used in *Descriptor-based series registration ImageJ* plug-in for image registration.

2.5.4 Chromatin domain tracking parameters

Tracking was performed using *ImageJ* plug-in *TrackMate* (Tinevez et al. 2017) with the parameters detailed in table 2.2 for long-term analysis and the parameters in table 2.3 for short-term analysis.

Estimated diameter	800nm
LOG detector	Yes
LAP tracker	Yes
Frame-to-frame linking:	
Max distance	10 pixels
Track Feature penalties	Mean intensity and estimated diameter
Track segment gap closing:	
Max distance	10 pixels
Max frame gap	3 frames
Track segment splitting:	
Max distance	4 pixels
Track segment merging:	
Max distance	4 pixels
Track filters:	
Track start filter	Below 10
Duration of track filter	Above 40

Table 2.2: Parameters used in *TrackMate ImageJ* plug-in for chromatin domain tracking in long-term imaging.

Estimated diameter	800nm
LOG detector	Yes
LAP tracker	Yes
Frame-to-frame linking:	
Max distance	8 pixels
Track Feature penalties	Mean intensity and estimated diameter
Track segment gap closing:	
Max distance	8 pixels
Max frame gap	2 frames
Track segment splitting:	
Max distance	4 pixels
Track segment merging:	
Max distance	4 pixels
Track filters:	
Track start filter	Below 10
Duration of track filter	Above 120

Table 2.3: Parameters used in *TrackMate ImageJ* plug-in for chromatin domain tracking in short-term imaging.

Chapter 3

Chromatin domain dynamics

Chromosomes of higher eukaryotes are subjected to hierarchical folding to constrain the genome to nuclear dimensions. Organising the genome in such a manner leads to the appearance of structures of different scales that influence both the architecture of the nucleus and gene expression. Genome three-dimensional (3D) organisation has predominantly been studied through next generation sequencing methodologies, and conclusions are often made from population averages, rather than single cell data. Techniques that allow for imaging of single cells, such as FISH, often rely on cell fixation processes. Information about structural traits of the genome can be extracted using these methods, but the acquisition of information on the dynamics of the structures observed is not possible. Live-cell imaging techniques have been used to probe the kinetics of chromatin structures, however, these have been mostly limited to one or two *foci*, integrated repetitive arrays, or have involved indiscriminate labelling of bulk chromatin (Gasser 2002; Chambeyron et al. 2005). It has remained challenging to image living cells during long periods to extract direct information about the dynamics of chromatin domain structures.

As the domain structure of the genome is mirrored by its replication timing (Pope et al. 2014), I was able to use a recently developed technique, termed RAPID-release, where a short pulse of EGFP-labelled histones, during S-phase, is generated and incorporated into distinct chro-

matin domains. As EGFP-labeled H3.1 has a slow turnover in human chromatin (Kimura, Sugaya, and Cook 2002), and as tagged histones are relatively inert compared with fluorescent nucleotides, they have the potential to be used as location markers for extended periods of time.

I capitalised on this unique labelling ability to investigate the behaviour of chromatin domains in living cells across different time-scales. This was achieved by tracking their positions, in absolute terms, as time progressed. I started by employing fluorescence spinning disc confocal microscopy, however, the high laser power required by the technique caused bleaching of the fluorophores early in the time series, and phototoxicity problems were also observed. Therefore, I developed a different approach that employed lattice light sheet microscopy, a technique that uses lower laser power and, therefore, is less prone to causing flourophore bleaching and phototoxic damage. I was able to extract the coordinates of each labelled chromatin domain at each time-point, and effectively reconstruct the nucleus of single cells, and observe how their chromatin architecture changed through time.

To explore the hypothesis laid out in section 1.4, I assessed how the population of these structures behaved under standard conditions. I was able to identify two different types of chromatin domains which I termed, low mobility domains, and high mobility domains, depending on their dynamics. I also looked to understand if perturbations to the integrity of the genome could alter their dynamics. I triggered DNA damage in cells by exposing them to Zeocin and observed a generalised increase in the mobility of the labelled chromatin structures, suggesting DNA integrity is related with the dynamics of chromatin.

3.1 Labelling chromatin domains

The replication of discrete parts of the genome take place independently of each other and at different points of S-phase. These independently replicating domains mirror the domain structures observed using

Hi-C, and are generally referred to as Topologically Associated Domains (TADs; Benjamin D. Pope and Gilbert, 2014). Due to this inherent link between replication timing and the domain structure of genomes, I hypothesized that, depending on the stage of S-phase, discrete TADs could be labelled with a pulse of tagged histones. I posited that by only labelling domains that are replicating within a limited time window, it would be possible to tag these structures sparsely enough to allow observation without being hindered by an unmanageable number of labelled genomic structures.

RAPID-release is a pulse-labelling technique developed by Apta-Smith, Hernandez-Fernaud, and Bowman (2018) composed of two elements: (1) a tether that anchors itself to the outer mitochondrial membrane (OMM), composed of an anchor peptide, one half of a chemically-induced dimerisation (CID) pair, a target site for a TVMV protease, EGFP as a fluorescent tag, cargo/protein of interest, and (2) a cytoplasm-soluble element that is comprised of the other half of the CID pair, a TVMV protease together with its auto-inhibitory domain (AI), and a fluorescent tag. Upon the addition of the trigger molecule (rapamycin, RAP), FKBP and FRB dimerise, bringing into close proximity the TVMV protease and its cleavage site. Because the AI inhibits TVMV in a competitive manner, the increase in local concentration of substrate (cleavage sites) dictates that, when transiently uninhibited, the protease will be able to cleave its substrate to release the fused protein of interest (figure 3.1).

To test whether EGFP-labelled histones followed a similar incorporation pattern to those of nucleotide analogs used in iPOND-like techniques, I employed an asynchronous HeLa cell-line stably expressing the RAPID-release constructs, having histone H3.1 as cargo. I expected to observe different labelling patterns emerging across nuclei, as a consequence of cells being in different points of the cell cycle when the pulse took place.

Indeed, I observed cells that developed a homogeneous fluorescence throughout the nucleus (figure 3.2, green arrows) whereas other cells in

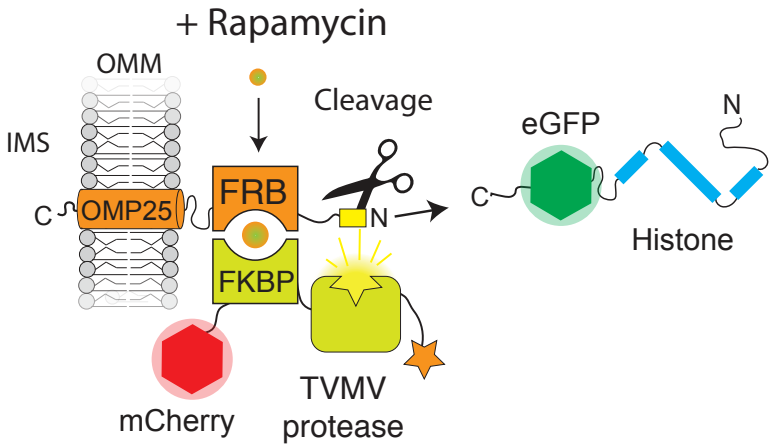

Figure 3.1: Diagram of RAPID-release. Upon addition of rapamycin to the media in which cells sit, the two components of the system dimerise, bringing TVMV in close proximity to its target site. Cleavage of the TVMV target releases EGFP-tagged histones that are quickly imported into the nucleus. Figure provided by Dr Andrew Bowman (unpublished).

the population had nuclei with more granular appearances (figure 3.2, white arrows). I postulated that the homogeneously fluorescent nuclei were not in S-phase upon RAP addition, and so, histones were imported into the nucleus but not incorporated into the genome. Conversely, I attributed the granularity of cells to the incorporation of EGFP-labelled histones into the chromatin fibre.

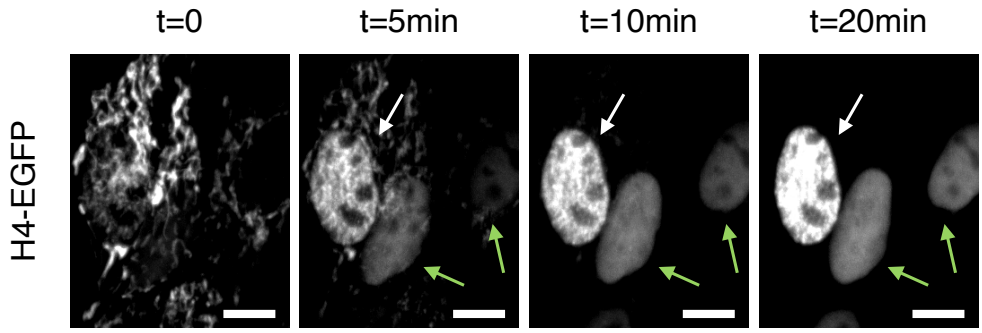

Figure 3.2: Nuclear labelling patterns generated by RAPID-release. Different cells present different nuclear labelling patterns after RAPID-release activation. Some are granular (white arrows), some are homogeneously fluorescent (green arrows). Scale bar, 10 μm.

3.1.1 Cell synchronisation for specific chromatin domain labelling

Upon analysis of the previously described data, it became clear that it was possible to label different chromatin domains using this technique, however, the patterns shown in figure 3.2 were not suitable for individual domain tracking. The granularity observed was composed of domains that were too numerous and that sat too close together to differentiate and be efficiently tracked. Therefore, Isought to understand if there was a particular window in the timing of S-phase where the employment of this technique could label chromatin domains that were sparsely populated enough, and of sufficiently large dimensions to be identified in isolation.

To achieve this, I subjected several populations of HeLa cells expressing RAPID-release to a double thymidine block. This procedure arrested cells at the beginning of S-phase. After releasing the block, RAP was added to the populations at different times to trigger the EGFP-labelled histone pulse at different stages of S-phase.

The prevalence of granular nuclei was greatly increased in comparison with their homogeneous counterparts, suggesting that more cells were going through S-phase when RAP was added.

I also observed that cells subjected to RAP in early S-phase presented

a granular appearance that was spread across the entirety of the nucleus, much like the cells indicated with white arrows in figure 3.2. At later stages, however, cells presented patterns where larger, more peripheral domains appeared (figure 3.3, yellow arrows). This is consistent with the literature in that small domains are located towards the centre of the nucleus and are the first ones to be replicated in S-phase, and larger heterochromatic domains replicate later in S-phase and are located in the periphery of nuclei (Rhind and D. M. Gilbert 2013).

Through analysis of my data I estimated that the best time to generate a histone pulse would be 5 h after the onset of S-phase. This was for two main reasons: (1) earlier pulses would label too many domains of too small dimensions that would be impossible to track effectively, and (2) a pulse generated later than 5 h post block lift would be too close to the end of S-phase, or indeed fall outside it. In the latter case, cells showed a small amount of peripheric replication that incorporated EGFP-labelled histones, but where a significant part of the nucleus presented a homogeneous texture similar to that presented by cells out of S-phase (figure 3.3, blue arrows).

I performed all subsequent experiments in cells subjected to a double thymidine block where RAP was added 5 h post block removal.

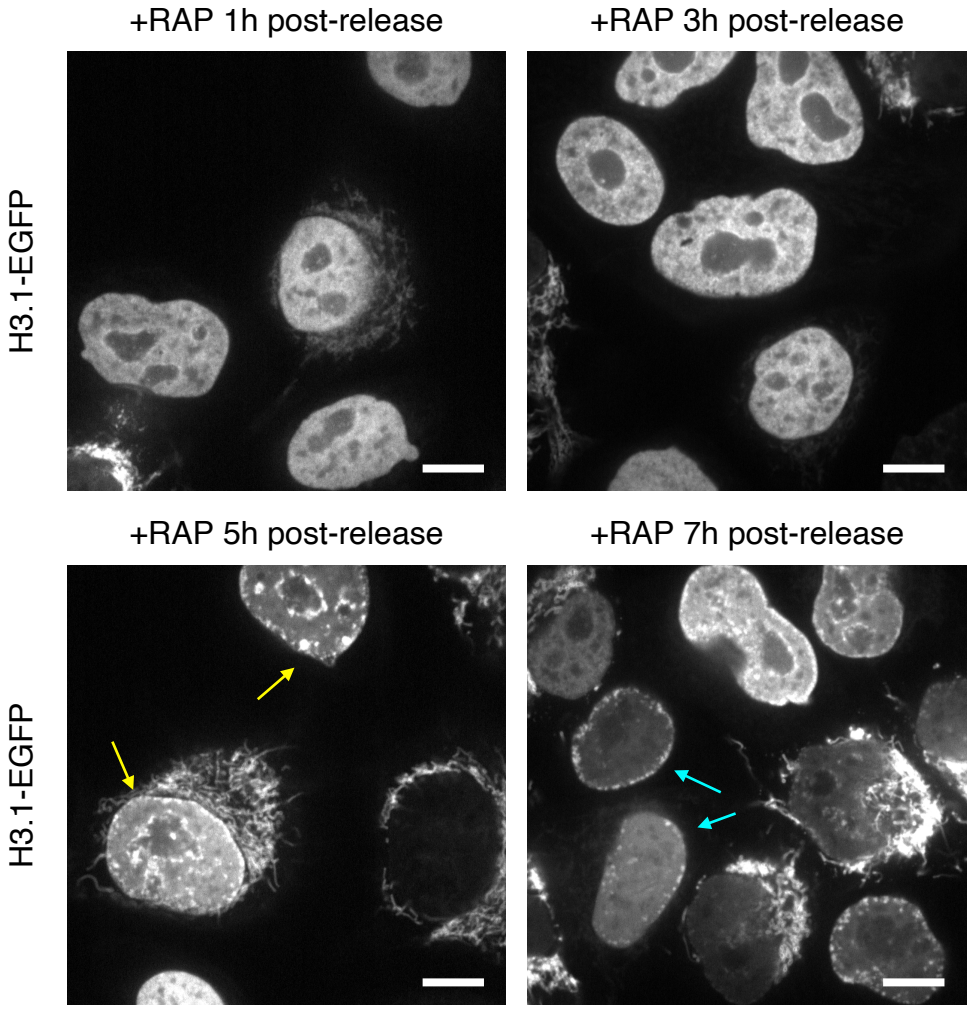

Figure 3.3: S-phase pulse timing. Cells exposed to RAP at later stages of S-phase present a greater number of large labelled domains and fewer homogeneous nuclei are observed. Scale bar, 10 μm.

3.1.2 Chromatin domains remain labelled across cell divisions

Next, I looked to understand if the labelling achieved through RAPID-release was stable enough for long-term imaging of these structures. I assumed that this would be the case if two daughter cells maintained similar nuclear labelling patters across, at least, one round of cell division.

To test this, a population of RAPID-release transfected cells were treated with RAP and diluted in suspension after 30 minutes. The cells were seeded onto an imaging slide and incubated for 12h.

I postulated that thinly seeded cells would settle distantly from each other, and if two cells were in close proximity they would likely be two daughter cells that arose from the division of the same parent. If both daughter cells presented the same nuclear pattern I could assume that the structures were maintained across cell divisions, and therefore stable.

Cells that sat close together presented a similar nuclear labelling pattern; while some pairs of cells presented homogeneously fluorescent nuclei, others had a chromatin labelling pattern similar to that generated when RAP is added in late in S-phase. Interestingly, some cells remained aggregated prior to settling. This allowed me to better compare and confirm the conservation across cell cycles, as evidenced by the second and third panels in figure 3.4. This suggested that chromatin domain labelling is stable enough for long-term imaging and analysis of the structures.

Besides assessing the potential ability to image chromatin domains in the long-term, the fact that labelling patterns remained conserved across cell divisions also suggested that these were functional chromatin structures whose replication timing was correlated with their architecture.

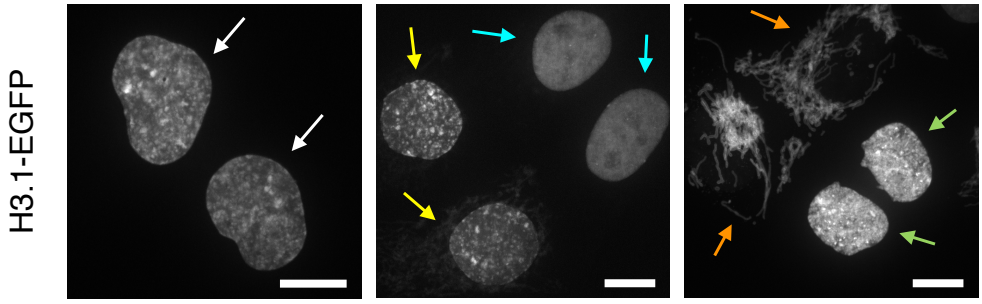

Figure 3.4: Stability of replication domains. Daughter cells resulting from a cell division retain a similar spacial genetic arrangement to each other, suggesting the location of TADs is conserved after a round of cell division. Arrows of the same colour indicate daughter cells resulting from the same parent. Scale bar, 10 μm.

3.2 Labelled chromatin replication domains mirror higher order genomic structures

To draw parallels between the observed domains labelled with EGFP and how these correspond to chromatin at the genomic level, I performed a series of chromatin immunoprecipitation and sequencing assays (ChIP-seq). Here, I triggered histone release from the OMM at different intervals post double thymidine block release (1h, 3h, 5h and 7h, in a way identical to section 3.1.1), and precipitated and sequenced the DNA fragments associated with EGFP to identify the structures.

Expectedly, the addition of RAP at 1 and 3h post block release led to the labelling of early replicating chromatin (figures 3.5 and 3.6). The differences between the enriched regions of 1h and 3h samples also illustrate the progression and propagation of DNA replication along the linear genome within the discrete replication domains, as the signal shifts along the genome. The contrast in enrichment between 3 and 5h is stark, suggesting that when RAP was added 5h post block release, late replicating chromatin was labelled instead. These regions were almost entirely inversely complementary to those of earlier samples and the difference between 5h and 3h was greater than that between 3h and 1h. These

observation aligned with the Repli-seq data and the replication timing of different regions of chromatin more widely. Indeed, late replicating chromatin was almost exclusively labelled in 5h samples. Repli-seq is a technique that allows for the identification of the timing of replication of the different parts of the genome. It relies on the incorporation of BrdU in nascent strands of newly replicated DNA, sorting of cells according to their stage of the cell cycle, and immunoprecipitation of the labelled DNA and its sequencing. Through this process it is possible to attribute a replication timing to the different regions of the genome (R. Hansen et al. 2010).

Interestingly, the patterns found in 7h samples was similar to that found in asynchronous samples, suggesting that, at this stage, cells had exited S-phase. This is because, if cells exit S-phase, few tagged histones will be incorporated, resulting in few reads. Therefore, cells that escape the double thymidine block will be the ones incorporating histones, presenting a labelling pattern similar to that of asynchronous cells. These data reinforced my assumption that in order to consistently label late replicating chromatin, the pulse of histones should be performed at 5h post block lift and that 7h is too late to label chromatin domains effectively.

Different replication timing chromatin also broadly aligned with TAD boundaries, further illustrating the replication timing regulation role of these structures, and suggesting that the labelled structures observed are in fact topologically associated domains, as has previously been observed (Pope et al, 2014). This allowed me to confidently associate the dynamics of the observed domains with that of TADs. Furthermore, the size of the enriched late replicating domains (5h) presented sizes of approximately 1-4 Mb in size, which is consistent with the size of TADs previously described, also shedding light on the size of the labelled structures in base-pairs terms.

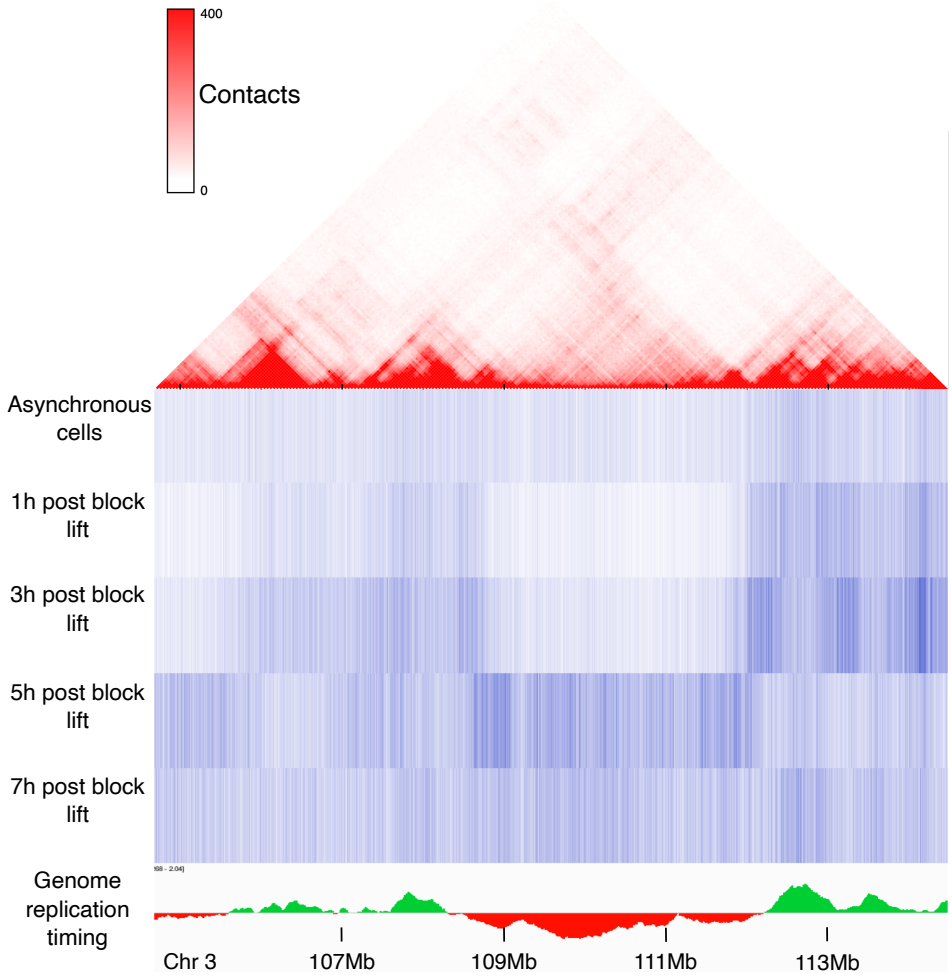

Figure 3.5: ChIP-seq of labelled chromatin. Chromatin immunoprecipitation of a region of chromosome 3 and its alignment to replication timing (Int93773609, *Florida State University Replication Domain Database*) and topologically associated domains (GM12878, YEU lab, Y. Wang et al. 2018). Green portion of the plot in *Genome replication timing* represents early replicating and red portion represents late replicating chromatin. Darker blue represents regions of greater EGFP enrichment.

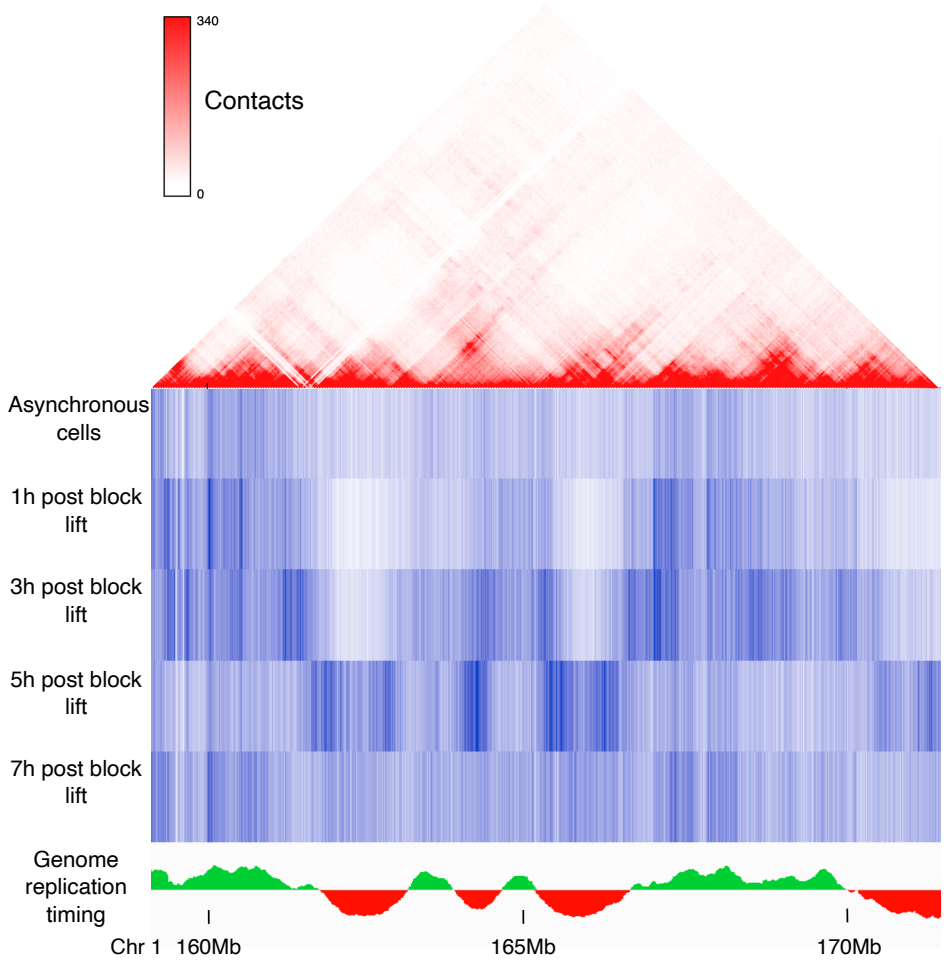

Figure 3.6: ChIP-seq of labelled chromatin. Chromatin immunoprecipitation of a region of chromosome 1 and its alignment to replication timing (Int93773609, *Florida State University Replication Domain Database*) and topologically associated domains (GM12878, YEU lab, Y. Wang et al. 2018). Green portion of the plot in *Genome replication timing* represents early replicating and red portion represents late replicating chromatin. Darker blue represents regions of greater EGFP enrichment.

3.3 Spinning disc confocal microscopy for long-term imaging of chromatin domains

To study the spatiotemporal dynamics of the labelled chromatin domains I started by imaging cells using a spinning disc confocal microscope where a Z-stack would be produced for each 1 minute time point, for the duration of two hours. I intended to reconstruct the nucleus in three-dimensions at each time point. Comparing the position of domains in three-dimensions (3D) would allow me to characterise their spatiotemporal dynamics, which could give insight into the way these structures behave.

Using this approach I observed chromatin domains splitting into several different structures and merging, once more, into a single domain (figure 3.7). Even though preliminary and limited in scope, this suggested RAPID-release and spinning disc confocal microscopy were tools that could give insight into the behaviour of chromatin domains at these time scales. However, when analysing data from later in the time-series I observed that the labelled domains were suffering photo-bleaching. Moreover, nuclei were suffering deformations that started to manifest between 40 and 60 minutes, and that these exacerbated further as imaging progressed. Nuclei at the beginning of the time series presented an oblate spheroid shape, sitting on the bottom of the slide and fitting comfortably within the 10 μm cross-sectional imaging window, whereas towards the end of the imaging period their shape had morphed into a sphere that could no longer be observed in its entirety within the 10 μm Z-space (figure 3.8).

I postulated that the photo-bleaching of EGFP stemmed from the intensity of the laser, and relatively long exposure time used. I also attributed the deformation of nuclei to photo-toxicity caused by the stated imaging conditions. Therefore, this limited the use of spinning disc confocal microscopy to relatively short time periods.

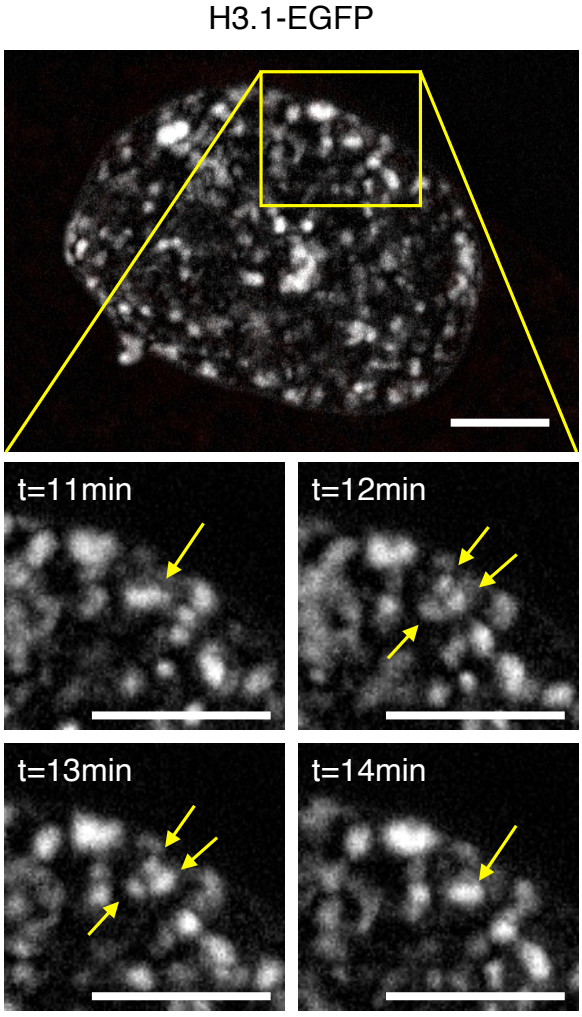

Figure 3.7: Examples of dynamic chromatin domains. In the time-span of 3 minutes one chromatin domain split into 3 different resolvable domains and converged back into one single domain. Scale bar, 5 μm.

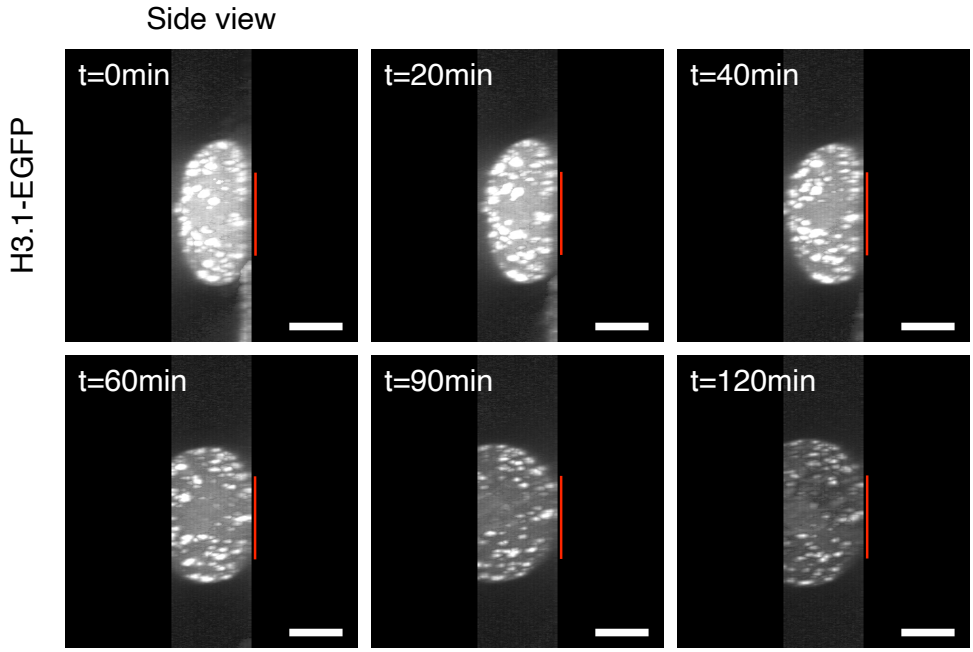

Figure 3.8: Effect of extended imaging on cell structure using confocal microscopy. Cells imaged for 2h under a spinning disc confocal microscope suffered nuclear deformation, causing the nucleus to partially leave the 10 μm-deep imaging window. Scale bar, 10 μm. Red line indicates the bottom of the imaging well.

3.4 Lattice light sheet microscopy as a method for data acquisition

To avoid the problems described above, I employed lattice light sheet microscopy (LLSM). Confocal microscopy operates by illuminating the entirety of the sample and collecting images from a particular Z-plane at one time, this means that to collect images from an n number of planes, the entire sample (and consequently, every plane) must be illuminated n times for every time point. Lattice light sheet microscopy, however, relies on the sole illumination of the plane being captured, this means that at each time-point, each imaging plane is illuminated once. Furthermore, lattice light sheet microscopes require exposure times tens of times lower than those of confocal microscopes for each capture, reducing even further the exposure of a sample to laser. I expected that this significant reduction in laser exposure would allow for long-term imaging of nuclei without significant bleaching of fluorophores and nuclear deformation.

Indeed, I observed that photo-bleaching was reduced to lower levels, and nuclear deformation no longer took place. Whereas spinning disc confocal microscopy caused nuclear deformation after 40 minutes of laser exposure, LLSM did not induce any changes to the nuclear integrity even after 2h of imaging. In fact I was able to image cells for as long as 3h without nuclei showing signs of swelling, allowing true long-term imaging of cells (figure 3.9).

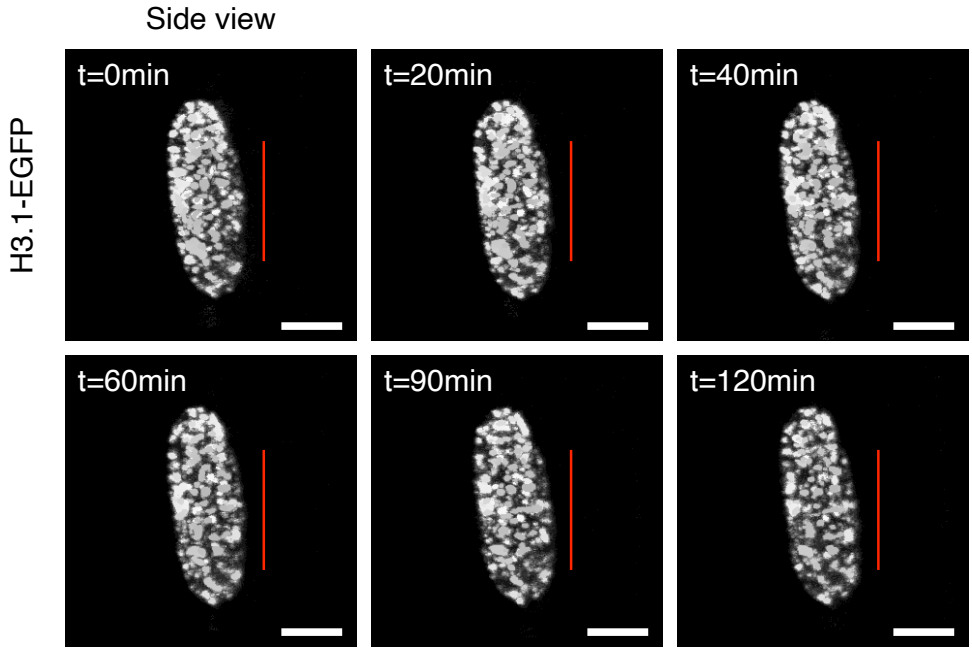

Figure 3.9: Effect of extended imaging on cell structure using lattice light sheet microscopy. Cells imaged for 2h in the lattice light sheet microscope do not suffer nuclear deformation, and photo-bleaching is significantly reduced. Scale bar, 5 μm. Red line indicates the bottom of the imaging well.

3.4.1 Exploring parameters of LLSM for chromatin domain imaging

Due to the reduced bleaching and photo-toxicity, it was possible to increase the temporal resolution and resolution in the Z-axis in my images. I attempted an array of different combinations of imaging parameters in several iterations (table 3.1) to try to optimise data collection.

I was able to increase temporal resolution from 1 minute to 30 seconds, and resolution in the Z-axis was increased 10 fold, from 1 μm to 100 nm. Because the objective is tilted at an angle of 57.2 degrees, a movement of 0.3 μm translates into an effective movement of 0.1 μm in the Z-axis. Furthermore, I increased the imaging window from 10 μm to 18 μm in case events such as mitosis, that lead to a change in cell dimensions, took place, so it would be possible to observe them in their entirety (table 3.2).

An important difference betIen confocal microscopy and LLSM, however, is the necessity for thermal equilibration of the sample and its holder prior to imaging. I observed that under certain circumstances, when imaging for longer than 30 minutes, the sample lost focus by drifting out of its focal plane. I postulated that this was due to the thermal expansion of the sample holder when inserted into the imaging chamber. The holder is made of surgical grade steel and suffers an increase in temperature from 20 degrees to 37 when inserted in the LLSM. This was not a phenomenon that had to be taken into consideration when imaging with the confocal microscope.

This issue was solved by allowing the sample to sit on its holder in the imaging chamber for 1h prior to the start of image acquisition. This period was sufficient to increase the holder's temperature to 37 degrees and eliminate drift, as it is possible to observe in figure 3.10.

The different iterations of imaging parameters and the thermal equilibration of the sample holder are a good illustration of the optimisation process that took place for the employment of LLSM in my research. This was especially important because this technique had never been employed at these time-scales until this point.

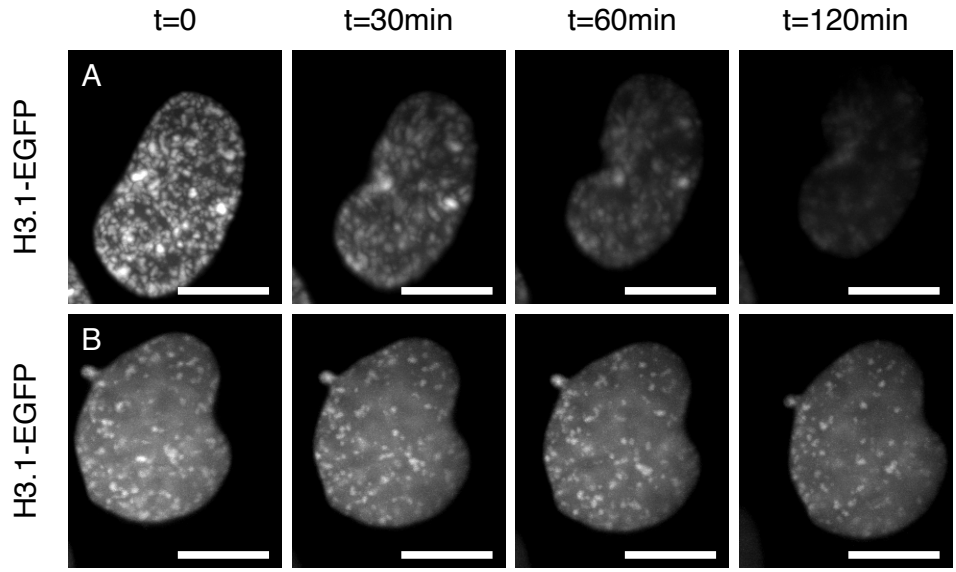

Figure 3.10: Effect of sample holder's thermal expansion on extended LLSM imaging. Thermal expansion of the sample holder generates drift from the focal plane that leads to a loss of focus, and therefore, renders the images collected after 20 minutes inadequate for domain dynamics analysis. **A**, Cell imaged without thermal equilibration prior to time-series capture. **B**, Cell imaged after thermal equilibration prior to time-series capture. Scale bar, 10 μm.

Parameters	First attempt	Second attempt	Final parameters
Laser power	1%	minimum	minimum
Number of planes	130	130	180
Exposure time (ms)	35	35	35
Step size (Z-axis, μ m)	0.5	0.3	0.3
Time-step (s)	60	30	30
Max. imaging time (h)	3	3	3

Table 3.1: Parameters attempted for long-term imaging of cells to increase the volume of data acquired whilst reducing bleaching and improving temporal resolution.

Parameters	Confocal	LLSM
Laser power	4%	minimum
Imaging window	10 μm	18 μm
Exposure time	180ms	35ms
Z-axis resolution	1 μm	0.1 μm
Temporal resolution	60s	30s

Table 3.2: Comparison between the parameters and capabilities of spinning disc confocal microscopy and those of LLSM.

3.4.2 Processing of LLSM data post-acquisition

Data deskew

The first step in processing LLSM data is to deskew each stack of images corresponding to each of the recorded time-points. Because the objective lens sits at a 57.2 degree angle from the horizontal plane, each plane in the Z-axis must be adapted, otherwise, when compiling a 3D image, these would manifest an angled skew of the same order. To deskew a Z-stack, images are shifted in accordance to the lens angle, and returned to a format that is faithful to the sample's true spatial characteristics.

Image deconvolution

From the deskewed data set I looked to increase the sharpness of the image, ensuring that the structures in which I was interested could be more easily discerned from the background and between themselves. This process relies on a calculated point spread function (PSF) generated by Slidebook, to infer the parts of the image that were the result of light diffraction, and which parts of the image correspond to actual cellular structures. This technique lead to the generation of sharper images where the labelled structures could easily be resolved from the background, but more importantly, this step made possible to resolve structures that sat close to each other and that would not be able to be resolved otherwise (figure 3.11).

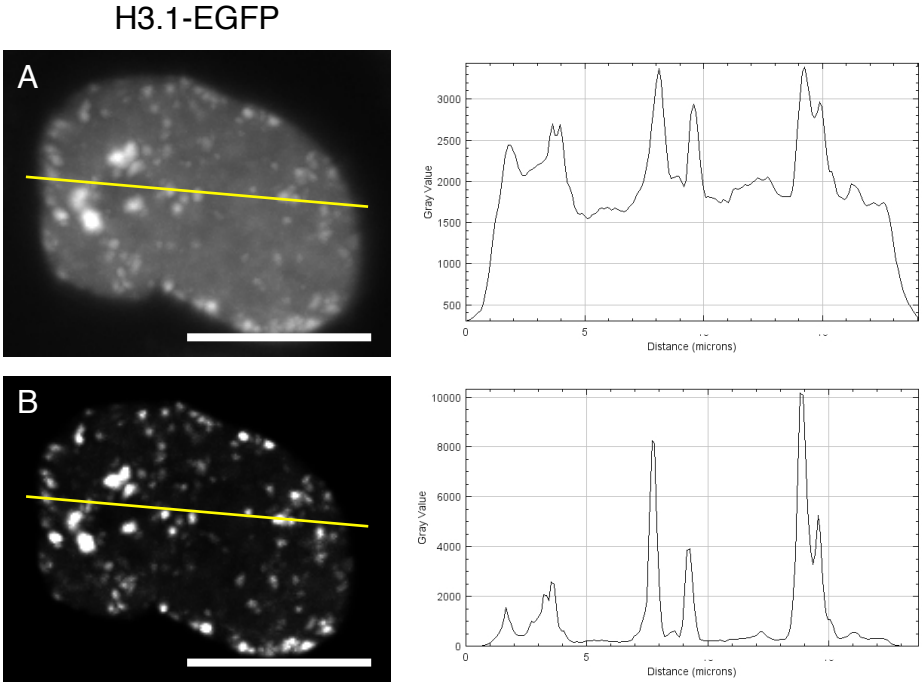

Figure 3.11: Deconvolution of acquired images. Deconvolved images present lower background than their non-deconvolved counterparts. Furthermore, chromatin domains are better resolved and, therefore, easier to identify in the nuclear space after the deconvolution process is applied. The yellow line indicates the plane whose profile is depicted in the right-hand side graphs. Scale bar, 10 μm.

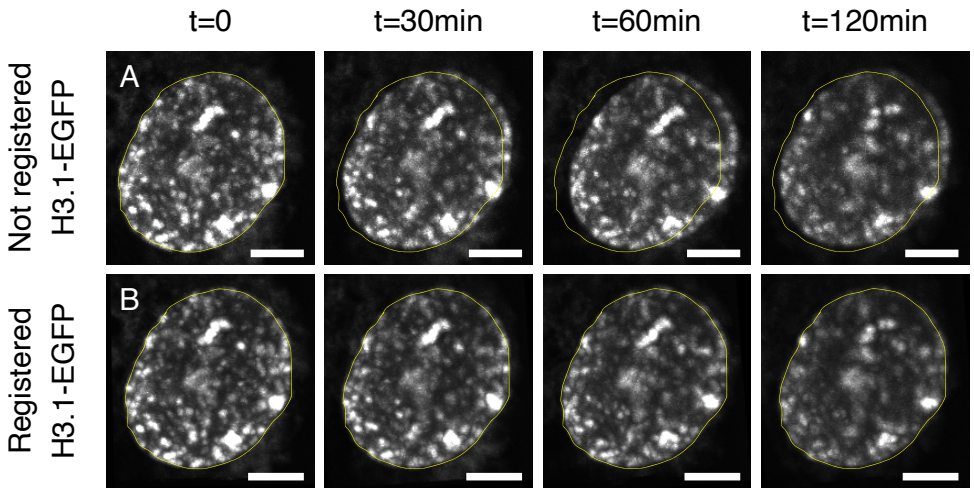

Figure 3.12: Registration of LLSM time series. Data sets that are processed through descriptor-based series registration present a static nucleus frame-by-frame, instead of a global drift of the organelle throughout the time series. **A**, Time-series before image registration. **B**, Time-series after image registration. The yellows line represents the place where the nucleus sat at $t = 0$. Scale bar, 5 μm.

Image registration

The final step in processing LLSM data was the removal of drift generated by cellular movement. Tracking the coordinates of structures within the nucleus without taking into consideration this movement would lead to skewed dynamics. To eliminate the movement of the nucleus, I employed the descriptor-based series registration plug-in for *ImageJ* (Schindelin et al. 2012) to maintain the nucleus static in relation to its surroundings, eliminating that component from the dynamics of chromatin domains. The software works by generating a rigid model of the nucleus at each time-point and then aligning them all. Because the model used is rigid, this dictates that the nucleus is not distorted in order to align images across time points, but only repositioned in three dimensions to achieve this goal (figure 3.12).

Domain tracking

The final goal of acquiring and processing the data was to identify the labelled chromatin domains and track them through time, in order to extract information about their dynamics (figure 3.13). To achieve this I employed TrackMate (Tinevez et al. 2017).

Its output consists of the spatial coordinates of each domain at each point of the time-series, allowing for the analysis of the movement of each structure through time. It also allows the identification of split and merge events analogous to those observed in section 3.3, figure 3.7.

The identification of each domain is dependent on its dimensions, and to identify and link two domains as part of the same track it uses a cost matrix, where domains at subsequent time-steps are associated to the same track. Linking happens between the domains that present the lowest cost in the matrix. This cost is primarily dependent on the distance between the two in subsequent time-points where greater distances yield higher linking costs. Further to this, it is possible to confer extra costs to the linking of domains, depending on characteristics other than distance, for example, mean intensity of domains and estimated diameter, allowing for more faithful linking throughout the time-series.

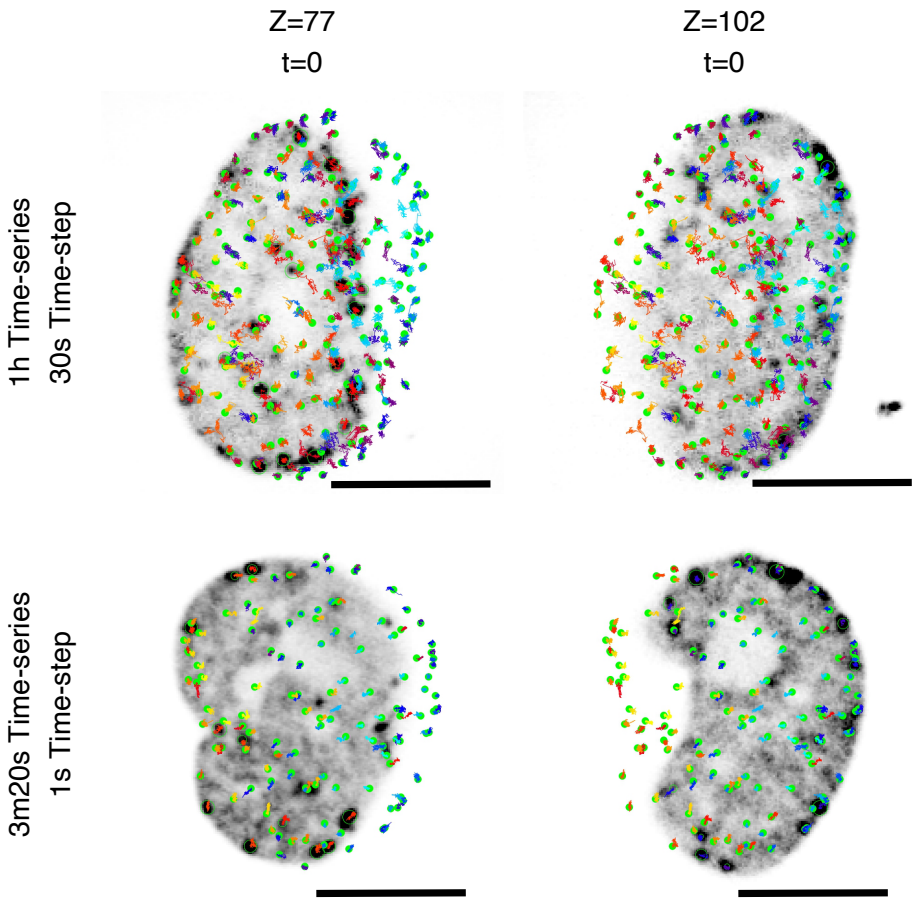

Figure 3.13: Track generation using TrackMate. Green dots represent the location of the centre of mass of domain at time = t, the coloured lines indicate the path each domain has explored throughout the entirety of the time-series. Due to imaging at an angle, some of the domain tracks appear outside of the representative slices shown. Scale bar, 10 μm.

3.5 Characterisation of the dynamics of chromatin domains

3.5.1 Spatial distribution of domains within the nucleus

To quantify the spatial distribution of chromatin domains I calculated the distance between each domain and the closest point of the nuclear periphery. I defined the nuclear periphery by generating a convex hull of the cloud of points, comprised of all the labelled chromatin domains that existed within the nucleus. A convex hull is the smallest convex volume that contains all points in a cloud. It generates a series of triangles using the outer most points, such that the volume of this envelope is minimised whilst containing all points. The convex hull for each cell was formed of approximately 60-70 points (domains) and was generated from their coordinates at $T = 0$, and remained static throughout the time-series to allow the domains that were part of its generation to migrate in relation to it (figure 3.14). I employed this technique due to the high number of domains that sit at the very edge of nuclei. My observations showed that a great number of these domains did not move in relation to the nuclear envelope, which allowed for the calculation of convex hulls that were a good approximation to the location of the nuclear envelope. The lack of mobility in peripheral domains may also imply that many of the labelled domains could have a physical association with the nuclear lamina itself.

My data showed that the average of median location of the labelled chromatin domains across all time points was within 100 nm of the periphery of the nucleus (33 nm long-term and 43 nm short-term imaging, figure 3.15). This was consistent with what I observed in the images collected both in my preliminary data (figure 3.1) and the 3D images of nuclei. It was also possible to observe that at distances greater than 300 nm the number of domains was kept low but constant, suggesting that, even though late replicating domains generally sat in the periphery of the

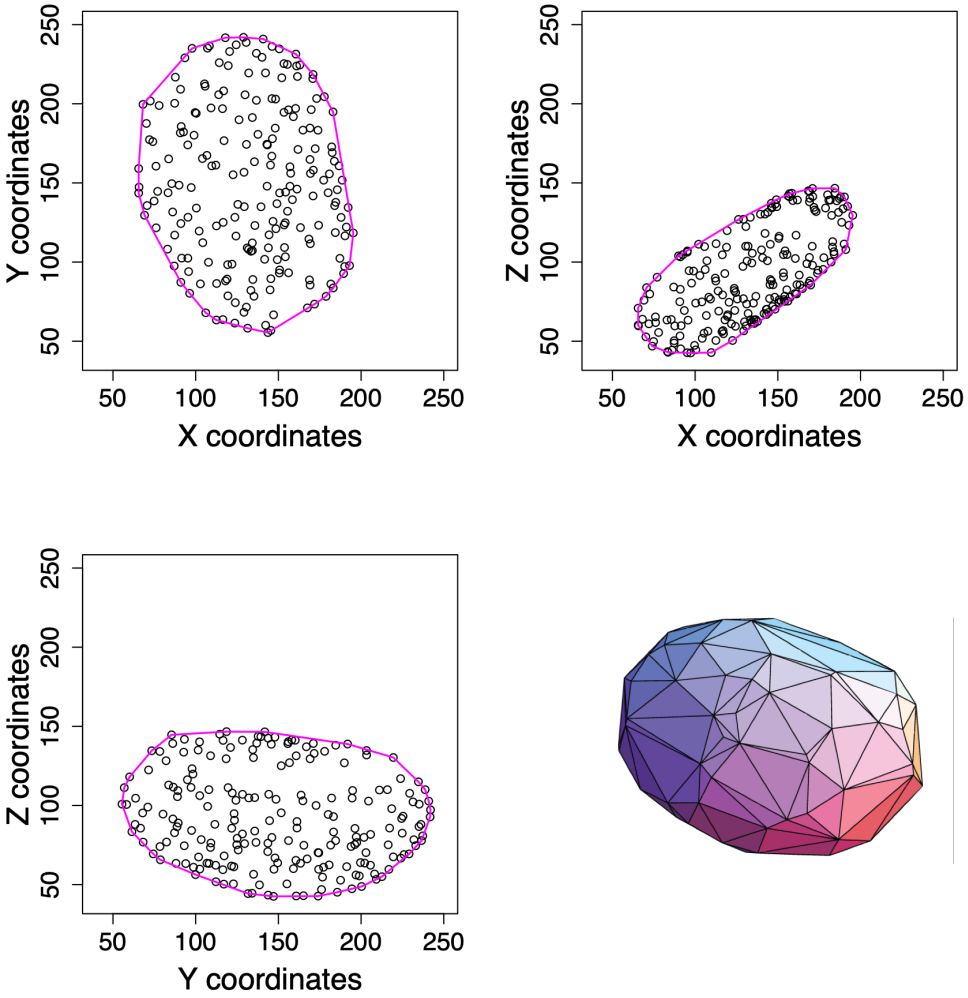

Figure 3.14: Convex hull generation. The convex hull connects the outermost points of a cloud and generates a convex polygon that resembles the nucleus. The first three tiles show the application of a convex hull to a long-term imaged cell, displayed according to all three dimensions. Bottom-right tile shows an illustrative 3D convex hull (adapted from *plotting - Convex hull in 3D - Mathematica Stack Exchange* 2021).

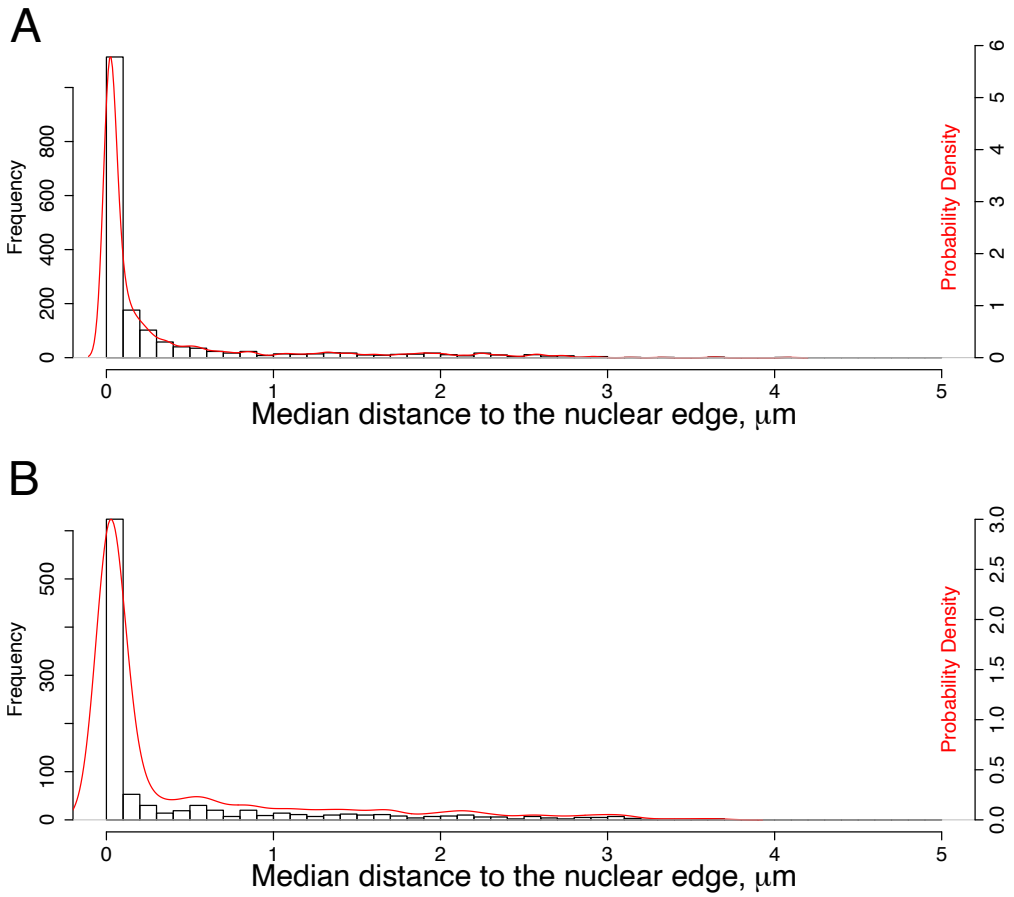

Figure 3.15: Median distance of chromatin domains to the periphery of the nucleus. **A**, **Long**-term imaging, 30 seconds time-step, 1h time-course. **B**, **Short**-term imaging, 1 second time-step, 3 minutes and 20 seconds time-course.

nucleus, some were located in the centre (figure 3.15). Central domains often associated with nucleoli, appearing to be anchored to these structures, however, some did not seem to be associated with any discernable nuclear structures (figures 3.3 and 3.11).

3.5.2 Splitting and merging events

One of the first dynamic events witnessed in my preliminary data was chromatin domains coalescing together and moving apart (figure 3.7). I looked to confirm that these events could be observed using LLSM. I found that they were still observable using this method, as evidenced in figure 3.16. I also intended to confirm that TrackMate could record them

faithfully. Through manual curation, I observed that these events were recorded by the software as merging and splitting events of the tracks it attributed to each chromatin domain.

Long timescales

When imaging cells for 1h and with a time-step of 30 seconds (long-term imaging) I observed that the majority of tracks (76.6%) did not present splitting or merging events, 13% exhibited both, 5.4% exhibited only splitting events, and 5% of tracks exhibited only merging events (figure 3.17 A). Of the tracks that presented this behaviour, approximately half only experienced it once. Tracks that split or merge multiple times became increasingly less frequent as the number of splits and merges mounted (figure 3.17 C). I also observed that tracks tendentiously split and merged a similar number of times *e.g.* if a track presents 3 merging events, it is likely that it will also present 3 splitting events. However, some merging events stemmed for the convergence of more than two tracks more often than the splitting of one track gave rose to several domains (figure 3.17 B). This asymmetry can be illustrated by the fact that within the universe of tracks that exhibited this behaviour, the average number of merging events was 1.63, and in the case of splitting events, it was 1.56, suggesting that in general there were more associating tracks than splitting ones.

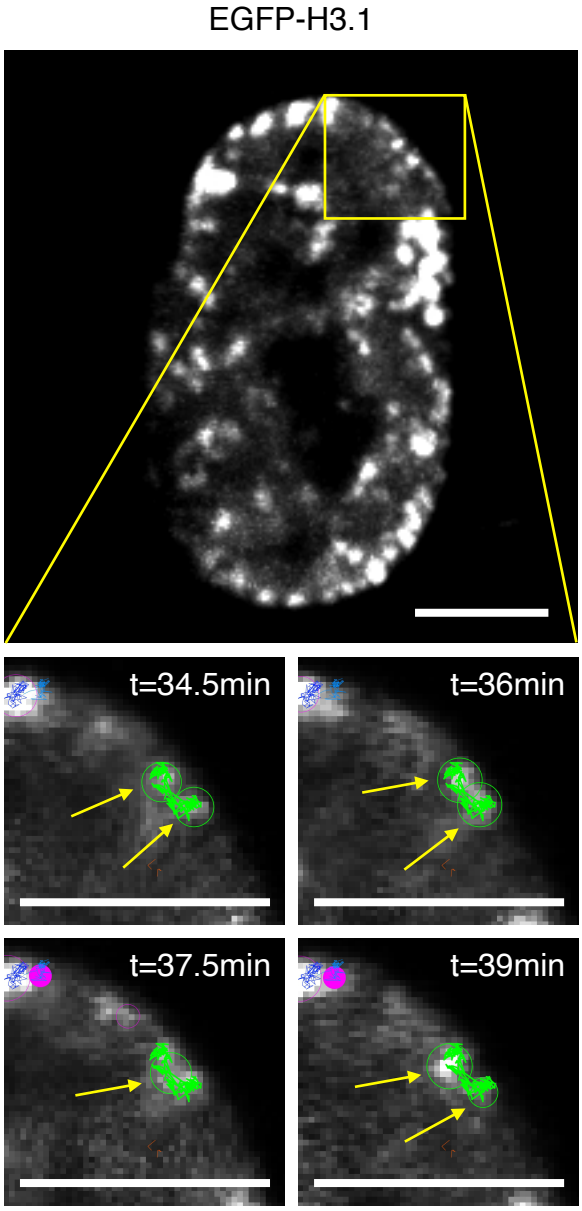

Figure 3.16: Chromatin domain coalescence and divergence. The track contains two distinct domains until $t = 37.5mins$, upon which they merge. After that event, the track splits into two different domains once again. The location of the detected domains is denoted by the green circles. Magenta circle denotes a labelled domain located outside the current plane. Scale bar, 5 μm.

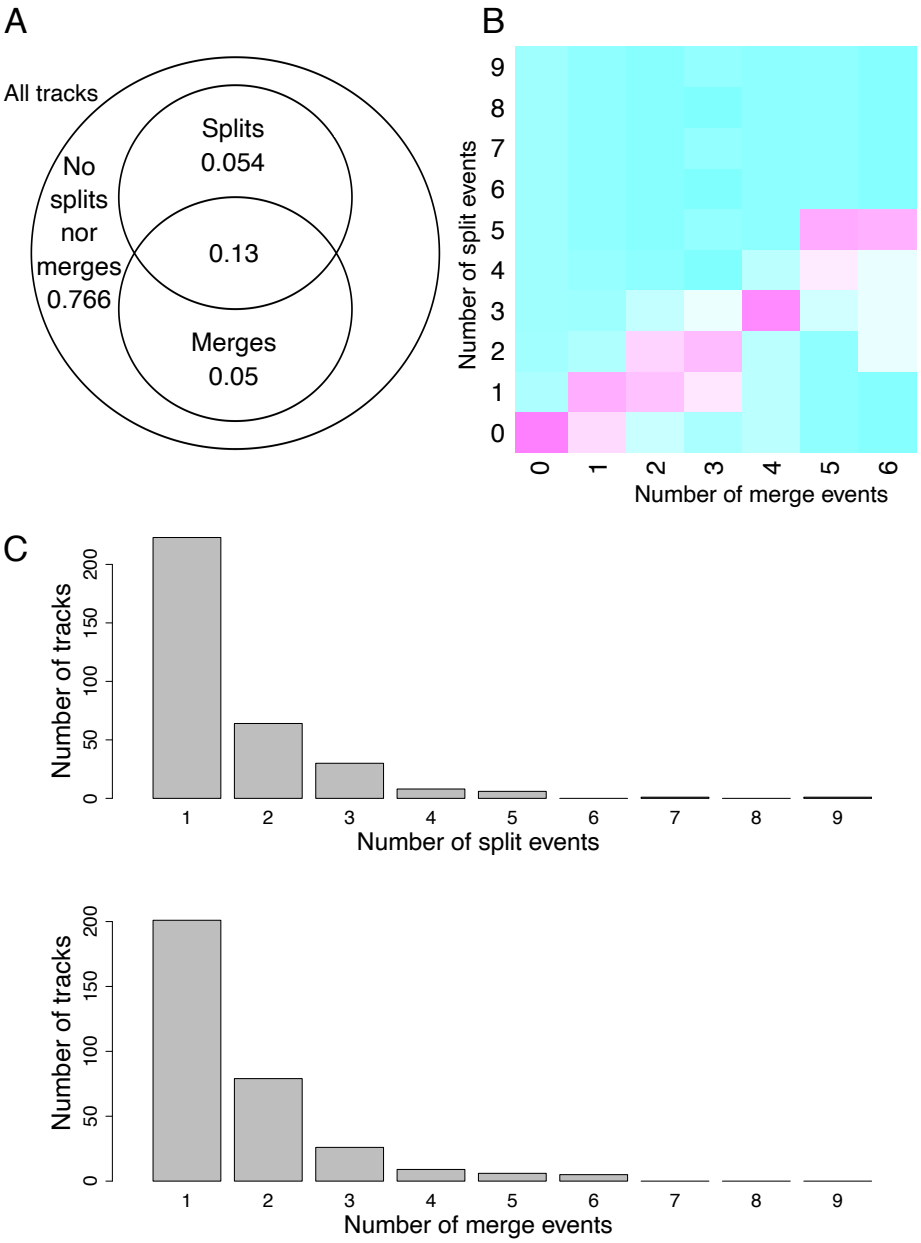

Figure 3.17: Splitting and merging events on **long** imaging time-scales. **A**, Proportions of chromatin domains that experience none, both, only splitting, or only merging events. **B**, Relationship between number of splitting and merging events. Magenta denotes a high percentage of split events of y magnitude for tracks that presented x number of merge events, and cyan denotes the contrary. **C**, Frequency of the number of splitting and merging events within the population of chromatin domains that experience this phenomenon.

Short timescales

When imaging cells for 3 minutes and 20 seconds and with a time-step of 1 second (short-term imaging) I observed that the majority of tracks (81.3%) did not present splitting or merging events, 14% exhibited both, 2.8% exhibited only splitting events, and 1.9% of tracks exhibited only merging events (figure 3.18 B). Of the tracks that presented this behaviour, it was more common for it to happen only once, with more events become increasingly rarer. However, splitting/merging tracks were proportionally less frequent than what was observed in long-term imaging (figure 3.18 A). On the other hand, the average number of splitting and merging events per track was greater in this case, increasing from 1.63 to 2.09 for merging and from 1.56 to 2.04 for splitting events (when comparing long and short-term imaging). As before, I also observed that tracks tendentiously split and merge a similar number of times, however, towards higher numbers of events the linear correlation between the two started to change, becoming less predictable (figure 3.17 C).

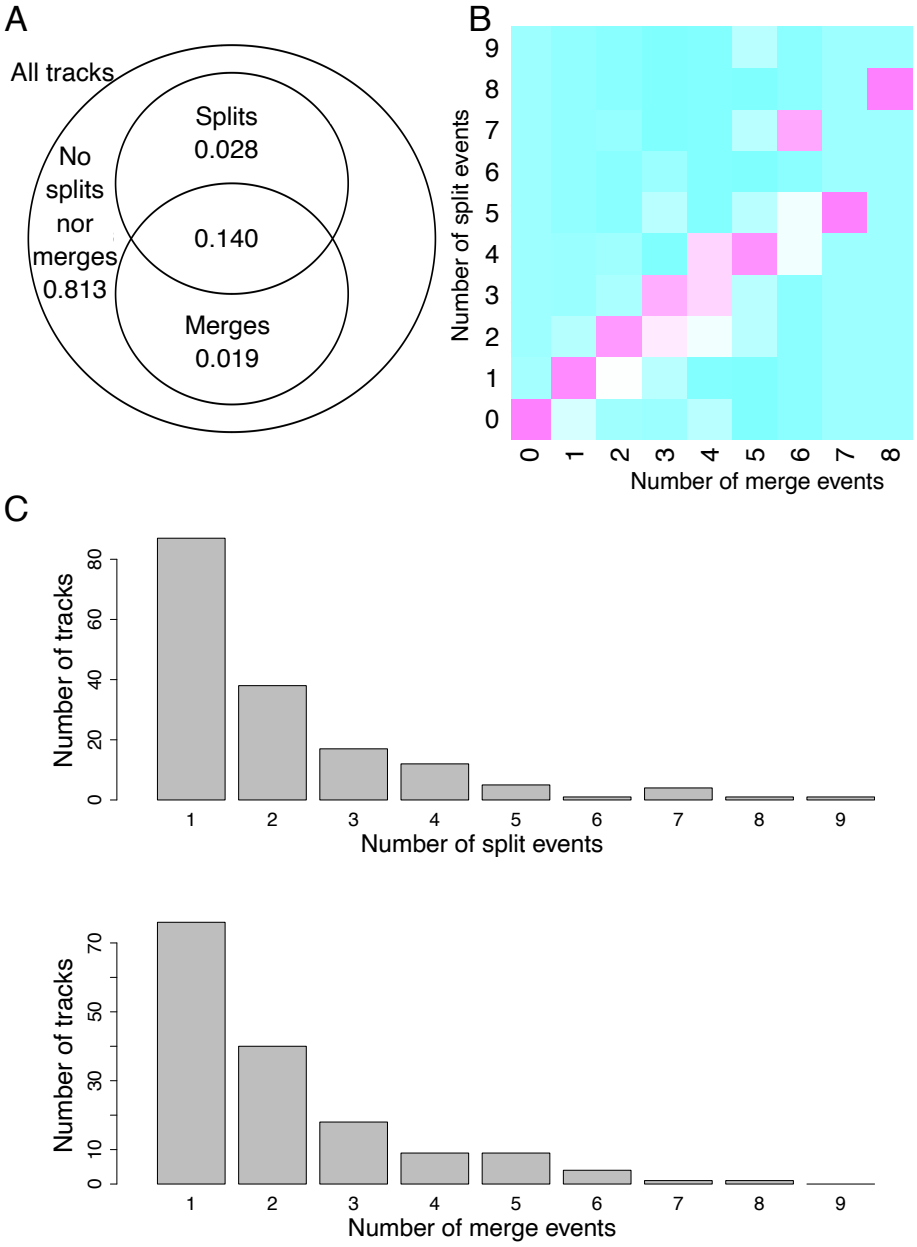

Figure 3.18: Splitting and merging events on **short** imaging time-scales. **A**, Proportions of chromatin domains that experience none, both, only splitting, or only merging events. **B**, Relationship between number of splitting and merging events. Magenta denotes a high percentage of split events of y magnitude for tracks that presented x number of merge events, and cyan denotes the contrary. **C**, Frequency of the number of splitting and merging events within the population of chromatin domains that experience this phenomenon.

3.5.3 Dynamics - Velocity, track length, and maximum displacement

To characterise the dynamics of chromatin domains I extracted information about their (1) average velocity across all time-steps, (2) the length of their tracks (defined as the sum of the distances between all consecutive time points), and (3) the maximum displacement, defined as distance between the two points of a track that sit farthest apart.

I observed that on long-term imaged domains, the mean average velocity was 0.231 $\mu m/min$, the average track length was 11.455 μm, and the average maximum displacement was 0.791 μm (figure 3.19). On short-term imaged domains the average mean velocity was 4.180 $\mu m/min$, the average track length was 13.030 μm, and the average maximum displacement was 0.507 μm (figure 3.20).

It was interesting to note that short-term imaged domains seemed to present higher levels of mobility than expected. They had higher velocities, greater track lengths and a higher than expected maximum displacement. I anticipated the opposite, since they were imaged for a fraction of the time of their long-term imaged counterparts (3 minutes and 20 seconds *versus* 1h). I believe that this discrepancy can be attributed to the higher sampling speed that short-term imaged domains experience, this attributed a more significant component of thermal noise to the calculated speed and track length. As short-termed imaged domains were imaged 60 times per minute, their position was recorded at the same rate, therefore, any displacement caused by thermal noise would be also recorded 60 times per minute. In the end, the accumulation of shorter movements equates to a high calculated track length. On the other hand, long-term imaged domains were sampled twice per minute, having the movement attributed to thermal noise only sampled as many times, as a consequence, the thermal component of calculated movement of the domains is less significant. This means, short-term and long-term sampling provide information about two distinct types of movement, the former informs on very short term fluctuations in position, whereas the latter

provides insight into how chromatin domains behave in long time-scales.

I also observed that all three metrics presented a positively skewed distribution, suggesting that even though the great majority of domains behaved similarly to each other, there were those that fell outside the expected range. Therefore, I assumed that there were two distinct populations of dynamic domains, one whose maximum displacement seemed to approximately fit a normal distribution, and another whose maximum displacements caused the skew in the distribution. Tracks above a maximum displacement threshold of 1.2 μm for long-term, and 0.8 μm for short-term imaged domains (approximately double the value at which the probability density is maximum) were termed High Mobility Domains (HMDs), and in contrast, those falling below the threshold were termed Low Mobility Domains (LMDs), and some randomly selected tracks of HMDs and LMDs were manually analysed (see section 3.5.4 and figures 3.24 and 3.25 for further analysis).

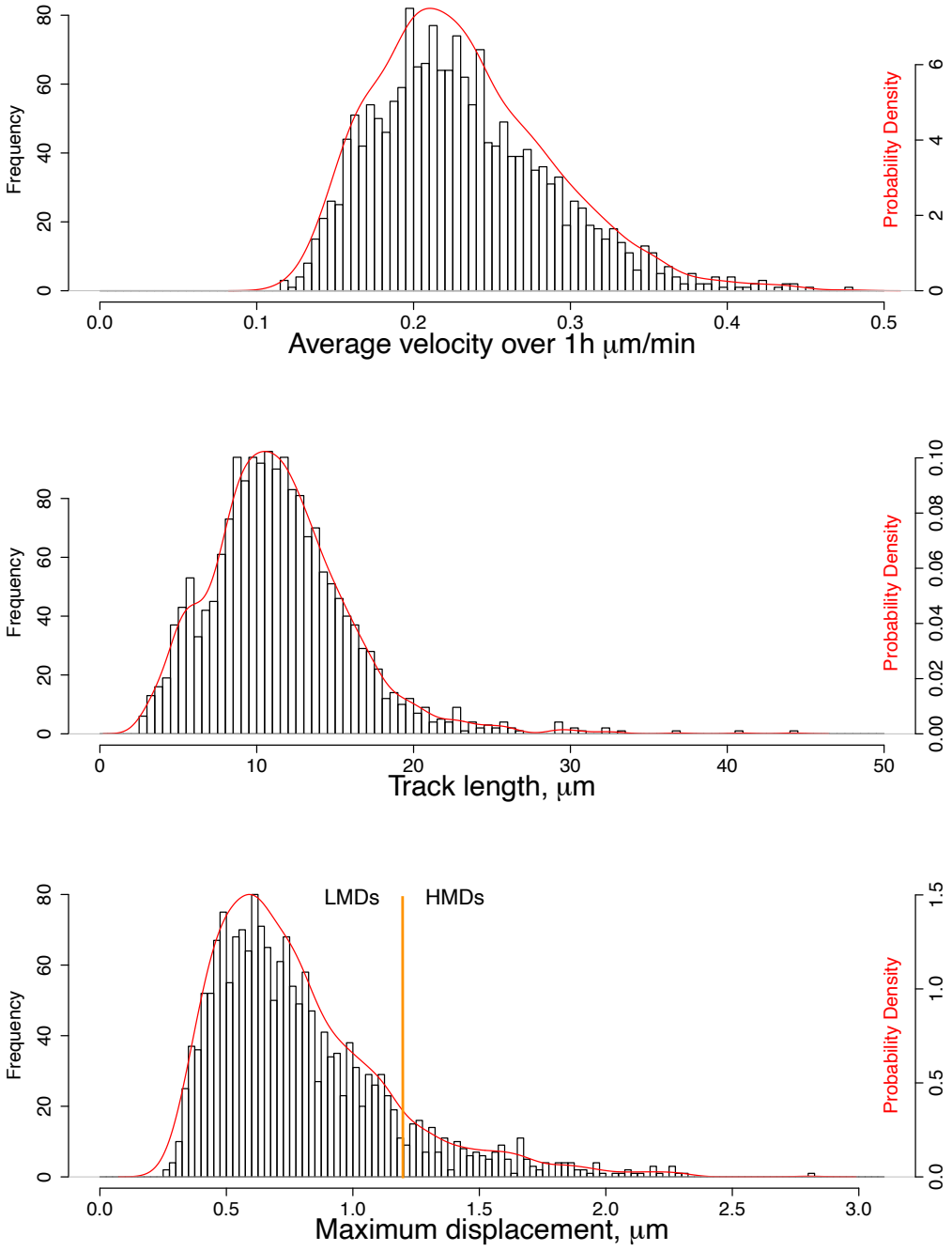

Figure 3.19: Velocity, track length and maximum displacement of chromatin domains in **long**-term imaged cells. Domains that present maximum displacements lower than 1.2 μm are termed Low Mobility Domains (LMDs), and domains that present maximum displacements greater than that threshold are termed High Mobility Domains (HMDs).

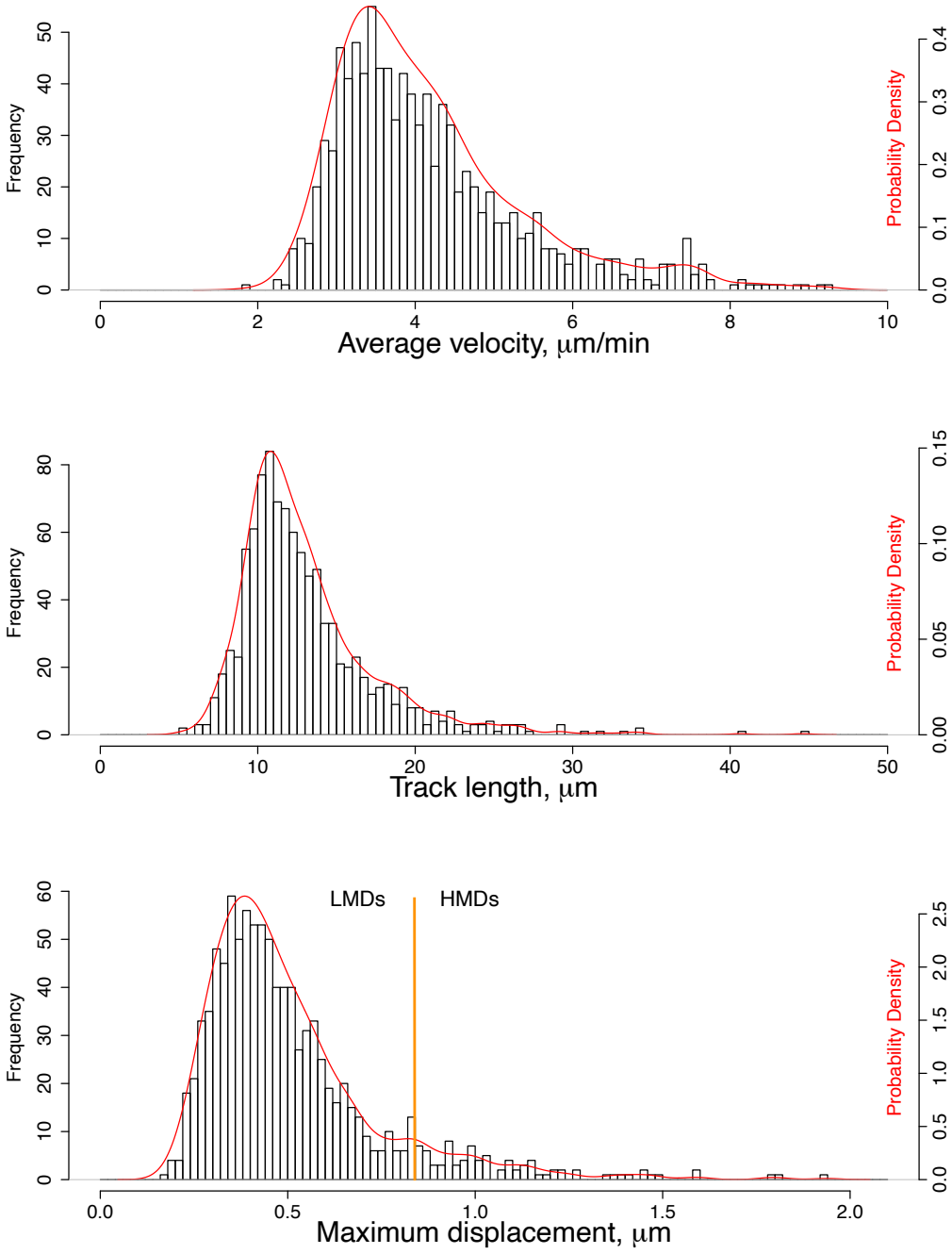

Figure 3.20: Velocity, track length and maximum displacement of chromatin domains in **short**-term imaged cells. Domains that present maximum displacements lower than 0.8 μm are termed Low Mobility Domains (LMDs), and domains that present maximum displacements greater than that threshold are termed High Mobility Domains (HMDs).

3.5.4 High mobility and low mobility chromatin domains

Location of the different populations

My first approach was to establish a relationship between the location of chromatin domains (in relation to the nuclear periphery) and their maximum displacement. I expected that if phenomena like anchoring to the lamina were taking place, domains would be more likely to present low mobility if peripherally located, conversely, domains sitting more internally would be tendentiously more mobile.

My data shows that the majority of chromatin domains labelled through our method sat peripherally within the nuclear space. This was to be expected taking into consideration that these are late replicating domains (figures 3.21 and 3.22). My data also showed that both LMDs and HMDs manifested themselves throughout the nucleus, however, LMDs were present in far greater numbers towards the periphery, translating into a lower median maximum displacement around this region. The median maximum displacement increased in locations not adjacent to the nuclear lamina, as HMDs became more abundant in relation to LMDs. This was especially clear in long-term imaged cells (figure 3.21). For example, the mean maximum displacement of domains located within 0.5 μm of the lamina was 0.67 μm, whereas this number was 0.85 and 0.83 μm for domains located between 0.5 and 1, and 1 and 1.5 μm, respectively, and broadly increasing thereafter. This suggests that the characteristic low mobility of LMDs may be the result of physical restraints that take place at peripheral locations, and that, at internal parts of the nucleus, these restrains are not as significant.

When imaging cells in the short-term, it was possible to observe that the distribution of chromatin domains presented a similar pattern to that of long-term-imaged cells, where the great majority of domains located to the periphery. In this case, however, a clear difference in mean maximum displacement between domains located adjacent to the nucleus, and in-

ternal domains had not yet developed. Domains located within 0.5 μm of the lamina had a maximum displacement of 0.44 μm, whereas this number was 0.47 and 0.46 μm for domains located between 0.5 and 1, and 1 and 1.5 μm, respectively (figure 3.22). This suggests that the effect of restraints on the movement of chromatin domains is not yet observable at this timescale since the median maximum displacement of domains was similar regardless of distance to the periphery. It also suggests that maximum displacements in the interior of the nucleus that exceed those seen in the periphery requires greater timescales, possibly in the 10s of minutes.

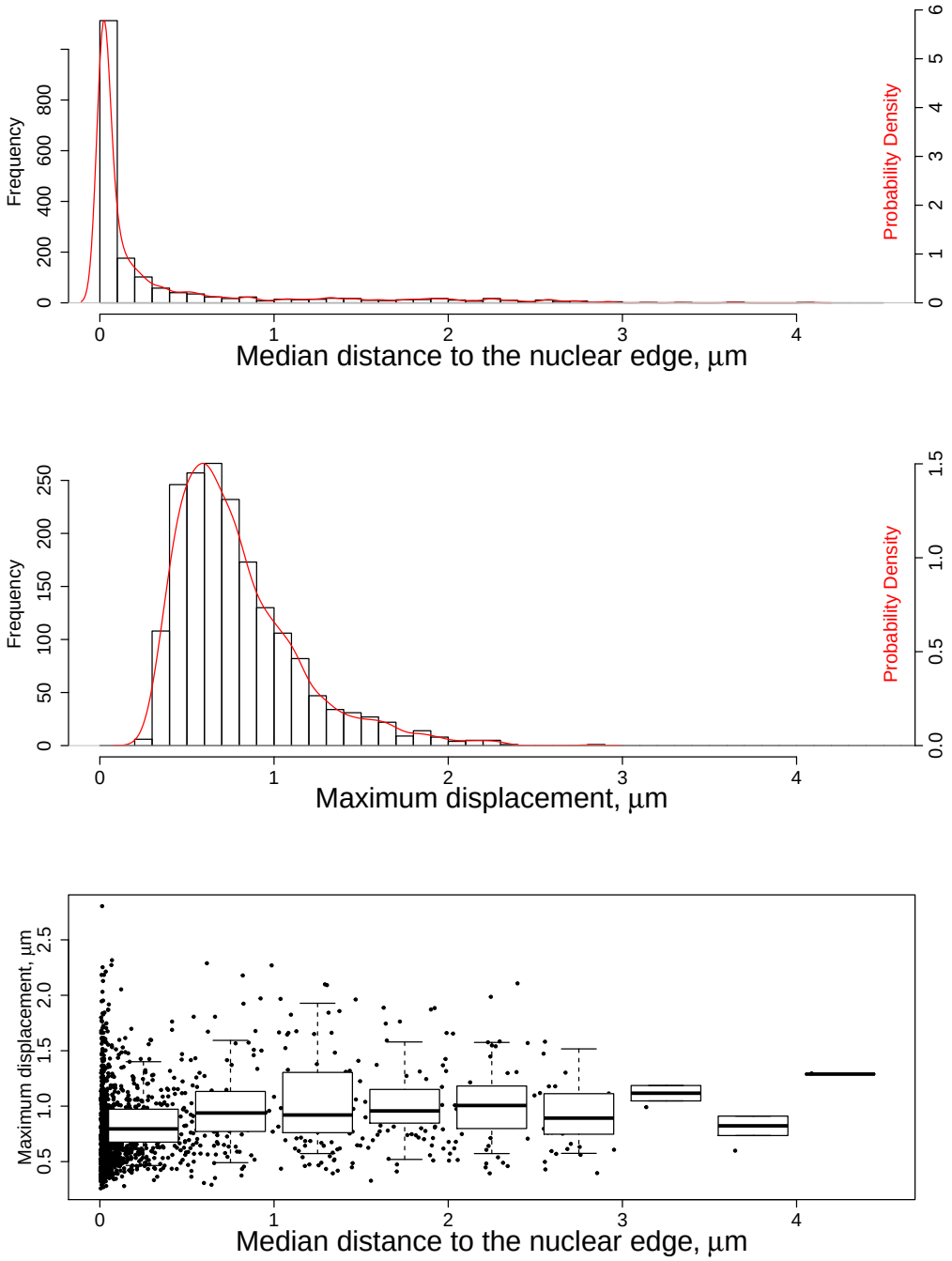

Figure 3.21: Relationship between distance to nuclear periphery and maximum displacement in **long**-term-imaged cells. Each box plotted encompasses an interval of 0.5 μm in distance from the nuclear periphery.

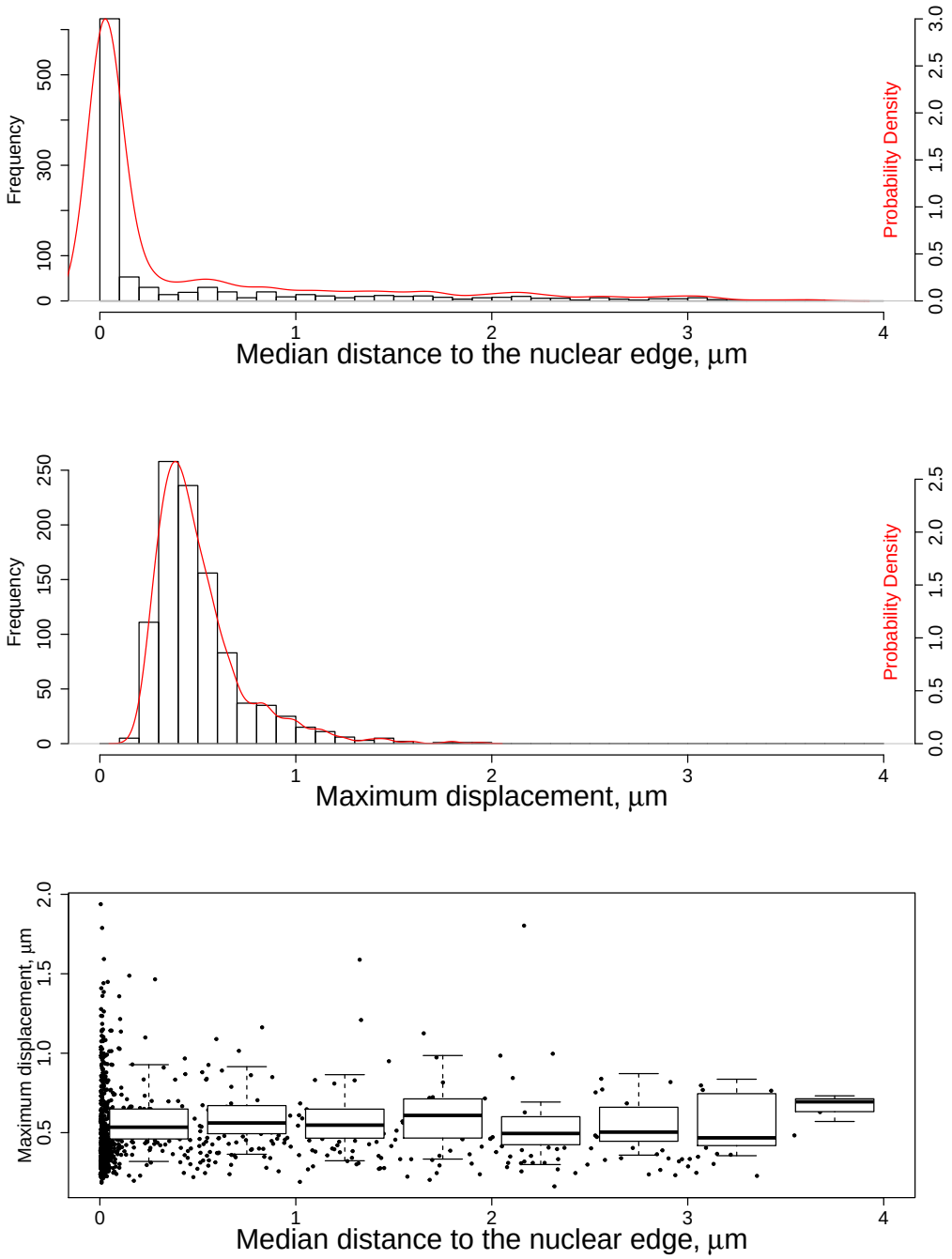

Figure 3.22: Relationship between distance to nuclear periphery and maximum displacement in **short**-term-imaged cells. Each box plotted encompasses an interval of 0.5 μm in distance from the nuclear periphery.

Examples of individual domain dynamics

For a more detailed analysis of LMDs and HMDs I looked at the tracks of 3 LMDs and 8 HMDs chosen at random in order to observe how the behaviour of the two populations differed. I observed that LMDs (**a**, **b**, and **c** in figure 3.24) remained in place and that their movement was limited to a space of approximately 300 nm in diameter after 1h of imaging (long-term imaging). Conversely, HMDs (**d** to **k** in figure 3.24) presented track lengths greater than 20 μm. The movements that HMDs experienced, although different in appearance, presented recurring patterns that were of interest.

It was common to observe domains moving in a particular direction over several minutes intercalated with periods of no significant movement (**d** and **e**), similarly, other domains such as **i** appeared static before rapidly changing locations and returning to a static state. I termed this type of movement an A-B movement since the domain moved from A to B, even if it experienced static periods. I observed domains that moved in a particular direction followed by periods of backtracking along the same route (**f** and **g**), I termed this an A-B-A movement. Some domains moved in a pattern which I described as A-B-C movement, where these would adopt discrete directions that changed multiple times (**h** and **j**). Finally, some HMDs presented motions similar to those of LMDs where there was not a discernable directionality to their movement, but exploring volumes with greater diameter, which I termed A movements. These observations suggest that HMDs are chromatin domains that experience forces that change their location over time, except for those domains like **k**, which seem to not have the same level of constraint as LMDs but also did not experience forces similar to those of other HMDs that actively alter their location.

I observed similar patterns on short-term-imaged cells (figure 3.25), although with lower maximum displacements. LMDs remained relatively static and no discernable difference was observed when compared to long-term imaged domains (domains **a**, **b** and **c**). The enhanced temporal

resolution also allowed me to observe the movement patterns of HMDs in greater detail. Domains **e**, **g**, and **h** are a good example of A-B movements, whereas **i** represents A movements. Backtracking (A-B-A movements) can be observed in domain **k**, and domains **d**, **f**, and **j** are good examples of A-B-C movement. These further support my observations above.

I looked to extract the mean squared displacement (MSD) of the entire population of domains, and that of the example domains. I assumed that the movement of domains could not be attributed to free diffusion since they are tethered by their position in the chromosome. However, I extracted this metric for several reasons: (1) to quantify the degree of restraint of chromatin domains *in vivo*, (2) to investigate how the movement of individual domains compares to the average, and (3) to investigate the dynamic phenomena observed on the HMDs.

The average MSD of the population of both the long-term and short-term imaged domains indicated that their movement was subdiffusive as predicted, the MSD curve tended towards a plateau as the calculation time step increased. The MSD of long-term imaged domains reached values greater than 0.2 μm^2 (figure 3.23 A) and short-termed imaged domains did not exceed 0.1 μm^2 (figure 3.23 B).

My data also showed that the MSD of the example long-term imaged LMDs selected remained low throughout the 1h time-course, not exceeding 0.1 μm^2 (**a**, **b**, and **c** of figure 3.24). I observed a similar pattern in the short-term imaged domains (figure 3.25) where LMDs presented MSD values of around half those of the population. This further suggests that LMDs face restraints to their movement as previously postulated.

LMDs MSD values contrasted greatly with those observed on HMDs, where the MSD reached values greater than 3 μm^2 and 1 μm^2, for long and short-term imaging, respectively. It was also possible to observe the resulting MSD associated with the different movement patters of HMDs. Domains that present A-B movements showed increases in MSD that cor-

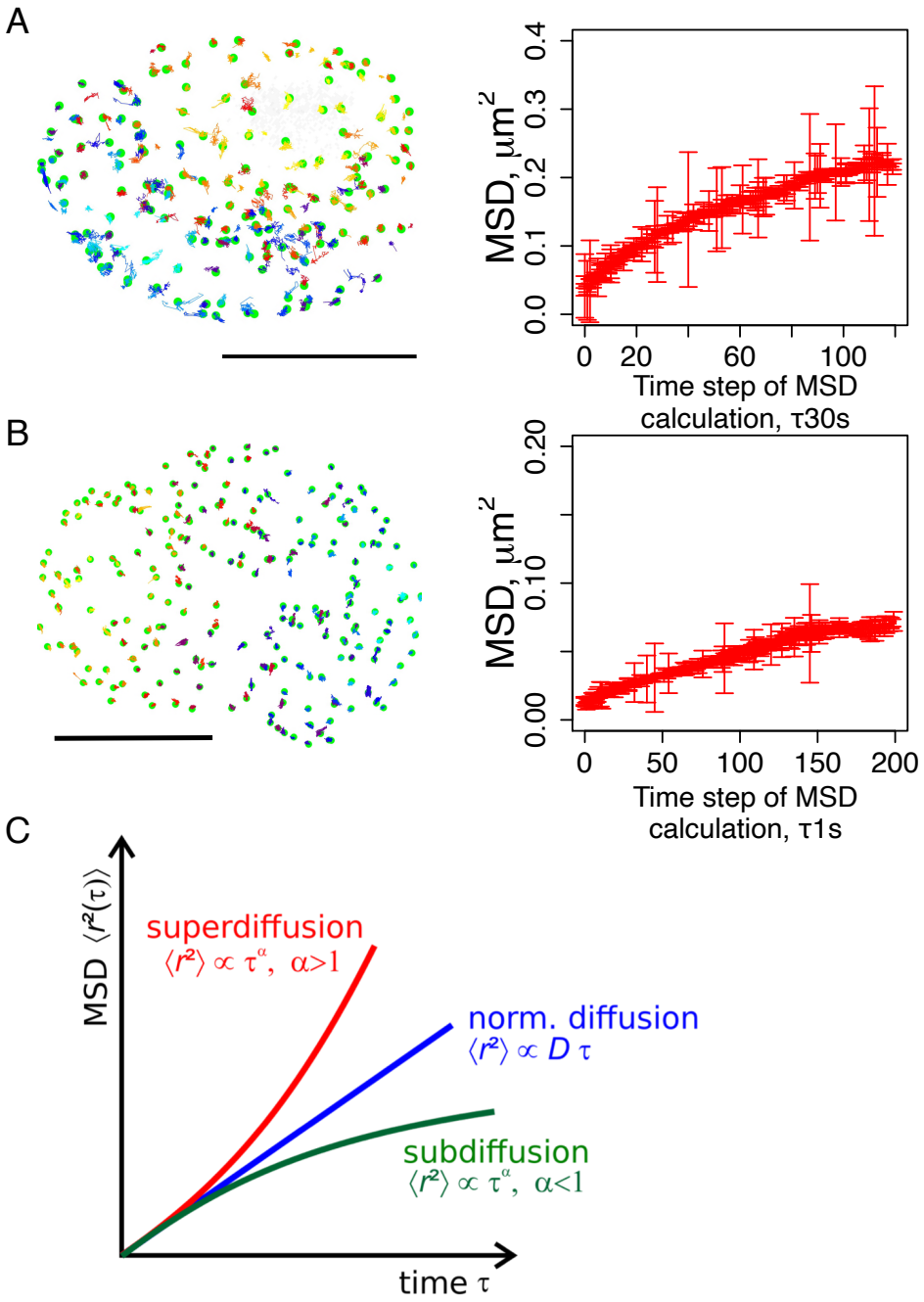

Figure 3.23: Chromatin domain MSD of **long** and **short**-term imaged cell populations. **A**, Example of domains and tracks identified in a nucleus imaged long-term, and the average MSD of the all chromatin domains analysed. **B**, Example of domains and tracks identified in a nucleus imaged short-term, and the average MSD of the all chromatin domains analysed. Scale bars, 10 μm. **C**, Profiles of the variation in MSD of a particle as a function of the type of the diffusion to which it is subject.

responded to the dynamic portion of the track, often displaying superdiffusion in these intervals, whereas plateaus in MSD could be seen when domains remained stationary, returning the movement to subdiffusion (**d**, **e**, and **i**, figure 3.24). When domains exhibited A-B-A movements, the MSD decreased during the periods where there was a reversal of direction, this was especially observable in **f** where the backtracking behaviour was more pronounced. However, this also took place when domains moved towards locations that were nearer to their initial position, even if this was not done along the path already explored, as evidenced in **h** and **j** (A-B-C movement). Interestingly, the MSD of domain **k** approximately followed that of the population average (A movement).

When analysing the MSD of short-term imaged domains (figure 3.25) I found a similar correlation between these movement patterns and changes in MSD. The observation that HMDs had a markedly greater MSD than the population average suggests that the movements of HMDs were likely to be a consequence of events in the nucleus that applied forces to these structures, and that their movement was a mixture of directed motion and confined diffusion. Conversely, the movement pattern of LMDs seemed to stem form physical constraints to the domains. Domains such as **k** (figure 3.24), however, seemed to sit somewhere in the middle, where there were constraints in place that prevented it from diffusing freely, however, not to the same degree observed in LMDs, but no forces seemed to be acting on them to generate movement in any particular direction.

I was also interested in investigating if HMDs had a preferred direction of travel in relation to the nuclear edge, *i.e.*, if there is a clear preference between travelling parallel or perpendicular to the nuclear lamina. To achieve this I calculated the distance between the domains in figures 3.24 and 3.25, and the convex hull of the nuclei to which they belonged. I did this at each time-point, and plotted their progression, together with the total displacement between each successive time-point.

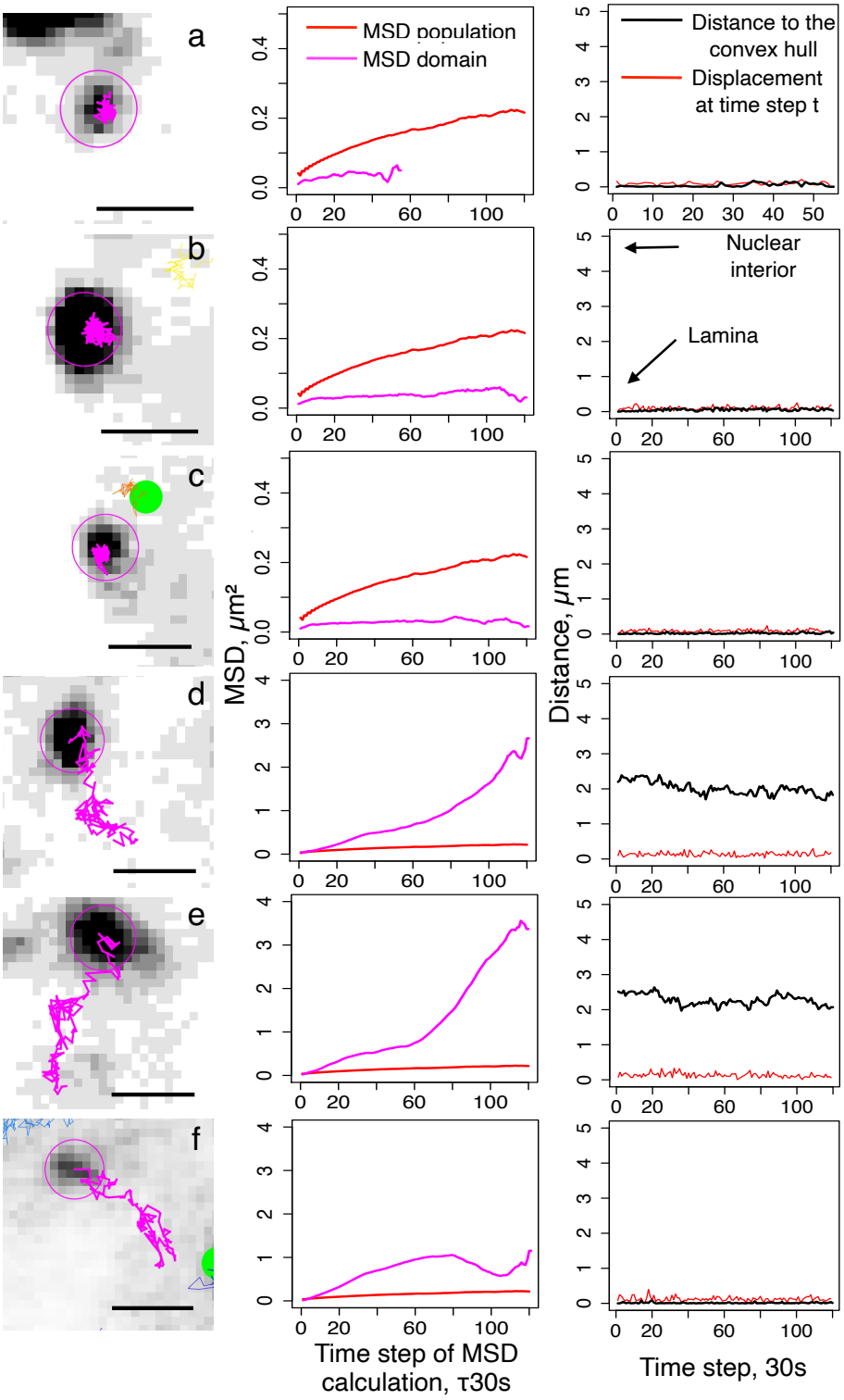
a
b
c
d
e
f
MSD population
MSD domain
Distance to the convex hull
Displacement at time step t
Nuclear interior
Lamina
MSD, μm²
Distance, μm
Time step of MSD calculation, τ30s
Time step, 30s

Figure 3.24

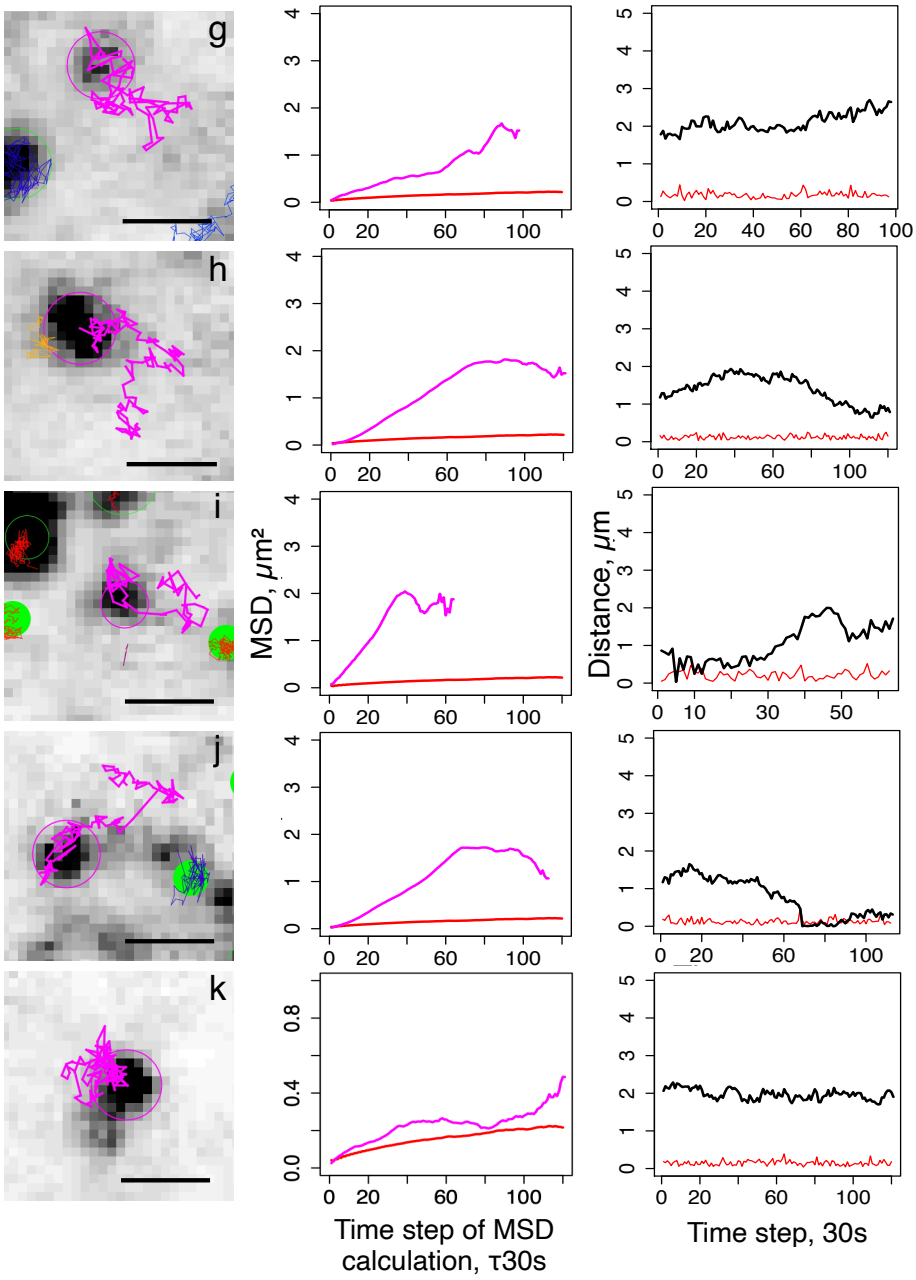

Figure 3.24: Dynamics of individual LMDs and HMDs, **long**-term imaging. Left side column displays the tracks of the randomly selected chromatin domains (magenta). Scale bar, 1 μm. Magenta circles represents position at $t = 0$, and green represents domains outside the visible plane. Middle column displays the mean squared displacement of the entire population of chromatin domains in red and that of the corresponding individual domains in magenta. Right side column displays the distance to the convex hull/nuclear edge (black) and displacement of the same domain between each consecutive time-point (red). LMDs: **a**, **b** and **c**. HMDs: movement type A-B, **d**, **e**, **i**; A-B-A, **f**, **g**; A-B-C, **h**, **j**; A, **k**.

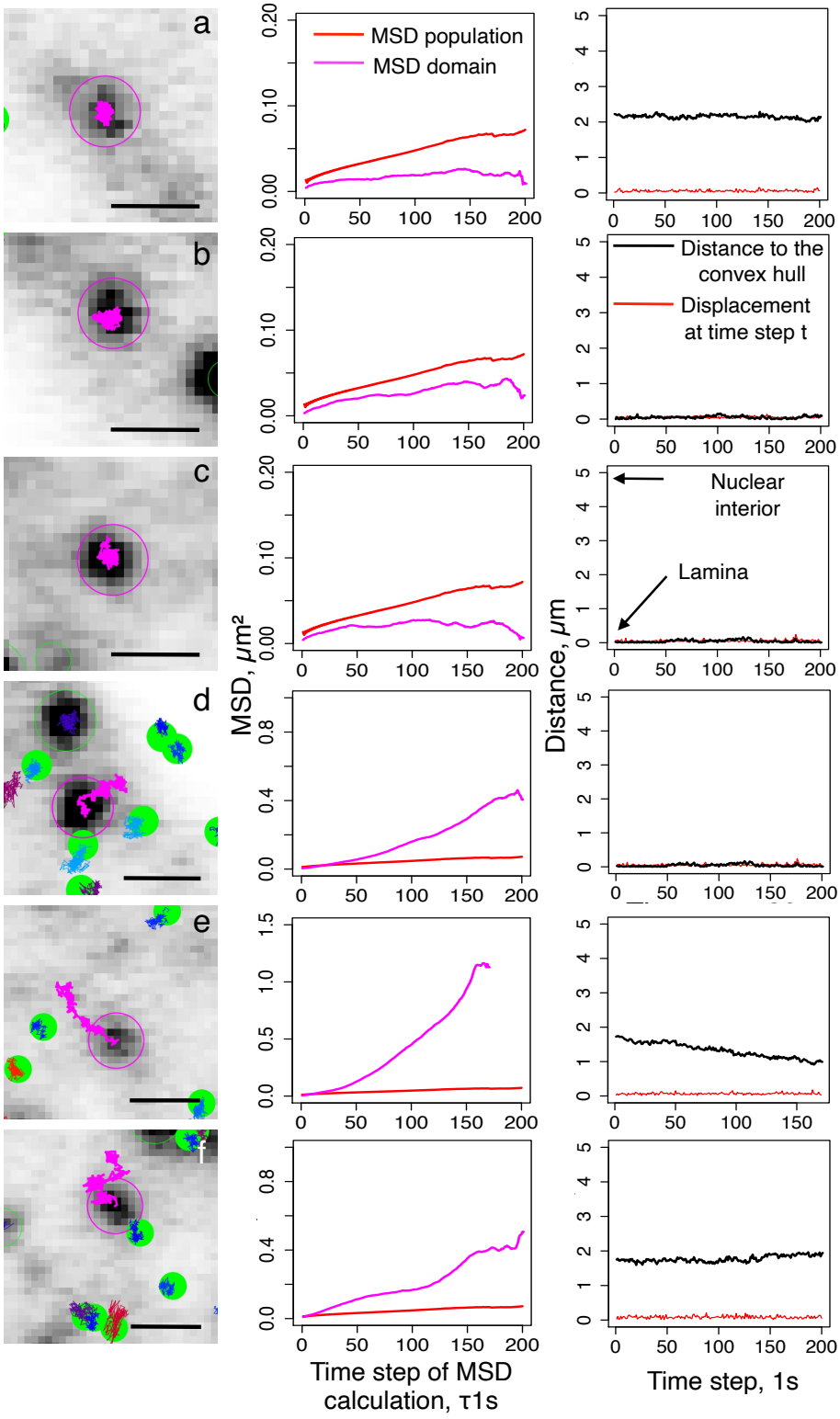
a
b
c
d
e
MSD population
MSD domain
Distance to the convex hull
Displacement at time step t
Nuclear interior
Lamina
MSD, μm²
Distance, μm
Time step of MSD calculation, τ1s
Time step, 1s

Figure 3.25

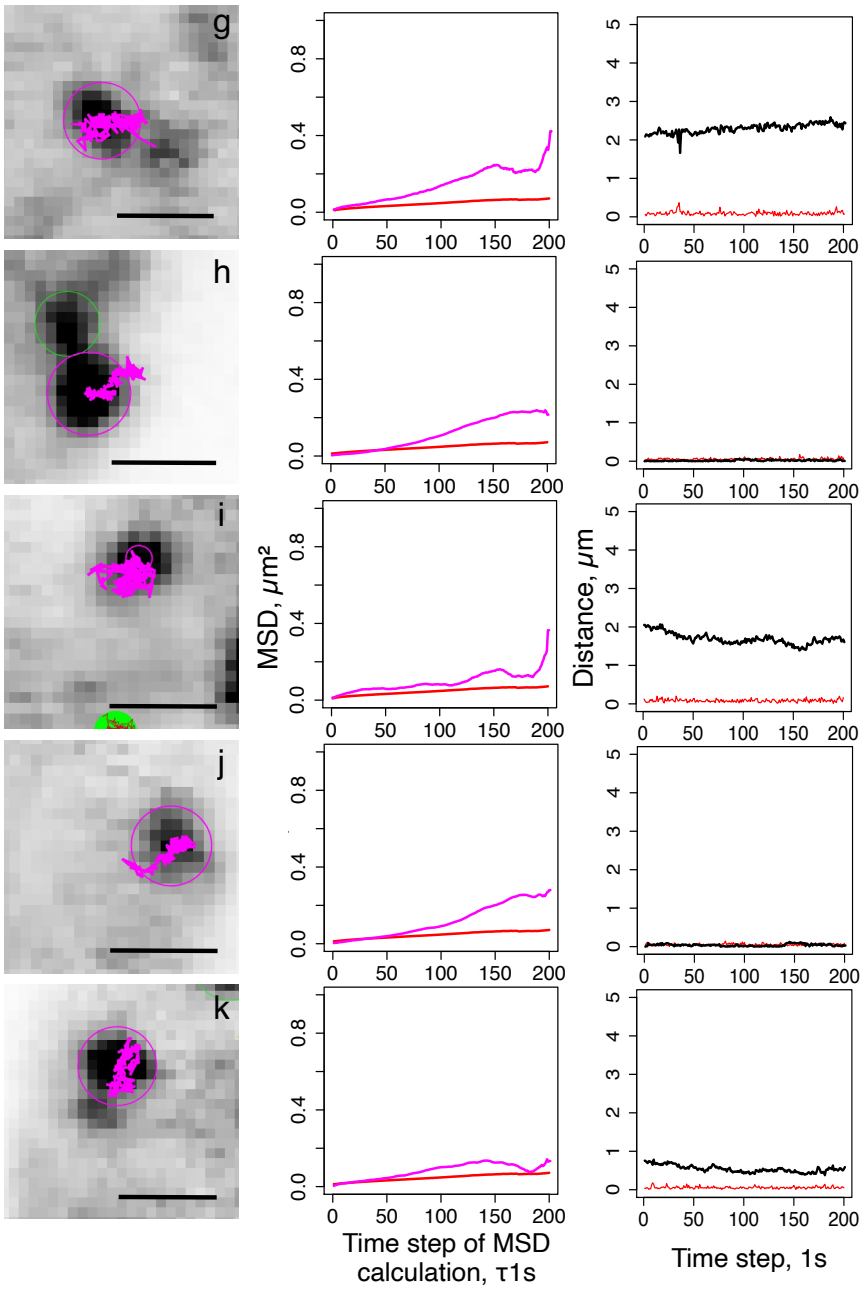

Figure 3.25: Dynamics of individual LMDs and HMDs, **short**-term imaging. Left side column displays the tracks of the randomly selected chromatin domains (magenta). Scale bar, 1 μm. Magenta circles represents position at $t = 0$, and green represents domains outside the visible plane. Middle column displays the mean squared displacement of the entire population of chromatin domains in red and that of the corresponding individual domains in magenta. Right side column displays the distance to the convex hull/nuclear edge (black) and displacement of the same domain between each consecutive time-point (red). LMDs: **a**, **b** and **c**. HMDs: movement type A-B, **e**, **g**, **h**; A-B-A, **k**; A-B-C, **d**, **f**, **j**; A, **i**.

I observed that 5 out of the 6 LMDs were located adjacent to the nuclear edge (**a**, **b**, and **c**, figure 3.24, and **b**, and **c**, figure 3.25), whereas the 6th LMD was located approximately 2 μm away from the periphery and towards the centre of the nucleus (**a**, figure 3.25). As expected, their position did not change significantly throughout the time-series, therefore, nor did their distance to the nuclear edge.

Of the 8 HMDs imaged over 1h, only one was located adjacent to the nuclear periphery and remained there for the duration of the time-course, suggesting its movement was entirely parallel to the lamina (**f**, figure 3.24). Other domains such as **d**, **e**, **g**, and to a certain extent **k**, even though not adjacent to the lamina, presented movements mostly parallel to the nuclear edge as well. However, **h**, **i**, and **j** displayed significant movement that was directed to or from the periphery. Indeed, domain **i** reached the periphery and moved away from it once more, whereas **j** reached the edge of the nucleus at time-step 70 and remained at that location for the remainder of the time-course. Of the 8 HMDs imaged short-term (figure 3.25), 3 were located adjacent to the nuclear edge, **d**, **h**, and **j**, remaining there for the duration of the time-course. Domain **k** was also located in close proximity to the lamina but not adjacent to it, it did, however, move towards the periphery during the 3 minutes and 20 seconds of imaging. Domains **e** and **i** also moved towards the periphery during the time-course. On the other hand, domains **f** and **g** moved mostly parallel to the lamina. Taking into consideration the different time-course lengths between the two imaging conditions I did not expect to see fluctuations in distance to the nuclear edge of the same order in short-term than on long-term imaging, however, it was useful to observe how the HMDs' position changed second-by-second in order to fill the gaps between the 30-second time-steps of long-term imaging.

My data suggests that there is not a clear preference in the direction of travel for HMDs in relation to the nuclear edge. These can indeed shuttle between the periphery and more central regions of the nucleus but this does not seem to constitute a trend. The same is true regarding

travelling in a plane parallel to the nuclear edge.

3.6 The impact of DNA damage on chromatin dynamics

The nucleus is a dynamic organelle that responds to a variety of stimuli. Its architecture can change drastically depending on the stage of the cell cycle, transcription patterns, and in response to DNA damage (Schneider and Grosschedl 2007). Therefore, after characterising the dynamics of chromatin domains in section 3.5 I looked to introduce perturbations to cells and assess their impact on nuclear dynamics.

It was interesting to me that only a small proportion of chromatin domains were highly mobile, furthermore, my observations of HMDs movement patterns and MSD suggested that forces were being applied to chromatin domains that led to their translocation. Recent theories have suggested that in order to repair double strand breaks through homologous directed repair, the damaged sites must be sequestered out of the heterochromatic compartments to which they belong in order to prevent deleterious chromosome crossovers (Tsouroula et al. 2016). I intended to investigate if the movements of the few HMDs observed above could be related to this phenomenon, and if it were not only the DSB sites that were removed from the compartment, but the whole TAD.

I induced DNA damage to cells by exposing them to zeocin, a bleomycin family glycopeptide antibiotic that generates DNA damage, both single stranded and double strand breaks, by intercalating into DNA (Chankova et al. 2007). Double strand breaks trigger the homologous recombination repair pathway (Wright, S. S. Shah, and Heyer 2018). I expected to observe significant dynamic events that could be associated with this type of repair as well as other phenomena that this perturbation could cause in order to draw conclusions and better understand dynamic chromatin.

Through this process I observed significant changes to the way chromatin domains move. The addition of zeocin had an impact on the split-

ting and merging events, the velocity of the domains, their maximum displacement, and mean squared displacement.

3.6.1 Zeocin induces DNA damage

To trigger DNA damage I exposed cells to 1000 $\mu g/ml$ of zeocin in imaging media for 1 and 4 hours. γH2AX is the phosphorylated form of histone H2AX (on serine 139), a protein from the histone H2A family, which enriches in sites of double strand breaks. Therefore, I used it as a marker to confirm the induction of DSBs (Scully and A. Xie 2013).

Cells that were exposed to zeocin presented γH2AX *foci* that were more numerous and of greater intensity. This took place in cells that had been exposed for both 1h and 4h, suggesting that the zeocin treatment triggered a significant amount of double-strand breaks throughout the nucleus and that DNA damage had been triggered in cells imaged after zeocin exposure (figure 3.26).

Whilst the majority of γH2AX did not co-localise with H3.1-EGFP labelled domains, a number of them presented an overlap with the γH2AX signal. This was both in the position and in the dimensions of the domain, suggesting that γH2AX propagation on DNA may be curtailed by the same factors that bind replication domains (figure 3.26, yellow and white arrows).

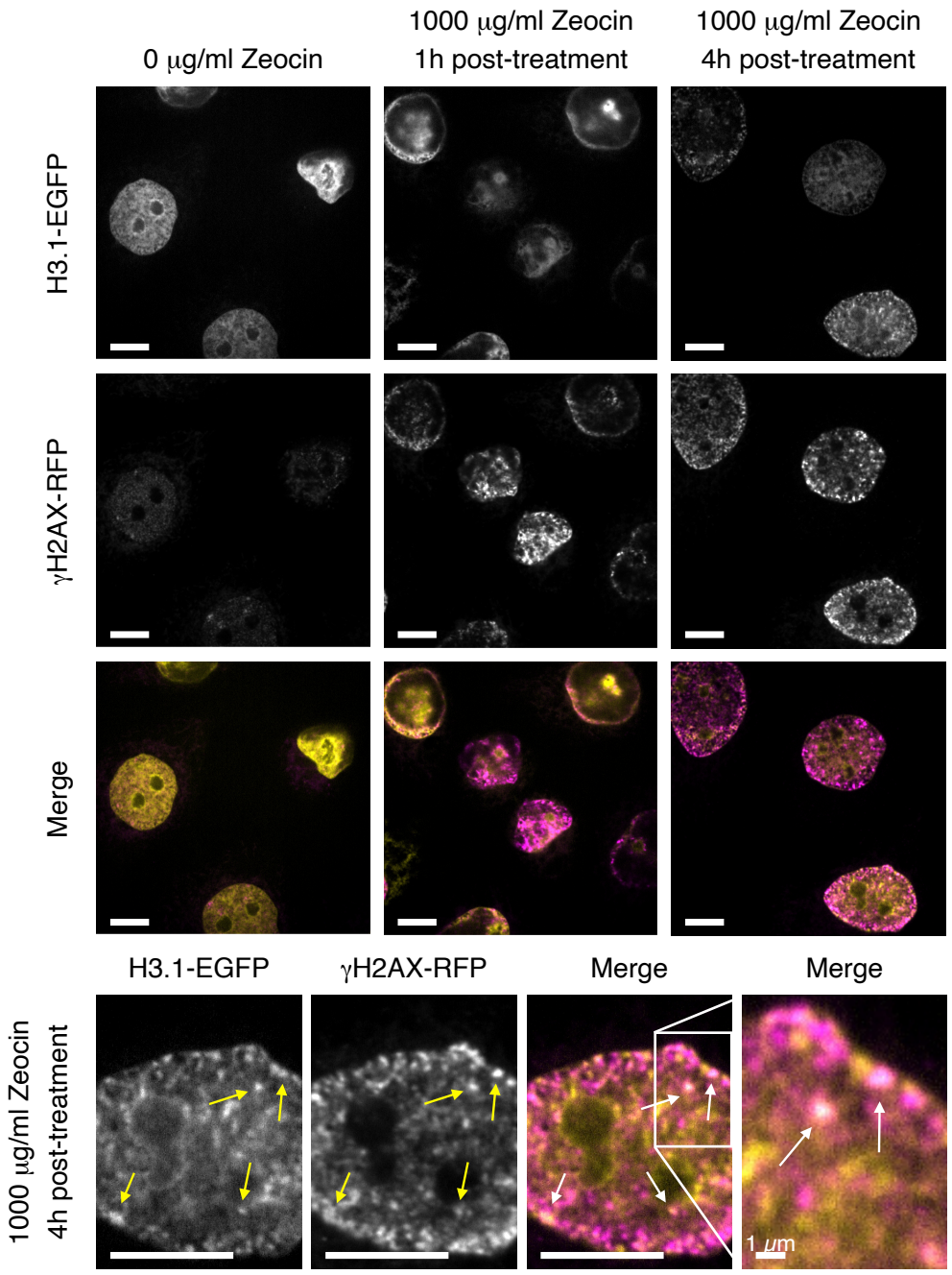

Figure 3.26: DNA damage by Zeocin. Yellow and white arrows indicate the co-localisation of H3.1-EGFP and γH2AX *foci*. Scale bar, 10 μm. EGFP channel in yellow and RFP in magenta.

3.6.2 Effect of DNA damage on the spatial distribution of domains within the nucleus

First, I looked at the impact of DNA damage on the distribution of domains across the nuclear volume using the nuclear periphery as a reference point. I observed that in long-term imaged cells, the average median distance to the periphery had changed from 33.1 nm to 30.1 and 35.4 nm, when cells were exposed to 500 and 1000 $\mu g/ml$ of zeocin, respectively. Despite this, differences were not significant according to a t-test (p=0.227, and 0.352, respectively), suggesting that at these time-scales DNA damage does not induce significant changes on the distribution of the labelled domains withing the nucleus (figure 3.27 A).

When analysing short-term imaged cells I observed that the average median distance to the periphery had changed from 42.8 nm to 49.6 and 38.1 nm when treated with 500 and 1000 $\mu g/ml$ zeocin, respectively. In this instance, the differences were statistically significant between 0 $\mu g/ml$ and the 500 $\mu g/ml$ zeocin treatment (p=0.0291) but not between 0 $\mu g/ml$ and 1000 $\mu g/ml$ of zeocin (p=0.179; figure 3.27 B).

These results were contradictory since in some instances, the addition of zeocin increased the median distance of domains to the periphery, whereas in other cases it reduced this distance. Furthermore, the majority of these differences were not statistically significant, only one reaching the p-value threshold of 0.05. Therefore, I concluded that there was not a meaningful relationship between the presence or absence of zeocin and the spatial distribution of chromatin domains within the nucleus in relation to the periphery.

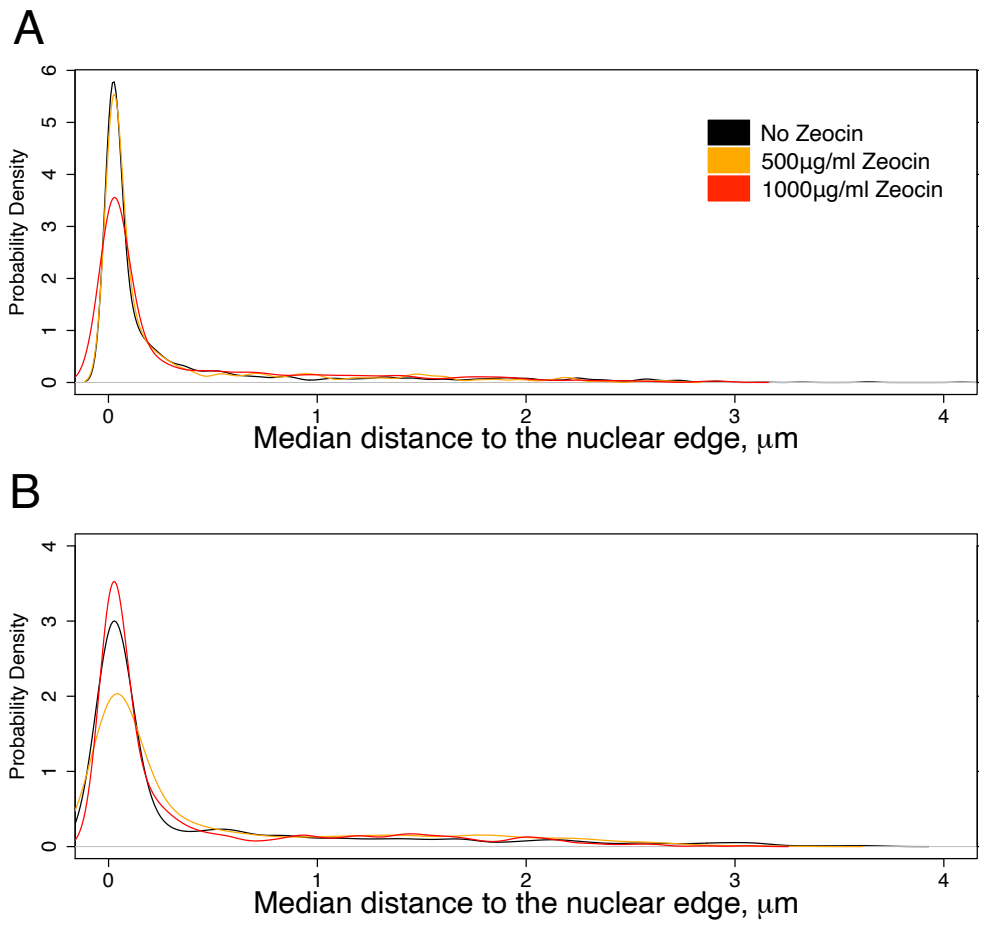

Figure 3.27: Effect of zeocin on domain distance to the nuclear periphery. **A**, **Long**-term imaging, 30 seconds time-step, 1h time-course. **B**, **Short**-term imaging, 1 second time-step, 3 minutes and 20 seconds time-course.

3.6.3 Effect of DNA damage on splitting and merging events

Next, I assessed the effect DNA damage had on splitting and merging events. I was interested in this metric because a potential increase in dynamic behaviour caused by the triggering of homologous recombination repair, could have led to an increase in splitting or merging events as a consequence of parts of chromosomes migrating within the nucleus.

I observed that, on long-term imaged cells, there was a negligible difference on the proportion of tracks that experience either splitting, merging, or both events. In the absence of zeocin, 77% of cells did not experience a splitting or merging event, this number was 80% and 77% for cells treated with 500 and 1000 $\mu g/ml$ of zeocin, respectively. However, I observed a significant reduction in the average number of splitting and merging events when cells were treated with 1000$\mu g/ml$ on tracks that experienced them. Under these conditions, the average number of splitting events was reduced from 1.56 to 1.31 (p=0.021) per track, and the number of merging events was reduced from 1.63 to 1.44 (p=0.024). Similarly, I saw a reduction in the number of splitting and merging events when the 500 $\mu g/ml$ treatment was employed, however, this was not significant (p=0.06 and p=0.11, for splitting and merging events, respectively; figure 3.28 A and B).

I also observed that the presence of zeocin interfered with the relationship between the number of splits and merges a track experienced. When zeocin was absent I observed that there was a slight bias towards merging events (as described in subsection 3.5.2). When zeocin was added, the bias towards merging events was widened, and the almost linear relationship between the two phenomena became less clear, as illustrated in figure 3.28 C).

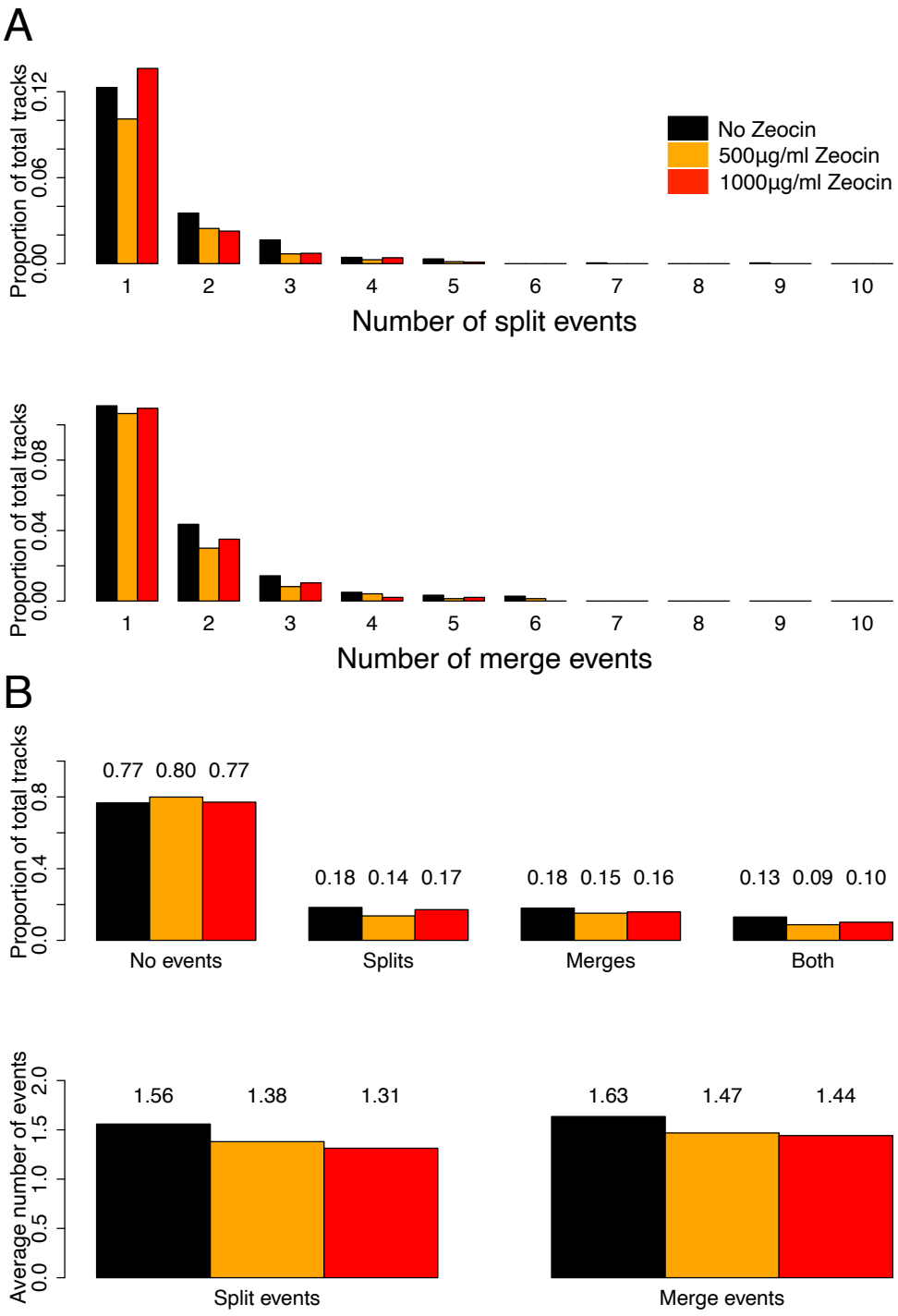
A
Proportion of total tracks
0.00
0.06
0.12
No Zeocin
500µg/ml Zeocin
1000µg/ml Zeocin
1
2
3
4
5
6
7
8
9
10
Number of split events
Proportion of total tracks
0.00
0.04
0.08
Number of merge events
B
Proportion of total tracks
0.0
0.4
0.8
0.77 0.80 0.77
0.18 0.14 0.17
0.18 0.15 0.16
0.13 0.09 0.10
No events
Splits
Merges
Both
Average number of events
0.0
0.5
1.0
1.5
2.0
1.56
1.38
1.31
1.63
1.47
1.44
Split events
Merge events

Figure 3.28

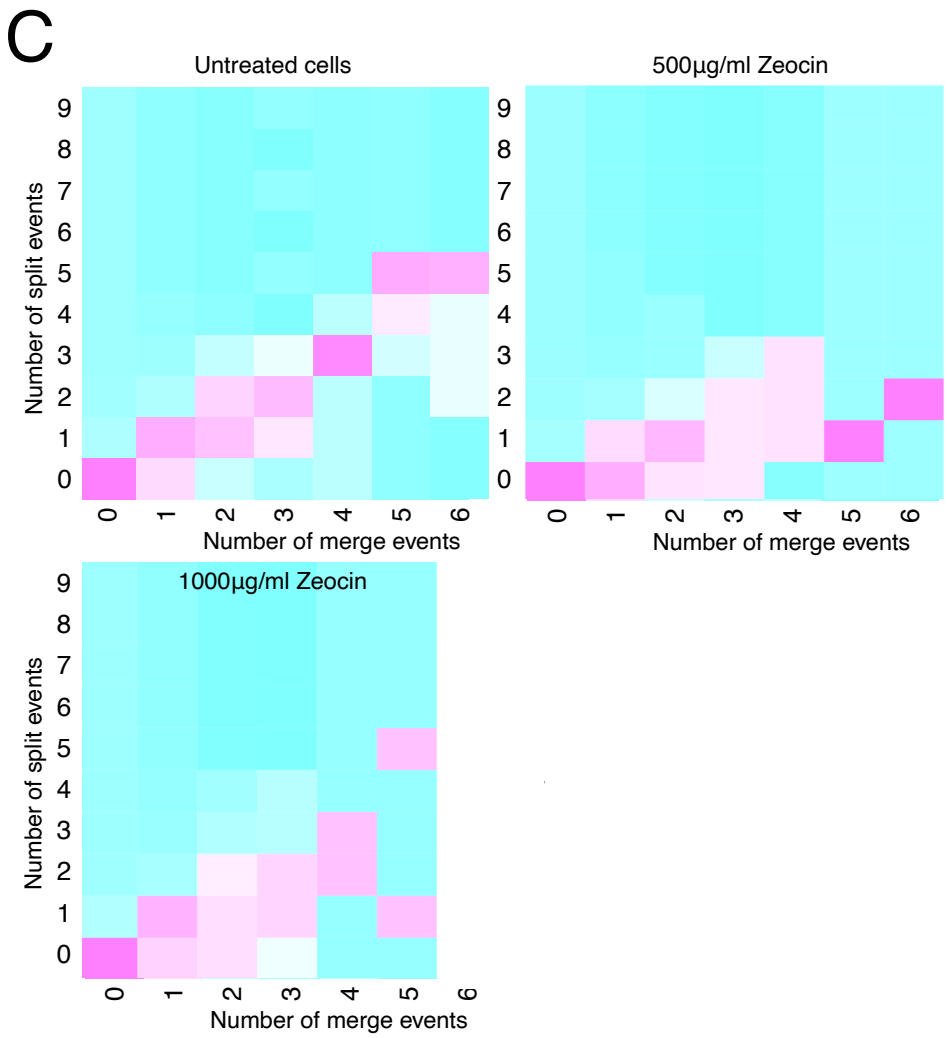

Figure 3.28: Effect of DNA damage on splitting and merging events in **long**-term imaged cell. **A**, Distribution of the amount of splitting and merging events experienced by domains of this subset in function of their zeocin treatment. **B**, Proportion of domains that experience splitting, merging, both, or none of these events, in function of zeocin treatment. **C**, Heat map of the relationship between splitting and merging events.

When analysing cells imaged short-term, I observed a different behaviour from that described above. In this instance, I observed an increase in the proportion of cells that exhibit splitting and merging events that follows the pattern of increasing zeocin concentration. The proportion of tracks that did not experience these events decreased from 81% to 76% and 74% in the presence of 500 and 1000 $\mu g/ml$ of zeocin, respectively (figure 3.29 B). However, the difference in the average number of splitting and merging events each track of the subset experienced was not significant, unlike what was observed in long-term imaging, this can be illustrated by the similar average of splitting and merging events each population experiences regardless of zeocin treatment (figure 3.29 A). I could also observe that the effect of zeocin on the relationship between the number of splitting and merging events was less pronounced in this instance, where the slight bias towards merging events was not as clear (figure 3.29 C).

On the whole, in long-term imaged cells, the number of tracks that experienced splitting, merging, or both events remained fairly constant in the presence of zeocin, but the number of events per track decreased. On the other hand, in short-term imaged cells, the number of tracks that experienced these events increased, however, the number of events per track did not manifest a clear trend in the presence or absence of zeocin. These data suggest that sequestration of DSB prior to repair could be reducing the freedom domains have to approach and separate from one another. This sequestration allied with the slower rate of image acquisition may mean that the increase in number of splitting and merging events can only be observed when imaging cells rapidly.

These observations further suggest that employing a combination of different temporal resolutions can increase insight into phenomena that would not be possible to capture in their entirety by utilising just one method, which displays the value in capturing nuclear dynamics at different time-scales.

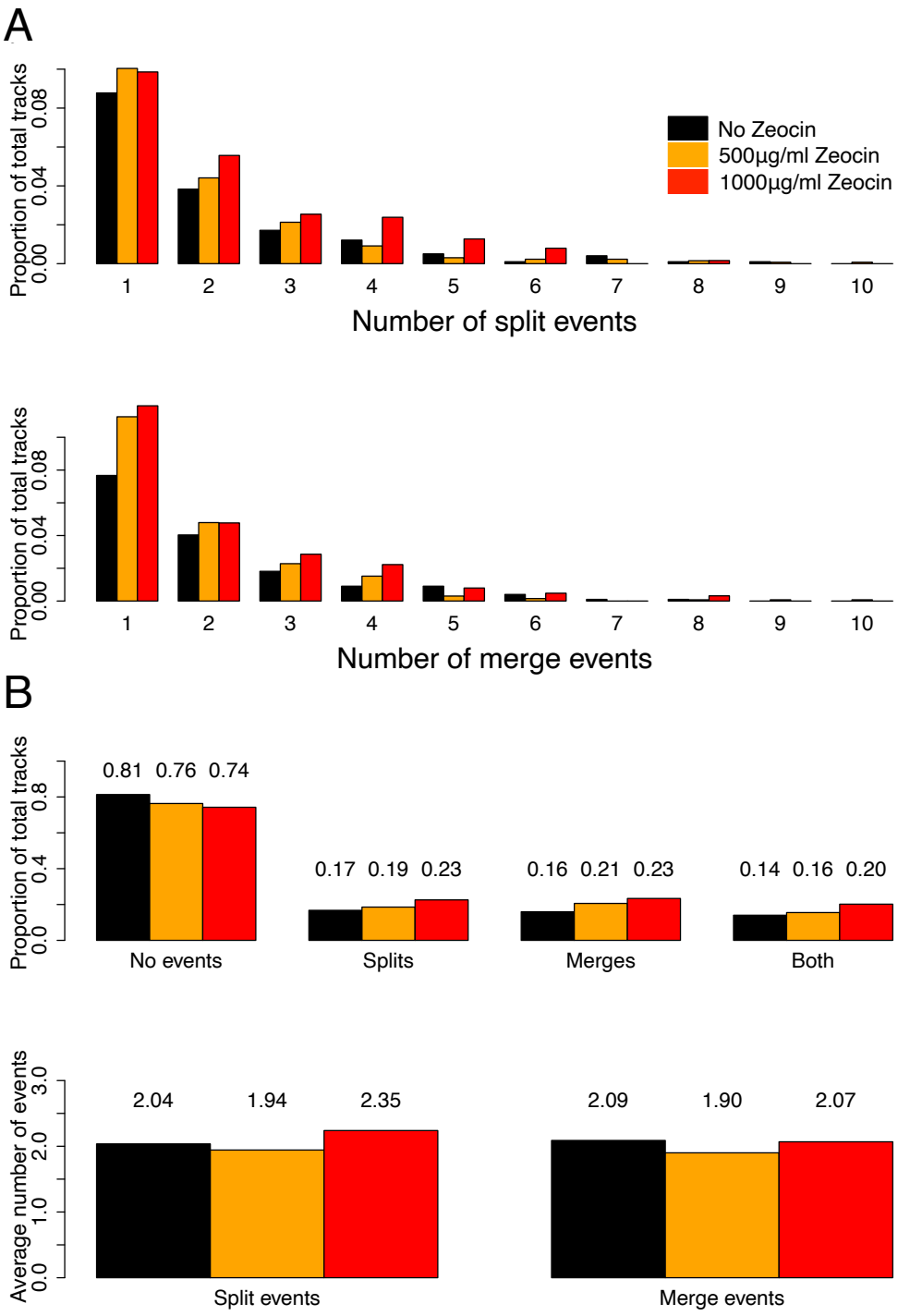
A
Proportion of total tracks
0.00
0.04
0.08
No Zeocin
500µg/ml Zeocin
1000µg/ml Zeocin
1
2
3
4
5
6
7
8
9
10
Number of split events
Number of merge events
B
0.81 0.76 0.74
0.17 0.19 0.23
0.16 0.21 0.23
0.14 0.16 0.20
0.0
0.4
0.8
No events
Splits
Merges
Both
Average number of events
0.0
1.0
2.0
3.0
2.04
1.94
2.35
2.09
1.90
2.07
Split events
Merge events

Figure 3.29

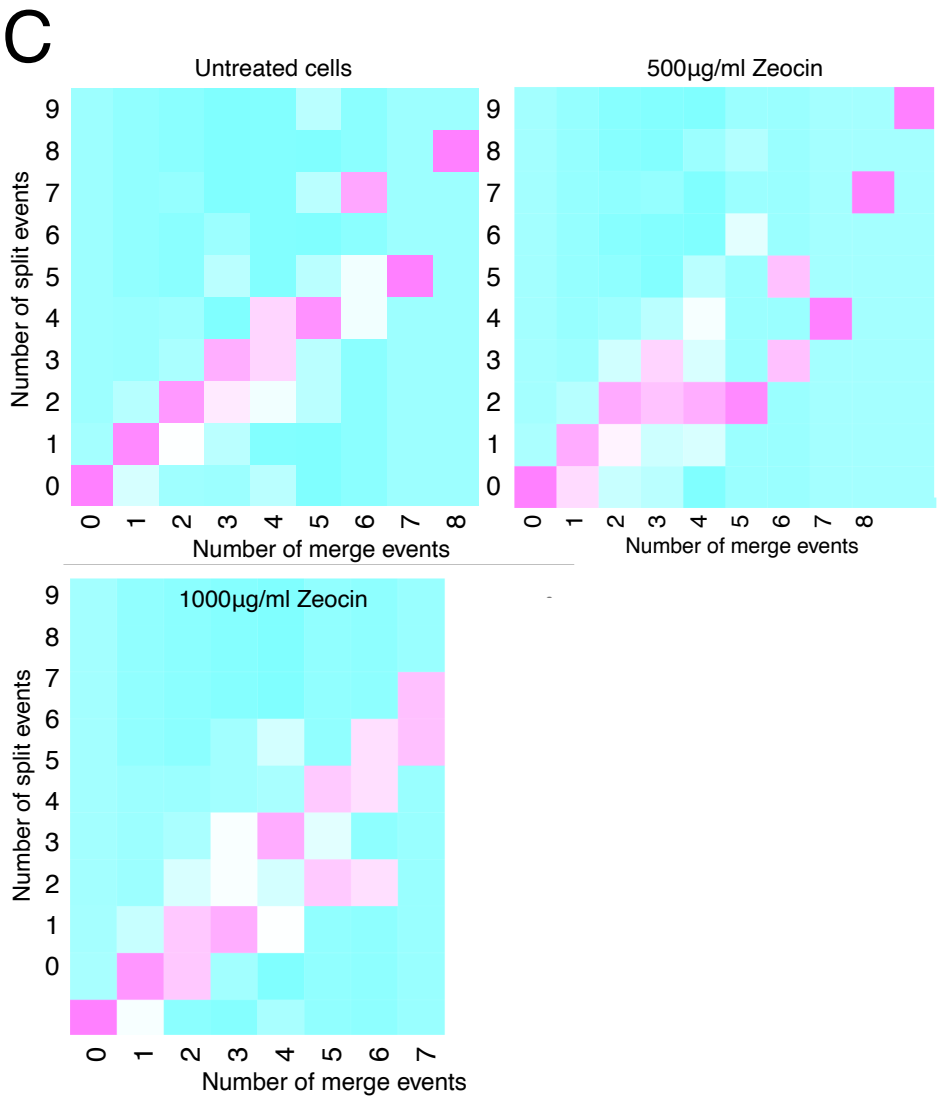

Figure 3.29: Effect of DNA damage on splitting and merging events in **short**-term imaged cell. **A**, Distribution of the amount of splitting and merging events experienced by domains of this subset in function of their zeocin treatment. **B**, Proportion of domains that experience splitting, merging, both, or none of these events, in function of zeocin treatment. **C**, Heat map of the relationship between splitting and merging events.

3.6.4 Effect of DNA damage on population dynamics

Velocity, track length and maximum displacement

To assess if DNA damage had a wide-spread impact on the dynamics of the chromatin domain population, I compared average velocity, average track length and maximum displacement of cells that were not treated, treated with 500 $\mu g/ml$, and 1000 $\mu g/ml$ of zeocin.

I observed that, in cells imaged over 1h, the mean of the average velocity had significantly increased from 0.231 $\mu m/min$ to 0.263 and 0.255 $\mu m/min$ when cells were exposed to 500 and 1000 $\mu g/ml$ of zeocin, respectively. Interestingly, the changes to average track length were not significant, having only changed from 11.455 μm to 11.703 and 11.273 μm. However, I did observe a marked change in the profile of the distribution; under the effect of zeocin, two peaks emerged from the domain populations, one approximately in the region of 8-9 μm, and another around the 13-14 μm mark for both 500 and 1000 $\mu g/ml$ treatments. The maximum displacement experienced a significant increase in both 500 and 1000 $\mu g/ml$ zeocin treatments, changing from 0.791 to 0.932 and 0.928 μm (figure 3.30).

Cells imaged over 3 minutes and 20 seconds presented similar behaviour, with a significant increase in mean average velocity from 4.180 $\mu m/min$ to 4.690 and 4.521 $\mu m/min$, with 500 and 1000 $\mu g/ml$ zeocin treatments. Domains imaged under these conditions presented significant changes on track length, unlike those imaged long-term. The average length of their tracks increased from 13.030 μm to 15.09 and 14.53 μm in the presence of 500 and 1000 $\mu g/ml$. However, they did not present changes in their distribution as long-term imaged cells did. Finally, these cells presented significant differences in maximum displacement between untreated cells and those treated with 500 and 1000 $\mu g/ml$ zeocin. In this particular case, maximum displacement increased from 0.507 to 0.566 and 0.544 μm, respectively (figure 3.31).

The positive skew in the distributions of all three metrics previously observed in untreated cells was also observed in the presence of zeocin. However, under these conditions there was an increase in the probability density towards higher values, which translates into an increase in the proportion of HMDs. Allied to this, an increase in maximum displacement without an accompanying increase in track length suggests that the movement of chromatin domains became more directional, as domains did not travel greater distances in total, but explored a greater nuclear volume. All this suggests that there are forces being applied to the labelled chromatin domains that exceed those of untreated cells. These changes could stem from physical changes to the DNA polymer itself due to lesions, and/or due to the sequestration and relocation of entire genomic regions for repair. In both cases, forces can be relayed to the labelled domains through the chromatin fibre, leading to their increased displacement, or indeed the labelled domains could be the ones onto which the forces are being applied.

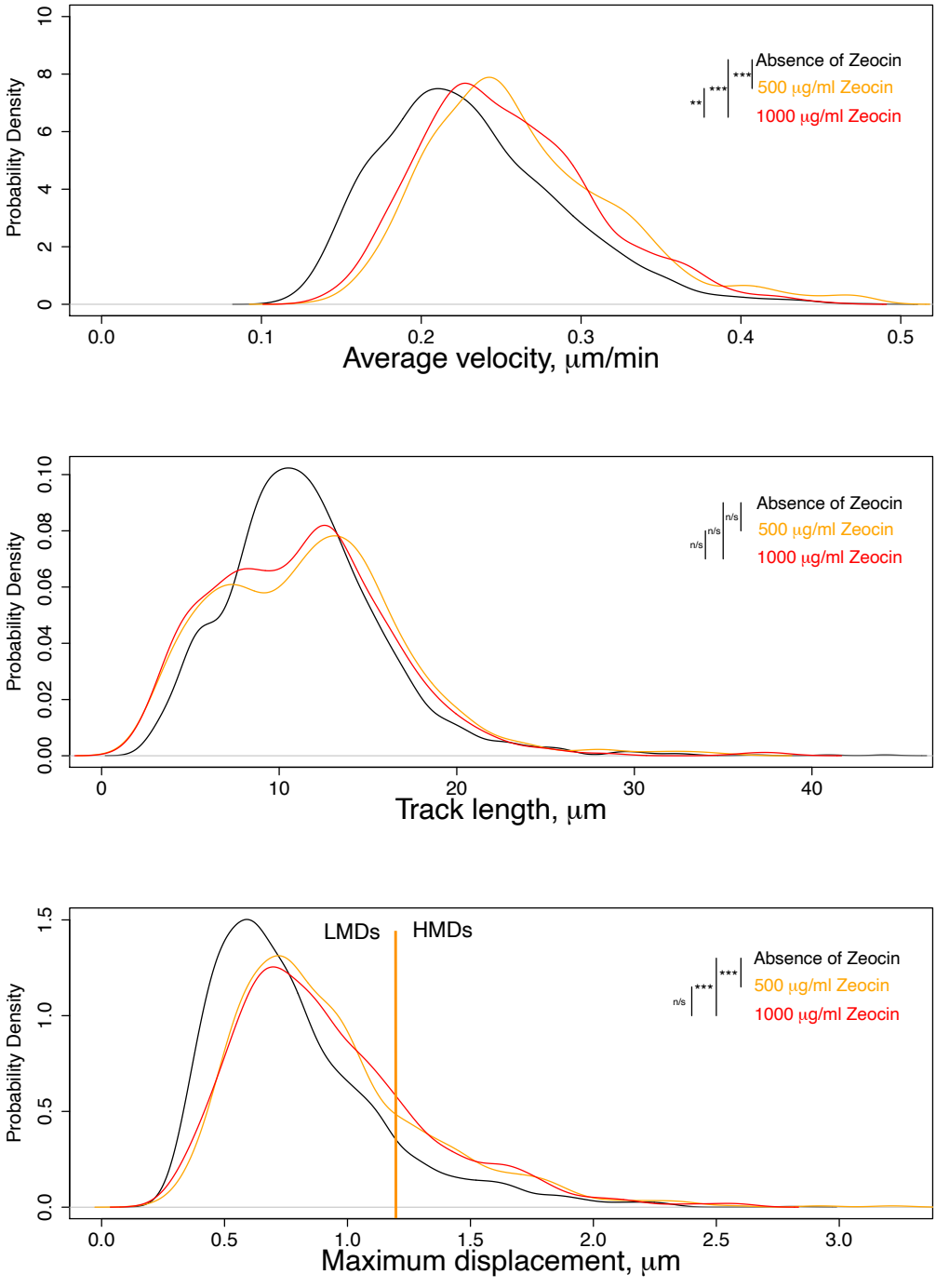

Figure 3.30: Effect of DNA damage on velocity, track length, and maximum displacement of **long**-term imaged chromatin domains.

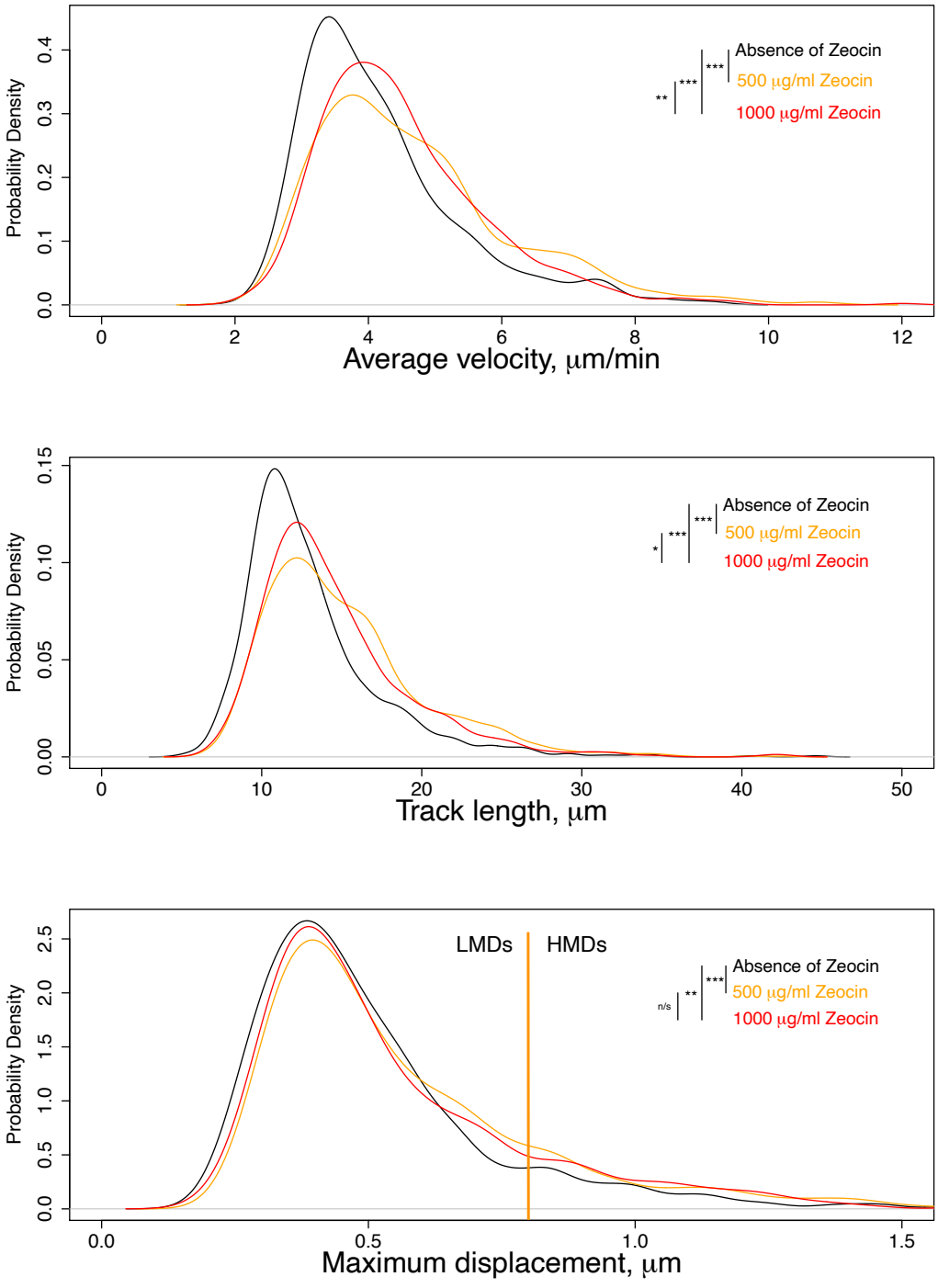

Figure 3.31: Effect of DNA damage on velocity, track length, and maximum displacement of **short**-term imaged chromatin domains.

Maximum displacements within individual cells and MSD of different populations

To better understand the phenomena described above, I performed a single cell analysis of maximum displacement values, rather than as an ensemble as presented above. Interestingly, the zeocin-treated cells congregated towards the top end of the spectrum, suggesting that, at the single cell level there was an increase in the number of HMDs, or an increased mobility when DNA damage was induced (figure 3.32 A). The greater values of maximum displacement for the two populations of cells treated with 500 and 1000 $\mu g/ml$ translated into an increase of MSD at a greater rate, when compared to their untreated counterparts, confirming that chromatin domains in nuclei that were subjected to DNA damage were exploring greater nuclear volumes (figure 3.32 B). Interestingly, I observed that in the long-term, the difference between the MSD of cells treated with 500 and 1000 $\mu g/ml$ of zeocin is negligible when compared to non treated cells.

In the short-term, the relationship between maximum displacement and zeocin treatment was less clear when analysing domains cell-by-cell (figure 3.33 A). Under these conditions, I also observed that the MSD of all three populations increased at a similar rates, however it was greater in zeocin-treated cells (figure 3.33 B).

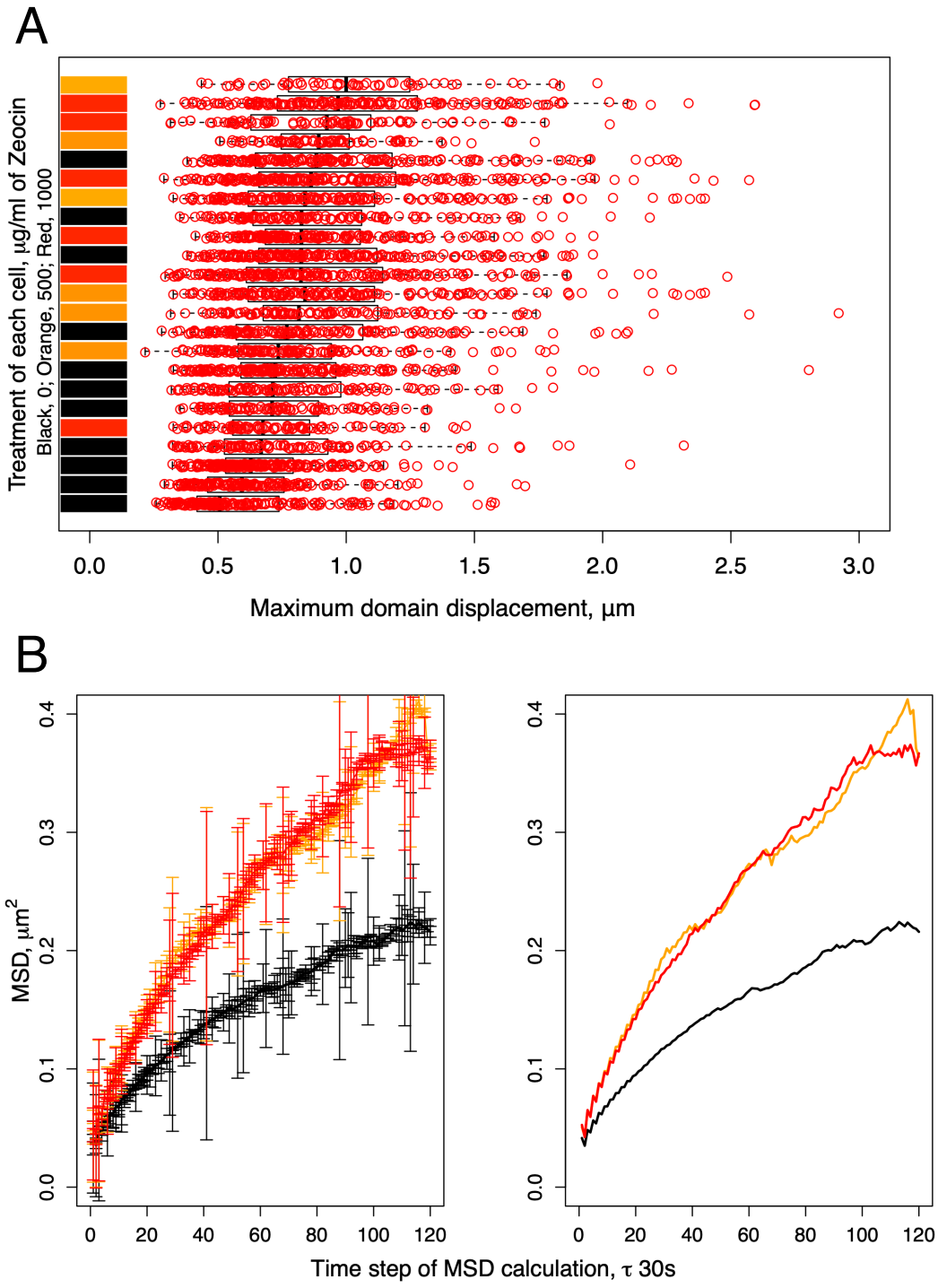

Figure 3.32: Effect of DNA damage on maximum displacement and MSD on **long**-term imaged cells. **A** Ranking of median maximum displacement of chromatin domains of each cell. **B** Mean squared displacement of each cell population. Black: non-treated; orange: 500 $\mu g/ml$ zeocin; red: 1000 $\mu g/ml$ zeocin.

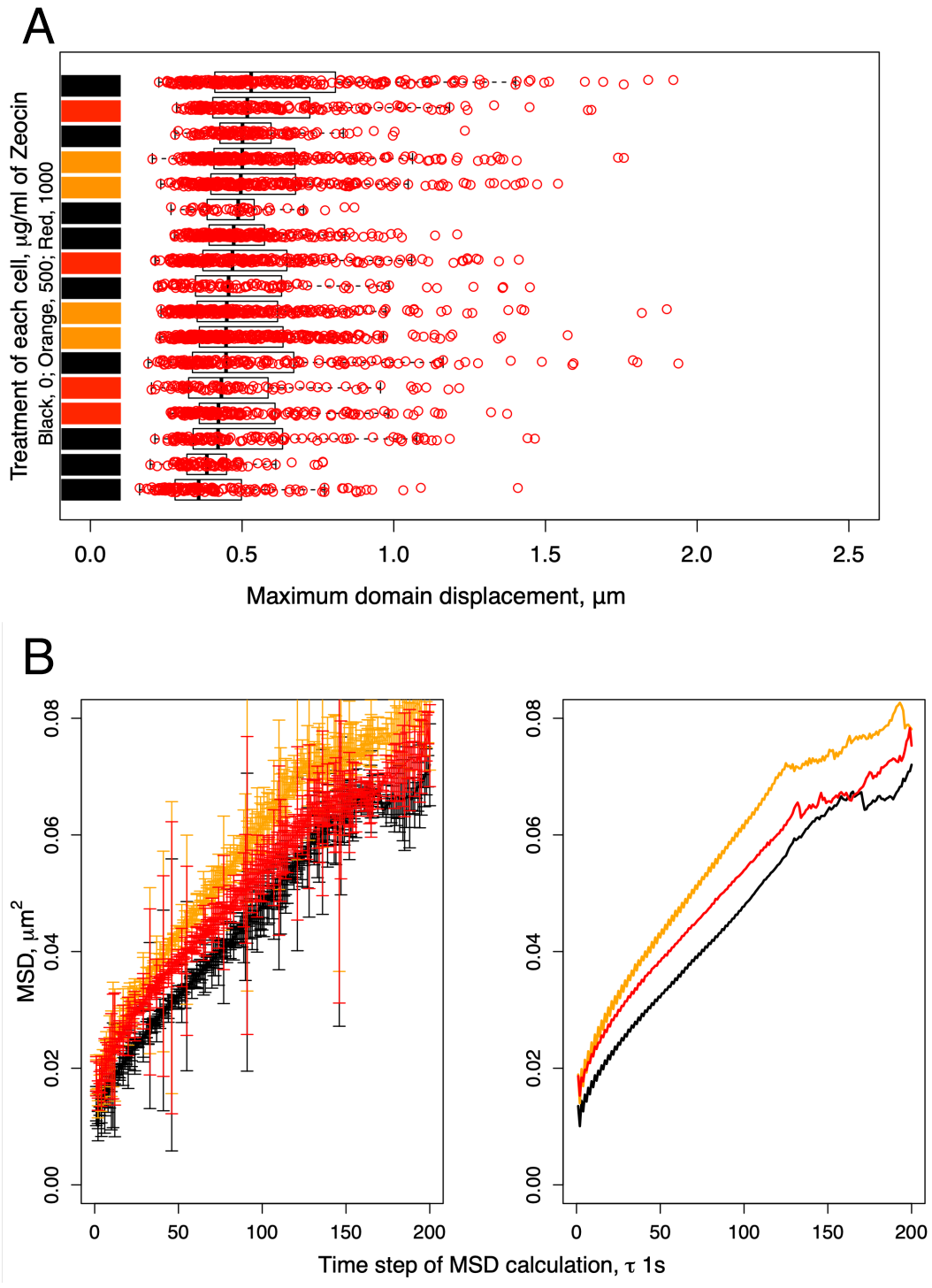

Figure 3.33: Effect of DNA damage on maximum displacement and MSD on **short**-term imaged cells. **A** Ranking of median maximum displacement of chromatin domains of each cell. **B** Mean squared displacement of each cell population. Black: non-treated; orange: 500 $\mu g/ml$ zeocin; red: 1000 $\mu g/ml$ zeocin.

3.6.5 Effect of DNA damage on location and movement of LMDs and HMDs

Effect of DNA damage on the location of LMDs and HMDs

DNA damage increased maximum displacement and the MSD of domain populations (section 3.6.4). However, according to my observation in section 3.6.2, the introduction of DNA damage did not significantly affect the spatial distribution of chromatin domains in relation to the nuclear periphery. This suggests that the increase in the maximum displacement of a population does not depend on the migration of chromatin domains from the nuclear edge into the centre of the nucleus. Therefore, I looked to understand if the increase in maximum displacement of the population was due to a generalised increase in maximum displacement of all domains, or if there was a subset of domains that was generating this change.

In long-term imaged cells, the increase in maximum displacement was due to the increase in HMDs from 11% of the entire population of domains to nearly twice this value (20.6% and 20.85% for 500 and 1000 $\mu g/ml$, respectively). This trend took place regardless of distance to the periphery of the nucleus; domains that were located within 500 nm from the periphery experienced a similar increase in relative numbers as those located more centrally (figure 3.34).

In short-term imaged cells, the proportion of HMDs increased from 10.59% of the total to 15.67% and 14.63% for 500 and 1000 $\mu g/ml$ zeocin treatment, respectively. This increase was smaller than the one observed in long-term imaged cells, which I attributed to the smaller imaging time window (figure 3.35).

These observations suggest that even though the probability of finding HMDs increases with distance to the periphery, the effect of zeocin on all domains is equivalent regardless of their location in relation to the periphery of the nucleus.

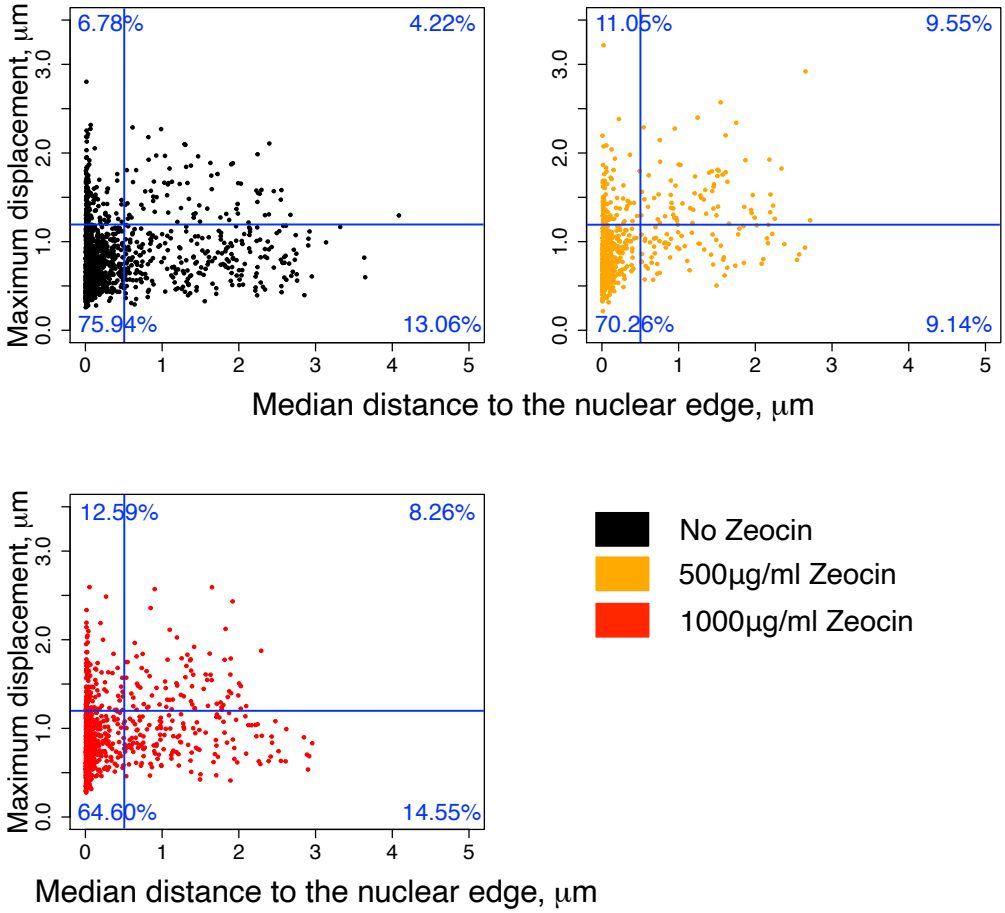

Figure 3.34: Effect of DNA damage on the maximum displacement of **long**-term imaged peripheral and central chromatin domains. The first quadrant (top left) contains peripheral HMDs, the second quadrant (top right) contains central HMDs, the third quadrant (bottom right) contains central LMDs, and the fourth quadrant (bottom left) contains peripheral LMDs.

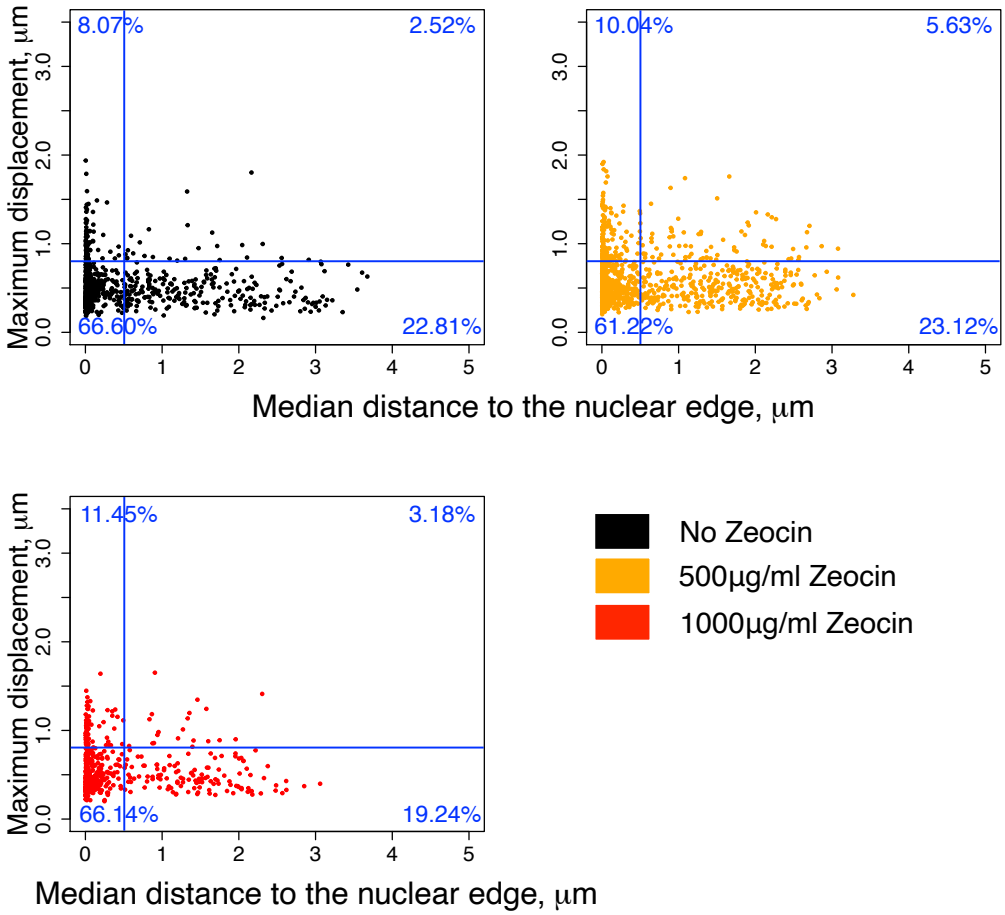

Figure 3.35: Effect of DNA damage on the maximum displacement of **short**-term imaged peripheral and central chromatin domains. The first quadrant (top left) contains peripheral HMDs, the second quadrant (top right) contains central HMDs, the third quadrant (bottom right) contains central LMDs, and the fourth quadrant (bottom left) contains peripheral LMDs.

Effect of DNA damage on movement directionality

I looked to explore the directionality of chromatin domain movement to assess if this was taking place parallel to the nuclear lamina, or, indeed, perpendicular to it. To achieve this, I compared the variation in distance to the nuclear periphery of each domains with their maximum displacement by calculating the ratio between the two distances. This relationship allowed me to compare the maximum distance travelled by a domain, and the component of that movement that relates to the direction perpendicular to the lamina. For example, if a HMD travels parallel to the lamina, its variation in distance to periphery (Δd) will be zero regardless of its maximum displacement (MaxD). Conversely, if a HMD travels perfectly towards (or from) the nuclear lamina, its variation in distance to periphery will equal its maximum displacement (figure 3.36 A).

When looking at the whole population of long-term imaged domains, there was a change in Δd:MaxD from 0.42 in untreated cells to 0.47 and 0.41 in cells treated with 500 and 1000 $\mu g/ml$ zeocin, respectively, however, these difference were not significant (p=0.233 and p=0.209). Different patterns emerged when considering HMDs and LMDs separately. In the case of HMDs, there was a significant increase in the perpendicularity of domain movements in relation to the nuclear periphery in cells treated with 500 $\mu g/ml$ (t-test; p=0.048) where the Δd:MaxD increased from 0.40 to 0.43. However, the increase to 0.42 in cells treated with 1000 $\mu g/ml$ was not significant (p=0.233). This was in contrast with LMDs, where decreases in Δd:MaxD from 0.43 in untreated cells to 0.38 and 0.39 in cells treated with 500 and 1000 $\mu g/ml$ zeocin, respectively, were both significant (p=0.00013 and p=0.0048; figure 3.36 B).

Short-term imaged cells saw significant differences in Δd:MaxD on the whole population between untreated cells and those treated with 500 $\mu g/ml$ of zeocin, where it increased from 0.43 to 0.49. There were also increases in the case of cells treated with 1000 $\mu g/ml$ zeocin (0.45), however, these were not significant (p=0.126). Unlike long-term imaged

domains where the perpendicularity of movements increased in HMDs but decreased in LMDs in the presence of zeocin, in short-term images domains it increased in both populations. In the HMD population, Δd:MaxD increased from 0.31 to 0.41 and 0.35 for 500 and 1000 $\mu g/ml$ zeocin treatments, respectively (p=0.0019 and p=0.322). The LMD population saw increases from 0.44 to 0.51 and 0.46 (p=1.51e-8 and p=0.096; 3.36 C).

These data suggest that in the long-term, HMDs increase the perpendicularity of their movements in relation to the nuclear lamina, but that LMDs do not experience this same increase in the same time scales upon DNA damage induction. This could be a consequence of the observations that have been previously made (Christopher Patrick Caridi et al. 2019) where DSB sites are translocated to the periphery for repair, either directly (where the labelled domains are being actively moved to the periphery) or indirectly (where forces being applied on different regions of the genome are being relayed to the labelled domains). The fact that in the short-term imaged cells, the differences between HMDs and LMDs are not as pronounced suggests that significant differences develop over periods of time greater than 3 minutes and 20 seconds but that, all domains experience changes in the direction of their movement when DNA damage is induced.

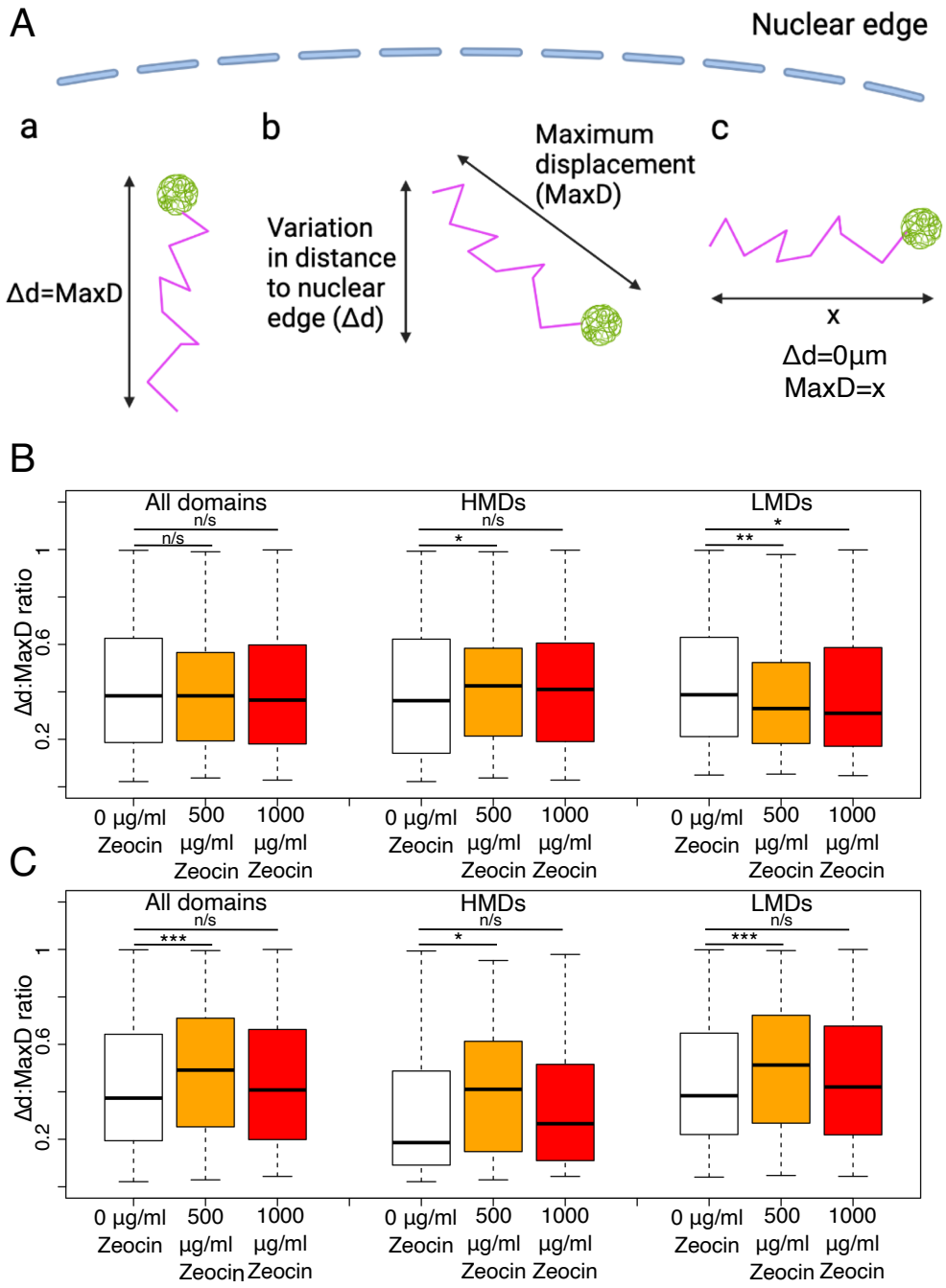

Figure 3.36: Effect of DNA damage in the directionality of chromatin domain movement in **long** and **short**-term imaged cells. **A** Diagram of the relationship between variation in distance to the periphery (Δd) and maximum displacement (MaxD). **B** Ratios between Δd and MaxD for the whole population of domains, HMDs and LMDs in **long**-term imaged cells. **C** Ratios between Δd and MaxD for the whole population of domains, HMDs and LMDs in **short**-term imaged cells.

Effect of DNA damage on example HMDs

Long-term imaged HMDs presented movement patterns identical to those described in section 3.5.4 (figure 3.37 A). Movements with the A-B pattern were evident in domains **d**, **f**, **g**, **h**, and **k**. Domains **a**, **c**, and **j** displayed A-B-C movements, and **b**, **e**, **i**, and **l** showed an A-B-A pattern. Some of these, however, displayed a combination of several patters, for example, domain **b** had elements of A-B-A movement but with backtracking events taking place in two different directions in separate occasions. Domain **g** moved in one particular direction with static periods (A-B) but with slight changes of direction (A-B-C). Domain **l** also presented elements of both A-B-A and A movement (figure 3.37).

In short-term imaged domains I could observe similar behaviour (figure 3.38 A). Domains **a**, **e**, **g** **j**, and **k** exhibited movement intercalated with stationary periods (A-B), **d** and **l** showed backtracking (A-B-A), and domains **b**, **c**, **h**, and **i** displayed changes of direction during their movement (A-B-C).

Despite an increase in number of HMDs, the movements that these displayed were not different from those described in section 3.5.4. This suggests that the forces that affected chromatin domains after DNA damage induction were similar to those operating in non-treated cells; however, due to the increase in HMDs, the forces were more common, further suggesting an increase in the number of dynamic events in the nucleus.

The relationship between MSD and the the movement patterns described in section 3.5.4 was maintained; the static and dynamic periods manifested themselves as plateaus and increases in MSD, whereas movements that brought the domains closer to their initial position led to a decrease in MSD. One difference between cells that were untreated, and their zeocin treated counterparts, was the values the MSD reached. In the former, MSDs did not reach values greater than 4, whereas the latter presented MSD values that reached between 4 and 5 for domains **a**, **d**, and **g**). The same correlation between MSD and movement pattern

was also observed in short-term imaged cells, however, in this instance, the MSD did not reach values that were clearly greater than those of untreated cells.

These data further suggest that the induction of DNA damage does not translate into a change in the movement patterns as seen above, but that it affects movement magnitude.

Taking into consideration that HMDs of cells treated with zeocin display a greater component of their movement towards and from the periphery of nuclei, I attempted to confirm if that could be observed in individual domains. I observed that in long-term imaged domains, some maintained a relatively stable distance to the periphery, suggesting that their movement was mostly parallel to the lamina (figure 3.37 , **a**, **b**, **e**). Others remained distant to the lamina but their position fluctuated more significantly (**d**, **j**, **k**, **l**), whereas some saw their position slowly approach or leave the nuclear periphery (**f**, **g**, **h**). Domain **c** started away from the periphery and then migrated to become adjacent to it, before becoming more internal once more; domain **i** followed the opposite pattern, where it began in the periphery, followed by a centrally-bound movement, before returning to the periphery.

In general, short-term imaged domains did not change their position in relation to the periphery in a significant manner, as expected due to the short imaging period (figure 3.38). This was especially clear in domains **e**, **f**, **g**, and **h**, other domains such as **a** and **i** presented a subtle drift towards, and then away, from the periphery during the time-course. Domains **b**, **c**, **d**, **j**, and **k** were located close to the periphery, or even adjacent to it, and migrated to and from the lamina during the time-course.

This suggests that the difference observed in the previous section cannot be clearly observed at this level of detail. The domains I analysed in detail did present differences in MSD, but their distance to the periphery profiles are not markedly different from untreated populations. This

suggests that the subtle differences are only observable when taking into account the entire population and not just a small subset of HMDs.

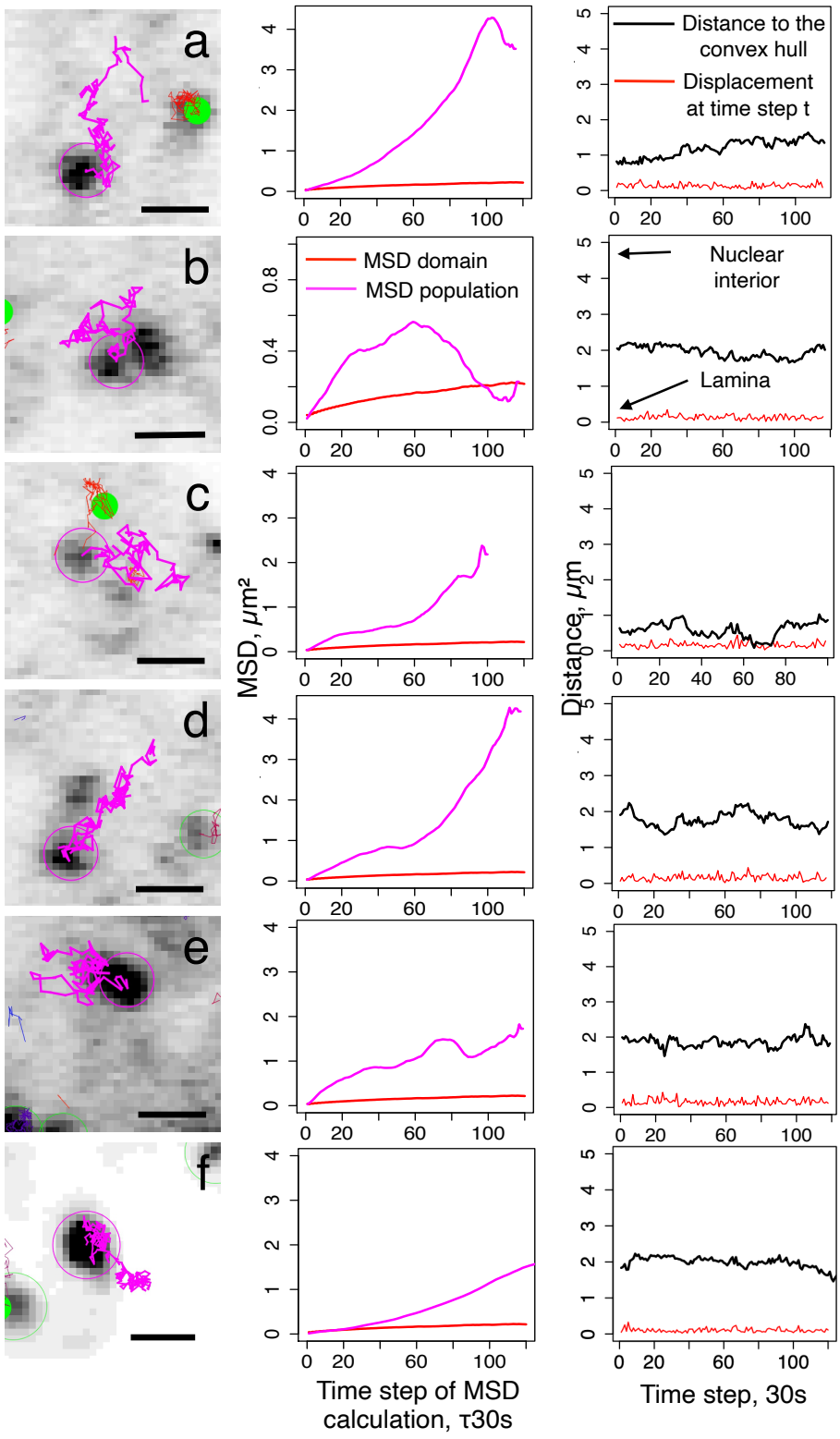
a
b
c
d
e
f
MSD domain
MSD population
Distance to the convex hull
Displacement at time step t
Nuclear interior
Lamina
MSD, μm²
Distance, μm
Time step of MSD calculation, τ30s
Time step, 30s

Figure 3.37

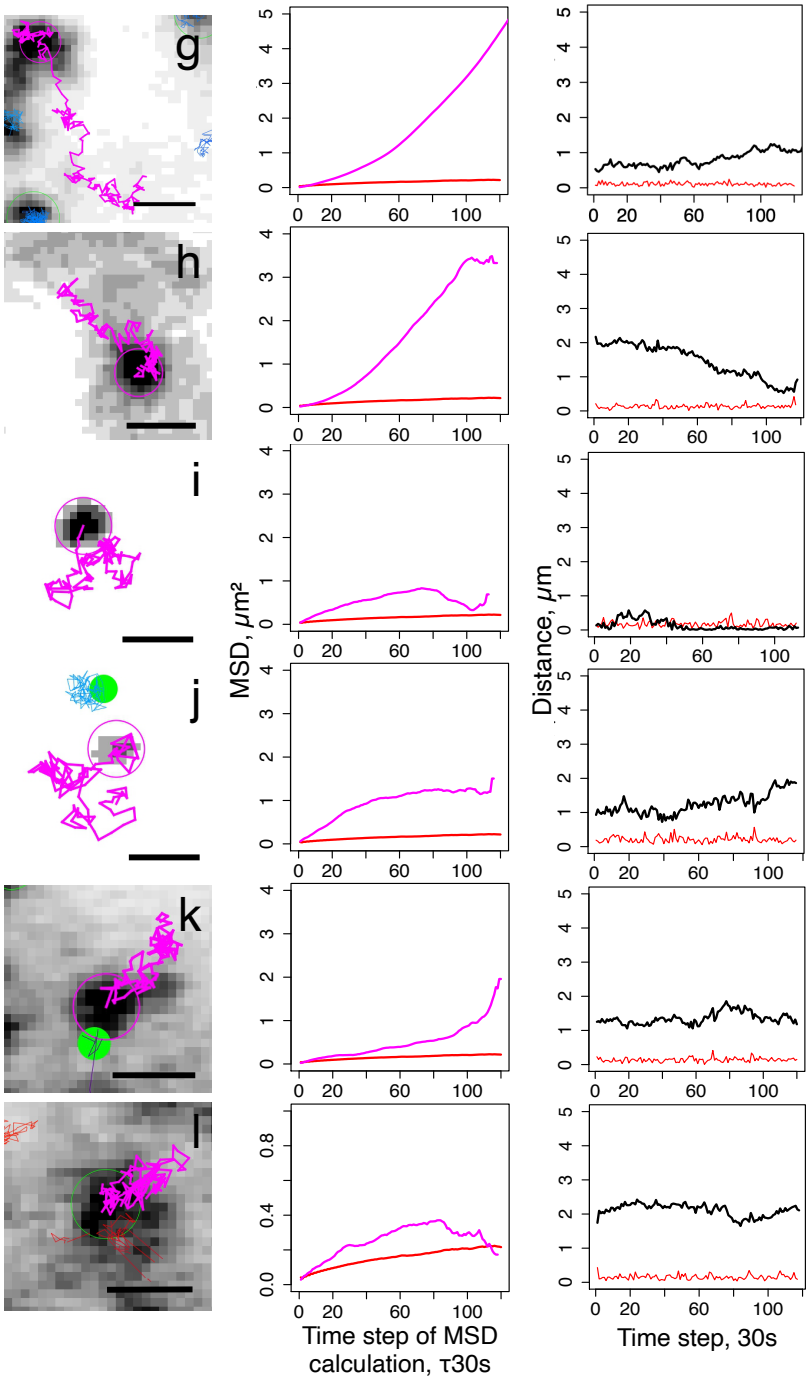

Figure 3.37: Dynamics of individual HMDs in the presence of zeocin, **long**-term imaging. Left side column displays the tracks of the randomly selected chromatin domains (magenta). Scale bar, 1 μm. The magenta circle represents position at $t = 0$, and green represents domains outside the visible plane. Middle column displays the mean squared displacement of the entire population of chromatin domains in red and that of the corresponding individual domains in magenta. Right side column displays the distance to the convex hull/nuclear edge (black) and displacement of the same domain between each consecutive time-point (red).

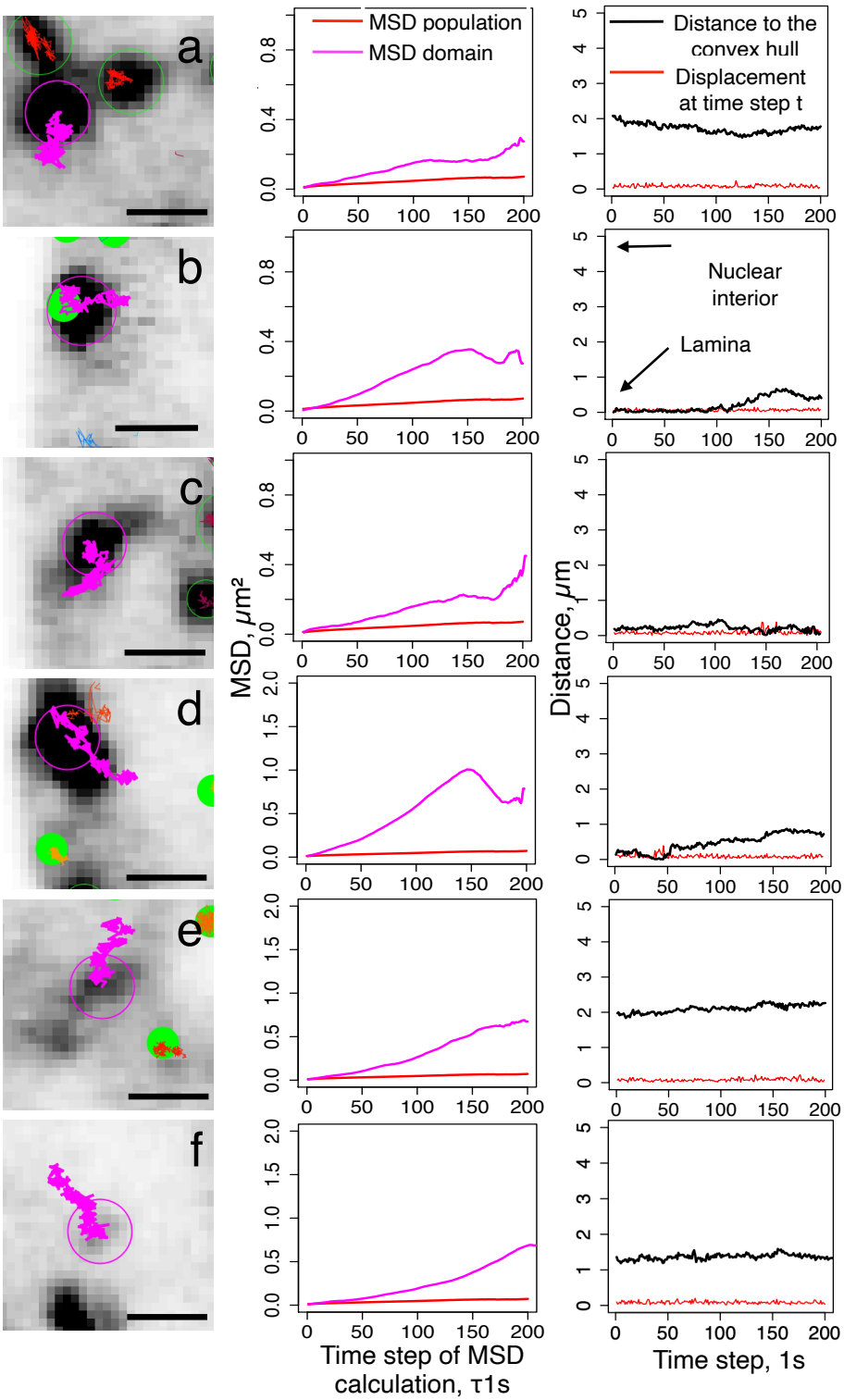
a
b
c
d
e
f
MSD population
MSD domain
Distance to the convex hull
Displacement at time step t
Nuclear interior
Lamina
MSD, μm²
Distance, μm
Time step of MSD calculation, τ1s
Time step, 1s

Figure 3.38

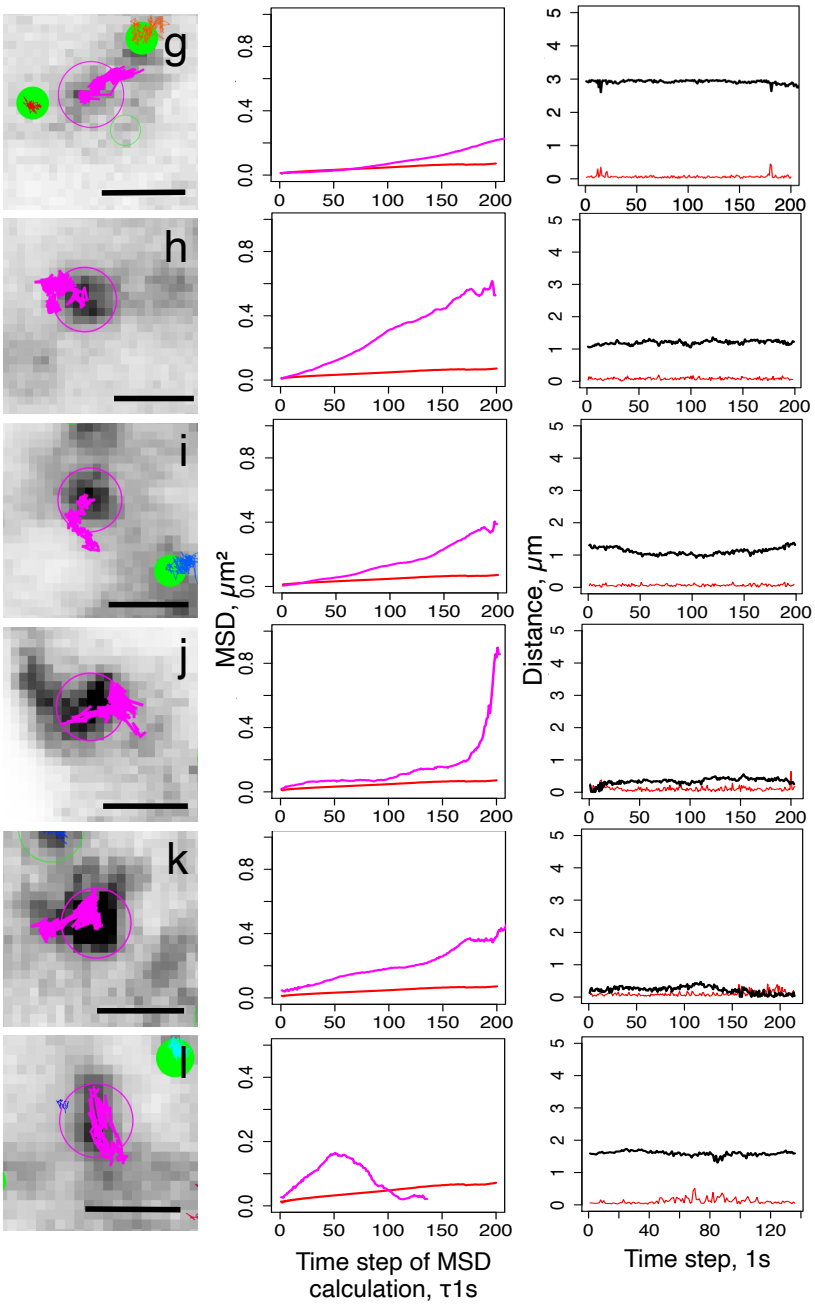

Figure 3.38: Dynamics of individual HMDs in the presence of zeocin, **short**-term imaging. Left side column displays the tracks of the randomly selected chromatin domains (magenta). Scale bar, 1 μm. The magenta circle represents position at $t = 0$, and green represents domains outside the visible plane. Middle column displays the mean squared displacement of the entire population of chromatin domains in red and that of the corresponding individual domains in magenta. Right side column displays the distance to the convex hull/nuclear edge (black) and displacement of the same domain between each consecutive time-point (red).

3.7 Discussion

To test the hypotheses previously put forward, the work developed in this chapter intended to (1) create a workflow to stably label and image chromatin domains in living cells, (2) analyse and characterise the dynamics of labelled chromatin using the developed methodology, and (3) explore how this could be used to study the effect of perturbations (DNA damage, in this instance) on the dynamics of chromatin.

Through the employment of RAPID-release, with appropriate timings, I was successful at labelling TADs in a stable fashion, and with the spacing and size necessary for effective tracking. Allied to this, through protocol optimisation, lattice light sheet microscopy provided a method of imaging cells with the necessary resolution in space and in time to extract both long-term and short-term data on the movement of these structures without causing widespread damage to cells. This was important because studying chromatin dynamics at the TAD length scale, in living cells, has remained challenging due to the limitations of the methods available.

Using the workflow developed, I extracted information about the spatial distribution, splitting and merging events, and dynamic characteristics of the labelled chromatin domains. Perhaps unsurprisingly, most of the domains that were labelled were located at the periphery of the nucleus since pulses were generated towards the end of S-phase, when peripheral heterochromatin is replicated. More striking, however, was that characteristics such as velocity, distance travelled, and maximum displacement followed a right skewed distribution. This allowed me to define two distinct populations of domains, LMDs and HMDs. The former representing the bulk of chromatin domains, characterised by low relative mobility, and the latter representing those that were more mobile and were in the minority, representing the tail of the distribution. HMDs were also relatively more abundant in in the centre of the nucleus where the minority of all labelled domains resided. Due to the lower mobility observed more prominently in peripheral domains, it is likely

that an important number of these were bound to the lamina and were, therefore, LADs. In fact, the least mobile of all domains were found immediately adjacent to the nuclear lamina. On the other hand, the relatively higher mobility of central domains could be explained by the lack of anchoring structures to restrain the movement of structures. However, some central domains presented very low mobility, which could indicate their anchoring to structures such as the nucleolus.

Characterising the dynamics of TADs using this methodology, and without perturbations to the cells, allowed for the creation of a benchmark of an array of parameters against which to compare the effect different treatments can have on chromatin dynamics. By building on the work described above, I observed how DNA damage affected previously observed dynamics in an effort to better understand the nuclear events witnessed. An obvious change after DNA damage induction was the increase in the dynamism of chromatin, where the velocity and maximum displacement of domains increased significantly. The number of HMDs also reflected this change, with their relative numbers approximately doubling in long-term imaged cells but not quite reaching this value in short-term imaged cells. Interestingly, this increase in HMD numbers happened consistently across the nucleus and regardless of distance to the periphery. This was unexpected because of the greater degree of constraint peripheral domains showed on average. Despite this, it was clear that with the induction of DNA damage, the forces acting upon chromatin domains became more frequent and led to greater distances travelled, even if the patterns of movement remained the same.

DSB repair requires the migration of genomic regions. In the case of heterochromatin repair, these regions must be translocated from the chromatin compartments to which they belong. Furthermore, other studies have highlighted that break sites can also be translocated to the periphery for this same purpose (Taddei and Gasser 2006). Therefore, it is likely that the movements observed are either a direct consequence of this, where domains themselves are translocated for repair, rather than

just the DSB sites, which is something not described before, or that they happen as an indirect consequence, caused by the movement of other parts of the genome that ultimately relay forces onto the labelled domains. In fact, the direction of movement of chromatin domains was affected by the induction of DNA damage, becoming more perpendicular to the lamina in HMDs. However, there was contradictory evidence on LMDs and the population as a whole between long-term and short-term imaged cells, warranting more work on this area. In fact, further work will be carried out to investigate the effects of DNA damage on chromatin using this methodology but with a focus on the agents that may be involved in the phenomena observed, such as RAD52, which is crucial in recombination of DNA, and actin, which has been linked with the translocation of DSB sites.

Apparent contradictions in the evidence provided by short-term and long-term imaged cells were also found in other aspects of chromatin dynamics, which puts in evidence the importance of being able to acquire images at different time-scales. Splitting and merging events are an example of this. I expected that as chromatin becomes more dynamic, I would observe more splitting and merging events, as domains could encounter each other and move away more often. Not only that, if portions of the genome were being actively translocated, be that entire domains, or fractions of a domain, this would reflect on the frequency of these events. Indeed, this was the case when imaging cells in the short-term, where the number of splitting and merging tracks increased, in addition, the number of times each track exhibited this behaviour also increased. In contrast, long-term imaged cells contradicted these observations with not only decreases in the number of splitting and merging tracks, but also with a reduction in the number of events per track. These seemingly discrepant data illustrate not only the need for imaging to take place at different time-scales, but also the need to understand the reasons behind their differences and ways of conciliating them to develop true understanding of chromatin dynamics. It is possible that the more

frequent acquisition of images allows for the visualisation of events that a more sporadic capture rate does not, this being wholly dependent on the time-scales of the events being observed.

It is difficult to assess whether all splitting and merging events have a biological significance, or if they only take place due to serendipitous proximity. However, some domains were observed travelling significant distances before merging. It is known that inter-TAD interactions exist and that these play a role in regulation (Nora et al. 2012; Bar Yaacov et al. 2019; Welch et al. 2020), therefore, it would be beneficial to further investigate if the events observed can be related to these interactions. There is also the possibility that merging and splitting of tracks arise due to movements into and from the compartments to which TADs belong, something that is known to happen for heterochromatin to undergo homologous recombination repair, or as a result of changes in transcription patterns (Tsouroula et al. 2016; Paulsen et al. 2019; Beagan et al. 2020; Bonev, Mendelson Cohen, et al. 2017).

Following domain tracks was also key in better understanding the influences to which domains are subject. It was clear that the movement of HMDs is not solely dependent on diffusion and that other forces are being applied to them besides the constraints conferred by being part of chromosomes. The movement of some domains presented clear subdiffusive behaviour intercalated with superdiffusivity periods. The former could be explained by both tethering to nuclear structures, but also that, by virtue of being part of a chromosome, they remain tethered to the remainder of the macromolecule, restricting their movements. The superdiffusive movement of HMDs could be linked to their interactions with actin and its associated machinery. It is known that nuclear actin mediates the translocation of chromatin in the nucleus; it has been shown that the polymerisation of F-actin is crucial in the translocation of DSB sites through the action of myosin motor proteins, especially in heterochromatin. This process could be linked to the translocation of the whole domains rather than just the damage sites. Studies involv-

ing actin polymeriser Arp2/3 could be employed to assess whether the movement witnessed in these circumstances is also dependent on F-actin assembly or if it does not impact whole domain translocations (Christopher P. Caridi et al. 2018). Alternatively, phalloidin studies could also be used towards this end. Furthermore, it would be of interest to understand how domains connect to any nuclear structures that could be driving their movement and applying forces to them. Chaperones such as UNC-45b (Lee, Melkani, and Bernstein 2014) and Smc5/6 (Chiolo et al. 2011) are involved in establishing a bridge between DNA and myosin motors, therefore, they are good candidates to understand the mechanisms behind HMD movement.

Alternatively, other active events taking place in chromatin, such as the threading of DNA strands through loop extrusion could be behind the movements observed (Sanborn et al. 2015). Relocation for regulatory purposes could also be the root of some of these translocations. Solely by employing the methods used in this work it is not possible to determine the source of the phenomena described, therefore, more work is needed to understand the mechanism behind this.

However useful in researching nuclear dynamics at the Mb scale, this methodology does not allow for tracking of the smaller and more numerous, early replicating domains, which limits its application. There is also a trade off between the duration of imaging and the time step that can be applied during acquisition, making it difficult to observe, in the same cell, those events that take place over tens of minutes and those that happen in a few seconds. Despite this, the workflow developed can be used for the investigation of other perturbations to cells, for example, the degradation of structural proteins, such as cohesin or CTCF, or inhibition of myosin motors and actin polymerisation (linked with DNA translocation). There is also scope to investigate the process of chromosome condensation, nuclear envelope reformation and chromatin decondensation, by exploring how the labelled domains condense into mitotic chromosomes using this method. This could shed light on whether the observed

chromatin domains are solely composed of chromatin that is contiguous along the linear chromosome or if DNA originating from different parts of the genome coalesce together to form these structures. Understanding these processes could play an important role on the investigation of genomic stability and the processes associated with it, representing an important contribution towards research around diseases where this aspect is of importance, such as many types of cancer.

In summary, through the generation of a short pulse of tagged histones towards the end of S-phase I labelled TADs in such a way that their movements could be tracked through time using LLSM. This led to the identification of two different populations of chromatin domains in function of the displacement they presented, LMDs and HMDs. Characterisation of these two populations alluded to the presence of both constraints and forces that act upon them. The induction of DNA damage saw the alteration of dynamic characteristics of chromatin through mechanisms that are not fully understood but that can further be investigated using the methods described in this chapter. Ultimately, this work has added to what is known about the dynamics of chromatin at the TAD length scale, and has laid the foundations for future discoveries in this area by setting up a robust methodological pipeline for the imaging of chromatin structures at different time scales.

Chapter 4

Expanding the capabilities of RAPID-release

Pulse-labelling techniques are powerful tools that have been employed with great success in all areas of molecular and cell biology. Important scientific discoveries such as Okazaki fragments and the secretory pathway of cells have been possible through the application of techniques of this type (Stein and Alexandrov 2014; Palade 1975).

However useful, there are limitations to their employment in cell biology and imaging. For example, incorporation of radioactive amino acids or functional amino acid derivatives allow for immediate labelling of structures, but present challenges concerning imaging processing, resulting from the requirement for derivatisation of the incorporated functional groups (Lang and Chin 2014). Other self-labelling techniques such as SNAP-tag, that allow for real-time imaging of living cells, also present difficulties for the study of events with fast kinetics. This derives from the time it takes to quench, pulse, and label the reporters, which can take from minutes to hours (Juillerat et al. 2003; Crivat and Taraska 2012; Clément et al. 2016).

The development of RAPID-release by Apta-Smith *et al* (2018) took a novel approach through the employment of a rapid pulse of labelled proteins that can be observed at the single-cell level, in real-time, using fluorescence microscopy. It relies on tethering of the protein of interest

to a cytosolic anchor soon after translation (in this case, the outer mitochondrial membrane [OMM]), which provides the time necessary for folding and maturation of the associated fluorescent tag, as well as for the accumulation of greater numbers of the protein to be pulsed. This is followed by the addition of Rapamycin (RAP), which promotes release of the anchored POI and the generation of the desired pulse through the activity of tobacco vein mottling virus (TVMV) protease (Stein and Alexandrov 2014; figure 3.1).

For processes whose kinetics exceed those of the folding and maturation of fluorescent protein tags, the above mentioned characteristics are key. Processes such as nuclear import and incorporation of histones into chromatin, which would be difficult to study using traditional pulse-labelling methods are a good example (Campos et al. 2010; Bonner et al. 1988; Reits and Neefjes 2001; Chudakov, S. Lukyanov, and K. A. Lukyanov 2005; Ishikawa-Ankerhold, Ankerhold, and Drummen 2012). The employment of RAPID-release for the study of chromatin domain dynamics in the previous chapter is evidence of how powerful this technique is, with the potential to study a broad range of other nuclear processes.

The work presented in this chapter aims to enhance RAPID-release in three ways: (1) To decrease variability in behaviour of the system between cells, whilst, at the same time, increasing the speed of release of the tethered cargo, (2) improve adaptability of the system, to be used in a variety of different research, and (3) to develop an orthologous system using distinct chemically-induced dimerisers and proteases, allowing for the generation of two independent pulses in the same cell. To achieve the first goal I attempted to stabilise the ratio between protease and tether by eliminating the reliance of RAPID-release on the transfection of two separate vectors, and replace this with one single vector with both components. To achieve the second aim, I made the system fully modular, and in order to achieve third goal, I replaced the Rapamycin-induced dimerisers with Abscisic acid (ABA) and Auxin (AUX)-induced

versions, and the TVMV protease with a HCV and TEV counterpart, as well as the associated target cleavage site.

My attempts were successful at decreasing the variability of the system across populations of cells as well as at increasing the average speed of release of tethered cargo. I was also successful at generating a modular system that is easy to edit and adapt to the needs of any project. However, the generation of an orthologous system to RAPID-release proved to be challenging, as the novel combinations of dimerisers and proteases failed to produce kinetics similar to those of RAP-TVMV.

4.1 A single vector construct improves upon consistency of a dual vector system

RAPID-release (Apta-Smith, Hernandez-Fernaud, and Bowman 2018) (figure 4.2A) relies upon the transfection of two distinct vectors: one encoding the tether, and another encoding the protease (figure 4.2 B). I posited that carrying out a double transfection with both elements of the system would yield high variability between the cells of a population regarding the level of expression of each individual vector, and that this would happen as a direct consequence of cells taking up different amounts of each plasmid. Asymmetries in expression between the two elements of the system would, therefore, be followed by a disparity in cargo release kinetics between cells, since the release rate of the tethered cargo is dependent on the ratio between the protease and the tether element, *i.e.*, the greater the protease to cargo ratio, the faster the release (figure 4.2 G).

To tackle this heterogeneity issue I looked to generate a single vector that contained the two elements as an Internal Ribosome Entry Site (IRES)-separated cistron (figure 4.2 B). IRES is an RNA element that allows for cap-independent translation initiation. If this element is placed after the primary open reading frame of an mRNA molecule, translation takes place from both the cap and the IRES site. If a stop codon is

placed immediately before IRES, two independent polypeptides can be generated from one single mRNA molecule (Renaud-Gabardos 2015).

I hypothesised that employing this method would not only eliminate the variability in protease:tether ratio generated by two-plasmid transfections, but also increase the ease with which this step is performed. This would hold true regardless of the number of plasmids a cell may take up.

4.1.1 Relative order of the RAPID-release elements and IRES

To decide the order in which the two elements should be in relation to IRES, my first approach was to design and generate two potential versions of this IRES-RAPID-release (IRR) system. One where the protease was encoded before IRES and the tether after, and the other in the opposite order. These two iterations of IRR were developed due to the fact that cap-dependent and IRES-dependent translation have different efficiencies, the latter being, in most cases, between 20 and 50% as efficient as the former (Mizuguchi et al. 2000). It was important to assess if the Protease:Tether ratios generated by each of the versions allowed the system to operate correctly, or if that difference in efficiency would have a significant impact in the way RAPID-release operated.

Transfection of each IRES construct showed EGFP anchored to the OMM, as well as mCherry soluble in the cytoplasm, in a pattern equal to that of the original RAPID-release. This was the case for both versions of IRR, suggesting both elements were being expressed as separate proteins independently of their order in relation to IRES, and proving that IRES does not interfere with the cellular localisation of upstream or downstream constructs (figure 4.1).

However, I also observed that cells transfected with the Protease-IRES-Tether version of IRR presented a high level of background cargo release in the absence of Rapamycin (figure 4.1, yellow arrows), something that was not observed in cells transfected with the Tether-IRES-

Protease version. This created a problem for the correct functioning of RAPID-release, which relies on the creation of an intense pulse of labelled cargo. The inadvertent release from the cytosolic anchor cripples its function and reduces its benefits. I did not believe that this could be attributed to IRES affecting the function of OMP25, as this element is present in the C-terminus of the tether construct. OMP25 is located far downstream from the IRES in the case of Protease-IRES-Tether, where I observe the higher EGFP background, but adjacent to IRES in the Tether-IRES-Protease version, where this phenomenon was not observed.

I believe, therefore, that the background is a consequence of spurious cleavage events of cargo from the OMM as a result of the high protease to tether ratio, promoted by the different efficiencies of cap-dependent and IRES-dependent translation. Under normal circumstances the auto-inhibitory domain would be capable of preventing pre-rapamycin release of cargo but the increased abundance of protease increases the likelihood of cleavage and, therefore, a background release of cargo can be observed. As a result of these findings I decided that the Tether-IRES-Protease version of IRR (figure 4.1 B) was the most appropriate to move forward towards my goal of improving upon RAPID-release, since it did not present a significant premature cargo release problem.

Further to this, in IRES-dependent translation, the IRES' origin recognition element causes the addition of a tetrapeptide (Met-Ala-Thr-Thr) at the beginning of the reading frame that follows. This does not represent a problem in the protease construct, however, it would limit the use of the system if the integrity of the N-terminus of a protein of interest were important for its function, as is the case with histones.

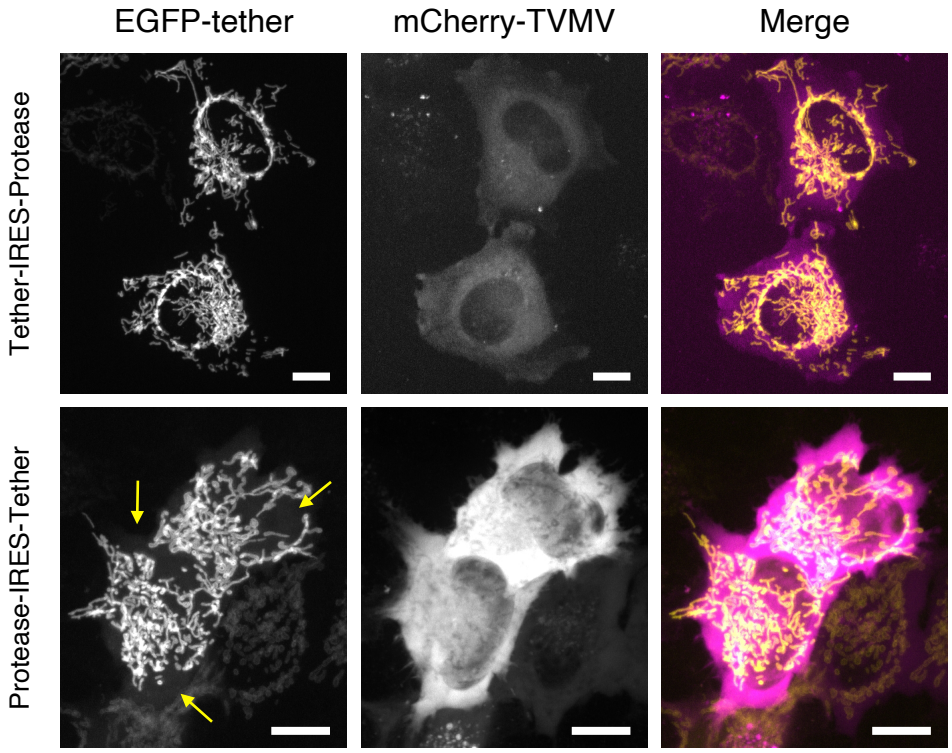

Figure 4.1: Element order affects the performance of RAPID-release. Cells expressing the Tether-IRES-protease (top row) version of IRR present less background cleavage than those expressing Protease-IRES-tether (bottom row, yellow arrows). The former expresses less protease in relation to tether than the latter (mCherry channel). Scale bar, 10 μm. EGFP channel in yellow and mCherry in magenta.

4.1.2 Two-vector *versus* polycistronic expression

My next step was to compare IRR to the two-plasmid version of RAPID-release to assess whether my approach would succeed at improving its kinetics.

I started by comparing the relative amounts of protease to tether construct between a population of cells transfected with the two original RAPID-release plasmids, and another transfected with IRR. Both were imaged using the same laser intensities and exposure times. I then extracted the mean pixel intensity of the EGFP signal, and that of the mCherry to calculate the ratio between protease and tether for cells in both populations, and compared the results between the two groups.

I observed that cells transfected with IRR presented significantly greater Protease:Tether ratio than their two-plasmid counterparts (0.440 and 0.328, respectively, p=0.00402, t-test). I also observed that the variance on these ratios was significantly reduced in IRR when compared to the original system ($p=1.053e-07$, f-test; figure 4.2 E). This suggested that there was an improvement in consistency of expression in the cells where IRR was employed, when compared to the two-plasmid version.

To evaluate whether the reduction in expression variability would also translate into a reduction in the variation of the kinetics of the system across cells, I next studied the rates of cargo release from the OMM. As a measure for cargo release I used the variation in the standard deviation (SD) of the maximum pixel intensity of the EGFP signal of the whole cell through time. This metric was chosen because prior to the addition of RAP the entirety of the EGFP signal originates from the mitochondria, resulting in a high standard deviation between the intensity of pixels across the cell as a whole. However, once RAP is added and cargo starts to be released, EGFP becomes increasingly diffused, reducing the SD of the pixel intensity (figure 4.2 C and D). By analysing how fast this decline in SD occurs I can infer how fast cargo is released from the OMM in each cell. I recorded this variation upon the addition of RAP, and calculated the slope of the line fitted to the first five time-points. This

time window was chosen as it is the interval in which SD fits to a linear regression, and its variation can be attributed to the diffusion of EGFP after cleavage from the OMM.

I observed that the IRR system leads to a significant reduction in release rate variance ($p=8.42e-4$, f-test; figure 4.2 F). This is clear when analysing the release profiles in figure 4.2 D, where greater homogeneity between cells can be observed in IRR-transfected cells (right) than with the two-plasmid system (left). Furthermore, the IRR cells also presented a significant increase in the average rate or cargo release when compared to the two-plasmid system (0.063 and 0.035, respectively, $p=1.632e-05$, t-test; figure 4.2 F).

I, therefore, concluded that transforming RAPID-release from a two-plasmid into a one-plasmid system improved the consistency of its behaviour between cells and promoted faster kinetics, allowing faster cellular processes to be studied through its application. It is important to note, however, that in some specific instances, transfecting two different plasmids can generate Protease:Tether ratios that lead to faster release. However, employing the two-plasmid system to achieve faster release kinetics in a small number of cells stands as a trade-off between this and consistency across the cell population and low levels of background cleavage.

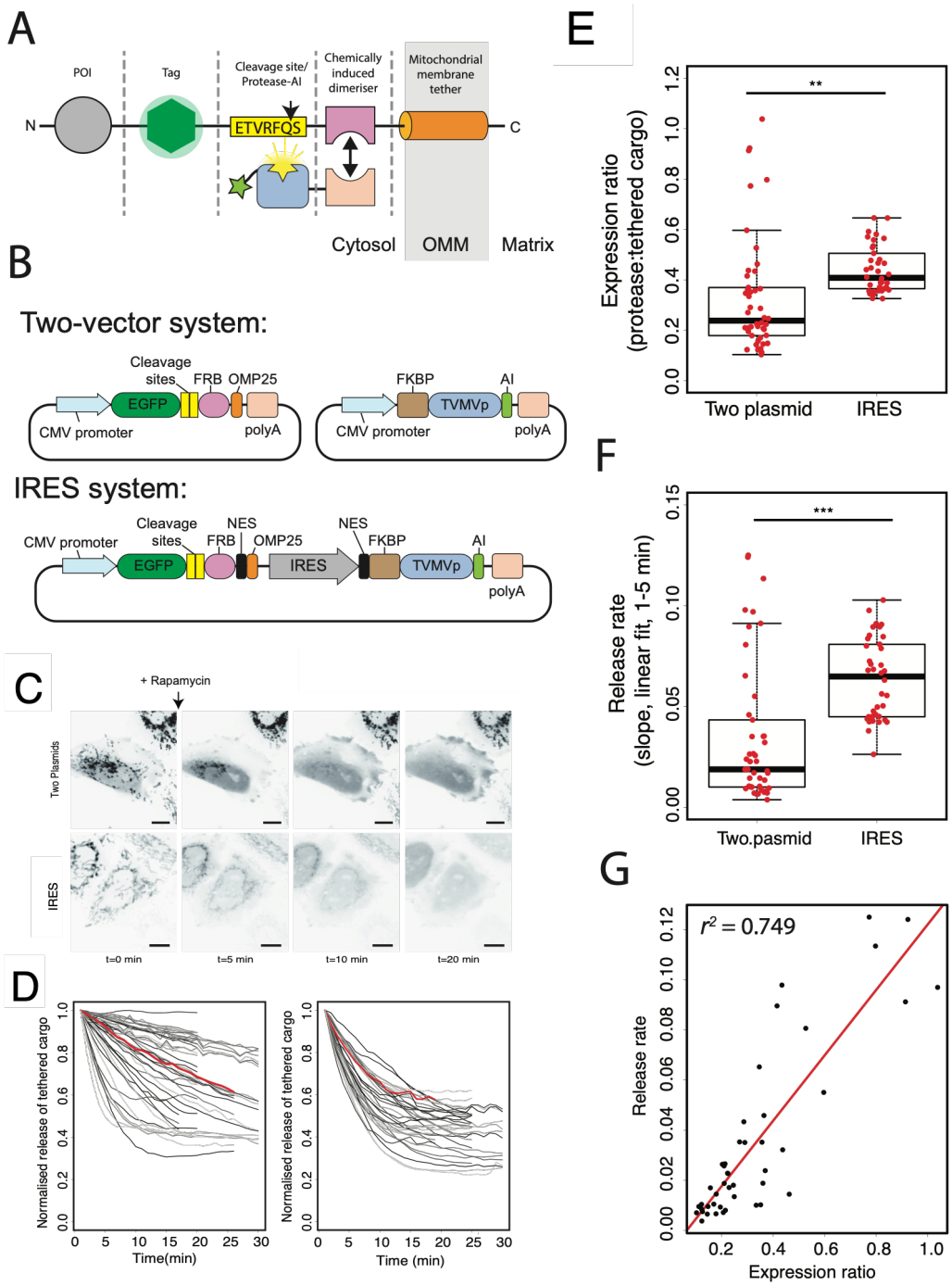
A
POI
Tag
Cleavage site/ Protease-AI
Chemically induced dimeriser
Mitochondrial membrane tether
N
ETVRFQS
C
Cytosol
OMM
Matrix
B
Two-vector system:
Cleavage sites
FRB
OMP25
EGFP
CMV promoter
polyA
FKBP
AI
TVMVp
IRES system:
NES
IRES
C
+ Rapamycin
Two Plasmids
IRES
t=0 min
t=5 min
t=10 min
t=20 min
D
Normalised release of tethered cargo
Time(min)
Time (min)
E
Expression ratio (protease:tethered cargo)
Two plasmid
IRES
F
Release rate (slope, linear fit, 1-5 min)
Two.pasmid
G
$r^2 = 0.749$
Release rate
Expression ratio

Figure 4.2

Figure 4.2: IRES-RAPID-release (IRR) *Vs* dual vector system. **A** An overview of the RAPID-release system with the tethered element above and the soluble element below. **B** structure of the original two-vector system and the IRR system. **C** An example release of EGFP from OMM upon addition of rapamycin for the two-plasmid and IRR systems. **D** SD of the max pixel intensity of individual cells through time (measure of release kinetics) two-vector (left) versus the IRR systems (right). Red traces depict cells shown in D. **E** The ratio between the protease and tethered construct is significantly greater in IRR than in the original two-vector system. IRR also presents significantly less variance in this metric, across the cell population. **F** Release rates of tethered cargo are significantly greater in IRR when compared with the two-vector system. The variance of release rates is less in IRR compared to the two-vector version. **G** The ratio of protease to tethered construct is directly proportional to the release rate.

4.2 Conferring a modular structure to IRES-RAPID-release

Redesigning RAPID-release to transform it into IRR gave me the opportunity to add features that were not present in the original system. First, I made the system modular. When designing IRR I placed a unique restriction site between each of the elements that compose it. This eased the addition and replacement of cargo and fluorophores, facilitating the study of different proteins of a pathway, or different pathways all together. Having the ability to exchange labels is also important in case fluorescence microscopy is not appropriate for the study of certain processes. The presence of unique restriction sites between any of the other modules of IRR also allows for the effortless alteration of any aspects of the system the user may deem necessary.

I also added a nuclear export sequence (NES) to both elements of the system, which is not present in the original RAPID-release (figure

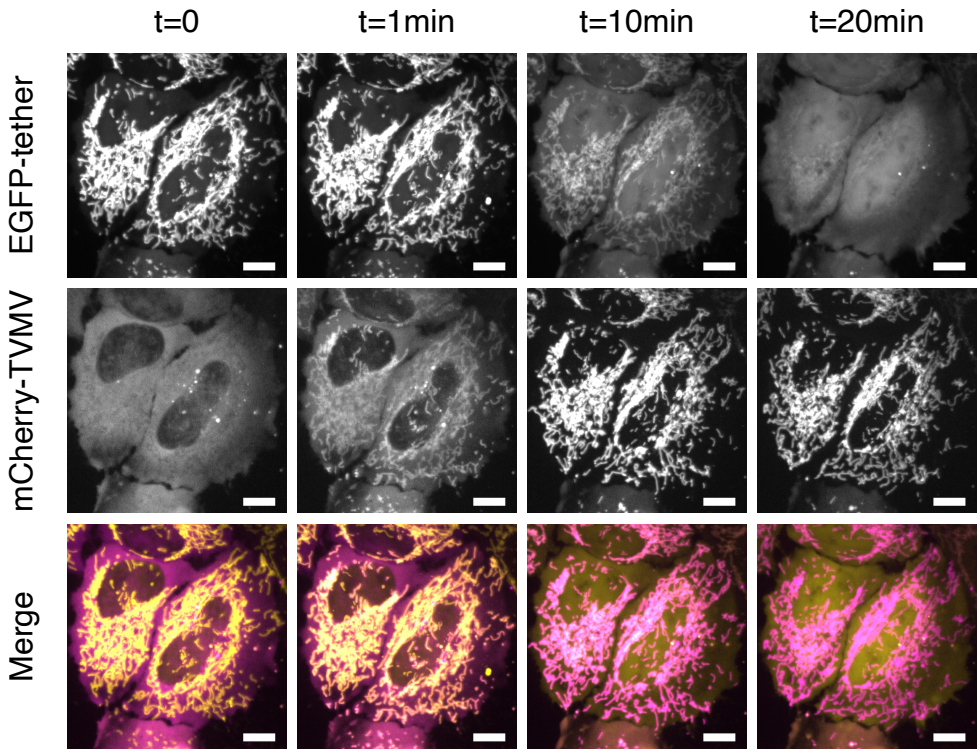

Figure 4.3: Tether release from cargo-free IRR. Upon addition of RAP, EGFP is cleaved from the OMM and diffuses through the cytoplasm. The addition of an NES prevents the protease and uncleaved tether from accumulating in the nucleus. Scale bar, 10 μm. EGFP channel in yellow and mCherry in magenta.

4.2 B), to decrease the probability that once translated, a tether element containing a nuclear protein would be imported before it had the chance to be anchored to the OMM. The NES added to the soluble element prevents it from accumulating in the nucleus, freeing it from mCherry, which allows for the labelling of intra-nuclear structures using fluorophores that operate in this channel without the interference of this element (figure 4.3).

Adding and changing cargo with IRR

To test the modularity and versatility of IRR, I added two different cargo proteins to the system – histone H3.1 and the ribosomal protein RPL11. Both of these proteins are imported into the nucleus upon translation. In the case of histone H3.1 it is incorporated into chromatin as

part of the nucleosome, and RPL11 is transported to the nucleolus to be assembled into ribosomes as part of a large ribosomal subunit (LSU) subcomplex, the 5S RNP, which is composed of the 5S RNA, RPL5 and RPL11 (Sloan, Bohnsack, and Watkins 2013).

Both of these proteins were added to IRR with ease, requiring only one PCR and one restriction endonuclease cloning event. They were added to the N-terminus of the tether as illustrated in figure 4.2 A, leaving them tagged by EGFP on their C-terminus. When expressed in context with IRR, both EGFP-labelled proteins were anchored to the OMM. Upon addition of rapamycin, they dissociated from the OMM and import into the nucleus was observed with kinetics similar to those described before (figure 4.4). It was also possible to observe the enrichment of RPL11 in the nucleolus as time progressed. This is encouraging data that exemplifies the versatility of IRR, and illustrates how its employment can have direct implications on the research of nuclear processes, or, indeed, implications in research of diseases such as Diamond-Blackfan anemia, which arises due to mutations on RPL11 (Gazda et al. 2008).

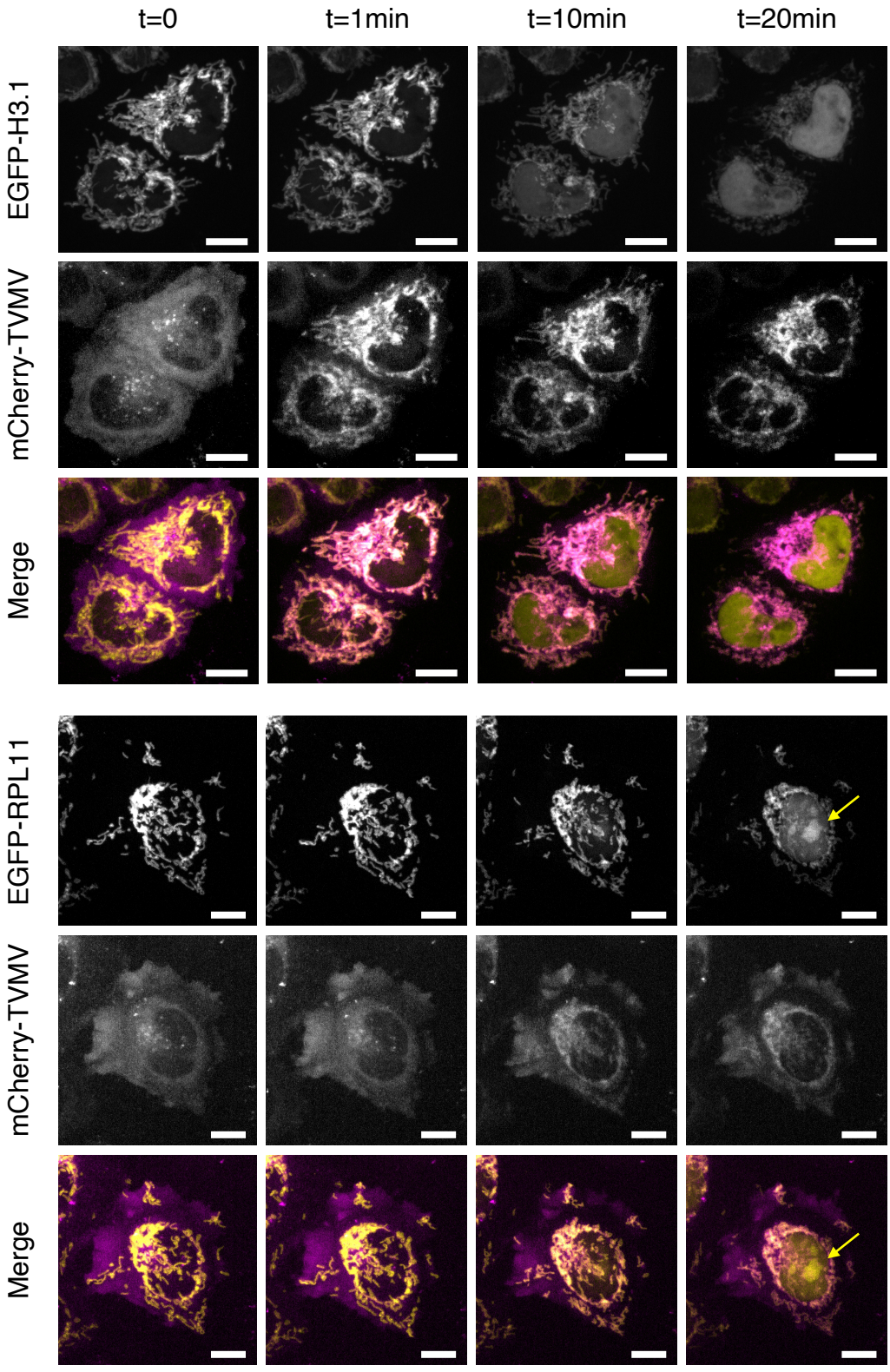

Figure 4.4: Compatibility of IRR with different proteins of interest. IRR with different cargo: H3.1, and RPL11. Yellow arrows indicate the nucleolus, where RPL11 accumulates after the addition of RAP. Scale bar, 10 μm. EGFP channel in yellow and mCherry in magenta.

Introducing HALO technology as an alternative fluorophore

I then looked to alter the fluorophore associated with IRR. This is important since altering the way a protein is labelled can open doors to new ways of studying their behaviour through different methods other than fluorescence microscopy, such as affinity chromatography/pulldowns, biotin conjugation, *etc.*

I chose to replace EGFP with HALO-tag, a self labelling protein tag that covalently binds to a synthetic ligand (by *Promega Corporation*, Kiwamu Takemoto, Tomoki Matsuda 2011). The protein tag encoded is a 33kDa catalytically inactive hydrolase that is not endogenous to human tissues and that under physiological conditions binds covalently to a small synthetic ligand in an irreversible manner. These ligands dictate the wavelength in which the tag can be observed, making it easier to change the colour of the label between experiments if necessary (He et al. 2011). By utilising the modular characteristics of IRR, I replaced EGFP with HALO and transfected the HALO-IRR (without cargo). The synthetic ligand was then added to cells, in this case OregonGreen (figure 4.5), and the HALO-OregonGreen pulse was initiated by addition of rapamycin.

As expected, the addition of RAP led to the dimerisation of FRP and FKBP, and the consequent enrichment of mCherry on the OMM. However, interestingly, this dimerisation did not translate into the release of the tethered HALO-OregonGreen in a pattern similar to the one observed in in figure 4.3. What I observed was the maintenance of the fluorophore on the OMM (figure 4.6 A). I postulated that the synthetic ligand in solution could be inhibiting the activity of TVMV and, therefore, preventing any release from the OMM. Therefore I added RAP to a population of cells transfected with IRR-HALO where OegonGreen had not been added. After 30 minutes I added the ligand and imaged the cells. I assumed that if Oregon Green was causing protease inhibition I would see the fluorophore diffused throughout the cell. On the other hand, if it was the HALO element itself that was preventing its own release from the OMM, or any other phenomenon, I expected to see enrichment of

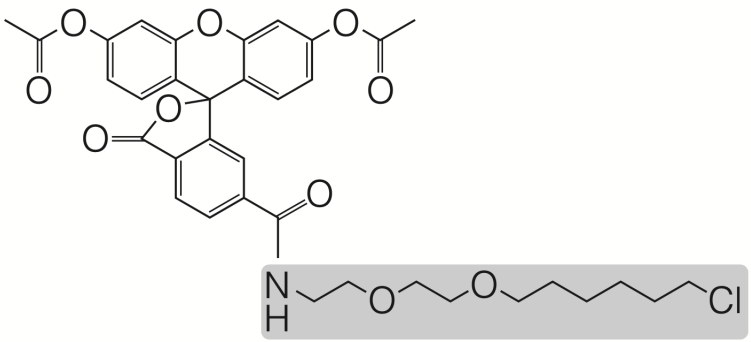

Figure 4.5: Chemical structure of OregonGreen fluorescent dye, a synthetic ligand compatible with HALO-tag. In grey the substrate for the HALO hydrolase where the covalent bond forms.

OregonGreen on the OMM.

I observed that, once again, mCherry had enriched the OMM, suggesting dimerisation was still taking place, but, more importantly, that OregonGreen was diffused throughout the cell (figure 4.6 B). This indicates that HALO had been released from the OMM upon the addition of RAP, suggesting that the OreonGreen dye inhibits the activity of TVMV but the Halo element itself does not.

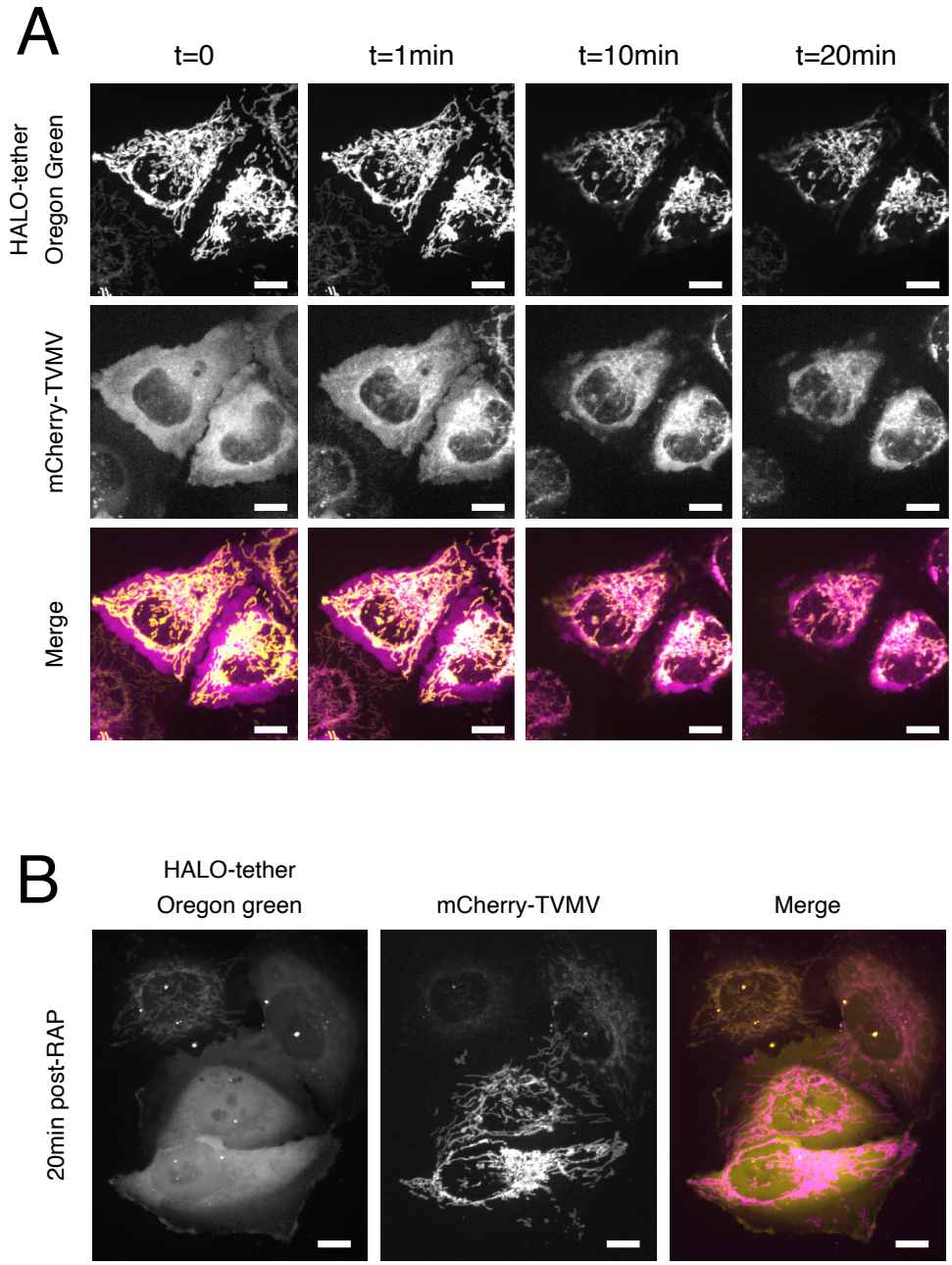

Figure 4.6: Effect of OregonGreen on HALO-IRR kinetics. **A** The use of HALO technology where the OregonGreen is added to the medium prior to RAP prevents the release of tethered cargo by TVMV cleavage. **B** When OregonGreen is added to cells after RAP, the cleavage of tether construct is rescued. Scale bar, 10 μm. EGFP channel in yellow and mCherry in magenta.

4.3 Development of a system orthologous to IRES-RAPID-release

IRR's newly conferred modularity created the opportunity to develop an orthologous system that relied on the same principles as RAPID-release, but that employed different sets of dimerisers and proteases. I developed this orthologous IRR for two reasons: (1) some element in the original IRR could be incompatible with some types of research (where, for example, rapamycin may be needed for other purposes), and (2) it would create the ability to generate two distinct pulses within the same population of cells independent of each other.

4.3.1 RAP-TVMV, ABA-HCV, and AUX-TEV

I started by employing the enhanced modularity of the system to easily replace the key elements of IRR. A version was generated where abscisic acid (ABA) receptor PYL1 (PYL1) replaced FKBP, Abelson Interactor 1 (ABI1) replaced FRP (PYL1 and ABI1 dimerise in the presence of ABA) (Liang, Ho, and Crabtree 2011), and Hepatitis C Virus (HCV) protease replaced TVMV (figure 4.8 A). Another version was also produced where Transport Inhibitor Response 1 (TIR1) replaced FKBP, Auxin-inducible degron (AID) replaced FRB (which dimerises in the presence of auxin (AUX)), and Tobacco Etch Virus (TEV) protease replaced TVMV.

The two dimerisation pairs and proteases were chosen because the small molecules that activate them have no analogs in human cells and, therefore, any cross-talk between the system and physiological processes would be unlikely. Similarly to TVMV in IRR, the proteases chosen included auto-inhibitory domains (AI) that were designed to prevent the spurious cleavage of cargo off the OMM through competitive inhibition, prior to the addition of the dimerisation-inducing small molecule. The AI used with HCV was previously designed by Ingallinella et al. 2000. The AI I used for TEV, however, was generated by me through mutation

of the native TEV substrate (ENLYFQ—(G/S)), where a proline was inserted in the position immediately after the cleave site to generate the sequence ENLYFQ—PG. I posited that adding a proline residue to the position immediately after the cleavage site could inhibit the activity of TEV.

I was aware that the AUX triggered approach could lead to premature targeting and degradation of the protease and/or tether by the proteasome if TIR1 reached high enough levels (S. Li et al. 2019). To try to prevent this, AID was placed on the soluble portion of IRR, and TIR1 was anchored to the OMM. If this undesirable degradation were to take place none-the-less, there would not be a signal on the EGFP, mCherry, or both channels.

Upon testing I observed that the new orthologous systems were not functioning like the original rapamycin-induced system. The abscisic-acid triggered IRR (ABA-IRR) presented the same characteristics as rapamycin-triggered IRR (RAP-IRR) prior to the addition of their respective small molecule trigger; there was enrichment of the tether on the OMM, and the protease was diffused through the cytoplasm. It was also encouraging to observe that upon the addition of ABA, mCherry-HCV enriched on the OMM, suggesting that the ABA-dependent dimerisation took place. However, even though dimerisation occurred, HCV did not cleave EGFP from the OMM at a rate similar to that of RAP-IRR since the increase in diffusible EGFP was negligible (figure 4.7 A and B).

The auxin-triggered IRR (AUX-IRR) presented yet a different set of issues, even if neither the tether nor the protease had been targeted for degradation by the proteasome. In this case, protease was diffused throughout the cytoplasm and the tether construct was enriched on the OMM as expected. However, it was clear that even prior to the addition of AUX there was already a significant presence of soluble EGFP in the cytoplasm, suggesting a significant constitutive cleavage of the cargo off the OMM (figure 4.7 C). I attributed this to the inefficiency of the AI that was developed precisely to prevent this phenomenon. As it was

stated in subsection 4.1.1, this undesirable outcome would undermine the applications or IRR and cripple its use. Furthermore, upon the addition of AUX there was not a rapid enrichment of mCherry-TEV to the OMM, as observed with RAP-IRR and ABA-IRR. Interestingly however, even though this phenomenon was not observed, the EGFP that still enriched the OMM at this point was completely released after 20 minutes (figure 4.7C).

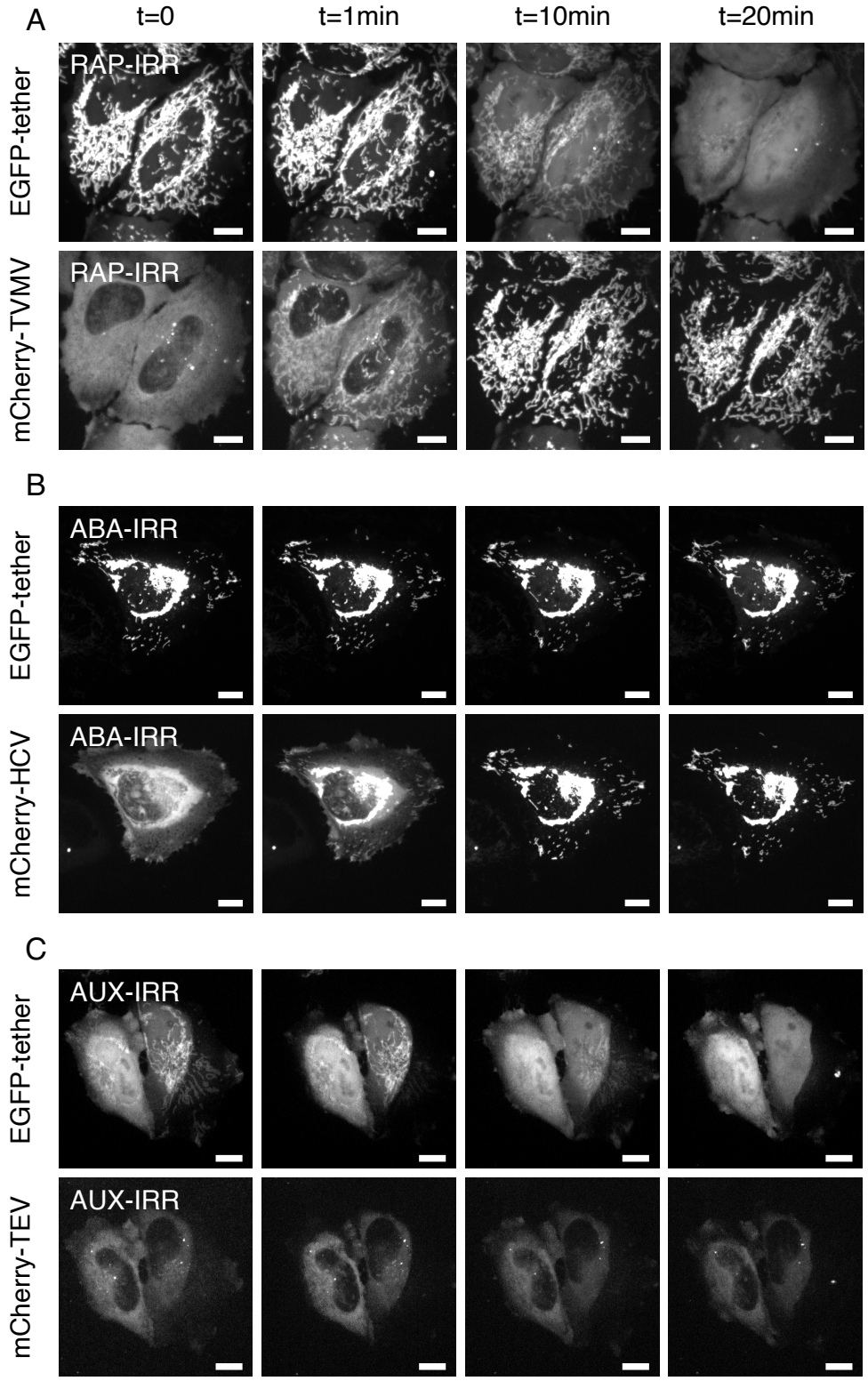

Figure 4.7: Testing of different orthologous dimerisers and proteases to RAP-IRR. **A**, Original RAP-IRR before and after the addition of RAP. **B**, ABA-IRR before and after the addition of ABA. **C**, AUX-IRR before and after the addition of AUX. Scale bar, 10 μm.

4.3.2 Optimisation of ABA-IRR

Taking into consideration the outcomes described in subsection 4.3.1, it was decided that AUX-IRR would be abandoned as potential orthologues but that ABA-IRR would be further investigated in the attempt to generate an alternative system. This was due to two reasons: (1) it was not clear if TIR1 and AID1 were dimerising at rates compatible with what is expected of IRR, and (2) the background cleavage of TEV was too high to fit the purpose of IRR.

To understand the reason behind the inactivity of HCV, I proceeded to generate all four possible combinations of dimerisers and proteases (RAP-TVMV, ABA-HCV, RAP-HCV, and ABA-TVMV) to compare the kinetics of these permutations. Generation of these permutations was facilitated by the modularity conferred upon the system when upgrading RAPID-release into IRR.

I expected that if HCV was not compatible with the structure of IRR it would fail to cleave cargo off the OMM regardless of the dimeriser associated with it. On the other hand, if the incompatibility was generated by the dimerisers themselves, I expected TVMV to be inhibited when paired with the ABA dimerisation pair, and HCV regain its activity once paired with the RAP dimerisation pair.

I observed that when paired with FKBR/FRB, HCV's activity was greatly improved, increasing from 0.017 to 0.040 (p=7.884e-14, t-test). I also observed that, just like HCV, if TVMV was paired with PYL1/ABI1 its activity was significantly inhibited, dropping from 0.055 to 0.022 (p=5.933e-16, t-test; figure 4.8 B and C). The permutation of these elements also showed that TVMV had a higher cleavage rate than HCV, 0.063 compared to 0.040, respectively (p=1.196e-07, t-test). Interestingly, this difference between TVMV and HCV was still observable even when both proteases were associated with the ABI1/PYL1 dimerisation pair and their activity was significantly reduced. Here, the cleavage rate of TVMV was also significantly greater than that of HCV (0.022 and 0.010, respectively, p=0.0394, t-test; figure 4.8 B and C).

These data suggest that the reason behind the inactivity of HCV in subsection 4.3.1 was not its incompatibility with IRR. The data points towards the ABA dimerisation pair conferring much slower cleavage kinetics upon fused proteases through a mechanism that is not yet known. It was clear that if I were to create an orthologous system and apply the ABA pair, these incompatibilities would have to be resolved.

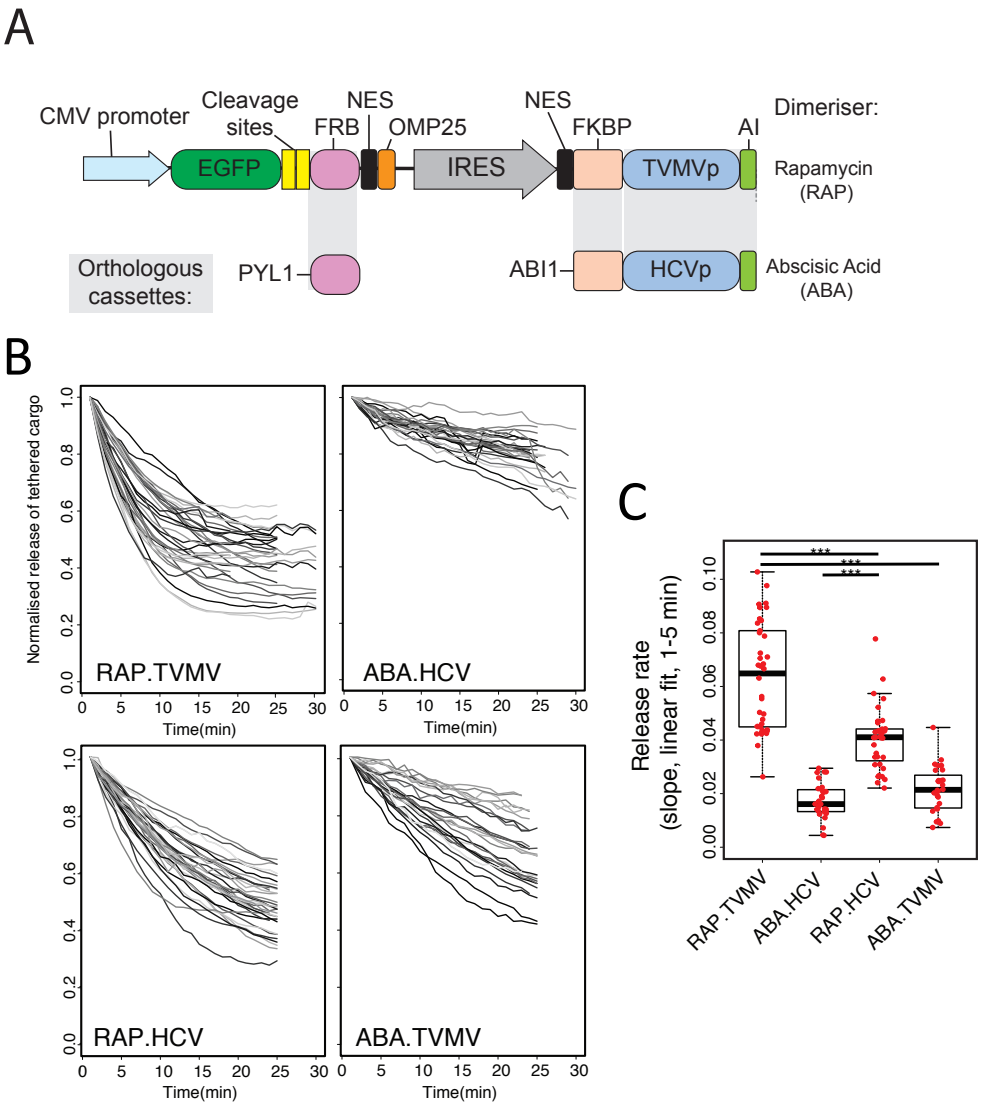

Figure 4.8: Combinatorial analysis of RAP and ABA dimerisers, and TVMV and HCV proteases. **A** Diagram of RAPID-release and its orthologous cassettes. **B** SD of the max pixel intensity of individual cells through time (measure of release kinetics) of all four combinations of dimerisers and protease. **C** Release rates of different combinations of dimerising domains (rapamycin or abscisic acid-triggered) and proteases (TVMV or HCV).

4.3.3 Modifying the abscisic acid dimerisation system to enhance release kinetics

I aimed to assess whether TVMV and HCV protease inhibition took place through chemical inhibition dependent on the ABA molecule itself. To achieve this, RAP-HCV was triggered by the addition of RAP in the presence of ABA. Under these condition, if ABA itself was causing the inhibition of proteolytic activity, there would be no release of cargo from the OMM. However, if this was not the mechanism of inhibition I would see similar kinetics independently of the presence or absence of abscisic acid.

I observed that RAP-HCV protease recruited to the OMM with comparable kinetics upon rapamycin addition, as expected, with the release profiles and rates showing no significant difference between the experiments performed in the absence or presence of ABA (0.040 vs 0.044, respectively, p=0.2944, t-test; figure 4.9 A). This suggested that chemical inhibition is not the mechanism through which the ABA dimerisation pair is inhibiting the associated proteases.

Following this, I postulated that the inhibition of protease activity derived from a steric hindrance of the proteases in reaching their cleavage sites.

To test this, I theorised that a different arrangement of the dimerisation domains would rescue proteolytic activity, by bringing into closer proximity the protease and the target site.

To achieve this, I pursued two strategies. Firstly, I analysed the crystal structure of the dimerised PYL1 and ABI1 (PDB: 3KDJ) and designed a circularly permutated version of ABI1, in such way that its C-terminus containing the HCV protease would come into closer proximity with its target site in the tethered element (figure 4.9 B). Secondly I performed a cassette swap of the ABI1 and PYL1 domains, so that ABI1 would be present in the tethered and PYL1 in the soluble element fused to the protease (figure 4.9 C). My rational was that because ABI1 and HCV are both relatively large globular proteins, their flexibility is limited,

but because PYL1 has smaller dimensions it could confer the protease construct greater flexibility in reaching its cleavage site, which may, in turn, rescue HCV activity.

My data shows that the circularly permutated ABI1 (CP-ABI1) domain in conjunction with the original PYL1 still dimerised in the presence of ABA, suggesting that the alteration of the polypeptide had not affected the system. However, I still observed low rates of cleavage, which were comparable to those seen with the original ABA pair. In fact, there was a significant decrease in cleavage rate from 0.017 to 0.011 in this instance ($p=0.001231$, t-test). The swap of ABI1 and PYL1 between elements proved successful in dimerising, however there was still not a significant difference between the two permutations in terms of release rates; the original disposition of the pair allowed for a release rate of 0.017, where the swapped domains presented one of 0.015 ($p=0.1491$, t-test; figure 4.9 D).

Both these results suggest that I either failed to bring the protease and the target site into close proximity, or that the mechanism through which PYL1/ABI1 inhibits HCV and TVMV is different to what I hypothesised. Closer inspection of the PYL1 structure revealed that the N and C-termini are also orientated away from the ABI1 interface, suggesting the former may be true, and that a double circular permutation may be necessary.

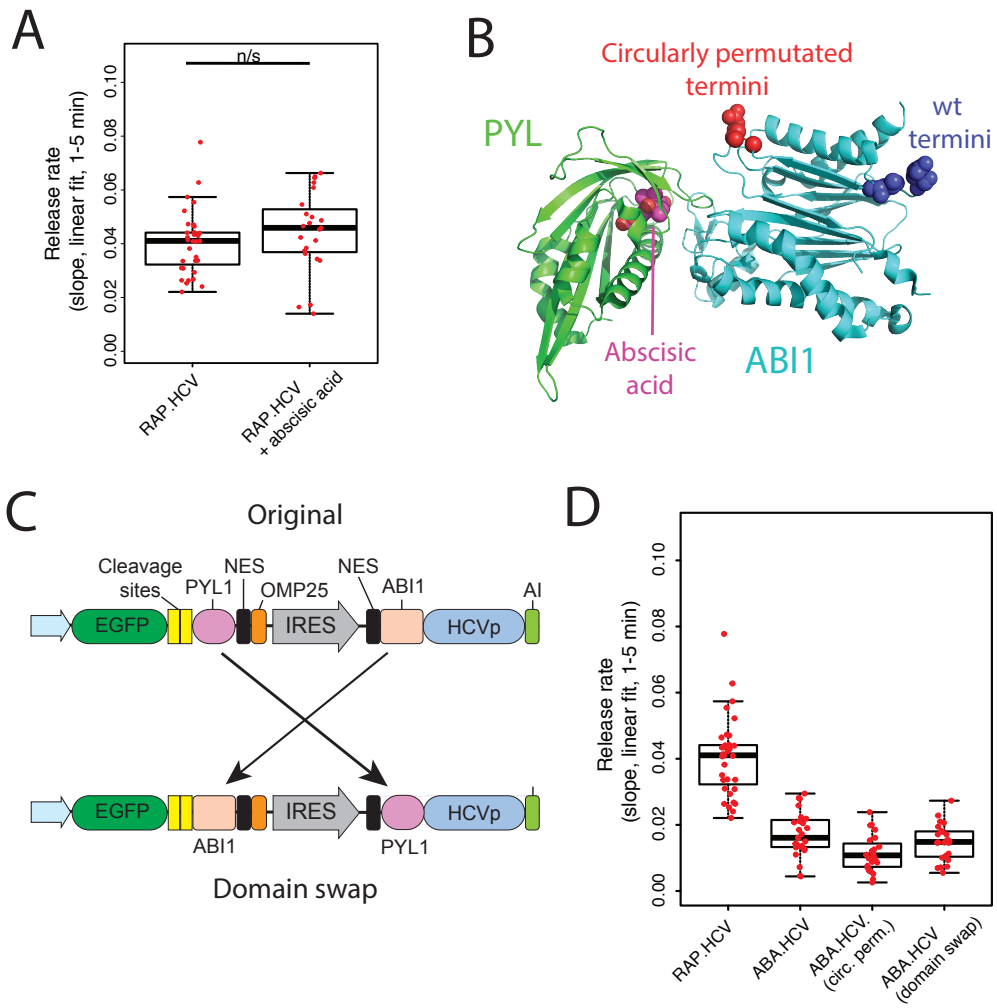

Figure 4.9: Proteolytic activity inhibition caused by ABA dimerisation system. **A** The inhibition of proteolytic activity is not caused by the presence of ABA. **B** Crystal structure of dimerised PYL1 and ABI1 in the presence of abscisic acid. Circularly permutated termini highlighted in red and dark blue. **C** Diagram of domain swap between the two cistrons of IRR. **D** Release rate alteration of ABA-HCV after the application of proteolytic activity-rescue measures.

4.4 Discussion

The optimisation and improvement of RAPID-release had three principal aims: (1) improve the existing system in terms of speed and consistency, (2) improve usability, and (3) create an orthologous system to the original RAP-IRR to allow dual pulse events.

I was successful at achieving aim number one by combining both tether and protease in a single IRES-based expression vector. This increased the average speed of cargo release and reduced variability across cell populations. A clear advantage of these improved characteristics is that cellular pathways with faster kinetics can now be studied more easily across a population of cells. This will ensure that the data of studies that rely on a high number of observations are now easier to acquire and analyse, since a higher proportion of cells will present adequate levels of both elements of the system.

My second aim of improving system adaptability and ease of use by introducing unique in-frame restriction sites between the functional elements was also successful. It was important for this aim to be achieved so IRR could be used as widely as possible. Increasing the ease with which fluorophores, cargo, and other elements can be exchanged will ensure that research of varied types will capitalise on IRR, even if their specific necessities are somewhat different to ours. However, it was made clear by my attempt to use HALO-tag as a replacement label that some changes to the system may not be possible, and that these must be thoroughly tested and understood. I would argue that this may even be the case with certain types of cargo. It is likely that some proteins may interfere with the system itself or that it may simply be incompatible with cell physiology for certain factors to exist anchored to the OMM without triggering cell death or affecting other signalling pathways.

I am aware, however, that more work needs to be done to achieve aim number three, and confer upon the system dual-release capabilities. It was useful to understand that the ABA dimerisation pair was preventing the cleavage of cargo from the OMM and that this likely happened due

to structural limitations and not chemical interaction between ABA and the proteases. In the future I intend to take this approach further and perform a circular permutation on PYL1 (similarly to ABI1 in 4.3.3). I will then aim to analyse the performance of all the combinations of CP-PYL1, CP-ABI1, PYL1, and ABI1. These alterations will provide further information on the ABA dimeriser's mechanism of inhibition of proteases, and hopefully, lead to the discovery of a combination of dimerisers that brings the tether and protease together but does not inhibit the crucial step that is cleavage of the anchored cargo.

It is perhaps also worth working towards the development of a functioning auto inhibitory domain for TEV and incorporate this protease in IRR. This would increase protease choice, which could be useful in terms of compatibility of the system with different areas of research, or even for flexibility in the rate of cargo release. It could also be interesting to test TEV with ABA dimerisation pair to see if the the same occurs with this combination in terms of proteolytic inhibition.

Nevertheless, fulfilling the first and second aims already presents a significant improvement to the system and its potential to be used in the study of dynamic cellular processes. I believe that my system is especially useful when studying processes that rely on protein movement across different cellular compartments, for example, the nucleus. Examples of where the RAPID-release approach could prove fruitful are processes such as histone deposition and turnover, the loading of chromatin binding proteins, such as cohesin, the ORC (origin recognition complex) or MCM2-7 (minichromosome maintenance protein complex), the study of ribosome synthesis, where ribosomal proteins must translocate to the nucleolus before re-export to the cytoplasm, and the study of proteins that form the nuclear lamina, especially those associated with laminopathies.

In the future, besides the completion of the orthologous system, I intend to adapt the system further. It is my objective to not only reduce promiscuous cleavage of tethered cargo (resulting from spurious inter-

actions of the proteases with their cleavage sites), but also increase the rate at which the tether is cleaved from the OMM, with an ultimate goal of achieving release kinetics comparable to cellular diffusion of larger macromolecules. One avenue would be to apply different optogenetic approaches to achieve both a reduction of background and an increase in release speed, such as the one published in M. W. Kim et al. (2017). In this study, the gating of release is achieved through cleavage-site sequestration by juxtaposed fusion to the LOV2 domain. The cleavage site (TEV in this case) is exposed only when blue light is shone on the cells, avoiding the requirement for an auto-inhibitory peptide. A second potential avenue would be to develop a protease amplifier strategy (Stein and Alexandrov 2014). As the current release rates are far slower than the catalytic turnover of the proteases, it is likely that the auto-inhibitory peptides retain significant functionality even after recruitment. An amplifier strategy would use a second protease to remove the AI upon recruitment, thus allowing the primary protease to work unhindered.

In summary, the work laid out here represents a contribution towards the existing array of pulse-labelling methodologies that can be used to study a variety of cellular processes. RAPID-release, its optimised version, and nascent orthologous systems, present their greatest potential when used in conjunction with microscopy and imaging, however, their potential in biochemical analysis should also not be discounted.

Chapter 5

Conclusion

The work developed in this thesis focused mainly on the investigation of chromatin through the employment of a newly developed pulse labelling technique – RAPID-release. Through its employment in concert with state-of-the-art microscopy, it allowed me to observe and analyse the movement of chromatin domains in living cells in the time scale of hours or as rapidly as every second. As such, using this method, I characterised how TADs behaved under normal conditions within the nucleus, and observed the phenomena in real-time. And by comparing the benchmark of dynamic parameters developed, I could compare how DNA damage affected the dynamics of chromatin. All this allowed me to confirm my hypotheses that TADs presented mostly low mobility at these time scales, but that a small proportion of these structures deviated from the majority by presenting a more dynamic behaviour. This work further showed that with the introduction of DNA damage, the subpopulation of dynamic chromatin domains could be expanded, linking DNA damage to the phenomena we observed.

I am confident, however, that the uses of the methodology I developed are not limited to the study of DNA damage, but can also be employed to better understand a wide range of actors that play roles in genome structure, integrity and regulation, as well as investigating the effect of different perturbations to cell homeostasis.

Despite the focus of this work being on chromatin dynamics, I am con-

fident that RAPID-release can be used in contexts different to straightforward genomic imaging, and that its versatility can be explored in other areas of cell function. This is especially true when paired with state-of-the-art microscopy, even if its use is not limited by this. Confidence in the versatility of the method inspired its optimisation and adaptation with the aims of making it suitable for use in kinetic, signalling, and structural studies, and its wider use would be a testament to its success.

I am confident that the work presented here amounts to a significant contribution in the topic of chromatin dynamics, and opens a path for further discoveries in this field. I am also confident that my efforts have widened the pool of pulse-labelling techniques available to molecular, cellular, and biochemical scientists in the pursuit of their research.

Bibliography

Agmon, Neta et al. (June 2013). "Effect of nuclear architecture on the efficiency of double-strand break repair". In: *Nature Cell Biology* 15.6, pp. 694–699. DOI: 10.1038/ncb2745. URL: https://www.nature.com/articles/ncb2745.

Allan, J. et al. (Aug. 1981). "Regulation of the higher-order structure of chromatin by histones H1 and H5". In: *Journal of Cell Biology* 90.2, pp. 279–288. ISSN: 00219525. DOI: 10.1083/jcb.90.2.279. URL: http://rupress.org/jcb/article-pdf/90/2/279/1267231/279.pdf.

Amendola, Mario and Bas Van Steensel (June 2014). *Mechanisms and dynamics of nuclear lamina-genome interactions*. DOI: 10.1016/j.ceb.2014.03.003.

Apta-Smith, Michael James, Juan Ramon Hernandez-Fernaud, and Andrew James Bowman (Oct. 2018). "Evidence for the nuclear import of histones H3.1 and H4 as monomers." In: *The EMBO journal* 37.19. ISSN: 1460-2075. DOI: 10.15252/embj.201798714. URL: http://www.ncbi.nlm.nih.gov/pubmed/30177573%20http://www.pubmedcentral.nih.gov/articlerender.fcgi?artid=PMC6166134.

Babokhov, Michael et al. (Feb. 2020). *Local Chromatin Motion and Transcription*. DOI: 10.1016/j.jmb.2019.10.018.

Bar Yaacov, Reut et al. (May 2019). "Functional characterization of the ZEB2 regulatory landscape". In: 28.9, pp. 1487–1497. URL: http://orcid.org/%20https://academic.oup.com/hmg/article/28/9/1487/5261438.

Barbieri, Mariano et al. (June 2017). "Active and poised promoter states drive folding of the extended HoxB locus in mouse embryonic stem cells". In: *Nature Structural and Molecular Biology* 24.6, pp. 515–524. ISSN: 15459985. DOI: 10.1038/nsmb.3402. URL: https://www.nature.com/articles/nsmb.3402.

Beagan, Jonathan A. et al. (June 2020). "Three-dimensional genome restructuring across timescales of activity-induced neuronal gene expression". In: *Nature Neuroscience* 23.6, pp. 707–717. ISSN: 15461726. DOI: 10.1038/s41593-020-0634-6. URL: https://www.nature.com/articles/s41593-020-0634-6.

Beagrie, Robert A. et al. (Mar. 2017). "Complex multi-enhancer contacts captured by genome architecture mapping". In: *Nature* 543.7646, pp. 519–524. ISSN: 14764687. DOI: 10.1038/nature21411. URL: https://www.nature.com/articles/nature21411.

Becker, Annabelle et al. (Mar. 2014). "ATM alters the otherwise robust chromatin mobility at sites of DNA Double-Strand Breaks (DSBs) in human cells". In: *PLoS ONE* 9.3. ISSN: 19326203. DOI: 10.1371/journal.pone.0092640. URL: https://pubmed.ncbi.nlm.nih.gov/24651490/.

Bednar, Jan et al. (Nov. 1998). "Nucleosomes, linker DNA, and linker histone form a unique structural motif that directs the higher-order folding and compaction of chromatin". In: *Proceedings of the National Academy of Sciences* 95.24, pp. 14173–14178. ISSN: 0027-8424. DOI: 10.1073/PNAS.95.24.14173. URL: https://www.pnas.org/content/95/24/14173%20https://www.pnas.org/content/95/24/14173.abstract.

Beliveau, Brian J., Alistair N. Boettiger, et al. (2015). "Single-molecule super-resolution imaging of chromosomes and in situ haplotype visualization using Oligopaint FISH probes". In: *Nature Communications* 6. ISSN: 20411723. DOI: 10.1038/ncomms8147. URL: www.nature.com/naturecommunications.

Beliveau, Brian J., Eric F. Joyce, et al. (Dec. 2012). "Versatile design and synthesis platform for visualizing genomes with Oligopaint FISH probes". In: 109.52, pp. 21301–21306. URL: www.pnas.org/cgi/doi/10.1073/pnas.1213818110.

Bickmore, Wendy A. (Aug. 2013). *The spatial organization of the human genome*. DOI: 10.1146/annurev-genom-091212-153515. URL: https://pubmed.ncbi.nlm.nih.gov/23875797/.

Bintu, Bogdan et al. (Oct. 2018). "Super-resolution chromatin tracing reveals domains and cooperative interactions in single cells". In: *Science* 362.6413. ISSN: 10959203. DOI: 10.1126/science.aau1783. URL: http://science.sciencemag.org/.

Boettiger, Alistair N. et al. (Jan. 2016). "Super-resolution imaging reveals distinct chromatin folding for different epigenetic states". In: *Nature* 529.7586, pp. 418–422. ISSN: 14764687. DOI: 10.1038/nature16496. URL: https://pubmed.ncbi.nlm.nih.gov/26760202/.

Boija, Ann et al. (Dec. 2018). "Transcription Factors Activate Genes through the Phase-Separation Capacity of Their Activation Domains". In: *Cell* 175.7, 1842–1855.e16. ISSN: 10974172. DOI: 10.1016/j.cell.2018.10.042.

Bonev, Boyan and Giacomo Cavalli (Oct. 2016). *Organization and function of the 3D genome*. DOI: 10.1038/nrg.2016.112. URL: www.nature.com/nrg.

Bonev, Boyan, Netta Mendelson Cohen, et al. (Oct. 2017). "Multiscale 3D Genome Rewiring during Mouse Neural Development". In: *Cell* 171.3, 557–572.e24. ISSN: 10974172. DOI: 10.1016/j.cell.2017.09.043.

Bonin, Keith et al. (May 2018). "Structured illumination to spatially map chromatin motions". In: *Journal of Biomedical Optics* 23.05, p. 1. ISSN: 1083-3668. DOI: 10.1117/1.JBO.23.5.056007. URL: https://www.spiedigitallibrary.org/journals/journal-of-biomedical-optics/volume-23/issue-05/056007/Structured-

illumination-to-spatially-map-chromatin-motions/10.1117/1.JBO.23.5.056007.full.

Bonner, W M et al. (1988). *Kinetics of Accumulation and Depletion of Soluble Newly Synthesized Histone in the Reciprocal Regulation of Histone and DNA Synthesis*. Tech. rep., pp. 6542–6550. URL: https://pubs.acs.org/sharingguidelines.

Boyle, Shelagh et al. (Feb. 2001). "The spatial organization of human chromosomes within the nuclei of normal and emerin-mutant cells". In: *Human Molecular Genetics* 10.3, pp. 211–219. ISSN: 09646906. DOI: 10.1093/hmg/10.3.211. URL: https://europepmc.org/article/MED/11159939.

Branco, Miguel R and Ana Pombo (Apr. 2006). "Intermingling of Chromosome Territories in Interphase Suggests Role in Translocations and Transcription-Dependent Associations". In: *PLoS Biology* 4.5. Ed. by Peter Becker, e138. ISSN: 1545-7885. DOI: 10.1371/journal.pbio.0040138. URL: https://dx.plos.org/10.1371/journal.pbio.0040138.

Bronshtein, I. et al. (Aug. 2015). "Loss of lamin A function increases chromatin dynamics in the nuclear interior". In: *Nature Communications* 6. ISSN: 20411723. DOI: 10.1038/ncomms9044. URL: https://pubmed.ncbi.nlm.nih.gov/26299252/.

Brown, Christopher R. et al. (Mar. 2008). "Global histone acetylation induces functional genomic reorganization at mammalian nuclear pore complexes". In: *Genes and Development* 22.5, pp. 627–639. ISSN: 08909369. DOI: 10.1101/gad.1632708. URL: http://www.genesdev.org..

Burgess, Rebecca C. et al. (Dec. 2014). "Activation of DNA Damage Response Signaling by Condensed Chromatin". In: *Cell Reports* 9.5, pp. 1703–1717. ISSN: 22111247. DOI: 10.1016/j.celrep.2014.10.060. URL: https://pubmed.ncbi.nlm.nih.gov/25464843/.

Campos, Eric I et al. (Nov. 2010). "The program for processing newly synthesized histones H3.1 and H4." In: *Nature structural & molecular*

biology 17.11, pp. 1343–51. ISSN: 1545-9985. DOI: 10.1038/nsmb.1911. URL: http://www.ncbi.nlm.nih.gov/pubmed/20953179%20http://www.pubmedcentral.nih.gov/articlerender.fcgi?artid=PMC2988979.

Cardoso, M. Cristina et al. (Feb. 2012). *Structure, function and dynamics of nuclear subcompartments*. DOI: 10.1016/j.ceb.2011.12.009. URL: https://pubmed.ncbi.nlm.nih.gov/22227228/.

Caridi, Christopher P. et al. (June 2018). "Nuclear F-actin and myosins drive relocalization of heterochromatic breaks". In: *Nature 2018 559:7712* 559.7712, pp. 54–60. ISSN: 1476-4687. DOI: 10.1038/s41586-018-0242-8. URL: https://www.nature.com/articles/s41586-018-0242-8.

Caridi, Christopher Patrick et al. (Sept. 2019). "Nuclear actin filaments in DNA repair dynamics". In: *Nature Cell Biology 2019 21:9* 21.9, pp. 1068–1077. ISSN: 1476-4679. DOI: 10.1038/s41556-019-0379-1. URL: https://www.nature.com/articles/s41556-019-0379-1.

Chai, Bob et al. (July 2005). "Distinct roles for the RSC and Swi/Snf ATP-dependent chromatin remodelers in DNA double-strand break repair". In: *Genes & Development* 19.14, pp. 1656–1661. ISSN: 0890-9369. DOI: 10.1101/GAD.1273105. URL: http://genesdev.cshlp.org/content/19/14/1656.full.

Chambeyron, Séverine et al. (May 2005). "Nuclear re-organisation of the Hoxb complex during mouse embryonic development". In: *Development* 132.9, pp. 2215–23. ISSN: 0950-1991. DOI: 10.1242/DEV.01813. URL: https://www.research.ed.ac.uk/en/publications/nuclear-re-organisation-of-the-hoxb-complex-during-mouse-embryoni.

Chang, Li Hsin, Sourav Ghosh, and Daan Noordermeer (Feb. 2020). *TADs and Their Borders: Free Movement or Building a Wall?* DOI: 10.1016/j.jmb.2019.11.025.

Chankova, S. G. et al. (Nov. 2007). "Induction of DNA double-strand breaks by zeocin in Chlamydomonas reinhardtii and the role of in-

creased DNA double-strand breaks rejoining in the formation of an adaptive response". In: *Radiation and Environmental Biophysics* 46.4, pp. 409–416. ISSN: 0301634X. DOI: 10.1007/s00411-007-0123-2. URL: https://link.springer.com/article/10.1007/s00411-007-0123-2.

Chen, Baohui et al. (Dec. 2018). "Efficient labeling and imaging of protein-coding genes in living cells using CRISPR-Tag". In: *Nature Communications* 9.1. ISSN: 20411723. DOI: 10.1038/s41467-018-07498-y. URL: https://pubmed.ncbi.nlm.nih.gov/30498221/.

Cheng, Tammy M.K. et al. (Apr. 2015). "A simple biophysical model emulates budding yeast chromosome condensation". In: *eLife* 2015.4, pp. 1–22. ISSN: 2050084X. DOI: 10.7554/eLife.05565.

Chiolo, I. et al. (Mar. 2011). "Double-strand breaks in heterochromatin move outside of a dynamic HP1a domain to complete recombinational repair". In: *Cell* 144.5, pp. 732–744. ISSN: 1097-4172. DOI: 10.1016/J.CELL.2011.02.012. URL: https://pubmed.ncbi.nlm.nih.gov/21353298/.

Chuang, CH et al. (Apr. 2006). "Long-range directional movement of an interphase chromosome site". In: *Current biology : CB* 16.8, pp. 825–831. ISSN: 0960-9822. DOI: 10.1016/J.CUB.2006.03.059. URL: https://pubmed.ncbi.nlm.nih.gov/16631592/.

Chudakov, Dmitriy M., Sergey Lukyanov, and Konstantin A. Lukyanov (Dec. 2005). *Fluorescent proteins as a toolkit for in vivo imaging*. DOI: 10.1016/j.tibtech.2005.10.005.

Clément, C. et al. (Jan. 2016). "Functional Characterization of Histone Chaperones Using SNAP-Tag-Based Imaging to Assess de Novo Histone Deposition". In: *Methods in Enzymology*. Vol. 573. Academic Press Inc., pp. 97–117. DOI: 10.1016/bs.mie.2016.04.004.

Crivat, Georgeta and Justin W. Taraska (Jan. 2012). *Imaging proteins inside cells with fluorescent tags*. DOI: 10.1016/j.tibtech.2011.08.002.

Croft, Jenny A. et al. (June 1999). "Differences in the localization and morphology of chromosomes in the human nucleus". In: *Journal of Cell Biology* 145.6, pp. 1119–1131. ISSN: 00219525. DOI: 10.1083/jcb.145.6.1119. URL: http://www.jcb.org.

Cuddapah, Suresh et al. (Jan. 2009). "Global analysis of the insulator binding protein CTCF in chromatin barrier regions reveals demarcation of active and repressive domains". In: *Genome Research* 19.1, pp. 24–32. ISSN: 10889051. DOI: 10.1101/gr.082800.108. URL: http://www.genome.org/cgi/content/full/19/1/24%20https://europepmc.org/article/PMC/2612964.

Dechat, Thomas et al. (Dec. 2004). "LAP2α and BAF transiently localize to telomeres and specific regions on chromatin during nuclear assembly". In: *Journal of Cell Science* 117.25, pp. 6117–6128. ISSN: 0021-9533. DOI: 10.1242/JCS.01529. URL: http://rsb.info.nih.gov/ij/.

Dekker, Job et al. (Feb. 2002). "Capturing chromosome conformation". In: *Science* 295.5558, pp. 1306–1311. ISSN: 00368075. DOI: 10.1126/science.1067799. URL: https://pubmed.ncbi.nlm.nih.gov/11847345/.

Dion, Vincent and Susan M. Gasser (Mar. 2013). *Chromatin movement in the maintenance of genome stability*. DOI: 10.1016/j.cell.2013.02.010.

Dion, Vincent, Véronique Kalck, et al. (May 2012). "Increased mobility of double-strand breaks requires Mec1, Rad9 and the homologous recombination machinery". In: *Nature Cell Biology* 14.5, pp. 502–509. ISSN: 14657392. DOI: 10.1038/ncb2465. URL: https://www.nature.com/articles/ncb2465.

Dixon, Jesse R., Inkyung Jung, et al. (Feb. 2015). "Chromatin architecture reorganization during stem cell differentiation". In: *Nature* 518.7539, pp. 331–336. ISSN: 14764687. DOI: 10.1038/nature14222. URL: https://www.nature.com/articles/nature14222.

Dixon, Jesse R., Siddarth Selvaraj, et al. (May 2012). "Topological domains in mammalian genomes identified by analysis of chromatin interactions". In: *Nature* 485.7398, pp. 376–380. ISSN: 00280836. DOI: 10.1038/nature11082. URL: https://www.nature.com/articles/nature11082.

Dundr et al. (Dec. 2007). "Actin-dependent intranuclear repositioning of an active gene locus in vivo". In: *The Journal of cell biology* 179.6, pp. 1095–1103. ISSN: 1540-8140. DOI: 10.1083/JCB.200710058. URL: https://pubmed.ncbi.nlm.nih.gov/18070915/.

Eagen, Kyle P., Tom A. Hartl, and Roger D. Kornberg (Nov. 2015). "Stable Chromosome Condensation Revealed by Chromosome Conformation Capture". In: *Cell* 163.4, pp. 934–946. ISSN: 10974172. DOI: 10.1016/j.cell.2015.10.026.

Evdokimova, VN et al. (2018). "Nuclear myosin/actin-motored contact between homologous chromosomes is initiated by ATM kinase and homology-directed repair proteins at double-strand DNA breaks to suppress chromosome rearrangements". In: *Oncotarget* 9.17, pp. 13612–13622. ISSN: 1949-2553. DOI: 10.18632/ONCOTARGET.24434. URL: https://pubmed.ncbi.nlm.nih.gov/29568381/%20https://pubmed.ncbi.nlm.nih.gov/29568381/?dopt=Abstract.

Fedorova, Elena and Daniele Zink (Nov. 2008). *Nuclear architecture and gene regulation*. DOI: 10.1016/j.bbamcr.2008.07.018.

Ferrai, Carmelo et al. (Jan. 2010). "Poised transcription factories prime silent uPA gene prior to activation". In: *PLoS Biology* 8.1, p. 1000270. ISSN: 15449173. DOI: 10.1371/journal.pbio.1000270. URL: www.plosbiology.org.

Filippova, G N et al. (June 1996). "An exceptionally conserved transcriptional repressor, CTCF, employs different combinations of zinc fingers to bind diverged promoter sequences of avian and mammalian c-myc oncogenes." In: *Molecular and Cellular Biology* 16.6, pp. 2802–2813. ISSN: 0270-7306. DOI: 10.1128/mcb.16.6.2802. URL: https://pubmed.ncbi.nlm.nih.gov/8649389/.

Finch, J T and A Klug (June 1976). "Solenoidal model for superstructure in chromatin". In: *Proceedings of the National Academy of Sciences* 73.6, pp. 1897–1901. ISSN: 0027-8424. DOI: 10.1073/PNAS.73.6.1897. URL: https://www.pnas.org/content/73/6/1897%20https://www.pnas.org/content/73/6/1897.abstract.

Finn, Elizabeth H. et al. (Mar. 2019). "Extensive Heterogeneity and Intrinsic Variation in Spatial Genome Organization". In: *Cell* 176.6, 1502–1515.e10. ISSN: 10974172. DOI: 10.1016/j.cell.2019.01.020. URL: https://pubmed.ncbi.nlm.nih.gov/30799036/.

Fortin, Jean-Philippe and Kasper D. Hansen (Dec. 2015). "Reconstructing A/B compartments as revealed by Hi-C using long-range correlations in epigenetic data". In: *Genome Biology* 16.1, p. 180. ISSN: 1474-760X. DOI: 10.1186/s13059-015-0741-y. URL: https://genomebiology.biomedcentral.com/articles/10.1186/s13059-015-0741-y.

Fraser, James et al. (Sept. 2015). "An Overview of Genome Organization and How We Got There: from FISH to Hi-C". In: *Microbiology and Molecular Biology Reviews* 79.3, pp. 347–372. ISSN: 1092-2172. DOI: 10.1128/mmbr.00006-15. URL: http://mmbr.asm.org/.

Fu, Yi et al. (May 2016). "CRISPR-dCas9 and sgRNA scaffolds enable dual-colour live imaging of satellite sequences and repeat-enriched individual loci". In: *Nature Communications* 7.1, pp. 1–8. ISSN: 20411723. DOI: 10.1038/ncomms11707. URL: www.nature.com/naturecommunications.

Fullwood, Melissa J. et al. (Nov. 2009). "An oestrogen-receptor-α-bound human chromatin interactome". In: *Nature* 462.7269, pp. 58–64. ISSN: 00280836. DOI: 10.1038/nature08497. URL: http://cms1.gis.a-star.edu.sg.

Futcher, Bruce (1999). *Cell cycle synchronization*. Ed. by Gaspar Banfalvi. Vol. 21. Methods in Molecular Biology 2-3. Totowa, NJ: Humana Press, pp. 79–86. ISBN: 978-1-61779-181-9. DOI: 10.1023/A:1009872403440. URL: http://link.springer.com/10.1007/978-1-61779-182-6.

Gandhi, M. et al. (June 2012). "Homologous chromosomes make contact at the sites of double-strand breaks in genes in somatic G0/G1-phase human cells". In: *Proceedings of the National Academy of Sciences* 109.24, pp. 9454–9459. ISSN: 0027-8424. DOI: 10.1073/pnas.1205759109. URL: http://www.pnas.org/cgi/doi/10.1073/pnas.1205759109.

Gasser, Susan M. (May 2002). *Nuclear architecture: Visualizing chromatin dynamics in interphase nuclei*. DOI: 10.1126/science.1067703. URL: https://pubmed.ncbi.nlm.nih.gov/12029120/%20https://science.sciencemag.org/content/296/5572/1412.

Gazda, Hanna T. et al. (Dec. 2008). "Ribosomal Protein L5 and L11 Mutations Are Associated with Cleft Palate and Abnormal Thumbs in Diamond-Blackfan Anemia Patients". In: *American Journal of Human Genetics* 83.6, pp. 769–780. ISSN: 00029297. DOI: 10.1016/j.ajhg.2008.11.004. URL: https://pubmed.ncbi.nlm.nih.gov/19061985/.

Gentile, Claudia et al. (July 2019). "PRC2-Associated Chromatin Contacts in the Developing Limb Reveal a Possible Mechanism for the Atypical Role of PRC2 in HoxA Gene Expression". In: *Developmental Cell* 50.2, 184–196.e4. ISSN: 1534-5807. DOI: 10.1016/J.DEVCEL.2019.05.021.

Germier, Thomas et al. (Oct. 2017). "Real-Time Imaging of a Single Gene Reveals Transcription-Initiated Local Confinement". In: *Biophysical Journal* 113.7, pp. 1383–1394. ISSN: 15420086. DOI: 10.1016/j.bpj.2017.08.014. URL: https://pubmed.ncbi.nlm.nih.gov/28978433/.

Gibcus, JH and J Dekker (Mar. 2013). "The hierarchy of the 3D genome". In: *Molecular cell* 49.5, pp. 773–782. ISSN: 1097-4164. DOI: 10.1016/J.MOLCEL.2013.02.011. URL: https://pubmed.ncbi.nlm.nih.gov/23473598/.

Gibson, Bryan A. et al. (Oct. 2019). "Organization of Chromatin by Intrinsic and Regulated Phase Separation". In: *Cell* 179.2, 470–484.e21.

ISSN: 10974172. DOI: 10.1016/j.cell.2019.08.037. URL: https://pubmed.ncbi.nlm.nih.gov/31543265/.

Gilbert, Nick (Apr. 2019). *Biophysical regulation of local chromatin structure*. DOI: 10.1016/j.gde.2019.06.001. URL: https://www.research.ed.ac.uk/en/publications/biophysical-regulation-of-local-chromatin-structure.

Goloborodko, Anton, John F. Marko, and Leonid A. Mirny (May 2016). "Chromosome Compaction by Active Loop Extrusion". In: *Biophysical Journal* 110.10, pp. 2162–2168. ISSN: 15420086. DOI: 10.1016/j.bpj.2016.02.041.

Gonzalez-Suarez, Ignacio et al. (Aug. 2009). "Novel roles for A-type lamins in telomere biology and the DNA damage response pathway". In: *The EMBO Journal* 28.16, pp. 2414–2427. ISSN: 1460-2075. DOI: 10.1038/EMBOJ.2009.196. URL: https://www.embopress.org/doi/full/10.1038/emboj.2009.196%20https://www.embopress.org/doi/abs/10.1038/emboj.2009.196.

Goodarzi, Aaron A, Thomas Kurka, and Penelope A Jeggo (June 2011). "KAP-1 phosphorylation regulates CHD3 nucleosome remodeling during the DNA double-strand break response". In: *Nature Structural & Molecular Biology 2011 18:7* 18.7, pp. 831–839. ISSN: 1545-9985. DOI: 10.1038/nsmb.2077. URL: https://www.nature.com/articles/nsmb.2077.

Gruber, Stephan, Christian H Haering, and Kim Nasmyth (Mar. 2003). "Chromosomal Cohesin Forms a Ring". In: *Cell* 112.6, pp. 765–777. ISSN: 0092-8674. DOI: 10.1016/S0092-8674(03)00162-4. URL: http://www.cell.com/article/S0092867403001624/fulltext%20http://www.cell.com/article/S0092867403001624/abstract%20https://www.cell.com/cell/abstract/S0092-8674(03)00162-4.

Gu, Bo et al. (Mar. 2018). "Transcription-coupled changes in nuclear mobility of mammalian cis-regulatory elements". In: *Science* 359.6379,

pp. 1050–1055. ISSN: 10959203. DOI: 10.1126/science.aao3136. URL: http://science.sciencemag.org/.

Guacci, Vincent, Douglas Koshland, and Alexander Strunnikov (Oct. 1997). "A Direct Link between Sister Chromatid Cohesion and Chromosome Condensation Revealed through the Analysis of MCD1 in S. cerevisiae". In: *Cell* 91.1, pp. 47–57. ISSN: 0092-8674. DOI: 10.1016/S0092-8674(01)80008-8. URL: http://www.cell.com/article/S0092867401800088/fulltext.

Guelen, Lars et al. (June 2008). "Domain organization of human chromosomes revealed by mapping of nuclear lamina interactions". In: *Nature* 453.7197, pp. 948–951. ISSN: 14764687. DOI: 10.1038/nature06947. URL: https://pubmed.ncbi.nlm.nih.gov/18463634/.

Hansen, A.S. et al. (Dec. 2018). "Recent evidence that TADs and chromatin loops are dynamic structures". In: *Nucleus (Austin, Tex.)* 9.1, pp. 20–32. ISSN: 1949-1042. DOI: 10.1080/19491034.2017.1389365. URL: https://pubmed.ncbi.nlm.nih.gov/29077530/.

Hansen, RS et al. (2010). "Sequencing newly replicated DNA reveals widespread plasticity in human replication timing". In: *Proceedings of the National Academy of Sciences of the United States of America* 107.1, pp. 139–144. ISSN: 1091-6490. DOI: 10.1073/PNAS.0912402107. URL: https://pubmed.ncbi.nlm.nih.gov/19966280/.

Hauer, Michael H. et al. (Feb. 2017). "Histone degradation in response to DNA damage enhances chromatin dynamics and recombination rates". In: *Nature Structural and Molecular Biology* 24.2, pp. 99–107. ISSN: 15459985. DOI: 10.1038/nsmb.3347. URL: https://www.nature.com/articles/nsmb.3347.

He, Yuanzheng et al. (July 2011). "Identification of a lysosomal pathway that modulates glucocorticoid signaling and the inflammatory response". In: *Science Signaling* 4.180. ISSN: 19450877. DOI: 10.1126/scisignal.2001450. URL: https://pubmed.ncbi.nlm.nih.gov/21730326/.

Hepperger, Claudia et al. (2008). "Three-dimensional positioning of genes in mouse cell nuclei". In: DOI: 10.1007/s00412-008-0168-2. URL: http://www.ensembl.org.

Heride, Claire et al. (Dec. 2010). "Distance between homologous chromosomes results from chromosome positioning constraints". In: *Journal of Cell Science* 123.23, pp. 4063–4075. ISSN: 00219533. DOI: 10.1242/jcs.066498. URL: http://www.ncbi.nlm.nih.gov/projects/mapview/maps.cgi?TAXID.

Hirano, Tatsuya (Aug. 2012). *Condensins: Universal organizers of chromosomes with diverse functions*. DOI: 10.1101/gad.194746.112. URL: http://www.genesdev.org/cgi/doi/10.1101/gad.194746.112..

— (Feb. 2016). *Condensin-Based Chromosome Organization from Bacteria to Vertebrates*. URL: http://www.cell.com/article/S0092867416300472/fulltext.

Hnisz, Denes et al. (Mar. 2017). *A Phase Separation Model for Transcriptional Control*. DOI: 10.1016/j.cell.2017.02.007.

Holcman, D., N. Hoze, and Z. Schuss (Nov. 2015). *Analysis and Interpretation of Superresolution Single-Particle Trajectories*. DOI: 10.1016/j.bpj.2015.09.003. URL: https://pubmed.ncbi.nlm.nih.gov/26536253/.

Hübner, Michael R., Mélanie A. Eckersley-Maslin, and David L. Spector (Apr. 2013). "Chromatin organization and transcriptional regulation". In: *Current Opinion in Genetics & Development* 23.2, pp. 89–95. ISSN: 0959437X. DOI: 10.1016/j.gde.2012.11.006. URL: http://www.ncbi.nlm.nih.gov/pubmed/23270812%20http://www.pubmedcentral.nih.gov/articlerender.fcgi?artid=PMC3612554%20https://linkinghub.elsevier.com/retrieve/pii/S0959437X12001360.

Ingallinella, P. et al. (Oct. 2000). "Optimization of the P'-region of peptide inhibitors of hepatitis C virus NS3/4A protease". In: *Biochemistry* 39.42, pp. 12898–12906. ISSN: 00062960. DOI: 10.1021/bi001590g.

URL: https://pubmed.ncbi.nlm.nih.gov/11041854/%20https://pubmed.ncbi.nlm.nih.gov/11041854/?dopt=Abstract.

Ishikawa-Ankerhold, Hellen C., Richard Ankerhold, and Gregor P. C. Drummen (Apr. 2012). "Advanced Fluorescence Microscopy Techniques—FRAP, FLIP, FLAP, FRET and FLIM". In: *Molecules* 17.4, pp. 4047–4132. ISSN: 1420-3049. DOI: 10.3390/molecules17044047. URL: http://www.mdpi.com/1420-3049/17/4/4047.

Jinek, Martin et al. (Aug. 2012). "A programmable dual-RNA-guided DNA endonuclease in adaptive bacterial immunity". In: *Science* 337.6096, pp. 816–821. ISSN: 10959203. DOI: 10.1126/science.1225829. URL: http://science.sciencemag.org/.

Juillerat, Alexandre et al. (Apr. 2003). "Directed evolution of O6-alkylguanine-DNA alkyltransferase for efficient labeling of fusion proteins with small molecules in vivo". In: *Chemistry and Biology* 10.4, pp. 313–317. ISSN: 10745521. DOI: 10.1016/S1074-5521(03)00068-1.

Kagey, Michael H. et al. (Sept. 2010). "Mediator and cohesin connect gene expression and chromatin architecture". In: *Nature* 467.7314, pp. 430–435. ISSN: 14764687. DOI: 10.1038/nature09380. URL: https://www.nature.com/articles/nature09380.

Kamiyama, Daichi et al. (Mar. 2016). "Versatile protein tagging in cells with split fluorescent protein". In: *Nature Communications* 7. ISSN: 20411723. DOI: 10.1038/ncomms11046. URL: https://pubmed.ncbi.nlm.nih.gov/26988139/.

Kempfer, Rieke and Ana Pombo (2020). "Methods for mapping 3D chromosome architecture". In: *NAture reviews — GENEtICS* 21. DOI: 10.1038/s41576-019-0195-2. URL: www.nature.com/nrg.

Khorasanizadeh, Sepideh (Jan. 2004). "The Nucleosome: From Genomic Organization to Genomic Regulation". In: *Cell* 116.2, pp. 259–272. ISSN: 0092-8674. DOI: 10.1016/S0092-8674(04)00044-3. URL: http://www.cell.com/article/S0092867404000443/fulltext.

Kim, Min Woo et al. (Nov. 2017). "Time-gated detection of protein-protein interactions with transcriptional readout". In: *eLife* 6. ISSN: 2050084X. DOI: 10.7554/eLife.30233.

Kim, Tae Hoon et al. (Mar. 2007). "Analysis of the Vertebrate Insulator Protein CTCF-Binding Sites in the Human Genome". In: *Cell* 128.6, pp. 1231–1245. ISSN: 00928674. DOI: 10.1016/j.cell.2006.12.048.

Kimura, Hiroshi, Kimihiko Sugaya, and Peter R. Cook (Dec. 2002). "The transcription cycle of RNA polymerase II in living cells". In: *Journal of Cell Biology* 159.5, pp. 777–782. ISSN: 0021-9525. DOI: 10.1083/JCB.200206019. URL: http://www.jcb.org/cgi/doi/10.1083/jcb.200206019.

Kind, J et al. (Mar. 2013). "Single-cell dynamics of genome-nuclear lamina interactions". In: *Cell* 153.1, pp. 178–192. ISSN: 1097-4172. DOI: 10.1016/J.CELL.2013.02.028. URL: https://pubmed.ncbi.nlm.nih.gov/23523135/.

Kinoshita, Kazuhisa and Tatsuya Hirano (June 2017). "Dynamic organization of mitotic chromosomes". In: *Current Opinion in Cell Biology* 46, pp. 46–53. ISSN: 0955-0674. DOI: 10.1016/J.CEB.2017.01.006.

Koonin, Eugene V. and Yuri I. Wolf (June 2010). "Constraints and plasticity in genome and molecular-phenome evolution". In: *Nature Reviews Genetics* 11.7, pp. 487–498. ISSN: 14710056. DOI: 10.1038/nrg2810. URL: www.nature.com/reviews/genetics.

Kundu, Sharmistha et al. (Feb. 2017). "Polycomb Repressive Complex 1 Generates Discrete Compacted Domains that Change during Differentiation". In: *Molecular Cell* 65.3, 432–446.e5. ISSN: 10974164. DOI: 10.1016/j.molcel.2017.01.009. URL: https://pubmed.ncbi.nlm.nih.gov/28157505/.

Lang, Kathrin and Jason W. Chin (May 2014). *Cellular incorporation of unnatural amino acids and bioorthogonal Labeling of Proteins*. DOI: 10.1021/cr400355w.

Lee, CF, GC Melkani, and SI Bernstein (2014). "The UNC-45 myosin chaperone: from worms to flies to vertebrates". In: *International re-*

view of cell and molecular biology 313, pp. 103–144. ISSN: 1937-6448. DOI: 10.1016/B978-0-12-800177-6.00004-9. URL: https://pubmed.ncbi.nlm.nih.gov/25376491/.

Li, Heng and Richard Durbin (July 2009). "Fast and accurate short read alignment with Burrows-Wheeler transform". In: *Bioinformatics* 25.14, pp. 1754–1760. DOI: 10.1093/BIOINFORMATICS/BTP324.

Li, Shiqian et al. (Sept. 2019). "An efficient auxin-inducible degron system with low basal degradation in human cells". In: *Nature Methods* 16.9, pp. 866–869. ISSN: 15487105. DOI: 10.1038/s41592-019-0512-x. URL: https://www.nature.com/articles/s41592-019-0512-x.

Liang, Fu Sen, Wen Qi Ho, and Gerald R. Crabtree (Mar. 2011). "Engineering the ABA Plant stress pathway for regulation of induced proximity". In: *Science Signaling* 4.164, rs2–rs2. ISSN: 19450877. DOI: 10.1126/scisignal.2001449.

Lieber, Michael R. (July 2010). *The mechanism of double-strand DNA break repair by the nonhomologous DNA end-joining pathway.* DOI: 10.1146/annurev.biochem.052308.093131. URL: https://pubmed.ncbi.nlm.nih.gov/20192759/.

Lieberman-Aiden, Erez et al. (Oct. 2009). "Comprehensive mapping of long-range interactions reveals folding principles of the human genome". In: *Science* 326.5950, pp. 289–293. ISSN: 00368075. DOI: 10.1126/science.1181369. URL: https://www.ncbi.nlm.nih.gov/pmc/articles/PMC2858594/.

Lombardi, Maria L. et al. (July 2011). "The interaction between nesprins and sun proteins at the nuclear envelope is critical for force transmission between the nucleus and cytoskeleton". In: *Journal of Biological Chemistry* 286.30, pp. 26743–26753. ISSN: 00219258. DOI: 10.1074/jbc.M111.233700. URL: https://pubmed.ncbi.nlm.nih.gov/21652697/.

Losada, Ana, Michiko Hirano, and Tatsuya Hirano (July 1998). "Identification of Xenopus SMC protein complexes required for sister chromatidcohesion". In: *Genes & Development* 12.13, pp. 1986–1997. ISSN:

0890-9369. DOI: 10.1101/GAD.12.13.1986. URL: http://genesdev.cshlp.org/content/12/13/1986.full.

Lottersberger, Francisca et al. (Nov. 2015). "53BP1 and the LINC Complex Promote Microtubule-Dependent DSB Mobility and DNA Repair". In: *Cell* 163.4, pp. 880–893. ISSN: 10974172. DOI: 10.1016/j.cell.2015.09.057. URL: https://pubmed.ncbi.nlm.nih.gov/26544937/%20http://dx.doi.org/10.1016/j.cell.2015.09.057.

Loviglio, M. N. et al. (June 2017). "Chromosomal contacts connect loci associated with autism, BMI and head circumference phenotypes". In: *Molecular Psychiatry* 22.6, pp. 836–849. ISSN: 14765578. DOI: 10.1038/mp.2016.84. URL: www.nature.com/mp.

Luger, Karolin et al. (Sept. 1997). "Crystal structure of the nucleosome core particle at 2.8Å resolution". In: *Nature* 389.6648, pp. 251–260. ISSN: 0028-0836. DOI: 10.1038/38444. URL: http://www.ncbi.nlm.nih.gov/pubmed/9305837%20http://www.nature.com/articles/38444.

Luijsterburg, Martijn S. et al. (Apr. 2012). "DDB2 promotes chromatin decondensation at UV-induced DNA damage". In: *Journal of Cell Biology* 197.2, pp. 267–281. ISSN: 00219525. DOI: 10.1083/jcb.201106074. URL: https://pubmed.ncbi.nlm.nih.gov/22492724/.

Ma, Hanhui, Li Chun Tu, Ardalan Naseri, Yu Chieh Chung, et al. (Nov. 2018). "CRISPR-Sirius: RNA scaffolds for signal amplification in genome imaging". In: *Nature Methods* 15.11, pp. 928–931. ISSN: 15487105. DOI: 10.1038/s41592-018-0174-0. URL: https://pubmed.ncbi.nlm.nih.gov/30377374/.

Ma, Hanhui, Li Chun Tu, Ardalan Naseri, Maximiliaan Huisman, et al. (May 2016). "Multiplexed labeling of genomic loci with dCas9 and engineered sgRNAs using CRISPRainbow". In: *Nature Biotechnology* 34.5, pp. 528–530. ISSN: 15461696. DOI: 10.1038/nbt.3526. URL: https://pubmed.ncbi.nlm.nih.gov/27088723/.

Maass, Philipp G. et al. (Mar. 2018). "Inter-chromosomal Contact Properties in Live-Cell Imaging and in Hi-C". In: *Molecular Cell* 69.6,

1039–1045.e3. ISSN: 10974164. DOI: 10.1016/j.molcel.2018.02.007. URL: https://pubmed.ncbi.nlm.nih.gov/29526697/.

Manley, Suliana et al. (Feb. 2008). "High-density mapping of single-molecule trajectories with photoactivated localization microscopy". In: *Nature Methods* 5.2, pp. 155–157. ISSN: 15487091. DOI: 10.1038/nmeth.1176. URL: https://pubmed.ncbi.nlm.nih.gov/18193054/.

Marnef, Aline et al. (Sept. 2019). "A cohesin/HUSH- and LINC-dependent pathway controls ribosomal DNA double-strand break repair". In: *Genes & Development* 33.17-18, pp. 1175–1190. ISSN: 0890-9369. DOI: 10.1101/GAD.324012.119. URL: http://genesdev.cshlp.org/content/33/17-18/1175.full.

Marshall, W. F. et al. (Dec. 1997). "Interphase chromosomes undergo constrained diffusional motion in living cells". In: *Current Biology* 7.12, pp. 930–939. ISSN: 09609822. DOI: 10.1016/S0960-9822(06)00412-X. URL: https://pubmed.ncbi.nlm.nih.gov/9382846/.

Michaelis, Christine, Rafal Ciosk, and Kim Nasmyth (Oct. 1997). "Cohesins: Chromosomal proteins that prevent premature separation of sister chromatids". In: *Cell* 91.1, pp. 35–45. ISSN: 00928674. DOI: 10.1016/S0092-8674(01)80007-6. URL: http://www.cell.com/article/S0092867401800076/fulltext%20http://www.cell.com/article/S0092867401800076/abstract%20https://www.cell.com/cell/abstract/S0092-8674(01)80007-6%20https://pubmed.ncbi.nlm.nih.gov/9335333/.

Miné-Hattab, Judith and Rodney Rothstein (May 2012). "Increased chromosome mobility facilitates homology search during recombination". In: *Nature Cell Biology* 14.5, pp. 510–517. ISSN: 14657392. DOI: 10.1038/ncb2472. URL: https://pubmed.ncbi.nlm.nih.gov/22484485/%20https://www.nature.com/articles/ncb2472.

Mizuguchi, Hiroyuki et al. (Apr. 2000). "IRES-Dependent Second Gene Expression Is Significantly Lower Than Cap-Dependent First Gene Expression in a Bicistronic Vector". In: *Molecular Therapy* 1.4, pp. 376–382. ISSN: 15250016. DOI: 10.1006/mthe.2000.0050.

Moindrot, Benoit et al. (Oct. 2012). "3D chromatin conformation correlates with replication timing and is conserved in resting cells". In: *Nucleic Acids Research* 40.19, pp. 9470–9481. ISSN: 0305-1048. DOI: 10.1093/NAR/GKS736. URL: https://academic.oup.com/nar/article/40/19/9470/2414837.

Monahan, Kevin, Adan Horta, and Stavros Lomvardas (Jan. 2019). "LHX2- and LDB1-mediated trans interactions regulate olfactory receptor choice". In: *Nature* 565.7740, pp. 448–453. ISSN: 14764687. DOI: 10.1038/s41586-018-0845-0. URL: https://www.nature.com/articles/s41586-018-0845-0.

Mondal, T. et al. (July 2010). "Characterization of the RNA content of chromatin". In: *Genome Research* 20.7, pp. 899–907. ISSN: 1088-9051. DOI: 10.1101/gr.103473.109. URL: http://www.ncbi.nlm.nih.gov/pubmed/20404130%20http://www.pubmedcentral.nih.gov/articlerender.fcgi?artid=PMC2892091%20http://genome.cshlp.org/cgi/doi/10.1101/gr.103473.109.

Mumbach, Maxwell R. et al. (Nov. 2016). "HiChIP: Efficient and sensitive analysis of protein-directed genome architecture". In: *Nature Methods* 13.11, pp. 919–922. ISSN: 15487105. DOI: 10.1038/nmeth.3999. URL: https://www.nature.com/articles/nmeth.3999.

Nagano, Takashi, Yaniv Lubling, Csilla Várnai, et al. (July 2017). "Cell-cycle dynamics of chromosomal organization at single-cell resolution". In: *Nature* 547.7661, pp. 61–67. ISSN: 14764687. DOI: 10.1038/nature23001. URL: https://pubmed.ncbi.nlm.nih.gov/28682332/.

Nagano, Takashi, Yaniv Lubling, Eitan Yaffe, et al. (Dec. 2015). "Single-cell Hi-C for genome-wide detection of chromatin interactions that occur simultaneously in a single cell". In: *Nature Protocols* 10.12, pp. 1986–2003. ISSN: 17502799. DOI: 10.1038/nprot.2015.127. URL: https://pubmed.ncbi.nlm.nih.gov/26540590/.

Nagashima, Ryosuke et al. (May 2019). "Single nucleosome imaging reveals loose genome chromatin networks via active RNA polymerase II". In: *Journal of Cell Biology* 218.5, pp. 1511–1530. ISSN: 15408140.

DOI: 10.1083/jcb.201811090. URL: https://pubmed.ncbi.nlm.nih.gov/30824489/.

Nakamura, Hiromu, Toshiteru Morita, and Chikako Sato (1986). "Structural organizations of replicon domains during DNA synthetic phase in the mammalian nucleus". In: *Experimental Cell Research* 165.2, pp. 291–297. ISSN: 00144827. DOI: 10.1016/0014-4827(86)90583-5. URL: https://pubmed.ncbi.nlm.nih.gov/3720850/.

Nakayasu, H. and R. Berezney (1989). "Mapping replicational sites in the eucaryotic cell nucleus." In: *The Journal of cell biology* 108.1, pp. 1–11. ISSN: 00219525. DOI: 10.1083/jcb.108.1.1. URL: https://pubmed.ncbi.nlm.nih.gov/2910875/.

Narendra, Varun et al. (Feb. 2015). "CTCF establishes discrete functional chromatin domains at the Hox clusters during differentiation". In: *Science* 347.6225, pp. 1017–1021. ISSN: 10959203. DOI: 10.1126/science.1262088. URL: https://pubmed.ncbi.nlm.nih.gov/25722416/.

Naumova, Natalia et al. (Nov. 2013). "Organization of the mitotic chromosome". In: *Science* 342.6161, pp. 948–953. ISSN: 10959203. DOI: 10.1126/science.1236083. URL: https://science.sciencemag.org/content/342/6161/948.

Neely, Kristen E. et al. (Oct. 1999). "Activation domain-mediated targeting of the SWI/SNF complex to promoters stimulates transcription from nucleosome arrays". In: *Molecular Cell* 4.4, pp. 649–655. ISSN: 10972765. DOI: 10.1016/S1097-2765(00)80216-6. URL: http://www.cell.com/article/S1097276500802166/fulltext.

Neumann, Frank R. et al. (Feb. 2012). "Targeted INO80 enhances subnuclear chromatin movement and ectopic homologous recombination". In: *Genes and Development* 26.4, pp. 369–383. ISSN: 08909369. DOI: 10.1101/gad.176156.111. URL: http://www.genesdev.org/cgi/doi/10.1101/gad.176156.111..

Nora, Elphège P. et al. (May 2012). "Spatial partitioning of the regulatory landscape of the X-inactivation centre". In: *Nature* 485.7398, pp. 381–

385. ISSN: 00280836. DOI: 10.1038/nature11049. URL: https://www.nature.com/articles/nature11049.

Nuebler, Johannes et al. (July 2018). "Chromatin organization by an interplay of loop extrusion and compartmental segregation". In: *Proceedings of the National Academy of Sciences* 115.29, E6697–E6706. ISSN: 0027-8424. DOI: 10.1073/PNAS.1717730115. URL: https://www.pnas.org/content/115/29/E6697.

Ohlsson, Rolf, Rainer Renkawitz, and Victor Lobanenkov (Sept. 2001). *CTCF is a uniquely versatile transcription regulator linked to epigenetics and disease*. DOI: 10.1016/S0168-9525(01)02366-6.

Ohta, Shinya et al. (Sept. 2010). "The Protein Composition of Mitotic Chromosomes Determined Using Multiclassifier Combinatorial Proteomics". In: *Cell* 142.5, pp. 810–821. ISSN: 00928674. DOI: 10.1016/j.cell.2010.07.047. URL: https://pubmed.ncbi.nlm.nih.gov/20813266/.

Palade, George (Sept. 1975). "Intracellular Aspects of the Process of Protein Synthesis". In: *Science* 189.4206, pp. 867–867. ISSN: 0036-8075. DOI: 10.1126/science.189.4206.867-b. URL: https://pubmed.ncbi.nlm.nih.gov/1096303/.

Paulsen, Jonas et al. (May 2019). "Long-range interactions between topologically associating domains shape the four-dimensional genome during differentiation". In: *Nature Genetics* 51.5, pp. 835–843. ISSN: 15461718. DOI: 10.1038/s41588-019-0392-0. URL: https://www.nature.com/articles/s41588-019-0392-0.

Peric-Hupkes, Daan et al. (May 2010). "Molecular Maps of the Reorganization of Genome-Nuclear Lamina Interactions during Differentiation". In: *Molecular Cell* 38.4, pp. 603–613. ISSN: 10972765. DOI: 10.1016/j.molcel.2010.03.016. URL: https://pubmed.ncbi.nlm.nih.gov/20513434/.

Phillips, Jennifer E. and Victor G. Corces (June 2009). *CTCF: Master Weaver of the Genome*. DOI: 10.1016/j.cell.2009.06.001. URL: https://pubmed.ncbi.nlm.nih.gov/19563753/.

Phillips-Cremins, Jennifer E. et al. (June 2013). "Architectural protein subclasses shape 3D organization of genomes during lineage commitment". In: *Cell* 153.6, pp. 1281–1295. ISSN: 10974172. DOI: 10.1016/j.cell.2013.04.053. URL: http://dx.doi.org/10.1016/j.cell.2013.04.053.

plotting - Convex hull in 3D - Mathematica Stack Exchange (2021). URL: https://mathematica.stackexchange.com/questions/190428/convex-hull-in-3d-two-colorings-for-some-of-the-faces (visited on 06/26/2021).

Pombo, Ana and Miguel R. Branco (Oct. 2007). *Functional organisation of the genome during interphase*. DOI: 10.1016/j.gde.2007.08.008.

Pope, Benjamin D. et al. (Nov. 2014). "Topologically associating domains are stable units of replication-timing regulation". In: *Nature* 515.7527, pp. 402–405. ISSN: 14764687. DOI: 10.1038/nature13986. URL: https://www.nature.com/articles/nature13986.

Prokocimer, Miron et al. (July 2009). "Nuclear lamins: key regulators of nuclear structure and activities". In: *Journal of Cellular and Molecular Medicine* 13.6, pp. 1059–1085. ISSN: 15821838. DOI: 10.1111/j.1582-4934.2008.00676.x. URL: http://doi.wiley.com/10.1111/j.1582-4934.2008.00676.x.

Quinodoz, Sofia A. et al. (July 2018). "Higher-Order Inter-chromosomal Hubs Shape 3D Genome Organization in the Nucleus". In: *Cell* 174.3, 744–757.e24. ISSN: 10974172. DOI: 10.1016/j.cell.2018.05.024. URL: https://pubmed.ncbi.nlm.nih.gov/29887377/.

Rao, Suhas S.P., Su Chen Huang, et al. (Oct. 2017). "Cohesin Loss Eliminates All Loop Domains". In: *Cell* 171.2, 305–320.e24. ISSN: 10974172. DOI: 10.1016/j.cell.2017.09.026. URL: https://doi.org/10.1016/j.cell.2017.09.026.

Rao, Suhas S.P., Miriam H. Huntley, et al. (Dec. 2014). "A 3D map of the human genome at kilobase resolution reveals principles of chromatin looping". In: *Cell* 159.7, pp. 1665–1680. ISSN: 10974172. DOI: 10.

1016/j.cell.2014.11.021. URL: https://pubmed.ncbi.nlm.nih.gov/25497547/.

Reits, E. A.J. and J. J. Neefjes (2001). *From fixed to FRAP: Measuring protein mobility and activity in living cells*. DOI: 10.1038/35078615.

Renaud-Gabardos, Edith (2015). "Internal ribosome entry site-based vectors for combined gene therapy". In: *World Journal of Experimental Medicine* 5.1, p. 11. ISSN: 2220-315X. DOI: 10.5493/wjem.v5.i1.11. URL: /pmc/articles/PMC4308528/%20/pmc/articles/PMC4308528/?report=abstract%20https://www.ncbi.nlm.nih.gov/pmc/articles/PMC4308528/.

Rhind, Nicholas and David M. Gilbert (Aug. 2013). "DNA replication timing". In: *Cold Spring Harbor Perspectives in Biology* 5.8, a010132. ISSN: 19430264. DOI: 10.1101/cshperspect.a010132. URL: http://cshperspectives.cshlp.org/%20https://pubmed.ncbi.nlm.nih.gov/23838440/.

Ricci, Maria Aurelia et al. (Mar. 2015). "Chromatin Fibers Are Formed by Heterogeneous Groups of Nucleosomes In Vivo". In: *Cell* 160.6, pp. 1145–1158. ISSN: 0092-8674. DOI: 10.1016/J.CELL.2015.01.054.

Rivera-Mulia, Juan Carlos and David M. Gilbert (June 2016). *Replicating Large Genomes: Divide and Conquer*. DOI: 10.1016/j.molcel.2016.05.007. URL: http://dx.doi.org/10.1016/j.molcel.2016.05.007.

Robinett, Carmen C. et al. (1996). "In vivo localization of DNA sequences and visualization of large-scale chromatin organization using lac operator/repressor recognition". In: *Journal of Cell Biology* 135.6 II, pp. 1685–1700. ISSN: 00219525. DOI: 10.1083/jcb.135.6.1685. URL: https://pubmed.ncbi.nlm.nih.gov/8991083/.

Rodley, C. D.M. et al. (Nov. 2009). "Global identification of yeast chromosome interactions using Genome conformation capture". In: *Fungal Genetics and Biology* 46.11, pp. 879–886. ISSN: 10871845. DOI: 10.1016/j.fgb.2009.07.006. URL: https://pubmed.ncbi.nlm.nih.gov/19628047/.

Ryba, Tyrone et al. (June 2010). "Evolutionarily conserved replication timing profiles predict long-range chromatin interactions and distinguish closely related cell types". In: *Genome Research* 20.6, pp. 761–770. ISSN: 10889051. DOI: 10.1101/gr.099655.109. URL: http://www.genome.org/cgi/doi/10.1101/gr.099655.109..

Saad, Hicham et al. (2014). "DNA Dynamics during Early Double-Strand Break Processing Revealed by Non-Intrusive Imaging of Living Cells". In: *PLoS Genetics* 10.3. ISSN: 15537404. DOI: 10.1371/journal.pgen.1004187. URL: https://pubmed.ncbi.nlm.nih.gov/24625580/.

Sabari, Benjamin R. et al. (July 2018). "Coactivator condensation at super-enhancers links phase separation and gene control". In: *Science* 361.6400, eaar3958. ISSN: 0036-8075. DOI: 10.1126/science.aar3958. URL: https://pubmed.ncbi.nlm.nih.gov/29930091/.

Sanborn, Adrian L. et al. (Nov. 2015). "Chromatin extrusion explains key features of loop and domain formation in wild-type and engineered genomes". In: *Proceedings of the National Academy of Sciences of the United States of America* 112.47, E6456–E6465. ISSN: 10916490. DOI: 10.1073/pnas.1518552112. URL: www.pnas.org/cgi/doi/10.1073/pnas.1518552112.

Schalch, Thomas et al. (July 2005). "X-ray structure of a tetranucleosome and its implications for the chromatin fibre". In: *Nature 2005 436:7047* 436.7047, pp. 138–141. ISSN: 1476-4687. DOI: 10.1038/nature03686. URL: https://www.nature.com/articles/nature03686.

Schindelin, Johannes et al. (July 2012). *Fiji: An open-source platform for biological-image analysis*. DOI: 10.1038/nmeth.2019. URL: http://fiji.sc/Adding%7B%5C_%7DUpdate%7B%5C_%7DSites.

Schmidt, Dominic et al. (May 2010). "A CTCF-independent role for cohesin in tissue-specific transcription". In: *Genome Research* 20.5, pp. 578–588. ISSN: 10889051. DOI: 10.1101/gr.100479.109. URL: http://www.genome.org/cgi/doi/10.1101/gr.100479.109..

Schneider, Robert and Rudolf Grosschedl (Dec. 2007). *Dynamics and interplay of nuclear architecture, genome organization, and gene ex-*

pression. DOI: 10.1101/gad.1604607. URL: https://pubmed.ncbi.nlm.nih.gov/18056419/.

Schoenfelder, Stefan et al. (Sept. 2015). "Polycomb repressive complex PRC1 spatially constrains the mouse embryonic stem cell genome". In: *Nature Genetics* 47.10, pp. 1179–1186. ISSN: 15461718. DOI: 10.1038/ng.3393. URL: https://pubmed.ncbi.nlm.nih.gov/26323060/.

Scully, Ralph and Anyong Xie (Oct. 2013). *Double strand break repair functions of histone H2AX*. DOI: 10.1016/j.mrfmmm.2013.07.007. URL: https://www.ncbi.nlm.nih.gov/pmc/articles/PMC3818383/.

Seeber, Andrew, Vincent Dion, and Susan M. Gasser (Sept. 2013). "Checkpoint kinases and the INO80 nucleosome remodeling complex enhance global chromatin mobility in response to DNA damage". In: *Genes and Development* 27.18, pp. 1999–2008. ISSN: 08909369. DOI: 10.1101/gad.222992.113. URL: http://www.genesdev.org/cgi/.

Seeber, Andrew, Michael H. Hauer, and Susan M. Gasser (Nov. 2018). *Chromosome dynamics in response to DNA damage*. DOI: 10.1146/annurev-genet-120417-031334. URL: https://pubmed.ncbi.nlm.nih.gov/30208290/.

Selvaraj, Siddarth et al. (Dec. 2013). "Whole-genome haplotype reconstruction using proximity-ligation and shotgun sequencing". In: *Nature Biotechnology* 31.12, pp. 1111–1118. ISSN: 10870156. DOI: 10.1038/nbt.2728. URL: https://www.nature.com/articles/nbt.2728.

Sexton, Tom et al. (Feb. 2012). "Three-dimensional folding and functional organization principles of the Drosophila genome". In: *Cell* 148.3, pp. 458–472. ISSN: 10974172. DOI: 10.1016/j.cell.2012.01.010. URL: http://www.cell.com/article/S0092867412000165/fulltext.

Shaban, Haitham A., Roman Barth, and Kerstin Bystricky (2018). *Nanoscale mapping of chromatin dynamics in living cells*. DOI: 10.1101/405969. URL: https://doi.org/10.1101/405969.

Shaban, Haitham A. and Andrew Seeber (May 2020). *Monitoring global chromatin dynamics in response to DNA damage*. DOI: 10.1016/j.mrfmmm.2020.111707.

Shah, Sheel et al. (2018). "Dynamics and Spatial Genomics of the Nascent Transcriptome by Intron seqFISH". In: *Cell* 174, pp. 363–376. DOI: 10.1016/j.cell.2018.05.035. URL: https://doi.org/10.1016/j.cell.2018.05.035.

Shen, Yin et al. (July 2012). "A map of the cis -regulatory sequences in the mouse genome". In: *Nature 2012 488:7409* 488.7409, pp. 116–120. ISSN: 1476-4687. DOI: 10.1038/nature11243. URL: https://www.nature.com/articles/nature11243.

Shinkai, Soya et al. (Oct. 2016). "Dynamic Nucleosome Movement Provides Structural Information of Topological Chromatin Domains in Living Human Cells". In: *PLoS Computational Biology* 12.10, e1005136–e1005136. ISSN: 15537358. DOI: 10.1371/journal.pcbi.1005136. URL: http://www.mext.go.jp/english/.

Shoeman, R. L. and P. Traub (June 1990). "The in vitro DNA-binding properties of purified nuclear lamin proteins and vimentin." In: *Journal of Biological Chemistry* 265.16, pp. 9055–9061. ISSN: 0021-9258. DOI: 10.1016/S0021-9258(19)38810-6.

Shrinivas, Krishna et al. (Aug. 2019). "Enhancer Features that Drive Formation of Transcriptional Condensates". In: *Molecular Cell* 75.3, 549–561.e7. ISSN: 10974164. DOI: 10.1016/j.molcel.2019.07.009.

Simonis, Marieke et al. (Nov. 2006). "Nuclear organization of active and inactive chromatin domains uncovered by chromosome conformation capture-on-chip (4C)". In: *Nature Genetics* 38.11, pp. 1348–1354. ISSN: 10614036. DOI: 10.1038/ng1896. URL: https://www.nature.com/articles/ng1896.

Sloan, Katherine E., Markus T. Bohnsack, and Nicholas J. Watkins (Oct. 2013). "The 5S RNP Couples p53 Homeostasis to Ribosome Biogenesis and Nucleolar Stress". In: *Cell Reports* 5.1, pp. 237–247. ISSN: 22111247. DOI: 10.1016/j.celrep.2013.08.049. URL: https://pubmed.ncbi.nlm.nih.gov/24120868/.

Sofueva, Sevil et al. (Dec. 2013). "Cohesin-mediated interactions organize chromosomal domain architecture". In: *EMBO Journal* 32.24, pp. 3119–3129. ISSN: 02614189. DOI: 10.1038/emboj.2013.237. URL: https://www.embopress.org/doi/full/10.1038/emboj.2013.237%20https://www.embopress.org/doi/abs/10.1038/emboj.2013.237.

Solomon, David A, Jung-Sik Kim, and Todd Waldman (2014). "Cohesin gene mutations in tumorigenesis: from discovery to clinical significance". In: *BMB Rep* 47.6, pp. 299–310. DOI: 10.5483/BMBRep.2014.47.6.092. URL: www.bmbreports.orghttp://dx.doi.org/10.5483/BMBRep.2014.47.6.092.

Soutoglou, Evi et al. (June 2007). "Positional stability of single double-strand breaks in mammalian cells". In: *Nature Cell Biology* 9.6, pp. 675–682. ISSN: 14657392. DOI: 10.1038/ncb1591. URL: https://www.nature.com/articles/ncb1591.

Spichal, M et al. (2016). "Evidence for a dual role of actin in regulating chromosome organization and dynamics in yeast". In: *Journal of cell science* 129.4, pp. 681–692. ISSN: 1477-9137. DOI: 10.1242/JCS.175745. URL: https://pubmed.ncbi.nlm.nih.gov/26763908/.

Stadhouders, Ralph et al. (Feb. 2018). "Transcription factors orchestrate dynamic interplay between genome topology and gene regulation during cell reprogramming". In: *Nature Genetics* 50.2, pp. 238–249. ISSN: 15461718. DOI: 10.1038/s41588-017-0030-7. URL: https://www.nature.com/articles/s41588-017-0030-7%20https://www.nature.com/articles/s41588-017-0030-7/.

Stanley, Fintan K.T., Shaun Moore, and Aaron A. Goodarzi (Oct. 2013). "CHD chromatin remodelling enzymes and the DNA damage re-

sponse". In: *Mutation Research/Fundamental and Molecular Mechanisms of Mutagenesis* 750.1-2, pp. 31–44. ISSN: 0027-5107. DOI: 10.1016/J.MRFMMM.2013.07.008.

Stein, Viktor and Kirill Alexandrov (Nov. 2014). "Protease-based synthetic sensing and signal amplification". In: *Proceedings of the National Academy of Sciences of the United States of America* 111.45, pp. 15934–15939. ISSN: 10916490. DOI: 10.1073/pnas.1405220111. URL: https://www.pnas.org/content/111/45/15934.

Szczepińska, Teresa, Anna Maria Rusek, and Dariusz Plewczynski (July 2019). "Intermingling of chromosome territories". In: *Genes, Chromosomes and Cancer* 58.7, pp. 500–506. ISSN: 1045-2257. DOI: 10.1002/gcc.22736. URL: https://onlinelibrary.wiley.com/doi/abs/10.1002/gcc.22736.

Taddei, Angela and Susan M. Gasser (May 2006). "Repairing subtelomeric DSBs at the nuclear periphery". In: *Trends in Cell Biology* 16.5, pp. 225–228. ISSN: 0962-8924. DOI: 10.1016/J.TCB.2006.03.005. URL: http://www.cell.com/article/S0962892406000857/fulltext.

Takebayashi, S et al. (July 2012). "Chromatin-interaction compartment switch at developmentally regulated chromosomal domains reveals an unusual principle of chromatin folding". In: *Proceedings of the National Academy of Sciences of the United States of America* 109.31, pp. 12574–12579. ISSN: 1091-6490. DOI: 10.1073/PNAS.1207185109. URL: https://pubmed.ncbi.nlm.nih.gov/22807480/.

Tanenbaum, ME et al. (Oct. 2014). "A protein-tagging system for signal amplification in gene expression and fluorescence imaging". In: *Cell* 159.3, pp. 635–646. ISSN: 1097-4172. DOI: 10.1016/J.CELL.2014.09.039. URL: https://pubmed.ncbi.nlm.nih.gov/25307933/.

Thoma, F., Th Koller, and A. Klug (Nov. 1979). "Involvement of histone H1 in the organization of the nucleosome and of the salt-dependent superstructures of chromatin". In: *Journal of Cell Biology* 83.2 I, pp. 403–427. ISSN: 00219525. DOI: 10.1083/jcb.83.2.403. URL:

http://rupress.org/jcb/article-pdf/83/2/403/1074074/403.pdf.

Thomson, Inga et al. (Jan. 2004). "The Radial Positioning of Chromatin Is Not Inherited through Mitosis but Is Established de Novo in Early G1". In: *Current Biology* 14.2, pp. 166–172. ISSN: 09609822. DOI: 10.1016/j.cub.2003.12.024. URL: http://www.cell.com/article/S0960982203009357/fulltext.

Tinevez, Jean Yves et al. (Feb. 2017). "TrackMate: An open and extensible platform for single-particle tracking". In: *Methods* 115, pp. 80–90. ISSN: 10959130. DOI: 10.1016/j.ymeth.2016.09.016.

Tsouroula, K et al. (July 2016). "Temporal and Spatial Uncoupling of DNA Double Strand Break Repair Pathways within Mammalian Heterochromatin". In: *Molecular cell* 63.2, pp. 293–305. ISSN: 1097-4164. DOI: 10.1016/J.MOLCEL.2016.06.002. URL: https://pubmed.ncbi.nlm.nih.gov/27397684/.

Tsukamoto, Toshiro et al. (Nov. 2000). "Visualization of gene activity in living cells". In: *Nature Cell Biology 2000 2:12* 2.12, pp. 871–878. ISSN: 1476-4679. DOI: 10.1038/35046510. URL: https://www.nature.com/articles/ncb1200%7B%5C_%7D871.

Van De Werken, Harmen J.G. et al. (Oct. 2012). "Robust 4C-seq data analysis to screen for regulatory DNA interactions". In: *Nature Methods* 9.10, pp. 969–972. ISSN: 15487091. DOI: 10.1038/nmeth.2173. URL: https://pubmed.ncbi.nlm.nih.gov/22961246/.

Wang, Haifeng et al. (Sept. 2019). "CRISPR-mediated live imaging of genome editing and transcription". In: *Science* 365.6459, pp. 1301–1305. ISSN: 0036-8075. DOI: 10.1126/SCIENCE.AAX7852. URL: https://science.sciencemag.org/content/early/2019/09/04/science.aax7852.

Wang, Siyuan et al. (May 2016). "An RNA-aptamer-based two-color CRISPR labeling system". In: *Scientific Reports* 6. ISSN: 20452322. DOI: 10.1038/srep26857. URL: https://pubmed.ncbi.nlm.nih.gov/27229896/.

Wang, Yanli et al. (Oct. 2018). "The 3D Genome Browser: a web-based browser for visualizing 3D genome organization and long-range chromatin interactions". In: *Genome Biology 2018 19:1* 19.1, pp. 1–12. ISSN: 1474-760X. DOI: 10.1186/S13059-018-1519-9. URL: https://genomebiology.biomedcentral.com/articles/10.1186/s13059-018-1519-9.

Weierich, Claudia et al. (2003). "Three-dimensional arrangements of centromeres and telomeres in nuclei of human and murine lymphocytes". In: *Chromosome Research 2003 11:5* 11.5, pp. 485–502. ISSN: 1573-6849. DOI: 10.1023/A:1025016828544. URL: https://link.springer.com/article/10.1023/A:1025016828544.

Welch, Lonnie R. et al. (Feb. 2020). "Single-Cell Analysis of the 3D Topologies of Genomic Loci Using Genome Architecture Mapping". In: *bioRxiv*, p. 2020.02.10.941047. DOI: 10.1101/2020.02.10.941047. URL: https://www.biorxiv.org/content/10.1101/2020.02.10.941047v2.

Whitefield, Daniel B. et al. (Dec. 2018). "Quantifying site-specific chromatin mechanics and DNA damage response". In: *Scientific Reports* 8.1, pp. 1–9. ISSN: 20452322. DOI: 10.1038/s41598-018-36343-x. URL: www.nature.com/scientificreports/.

Wright, William Douglass, Shanaya Shital Shah, and Wolf Dietrich Heyer (July 2018). *Homologous recombination and the repair of DNA double-strand breaks*. DOI: 10.1074/jbc.TM118.000372. URL: https://pubmed.ncbi.nlm.nih.gov/29599286/.

Xie, Xiaohui et al. (Apr. 2007). "Systematic discovery of regulatory motifs in conserved regions of the human genome, including thousands of CTCF insulator sites". In: *Proceedings of the National Academy of Sciences of the United States of America* 104.17, pp. 7145–7150. ISSN: 00278424. DOI: 10.1073/pnas.0701811104. URL: https://www.pnas.org/content/104/17/7145%20https://www.pnas.org/content/104/17/7145.abstract.

Yaffe, Eitan et al. (July 2010). "Comparative analysis of DNA replication timing reveals conserved large-scale chromosomal architecture". In: *PLoS Genetics* 6.7, pp. 1–12. ISSN: 15537390. DOI: 10.1371/journal.pgen.1001011. URL: https://pubmed.ncbi.nlm.nih.gov/20617169/.

Zhang, Yubo et al. (Nov. 2013). "Chromatin connectivity maps reveal dynamic promoter-enhancer long-range associations". In: *Nature* 504.7479, pp. 306–310. ISSN: 00280836. DOI: 10.1038/nature12716. URL: https://www.nature.com/articles/nature12716.

Zheng, Meizhen et al. (Feb. 2019). "Multiplex chromatin interactions with single-molecule precision". In: *Nature* 566.7745, pp. 558–562. ISSN: 14764687. DOI: 10.1038/s41586-019-0949-1. URL: https://doi.org/10.1038/s41586-019-0949-1.

Zidovska, Alexandra, David A. Weitz, and Timothy J. Mitchison (Sept. 2013). "Micron-scale coherence in interphase chromatin dynamics". In: *Proceedings of the National Academy of Sciences of the United States of America* 110.39, pp. 15555–15560. ISSN: 00278424. DOI: 10.1073/pnas.1220313110. URL: www.pnas.org/cgi/doi/10.1073/pnas.1220313110.

Zuin, Jessica et al. (Jan. 2014). "Cohesin and CTCF differentially affect chromatin architecture and gene expression in human cells". In: *Proceedings of the National Academy of Sciences of the United States of America* 111.3, pp. 996–1001. ISSN: 10916490. DOI: 10.1073/pnas.1317788111. URL: https://pubmed.ncbi.nlm.nih.gov/24335803/%20www.pnas.org/cgi/doi/10.1073/pnas.1317788111.

Zuleger, Nikolaj et al. (Feb. 2013). "Specific nuclear envelope transmembrane proteins can promote the location of chromosomes to and from the nuclear periphery". In: *Genome Biology* 14.2, R14. ISSN: 1474760X. DOI: 10.1186/gb-2013-14-2-r14. URL: http://genomebiology.biomedcentral.com/articles/10.1186/gb-2013-14-2-r14.